

May 2015

Modeling Lake Michigan Nearshore Carbon and Phosphorus Dynamics

Joseph Henry Fillingham
University of Wisconsin-Milwaukee

Follow this and additional works at: <https://dc.uwm.edu/etd>

 Part of the [Biogeochemistry Commons](#), [Environmental Sciences Commons](#), and the [Fresh Water Studies Commons](#)

Recommended Citation

Fillingham, Joseph Henry, "Modeling Lake Michigan Nearshore Carbon and Phosphorus Dynamics" (2015). *Theses and Dissertations*. 871.
<https://dc.uwm.edu/etd/871>

This Dissertation is brought to you for free and open access by UWM Digital Commons. It has been accepted for inclusion in Theses and Dissertations by an authorized administrator of UWM Digital Commons. For more information, please contact open-access@uwm.edu.

MODELING LAKE MICHIGAN NEARSHORE CARBON AND PHOSPHORUS
DYNAMICS

by

Joseph H Fillingham

A Dissertation Submitted in

Partial Fulfillment of the

Requirements for the Degree of

Doctor of Philosophy

in Freshwater Sciences

at

The University of Wisconsin-Milwaukee

May 2015

ABSTRACT
MODELING THE NEARSHORE BIOGEOCHEMISTRY OF LAKE MICHIGAN

by

Joseph H Fillingham

The University of Wisconsin-Milwaukee, 2015
Under the Supervision of Professor Harvey Bootsma

Dreissenid mussels, in particular quagga mussels (*Dreissena rostriformis bugensis*), are transforming the Lake Michigan ecosystem by clearing the water column, recycling phosphorus and modifying benthic habitat. These impacts are thought to have caused observed declines in the spring phytoplankton bloom in Lake Michigan, as well as changes to food web structure and declines in the abundance of critical invertebrate and fish species. In the nearshore zone, the resurgence of benthic *Cladophora* algae to nuisance levels not observed since phosphorus loading abatement policies instituted in the 1970s has also been attributed to water column clearing and phosphorus recycling by mussels. Using a long term data set collected in the Lake Michigan nearshore zone between 1980 and 2013, changes in water quality parameters are characterized, compared to those monitored in the lake offshore, and analyzed in the context of the dreissenid mussel invasion and nearshore *Cladophora* growth. Using this time series analysis as a historical foundation, a computer model of the Lake Michigan nearshore zone was used to identify and quantify the influence of dreissenid mussels on *Cladophora* growth and nearshore phosphorus and carbon pools and fluxes.

This is the first study of Lake Michigan to incorporate both dreissenid mussels and *Cladophora* algae in a dynamic phosphorus and carbon model. Model output for the summer and fall of 2013 was validated by comparison with an extensive data set of phosphorus and carbon measurements taken at a monitoring station at 9m depth in the Lake Michigan nearshore. The monitoring station and model domain are characterized by rocky substrate and quagga mussel densities of ~ 5500 individuals m^{-2} and summer, peak *Cladophora* biomass of 250 gDW m^{-2} . Following model validation, model test scenarios were simulated excluding mussels. Comparison of model simulations with and without mussels confirmed that dreissenid mussels in the Lake Michigan nearshore zone support *Cladophora* growth at nuisance levels by increasing light penetration and phosphorus recycling. The nearshore mussel-*Cladophora* complex substantially increased the storage of phosphorus and carbon in the nearshore zone, supporting the nearshore shunt hypothesis.

Mussels were found to support *Cladophora* production at levels which produced a net autotrophic nearshore zone with *Cladophora* production consistently exceeding mussel respiration and phytoplankton production during the summer. Due to tissue C:P ratios that were more than twice those of phytoplankton, *Cladophora* was able to utilize the available light and phosphorus provided by mussel grazing and recycling of phytoplankton to support high growth rates and to produce a large biomass. Even though the nutrients available for *Cladophora* growth came from phytoplankton recycled by mussels, the ability of *Cladophora* to store phosphorus in tissue and grow at a high rate with a high tissue C:P ratio lead to a net autotrophic nearshore ecosystem. Nearshore phytoplankton were consistently mixed into the model domain from the lake offshore due

to mussel grazing and water column clearing. The consistent input of offshore particulate phosphorus and carbon to the nearshore in model simulations suggested that the nearshore is dependent on offshore energy sources. Tributary loading of carbon and phosphorus can subsidize mussel grazing and therefore limit the demand of nearshore mussels for offshore carbon and phosphorus. There are large areas of Lake Michigan, however, well away from river input that sustain large populations of mussels and *Cladophora*. These areas are likely sourcing energy and nutrients from the lake offshore as demonstrated by the results of this study. Although there is room for model improvement, the findings of this study provide the first definitive evidence that nearshore dreissenid mussels support *Cladophora* growth in the Lake Michigan nearshore zone and in doing so, create a seasonal nearshore sink for phosphorus and carbon supplied by the lake offshore. The results of this research provide guidance for future monitoring and modeling work which will provide a clearer picture of the influence of nearshore dreissenid mussels and *Cladophora* on whole lake nutrient dynamics and energy pathways.

© Copyright by Joseph H Fillingham, 2015
All Rights Reserved

TABLE OF CONTENTS

List of Figures	viii
List of Tables	xv
Acknowledgements	xviii
Chapter 1: Introduction and Background	1
1.1 Introduction	1
1.2 Questions, Hypotheses, and Research Philosophy	9
Chapter 2: Change in the Lake Michigan Nearshore zone: 1980 – 2013	15
2.1 Introduction	16
2.2 Methods	19
2.3 Results	26
2.4 Discussion and Conclusions	44
Chapter 3: Modeling Nearshore Phosphorus Dynamics	51
3.1 Introduction	52
3.2 Data Collection and Sampling Methods	55
3.3 Model Description	58
3.4 Model Simulation Results	76
3.5 Discussion and Conclusions	105
Chapter 4: Modeling Nearshore Carbon and Phosphorus Dynamics	115
4.1 Introduction	116
4.2 Data Collection and Sampling Methods	118
4.3 Model Description	122

4.4 Model Simulation Results	137
4.5 Discussion	163
4.6 Conclusions	178
Chapter 5: Synthesis and Conclusions	180
References	189
Appendix A: Sampling Methods, Measurement Methods, and Data	206
Appendix B: MATLAB Code for Models and Functions	257

LIST OF FIGURES

- Figure 2.1:** Map of the Milwaukee, WI and the Lake Michigan nearshore zone with MMSD monitoring stations indicated with red dots and labeled. NS-7 and 8 were included in this study of historical nearshore water quality parameters. This map was modified from its original version which was provided by MMSD. 20
- Figure 2.2:** Number of chlorophyll *a* samples collected during each month and decade by the Milwaukee Metropolitan Sewerage District at nearshore monitoring stations 7 and 8. 22
- Figure 2.3:** Number of chlorophyll *a* samples collected during each month and decade by the EPA during offshore monitoring cruises at Lake Michigan southern basin stations: MI 11, 17, 18, 19, 23, and 27. 25
- Figure 2.4:** A) Chlorophyll *a* concentration, B) silica concentration, C) turbidity, and D) secchi depth annual means. Error bars indicate the 95% confidence interval of the annual mean. Linear regressions of the means from 1980 to 2013 are shown for each parameter as black lines. The slope, R^2 , and p values for each linear regression are: A) $m = -0.081$, $R^2 = 0.65$, $p < 0.001$, B) $m = 0.572$, $R^2 = 0.64$, $p < 0.001$, C) $m = -0.039$, $R^2 = 0.52$, $p < 0.001$, D) $m = 0.213$, $R^2 = 0.72$, $p < 0.001$. The cubic polynomial fit for each parameter annual means is shown as a gray line with R^2 and p values: A) 0.65, $p < 0.001$ B) 0.86, $p < 0.001$ C) 0.68, $p < 0.001$ and D) 0.81, $p < 0.001$. 27
- Figure 2.5:** A) Chlorophyll *a* concentration, B) silica concentration, C) turbidity, and D) secchi depth decade distributions. The mid line is the decade median and the dot is the decade mean. The rectangle indicates the 25th and 75th percentile of the decade distribution while the dashed whiskers indicate 1.5 times the 25th and 75th percentile range representing the maximum and minimum values with outliers removed. 29
- Figure 2.6:** Chlorophyll *a* concentration (A), silica concentration (B), turbidity (C), and secchi depth (D) monthly means sorted by decade. Error bars represent the 95% confidence intervals of the monthly means represented by: circles for the 1980s, squares for the 1990s, and triangles for the 2000s. 33
- Figure 2.7:** Ratios of chlorophyll *a* concentration ($\mu\text{g L}^{-1}$) to A) turbidity (NTU), and B) secchi depth (m). Black bars represent the 1980s, gray bars the 1990s, and white bars the 2000s. Error bars indicate the 95% confidence interval of the decade month ratio mean. 35
- Figure 2.8:** Lake Michigan, southern basin, offshore depth averaged chlorophyll *a* concentration collected by the EPA: A and B include all 36

available data, C and D include April data only, and E and F include August data only. A, D, and E are presented the same as in Fig. 4 where the linear fit R^2 and p values are: A) $R^2 = 0.15$, $p = 0.04$; C) $R^2 = 0.06$, $p = 0.24$; and D) $R^2 = 0.10$, $p = 0.13$, and the cubic R^2 and p values are A) $R^2 = 0.17$, $p = 0.03$; C) $R^2 = 0.17$, $p = 0.04$; and D) $R^2 = 0.11$, $p = 0.12$. B, D and F are presented the same as in Fig. 5.

Figure 2.9: Lake Michigan, southern basin, offshore depth averaged silica concentration collected by the EPA where: A and B include all available data; C and D include April data only; and E and F include August data only. A, D, and E are presented the same as in Fig. 4 where the linear fit R^2 and p values are: A) $R^2 = 0.88$, $p < 0.001$, C) $R^2 = 0.88$, $p < 0.001$, D) $R^2 = 0.86$, $p < 0.001$ and the cubic fit R^2 and p values are A) $R^2 = 0.95$ ($p < 0.001$), C) $R^2 = 0.92$ ($p < 0.001$), D) $R^2 = 0.92$ ($p < 0.001$) for the cubic polynomials. B, D and F are presented the same as in Fig. 5. 38

Figure 2.10: Nearshore and offshore chlorophyll a concentration annual means and linear regressions of the annual means. Both nearshore ($R^2 = 0.65$, $p < 0.001$) and offshore ($R^2 = 0.15$, $p = 0.04$) linear trends are significant. 39

Figure 2.11: Depth and decade mean chlorophyll *a* and silica concentrations in the nearshore (black bars) and offshore (white bars). Spring (A and C) indicates samples taken in May for the nearshore and April for the offshore, and summer (B and D) indicates samples take in August for both the nearshore and offshore. 41

Figure 2.12: Nearshore (A and C) and offshore (B and D) chlorophyll *a* and silica concentrations during spring (black bars) and summer (white bars) in the 1980s, 1990s, and 2000s. Error bars indicate the 95% confidence interval of the decade mean. Spring is represented by the month of May in the nearshore and April in the offshore. Summer is represented by the month of August for both the nearshore and offshore. 42

Figure 2.13: Lake Michigan southern basin total phosphorus loading in metric tons per annum (from Chapra and Dolan 2012) (A), and total and total soluble phosphorus loading from the Milwaukee, WI river confluence in the inner harbor in metric tons per annum (B). 46

Figure 3.1: Map of Lake Michigan around Milwaukee, WI. The 9m monitoring station is labeled AW9 and the 20m monitoring station is labeled AW20. Depth contours are labeled and shown every 10m. The Milwaukee Harbor break-wall is not shown. 56

Figure 3.2: Schematic diagram of the model variables and phosphorus fluxes 60

- Figure 3.3:** Mussel volumetric pumping rate as a function of temperature based on the results of Tyner (2013). The equation of best fit is $M_P = 0.633e^{0.074T}$, where $R^2 = 0.98$ ($p = 0.01$). 70
- Figure 3.4:** Light extinction coefficient (K_e) as a function of the depth averaged particulate phosphorus concentration (PP) at the Lake Michigan nearshore 9m monitoring station. Measurements were taken during the 2013 and 2014 monitoring seasons. The dots represent measured values of K_e and PP and the solid line represents the best fit linear regression of the data, where $K_e = 0.0383[PP] + 0.162$, and $R^2 = 0.55$ ($p < 0.01$). 73
- Figure 3.5:** Model input variables: A) bottom water temperature, B) east – west current velocity, where negative values are towards the west from the east, C) surface wind-wave height, D) water column turbulent diffusion coefficient, and E) near-bottom turbulent diffusion coefficient. The x-axis is the consistent for all subplots and is shown below E. 77
- Figure 3.6:** The model simulated near bottom PAR compared to the measured near bottom PAR at the 9m monitoring from May 30, 2013 - July 13, 2013. The solid line represents the perfect fit while the model vs. observed $R^2 = 0.47$ ($p < 0.001$). 79
- Figure 3.7:** Model phosphorus simulation results (lines) and measured values at the 9m monitoring station (dots): A) upper layer dissolved phosphorus; B) lower layer dissolved phosphorus; C) NBL dissolved phosphorus; D) upper layer particulate phosphorus; E) lower layer particulate phosphorus; and F) NBL particulate phosphorus. 81
- Figure 3.8:** A) Model simulated (line) and measured (dots) *Cladophora* biomass; B) Model simulated (line) and measured (dots) *Cladophora* tissue phosphorus content; and C) model simulated (line) and measured (dots) *Cladophora* areal phosphorus storage. Dots and error bars represent the mean and \pm the standard deviation of triplicate samples. 83
- Figure 3.9:** Model simulated mussel volumetric pumping rate (A), mussel grazing phosphorus flux (B), and the net dissolved phosphorus flux due to mussel excretion and *Cladophora* uptake ($J_{MX} - J_{CU}$) (C). Positive values indicate mussel DP excretion surpasses *Cladophora* DP uptake and negative values indicate mussel excretion is less than *Cladophora* uptake. 85
- Figure 3.10:** Sediment trap (white bars) with model simulated sediment trap (black bars) accumulated particulate phosphorus (top A, bottom B) and sediment trap particulate phosphorus accumulation rate (top C, bottom D) for deployment periods 1) July 11 – August 7, 2013, 2) August 7 – September 20, 2013, and 3) September 20 – November 7, 2013. Error bars on empirical 87

sediment traps represent the standard deviation of triplicate traps at each depth. Note the difference scales on each graph.

- Figure 3.11:** A) Model simulated areal sediment stored particulate phosphorus concentration, and B) model simulated near-bottom particulate phosphorus concentration (dashed line) and measured bottom turbidity (solid line). 89
- Figure 3.12:** A) Model simulated phosphorus budget including total domain phosphorus, total suspended phosphorus, *Cladophora* stored phosphorus, and sediment stored phosphorus; B) monthly average horizontal particulate (J_{PP}) dissolved (J_{DP}) and sloughed *Cladophora* (J_{SL}) fluxes into (positive) and out of (negative) the nearshore zone. 90
- Figure 3.13:** Response variation of model simulated A) mean *Cladophora* biomass, B) mean, net boundary, or cross-shore, dissolved phosphorus flux, and C) mean, net boundary particulate phosphorus flux as a function of perturbations of the mussel model parameters M_1 , M_2 , and ex (see Table 3 for parameter descriptions and units) from -50% to +50% of the base simulation values (see Table 6 for specific response variation values). The horizontal axis is the same in all three figures and is labeled beneath C. 101
- Figure 3.14:** A) Model simulated phosphorus budget including all simulated phosphorus pools for the no mussel test scenario, and B) monthly average horizontal particulate (J_{PP}) dissolved (J_{DP}) and sloughed *Cladophora* (J_{SL}) fluxes into (positive) and out of (negative) the nearshore zone for the no mussel test scenario. 103
- Figure 3.15:** Maximum *Cladophora* biomass simulated using constant vertical diffusivities for the calculation of vertical fluxes of particulate phosphorus (PP) and dissolved phosphorus (DP) between the bottom layer and the lower water column layer. The constant diffusivities were applied to both PP and DP (white circles and line) and DP alone (black squares and dashed line). In the latter case, the base simulation diffusivity was used to calculate PP fluxes. 111
- Figure 4.1:** Map of Lake Michigan and the Lake Express Car Ferry route (black line) from Milwaukee, WI to Muskegon, MI as labeled. 121
- Figure 4.2:** Conceptual diagram of the NCPM showing pools of particulate carbon and dissolved phosphorus (Table 1) and fluxes of carbon and phosphorus (Table 2). Particulate phosphorus is calculated as the sum of suspended particulate carbon pools: phytoplankton and particulate detritus. DIC and the influence of biology on DIC is not shown. 124
- Figure 4.3:** A) Transects (Fig 1) of monthly mean, Lake Express measured, pCO_2 (μatm) for May through October from Milwaukee, WI (W 87.9) to 135

Muskegon, MI (W 86.3) where negative longitude values indicate °W. B) The approximate depth along the lake transect.

Figure 4.4: Mean daily ferry measured and 9m station buoy measured $p\text{CO}_2$. 136
Gaps in the 9m station time series represent data which was removed due to system malfunction or occurred during system maintenance. Gaps in the Lake Express data are filled by linear interpolation between gap end points and occur in mid-July and late August through early September.

Figure 4.5: Model input variables: A) water temperature, B) surface PAR, C) 138
east – west current velocity, where negative values are towards the west from the east, D) surface wind-wave height, and E) the wind speed at ~10m above the lake surface. The x-axis is consistent for all subplots and is shown below E.

Figure 4.6: Measured (thin black line) and simulated (thick black line) 139
nearshore $p\text{CO}_2$ for each month of the simulation period when $p\text{CO}_2$ measurements at the 9m station were available during June – September as labeled.

Figure 4.7: Model simulated versus measured daily maximum PAR (dots) at 141
the bottom of the 9m station. The black line is the one to one, best fit line.

Figure 4.8: Measured (dots) and model simulated (black lines) dissolved 142
phosphorus (A), particulate phosphorus (B), chlorophyll *a* (C), and particulate carbon (D) concentrations.

Figure 4.9: Measured (dots) and model simulated (black lines) *Cladophora* 143
biomass (A), tissue phosphorus content (B), and areal stored phosphorus (C). Error bars represent one standard deviation of triplicate samples.

Figure 4.10: Model simulated mussel clearance rate, or volumetric pumping 145
rate (A), mussel particulate phosphorus grazing flux (B), and the net near bottom dissolved phosphorus flux due to mussel excretion and *Cladophora* uptake ($J_{\text{MX}} - J_{\text{CU}}$) (C). Positive values indicate mussel DP excretion surpasses *Cladophora* DP uptake and negative values indicate mussel excretion is less than *Cladophora* uptake.

Figure 4.11: The \log_{10} of each model areal carbon pool including DIC, 149
Cladophora, particulate detritus, sediment, and phytoplankton for the model domain of depth 9.2m.

Figure 4.12: A) Daily mean carbon fluxes through the model boundaries 150
including: nearshore-offshore suspended particulate carbon (J_{HPC}), nearshore-offshore DIC (J_{HDIC}), CO_2 through the air-water interface (J_{AWC}), and nearshore-offshore sloughed *Cladophora* (J_{SL}). B) Monthly mean carbon boundary fluxes listed the same as in A. Negative values indicate a flux out of

the model domain to either the offshore or the atmosphere and positive values indicate flux into the model domain from the offshore or the atmosphere.

Figure 4.13: A) Mean simulated daily, net carbon fluxes associated with *Cladophora*, phytoplankton, dreissenid mussels, and community (net) production, where negative values indicate respiration and positive values indicate photosynthesis. B) Monthly means of simulated net carbon fluxes associated with *Cladophora* (J_{CC}) and phytoplankton (J_{PC}) net production, and dreissenid mussel respiration (J_{MXC}). 153

Figure 4.14: Air-water CO₂ transfer velocity model comparison (A) where k_1 represents the parameterization of Wanninkhof (1992) and k_2 represents the parameterization of Zhao and Xie (2010). B) Cumulative sum of the air-water CO₂ flux associated with transfer velocity models: k_1 and k_2 . 154

Figure 4.15: Carbon fluxes in Figure 12, for the no dreissenid mussel test scenario. The y-axis scales are the same as in Figure 12 for direct comparison. 156

Figure 4.16: Mean daily carbon fluxes (A) and mean monthly carbon fluxes (B) associated with *Cladophora*, and phytoplankton production, as in Figure 13, for the no mussel test scenario. Y-axis scales are the same as in Figure 12 for direct comparison. 158

Figure 4.17: Comparison of monthly mean, biomass specific, net growth rates for *Cladophora* and phytoplankton for model simulations with and without mussels (labeled: no mussels). Rates are calculated as the ratio of net production in $\text{mmol C m}^{-2} \text{d}^{-1}$ to areal biomass in mmol C m^{-2} . 159

Figure 4.18: Comparison of model $p\text{CO}_2$ output for the period of June 2013 when $p\text{CO}_2$ observations were available. The alkalinity test represents the test scenario where alkalinity was set to a constant diel cycle represented by a cosine curve with a mean of 2.22 meq L^{-1} , a range of $\pm 0.01 \text{ meq L}^{-1}$ and daily maximums at midnight and minimums at noon. 162

Figure 4.19: Biomass specific, *Cladophora* net production calculated as the ratio of daily mean *Cladophora* net production and daily mean *Cladophora* biomass. 168

Figure 4.20: The difference between the NPFM and NCPM simulated bottom PAR (A), dissolved phosphorus in the near bottom layer (B), and *Cladophora* biomass (C). Values were calculated as: NPFM – NCPM so that negative values indicate periods where the NPFM produced output which was lower than the NCPM and positive values indicate periods where the NPFM produced output which was higher than the NCPM. 171

Figure A.7: CO₂ system measured A) air and water $p\text{CO}_2$ (ppm) and B) water temperature (°C) during the 2013 monitoring season at the 9m station. 222

LIST OF TABLES

<p>Table 2.1: Percent change in decadal means for each nearshore parameter. Negative values indicate a percent decrease between the labeled decades, and positive values indicate a percent increase between the labeled decades.</p>	30
<p>Table 2.2: Results of Welch’s t-tests for nearshore decadal means. For each parameter sample, the mean (standard deviation), t-statistic (degrees of freedom), test result, and the test p value are presented. A test result of 1 indicates a rejection of the null hypothesis of equal means at the 5% confidence level and a result of 0 indicates that the null hypothesis could not be rejected at the 5% confidence level. The results are presented so that the listed t-test is between the decade column and the following decade from left to right, where the test results under the 2000s are between the 1980s and 2000s.</p>	32
<p>Table 2.3: Mean silica concentration ($\mu\text{mol Si L}^{-1}$) for the nearshore spring (May) and summer (August) and offshore spring (April) and summer (August) along with 95% confidence intervals of each mean (CI) and estimated silica utilization ($\mu\text{mol Si L}^{-1}$) in the nearshore and offshore calculated as the difference between spring and summer mean concentrations.</p>	43
<p>Table 3.1: List of model variables, their units and description.</p>	61
<p>Table 3.2: List of model phosphorus fluxes, with units of $\text{mg P m}^{-2} \text{s}^{-1}$, and their description.</p>	62
<p>Table 3.3: Model constants listed with their description, value used during model simulations, and their units.</p>	63
<p>Table 3.4: Model variables and their accuracy metrics calculated based on measurements taken at the 9m monitoring station. Error is calculated as the mean relative error as in Eq. 9.</p>	80
<p>Table 3.5: Model constant parameters and their sensitivity analysis perturbation values ranging from -50% of the value used to +50% of the value used in the base model simulation. The $\pm 20\%$ and 40% perturbation values are not included. The center column with perturbation 0 lists the constant values used in the base simulation. See Table 3 for constant descriptions and units.</p>	95
<p>Table 3.6: Sensitivity test response matrix for mean <i>Cladophora</i> biomass, mean, net boundary particulate phosphorus flux, and mean, net boundary dissolved phosphorus flux. The percent constant perturbation is listed at the top of the table and values below indicate the variation response calculated as Eq. 23 associated with each model constant parameter.</p>	96

Table 3.7: The influence of mussels on the Lake Michigan nearshore zone calculated based on the differences between simulations with and without mussels. Positive values indicate an increase from the no mussel to mussel simulation and negative values indicate a decrease from the no mussel to the mussel simulation.	104
Table 4.1: Model carbon and phosphorus variables, their units, and descriptions.	125
Table 4.2: Carbon and phosphorus fluxes calculated by the model, their units, and descriptions.	127
Table 4.3: Model constants and parameters, their value, units, and descriptions.	132
Table 4.4: Model accuracy metrics for listed model variables calculated based on measurements taken at the 9m monitoring station. Error is calculated as the mean relative error as in Eq. 26.	147
Table 4.5: Model calculated net, monthly mean, production and respiration for phytoplankton, <i>Cladophora</i> , and mussels as well as the net, monthly mean, nearshore community production, and the net benthic community production, calculated as the sum of <i>Cladophora</i> net production and mussel respiration only. Negative values indicate net respiration and positive values indicate net production. Units for all values are $\text{mmol C m}^{-2} \text{d}^{-1}$.	167
Table A.1.1: Soluble reactive phosphorus concentration measured at the 9m and 20m monitoring stations during 2013 at the indicated depths. Units of all values are $\mu\text{g P L}^{-1}$. Zeros values indicate measurements below the method detection limit and dashed lines indicate times when samples were not collected or were excluded due to contamination.	208
Table A.1.2: Particulate phosphorus concentration measured at the 9m and 20m monitoring stations during 2013 at the indicated depths. Units of all values are $\mu\text{g P L}^{-1}$. Dashed lines indicate times when samples were not collected or were excluded due to contamination.	209
Table A.2: Mean and standard deviation of triplicate <i>Cladophora</i> biomass and tissue phosphorus content measurements at the 9m station during 2013.	210
Table A.3.1: Mean and standard deviation of measured mussel density and biomass at the 9m station during 2013.	211
Table A.3.2: The fraction of mussels within each length class for one representative sample from each day mussels were collected at the 9m station in 2013.	212

Table A.4: Sediment trap dry mass and particulate phosphorus concentrations measured during 2013 at the 9m station. Collection depth indicates whether the sediment trap was located in the upper apparatus (Top) or lower apparatus (Btm). Contaminated sediment trap samples which were not usable are indicated by a dashed line.	214
Table A.5: Chlorophyll <i>a</i> concentration measured at the 9m and 20m stations during 2013. Units of all values are in $\mu\text{g L}^{-1}$. Dashed lines indicate times when samples were not collected or were excluded due to contamination.	216
Table A.6: Particulate carbon concentration measured at the 9m and 20m stations during 2013. Units of all values are in $\mu\text{g L}^{-1}$. Dashed lines indicate times when samples were not collected or were excluded due to contamination.	218
Table A.7: Data collected using the buoy mounted CO_2 monitoring system at the 9m station during 2013. Values listed as NaN represent missing values due to equipment failure. Gaps in the time series were caused by equipment failure and periods of general maintenance.	222

ACKNOWLEDGEMENTS

I would like to first thank my wife, Katie Fillingham. There are no words for the love and support she has shown me throughout this long process and I will never be able to repay her for the lost weekends and the time spent apart. Katie's sacrifices for my success were often overlooked, but they will never be forgotten.

Thank you so much to my parents for their love, help and support throughout my graduate career and for giving me a place to stay and food to eat in Milwaukee when Katie and I moved to Washington, DC.

Thank you very much to those who worked beside me in the Bootsma Laboratory at the School of Freshwater Sciences. I could not have completed this research without the laboratory, field, and logistical support of Erin Wilcox, Ben Turschak, Zac Driscoll, Caroline Mosley, Emily Tyner, and Kerry Latham. All of your individual help and expertise made this research possible.

Many thanks to the members of my PhD committee, Dr. Val Klump, Dr. Qian Liao, Dr. Paul Roebber, and Dr. Jim Waples, who provided their knowledge and guidance throughout this project. I would like to thank Dr. Jim Waples in particular for all of his support throughout the last year of this project.

Dr. Harvey Bootsma is my advisor and mentor. I have learned so much from him as a scientist and a professional. Harvey provided me with every opportunity to succeed over the last six years. He was kind and flexible and afforded me the work life balance I needed to continue working on this project. I will be forever grateful to him.

CHAPTER 1

INTRODUCTION AND BACKGROUND

1.1 Introduction

Dreissenid mussels have been a transformative invasive species around the world. Their ability to colonize streams, rivers and lakes has resulted in drastic changes in aquatic ecosystems in both Europe and North America (Higgins and Vander Zanden, 2010; Karatayev et al., 2014). In the Laurentian Great Lakes of North America, dreissenid mussels (*Dreissena polymorpha* [zebra mussel] and more recently *Dreissena rostriformis bugensis* [quagga mussel]) have established massive populations in both littoral benthic (zebra and quagga) and profundal zones (quagga only), (Bunnell et al., 2009a; Karatayev et al., 2014; Nalepa et al., 2014, 2010, 2009). In Lake Michigan, quagga mussel densities have been observed as high as 10,000 individuals m⁻² in nearshore waters and as high as 100,000 m⁻² in the offshore benthos (Nalepa et al., 2014, 2010, 2009). These massive mussel populations have both positive and negative impacts. Their ability to increase water clarity has been considered positive for recreation, however, higher transparency has led to increased nuisance algal growth (Auer et al., 2010; Limburg et al., 2010). In addition, dreissenid mussels grow on water intake pipes causing fouling and creating substantial costs for water treatment and power generation (Connelly et al., 2007; Limburg et al., 2010). Many recent changes in the Great Lakes food webs, including declines in the spring phytoplankton bloom and changes to invertebrate and fish abundances, have also been attributed to dreissenids (Hecky et al., 2004; Madenjian et al., 2002; Pothoven and Madenjian, 2008; Vanderploeg et al., 2002).

Bivalve mollusks are known as ecosystem engineers due to their ability to modify benthic habitat, redistribute and recycle nutrients, and restructure food webs (Newell, 2004; Prins et al., 1998; Strayer et al., 1999; Vaughn et al., 2008). As suspension feeders, bivalves have a top-down impact by consuming phytoplankton (Buzzelli et al., 2013; Lonsdale et al., 2009; Pomeroy et al., 2006; Strayer et al., 1999). Due to their ability to recycle nutrients trapped in particulate organic material, clear the water column and increase light penetration, and modify benthic habitat and sediment dynamics, bivalves can also have a “bottom-up” influence on aquatic primary production (Cuhel and Aguilar, 2013; Karatayev et al., 2014; Newell, 2004; Pomeroy et al., 2006; Strayer et al., 1999; Wallace and Webster, 1996). The impact of bivalves is complicated by their nutrient requirements and the influence of food quality on excretion and egestion. By both selectively feeding on certain phytoplankton groups and selectively retaining and excreting nitrogen and phosphorus, bivalves can alter primary production by changing the availability of limiting nutrients, changing water column N:P ratios, and changing the phytoplankton community composition (Atkinson et al., 2013; Johengen et al., 2013).

The total influence of these ecosystem engineers is inevitably limited by the aquatic climate, basin morphology, and hydrodynamics which control metabolic rate, the delivery of food to the near bottom layer, and the fate of recycled nutrients and waste (Ackerman, 1999; L. Boegman et al., 2008; Bootsma and Liao, 2013; Dayton et al., 2014; Gerritsen et al., 1994; Pomeroy et al., 2006; Saurel et al., 2013). Bivalve colonies are spatially limited by benthic substrate type, species specific physiochemical factors, and water residence time (Dame and Prins., 1998; Jones et al., 2011; Jones and Ricciardi, 2005). Regardless of the resulting spatial heterogeneity of mussel benthic colonization,

basin morphology and hydrodynamics act to extend the influence of bivalves beyond their colonized area, as parcels of water depleted of particles can be advected downstream and throughout lakes (Atkinson and Vaughn, 2015; Bocaniov et al., 2014; Cha et al., 2011; Jonsson et al., 2014). The extended reach of bivalves allows them to have impacts on large coastal and lake systems well beyond their colonized area.

Following the invasion of zebra mussels in the Great Lakes in the late 1980s and their colonization of nearshore waters (Fleischer et al., 2001; Nalepa et al., 2014), Hecky et al. (2004) hypothesized that the an overarching influence of dreissenid mussels on Great Lake ecosystems was to restrict nutrient flow from tributaries to the pelagic while increasing littoral benthic production and diversity. This process was coined the “nearshore phosphorus shunt”. Since the invasion of the quagga mussels in the late 1990s and early 2000s, their population has expanded into the profundal zone (Nalepa et al., 2010, 2009). Through this change, maximum population densities of mussels shifted from < 30m depth to > 50m depth (Bunnell et al., 2009b; Nalepa et al., 2010). Vanderploeg et al. (2010) proposed that dreissenid mussels in the mid-depth regions of Lake Michigan were producing a sink for pelagic phytoplankton and severely reducing the size of the spring phytoplankton bloom. This new hypothesis was coined the “mid-depth sink”. With large populations of dreissenid mussels now living in both littoral benthic and profundal zones, both of these proposed processes, strongly tied to lake hydrodynamics, are likely acting in tandem to change nutrient and food web dynamics in the Great Lakes.

Benthic recycling of limiting nutrients such as phosphorus and silica in the profundal zone of Lake Michigan plays an important role in lake biogeochemistry and

has traditionally supported the spring diatom bloom and the food web (Brooks and Edgington, 1994; Conley et al., 1988; Klump et al., 2009; Schelske, 1985; Shafer and Armstrong, 1994). With the profundal benthos now dominated by quagga mussels and their filter feeding, recycling particulate organic material, and altering the state of accumulated sediment (Hecky et al., 2004; Nogaro and Steinman, 2014; Turner, 2010), dreissenid mussels are now likely playing a large role in the annual phosphorus budget of Lake Michigan. Using a phosphorus mass balance model to simulate total phosphorus budgets of the Great Lakes based on tributary input, settling, and inter-basin transport, Chapra and Dolan (2012) found that, following the dreissenid mussel invasion, Lakes Michigan, Huron, Erie, and Ontario required higher effective settling rates to reproduce observed TP concentrations. These results were indicative of the lake wide impact of dreissenid mussels and their ability to increase lake TP assimilation capacity.

By reducing phytoplankton populations in Lake Michigan while simultaneously increasing water transparency (Fahnenstiel et al., 2010b; Kerfoot et al., 2010; Mida et al., 2010; Pothoven and Fahnenstiel, 2013), dreissenid mussels are considered to have played a major role in benthic-pelagic coupling (Cuhel and Aguilar, 2013; Higgins and Vander Zanden, 2010; Higgins et al., 2014; Lowe and Pillsbury, 1995; Ozersky et al., 2012). This has likely had dramatic impacts on native species associated with benthic-pelagic coupling, although direct measurement of these impacts has been limited to correlative associations such as the 90% decline in the benthic amphipod *Diporeia* sp. following the invasion of quagga mussels (Nalepa et al., 2009, 2006). *Diporeia* is a key species in Lake Michigan playing a critical role in benthic-pelagic energy pathways by assimilating

massive amounts of carbon associated with the spring bloom and providing an important food source to predators (Fitzgerald and Gardner, 1993; Pothoven and Madenjian, 2008).

Benthic-pelagic coupling associated with dreissenid mussels in the littoral of the Great Lakes during the summer is thought to be manifested by the growth of the benthic, filamentous algae *Cladophora* (Auer et al., 2010 and Higgins et al., 2008). The growth and abundance of *Cladophora* in Lake Michigan was considered to be controlled by ambient available phosphorus concentrations which have dropped significantly in the lake pelagic since phosphorus loading regulations were implemented in the late 1970s (Chapra and Dolan, 2012; Mida et al., 2010; Pauer et al., 2011). *Cladophora* now grows to nuisance levels in the Great Lakes, similar to levels prior to phosphorus loading abatement in the 1970s, causing beach fouling, clogging of power plant and municipal water intake pipes, as well as ecosystem and human health concerns associated with *E. coli* and avian botulism (Auer et al., 2010; Chun et al., 2013; Higgins et al., 2008b, 2005b; Verhougstraete et al., 2010; Whitman et al., 2003). Links between the *Cladophora* resurgence and mussel activity have been made by comparison of areal mussel excretion rates relative to tributary loading and vertical mixing (Bootsma and Liao, 2013; Bootsma, 2009; Dayton et al., 2014; Ozersky et al., 2009), *in situ* and *in vitro* measurements of nutrient concentrations associated with mussel free and colonized nearshore substrates (Bootsma and Liao, 2013; Ozersky et al., 2013; Turner, 2010), and observations of benthic primary productivity (Davies and Hecky, 2005).

Hydrodynamic and lower trophic level, ecosystem models have been used to quantify the influence of dreissenid mussels on nutrient dynamics and primary production. Dreissenid mussels were recently incorporated into 3-D biogeochemical

models (Bocaniov et al., 2014) and 2-D models of Lake Erie (L. Boegman et al., 2008; Leon Boegman et al., 2008; Zhang et al., 2008). Dreissenid mussels have also been included in other modeling studies in the Great Lakes region such as Green Bay, Lake Michigan (Padilla et al., 1996), a 1-D model of eastern Lake Michigan (Rowe et al., 2015), and Lake Simcoe (Schwalb et al., 2015). In Lake Erie, the effect of dreissenid mussels on phytoplankton abundance was found to be moderated by a particulate boundary layer above profundal mussels beds due to limited vertical mixing rates. (Boegman et al., 2008a; Boegman et al., 2008b; Zhang et al., 2008). Similar results were found in simulations of Lake Simcoe which is primarily colonized by zebra mussels in shallow areas (Schwalb et al., 2015). The ability of mussels to recycle phosphorus while selectively feeding on specific phytoplankton groups was suggested to possibly stimulate growth of non-edible forms of algae and contribute to harmful algal blooms in Lake Erie (Boegman et al., 2008a; Zhang et al., 2011). In a 3D simulation of Lake Erie, Bocaniov et al. (2014) found that high mixing rates and mussels in the nearshore zone substantially impacted the phytoplankton concentration lake wide, providing evidence for the nearshore shunt hypothesis. Although the basin morphology and mussel distributions were very different between the two lakes, similar results were found in simulations of Lake Simcoe (Schwalb et al., 2015). In Green Bay, Padilla et al. (1996) showed that zebra mussels could reduce chlorophyll concentrations by 80%, and found little impact on zooplankton biomass. It was found that the impact of mussel filtering was similar to the impact of nutrient gradients in the eutrophic Green Bay estuary, highlighting the importance of tributary input to that system. In a 1-D column simulation, Rowe et al. (2015) found that mussel filtering substantially reduced the magnitude of the spring

phytoplankton bloom in Lake Michigan, however their total impact was strongly controlled by seasonal stratification and the rate of vertical mixing.

Although modeling studies in other lakes have discussed the role of nearshore mussels on lake phytoplankton abundance (Bocaniov et al., 2014; Rowe et al., 2015; Schwalb et al., 2015), no study published to date has simulated the growth of *Cladophora* in the presence of dreissenid mussels in the nearshore zone, and the role of both on nutrient dynamics and energy pathways (Auer et al., 2010; Dayton et al., 2014; Pauer et al., 2011). Modeling *Cladophora* growth in the Great Lakes was pioneered by Canale, Auer, and others in a series of papers published in the Journal of Great Lakes Research in 1982 (see e.g. Auer et al., 1982). *Cladophora* growth in Lake Huron was accurately simulated using a mechanistic model driven by water temperature, soluble reactive phosphorus (SRP) concentration, and near bottom photosynthetically available radiation (PAR). The *Cladophora* model was used as an effective predictive tool showing that reducing point source phosphorus inputs to the Great Lakes would reduce nearshore *Cladophora* growth and the inevitable accumulation of sloughed algae on shorelines (Auer et al., 2010; Higgins et al., 2008b). This work was followed by more recent modeling efforts driven by the resurgence *Cladophora* growth in the Great Lakes after the dreissenid mussel invasion. Studies were conducted on Lake Erie (Higgins et al., 2006, 2005a), Lake Ontario (Higgins et al., 2012; Malkin et al., 2008), and Lakes Michigan and Huron (Auer et al., 2010; Tomlinson et al., 2010). These studies have shown that recently observed nuisance levels of *Cladophora* can be accurately simulated by using observed levels of light penetration and soluble reactive phosphorus as model inputs. The findings of these modeling studies provide further indirect evidence of the

role of dreissenid mussels in supporting *Cladophora* growth in the nearshore zones of the Great Lakes, however, they do not include dynamic simulation of phosphorus dynamics and the role of mussels as a dissolved P source, limiting their ability to quantify the influence of nearshore mussels directly on *Cladophora* growth and nearshore nutrient fluxes (Auer et al., 2010; Bootsma, 2009; Ozersky et al., 2009).

Changes in upper trophic levels can alter the autotrophic or heterotrophic state of a system through trophic cascades (Carpenter et al., 1987, 1985; Cole et al., 2000; Schindler et al., 1997). The top-down and bottom-up influences of dreissenid mussels on phytoplankton and benthic algae, as well as their inevitable impacts on higher trophic levels, complicates the application of the trophic cascade model for understanding dreissenid mussel impacts on the Great Lakes. In the nearshore zone in summer, dreissenid mussels may be creating an autotrophic ecosystem through the support of *Cladophora* growth. In fact, *Cladophora* production has been shown to surpass that of phytoplankton in the nearshore zones of Lake Erie (Davies and Hecky, 2005), and Lake Ontario (Malkin et al., 2010), illustrating the potential importance of mussel supported *Cladophora* growth on lake carbon dynamics (Higgins and Vander Zanden, 2010; Higgins et al., 2014). Turschak et al. (2014) found evidence of a recent shift in the dependence of Lake Michigan offshore predators on nearshore energy subsidies. These nearshore energy sources could be, at least in part, *Cladophora* tissue grown in the nearshore in association with mussels and advected offshore after detachment and sloughing. Identifying and quantifying the specific role of dreissenid mussels on nearshore and lake wide nutrient and energy pathways is, therefore, critical to building

effective lake management strategies (Bootsma et al., 2012; Bunnell et al., 2013; Pauer et al., 2011).

1.2 Questions, Hypotheses, and Research Philosophy

The focus of this study is on Lake Michigan, the third largest Laurentian Great Lake by area, and the second largest by volume. Four specific questions were addressed.

1) What has been the influence of dreissenid mussels on carbon and nutrient dynamics in the nearshore zone of Lake Michigan through the last several decades of dreissenid mussel invasion and population change? 2) Do dreissenid mussels support the growth of nuisance *Cladophora* algae in the nearshore zone? 3) What impact, if any, do the nearshore benthic processes associated with dreissenid mussels and *Cladophora* algae have on phosphorus and carbon fluxes between the nearshore and offshore of Lake Michigan? 4) How do dreissenid mussels influence energy flow in the nearshore zone of Lake Michigan? At the ecosystem scale, do they facilitate autotrophy or heterotrophy?

It was hypothesized that dreissenid mussels have decreased nearshore phytoplankton abundance, increased water clarity and recycle enough phosphorus to increase *Cladophora* growth in the nearshore zone. Further, it was expected that dreissenid filtering would deplete the nearshore water column of particulate material at a rate faster than phytoplankton nearshore growth, and as a result nearshore mussel food requirements are met, to a large degree, by inputs of particulate organic phosphorus and carbon from offshore. Although this requirement may be subsidized by tributary input in some parts of Lake Michigan, *Cladophora* growth has been observed well away from tributary sources (Shuchman et al., 2013). In addition, it has been observed that tributary phosphorus input is insufficient to support observed rates of mussel dissolved phosphorus

excretion in nearshore areas (Bootsma, 2009; Ozersky et al., 2009) and that offshore phytoplankton sources can sustain nearshore mussel populations due to lake hydrodynamic mixing (Malkin et al., 2012). Therefore, this study specifically addresses the importance of offshore sources of particulate phosphorus and carbon, and their role supporting mussel metabolism and phosphorus supply in the nearshore.

Guided by findings in Lake Erie and Lake Ontario (Davies and Hecky, 2005; Malkin et al., 2010), it was also hypothesized that *Cladophora* photosynthesis would likely surpass that of nearshore phytoplankton. Approximately 30% of *Cladophora* tissue is carbon (Higgins et al., 2008b; Malkin et al., 2010) and 0.08 to 0.5 % of *Cladophora* tissue is phosphorus (Auer et al., 2010; Higgins et al., 2008b; Tomlinson et al., 2010) leading to a wide range of observed and modeled *Cladophora* carbon to phosphorus (C:P) ratios. Bootsma et al. (2012) measured *Cladophora*, phytoplankton, and mussel excretion C:P ratios in the nearshore zone of Lake Michigan near Milwaukee, WI between 2006 and 2009. These observations showed that *Cladophora* C:P ratios, in the range of 300 to 450 molar, were often more than twice those of phytoplankton, in the range of 150 to 250 molar, while the mussel excretion C:P ratio was similar to that of phytoplankton. Malkin (2007) measured *Cladophora* tissue C:P ratios in the nearshore zone of Lake Ontario in the range 630 to 1550 molar. Based on their high tissue C:P ratios, *Cladophora* is able to produce substantially more biomass from available phosphorus than phytoplankton (Bootsma et al., 2012). Although *Cladophora* growth is likely dependent on mussel phytoplankton grazing and phosphorus recycling, *Cladophora* production may occur at rates far greater than mussel respiration and phytoplankton production due to their ability to grow at high tissue C:P ratios and due to

the abundance of light at depth due to mussel water column clearing. It was, therefore, hypothesized that net *Cladophora* production, supported by mussel phosphorus recycling and water column clearing, may overcome mussel respiration to produce a net autotrophic nearshore zone during the summer.

To address these four questions and test our hypotheses, a numerical model of the Lake Michigan nearshore ecosystem were developed to allow for dynamic simulation of nearshore mussels, *Cladophora*, phosphorus and carbon. The model consists of empirically derived parameterizations and previously confirmed components including the Great Lakes *Cladophora* Model (Auer et al., 2010; Tomlinson et al., 2010) and mussel phosphorus excretion and respiration models (Bootsma, 2009; Tyner, 2013). The first modeling study is focused on the major pools and fluxes of phosphorus in the nearshore zone. The second modeling study incorporates particulate and dissolved inorganic carbon to evaluate the major pools and fluxes of both carbon and phosphorus in the nearshore zone. The models were compared to observations taken at a nearshore monitoring station in Lake Michigan just north of Milwaukee, WI which is characterized by a rocky benthos with populations of dreissenid mussels of 5500 individuals m⁻² and *Cladophora* biomass as high as 250 g dry weight m⁻² (Bootsma and Liao, 2013; Bootsma, 2009; Liao et al., 2009; Tomlinson et al., 2010). After model validation, test scenarios were performed in which the nearshore was simulated both with and without dreissenid mussels. By comparing the two scenarios, specific influences of dreissenid mussels on *Cladophora* and nearshore phosphorus and carbon pools and fluxes were identified and quantified.

Preceding the modeling studies, an analysis of a long term dataset of water quality parameters measured in the Lake Michigan nearshore zone from the early 1980s through 2013 was conducted. The purpose of this time series analysis was to identify major changes in the biogeochemistry of the nearshore zone in the context of both phosphorus loading abatement following the 1970s and the dreissenid mussel invasions of the 1990s and 2000s. The results of this analysis provided the foundation for assessing the impact of dreissenid mussels on the Lake Michigan nearshore and the lake as a whole. Although changes in primary production as well as phosphorus and silica concentrations over these periods have been characterized and studied in the Lake Michigan pelagic (Barbiero et al., 2002; Evans et al., 2011; Fahnenstiel et al., 2010b; Mida et al., 2010; Pothoven and Fahnenstiel, 2013; Reavie et al., 2014), only limited studies have been conducted in which the historical nature of the nearshore zone biogeochemistry has been established (Auer et al., 2010; Higgins et al., 2008b). Further, the influence of dreissenid mussels on the nearshore zone of Lake Michigan has remained mainly speculative (Seelbach et al., 2013).

In any modeling study the complexity of the model must be balanced by the computational costs, as well as the scope of the questions being addressed by using the model (Bennett et al., 2013; Chapra, 1997). Interestingly, no significant correlation has been found between aquatic ecosystem model complexity and model output accuracy (Arhonditsis and Brett, 2004; Robson, 2014). When applying models to questions regarding aquatic ecosystems, it therefore considered sound policy to walk before you run. An excellent example of a modeling study which appropriately fits the model to the research questions is Chapra and Dolan (2012). The authors used a simple reactor model

of the primary lake basins of the Great Lakes to study the influence of total phosphorus loading reductions on lake total phosphorus concentrations and inter-lake transport. As highlighted previously, the results of this study provided substantial evidence for dreissenid mussels increasing the TP assimilation capacity of several of the Great Lakes by identifying the divergence in model accuracy following the mussel invasion. Although the model was simple, it provided an extremely important result. With a focus here on the influence of mussels on *Cladophora* growth and nearshore phosphorus and carbon fluxes, with special attention paid to the fact that this is the first attempt to dynamically simulate dreissenid mussel metabolism, *Cladophora*, phosphorus and carbon in a nearshore context, a fairly simple conceptual model was considered an appropriate approach to addressing the questions posed here. By identifying and quantifying the role of nearshore dreissenid mussels on nearshore, as well as nearshore-offshore phosphorus and carbon fluxes, the results of this study will provide useful guidance for application of nearshore dynamics in larger scale and more complex lake biogeochemical models and for future research required to understand and accurately simulate nearshore dynamics in these models.

This dissertation consists of four additional chapters. Chapter 2 presents the time series analysis of the long term monitoring data set collected in the Lake Michigan nearshore zone and includes a comparison of the nearshore zone with the Lake Michigan offshore pelagic. Chapter 3 presents the nearshore phosphorus flux model, or NPFM for short. This model is a 1D box model which includes 3 vertical layers and simulates the phosphorus dynamics of the Lake Michigan nearshore including the biological influence of *Cladophora* algae and dreissenid quagga mussels. The vertical and nearshore-offshore

fluxes of particulate and dissolved phosphorus were calculated and evaluated as to their significance associated with dreissenid mussel filtering and nuisance *Cladophora* growth. Chapter 4 presents the the nearshore carbon and phosphorus model, or NCPM for short. The NCPM was modified from the NPFM by adding nearshore particulate and dissolved inorganic carbon dynamics. The NCPM simulates nearshore phytoplankton growth in addition to *Cladophora* growth and dreissenid mussels grazing so that distribution of primary production between water column phytoplankton and benthic *Cladophora*, or the autotrophic structure (Higgins et al., 2014), could be quantified and evaluated. Chapter 5 provides a summary and synthesis of the critical findings and conclusions of this research.

CHAPTER 2

CHANGE IN THE LAKE MICHIGAN NEARSHORE ZONE: 1980 – 2013

Abstract:

A long term water quality data set collected in the Lake Michigan nearshore zone was analyzed and compared to that of the lake offshore to quantify major changes in the nearshore ecosystem over the last three decades and to identify possible mechanisms responsible for these changes. There was a 70% decrease in nearshore chlorophyll *a* concentration, a 105% increase in silica concentration, a 65% decrease in turbidity and an 87% increase in secchi depth between the 1980s and the 2000s. Nearshore chlorophyll *a* declined significantly between each decade with most of the change occurring in the spring and fall. Nearshore silica, turbidity, and secchi depth only changed significantly between the 1990s and the 2000s signifying an important change in the nearshore ecosystem during this period. Changes in the Lake Michigan nearshore zone were similar to those found in the lake offshore, although, chlorophyll *a* concentration decreased faster than in the offshore resulting in a nearly uniform nearshore-offshore chlorophyll concentration during the 2000s. Silica utilization in the nearshore increased between the 1990s and the 2000s as offshore silica utilization decreased. Changes in the nearshore zone are attributed to the dreissenid mussel invasion in the late 1980s and early 1990s, and the expansion of quagga mussels to mid-depth and offshore waters during the 2000s. The decrease in chlorophyll *a* concentration and increase in water clarity in the nearshore zone has resulted in the dominance of benthic algae, such as *Cladophora*, and diatom epiphytes, likely causing the simultaneous increase in nearshore silica utilization. The results of the time-series analysis highlight the need for numerical modeling studies

focused on the complex nearshore-offshore coupled ecosystem which is now dominated by dreissenid mussels and nearshore benthic algae.

2.1 Introduction

Lake Michigan southern basin, spring chlorophyll *a* concentrations have dropped 50% and primary production has decreased 70% since the mid-1990s (Fahnenstiel et al., 2010b; Pothoven and Fahnenstiel, 2013). These profound changes to the base of the Lake Michigan food web have been attributed to the abundance of filter feeding quagga mussels (*Dreissena rostriformis bugensis*) in the offshore benthos (Fahnenstiel et al., 2010b; Kerfoot et al., 2010; Pothoven and Fahnenstiel, 2013; Vanderploeg et al., 2010). It has been considered likely that the observed loss in phytoplankton abundance and production may in turn be, at least partially, responsible for recent changes in macrozooplankton abundance and community composition, the near disappearance of the benthic amphipod *Diporeia sp.*, and declines in the abundance of planktivorous fish (Bunnell et al., 2013, 2009a, 2006; Nalepa et al., 2009; Pothoven and Fahnenstiel, 2013; Vanderploeg et al., 2012, 2002). Dreissenid mussels have changed the Lake Michigan nearshore as well as the offshore during this same period and are thought to have led to the resurgence of nuisance *Cladophora*, a benthic filamentous alga that grew at nuisance levels in the 1970s, but decreased in abundance following phosphorus loading reductions (Auer et al., 2010; Higgins et al., 2008b).

It has been hypothesized that the abundance of quagga mussels in the nearshore benthos has led to a “nearshore shunt” that effectively increases the efficiency of phosphorus retention in the nearshore (Bocaniov et al., 2014; Cha et al., 2011; Hecky et al., 2004). Mussel grazing of nearshore particulate matter leads to their excretion of

soluble reactive phosphorus (SRP) which can support *Cladophora* growth through the summer (Auer et al., 2010; Bootsma and Liao, 2013; Ozersky et al., 2009). Filtered particulate phosphorus (PP) that is egested as particulate detrital phosphorus is stored in nearshore sediments, further enhancing P retention in the nearshore (Bootsma and Liao, 2013; Hecky et al., 2004). The resurgence of *Cladophora* has also been attributed, in part, to the recent increase in Lake Michigan water clarity which is thought to be associated with mussel filter feeding (Auer et al., 2010; Malkin et al., 2008; Vanderploeg et al., 2010). These changes in the Lake Michigan nearshore may have broad implications for nutrient cycling and energy flow at the whole lake scale (Higgins et al., 2014). For example, recent evidence has shown a major shift in structure of the offshore food web, with greater reliance on nearshore energy sources (Turschak et al., 2014). In Lake Erie's eastern basin, observations in the nearshore and offshore before and after dreissenid invasion suggest a reversal of the historically high nearshore, low offshore chlorophyll *a* concentration gradient suggesting that the nearshore is now a sink for offshore phytoplankton (North et al., 2012).

The magnitude and temporal trends of changes in the Lake Michigan nearshore are not well documented, and remain somewhat anecdotal (Auer et al., 2010). Analysis of changes in the nearshore zone is needed to provide a more quantitative assessment of the mechanisms responsible for the observed changes and their potential impact at the whole-lake scale, which in turn can guide management strategies. To this end, nearshore chlorophyll *a* and dissolved silica concentrations and water clarity parameters measured in the western nearshore of Lake Michigan near Milwaukee, WI were analyzed with the

goal of quantifying temporal trends and identifying critical ecosystem changes from 1980 to 2013.

A brief review of observed and published changes in Lake Michigan is necessary to provide context for the following analyses of the lake nearshore zone. Total phosphorus (TP) loading to Lake Michigan decreased 41% between 1970 and 1980 primarily due to phosphorus loading regulations (Dolan and Chapra, 2012). Although below target levels, TP loading has only declined by a modest 17% between 1980 and 2010 with considerable year to year variation (Dolan and Chapra, 2012). The dreissenid invasion of Lake Michigan began with the zebra mussel in the early 1990s with the subsequent invasion of the quagga mussel in the late 1990s (Fleischer et al., 2001; Nalepa et al., 2001). Quagga mussels expanded into the offshore waters of Lake Michigan after 2005 and have managed to maintain large densities at depths greater than 50 m, regions zebra mussels were not able to substantially colonize (Bunnell et al., 2009a; Nalepa et al., 2010). The lake offshore has experienced significant declines in TP, chlorophyll *a* and primary productivity since 1980 due to both TP loading reductions and the filtering capacity of dreissenid mussels (Chapra and Dolan, 2012; Fahnenstiel et al., 2010b; Mida et al., 2010; Pothoven and Fahnenstiel, 2013). Silica concentrations in Lake Michigan increased slightly between 1980 and 2000 likely due to TP loading controls (Barbiero et al., 2002). Silica concentrations have increased significantly since the expansion of quagga mussels offshore and silica utilization has decreased 57% between the 1980s and 2000s (Mida et al., 2010). The most dramatic offshore changes in the last three decades have occurred since the quagga mussel offshore expansion in 2005 (Mida et al., 2010; Pothoven and Fahnenstiel, 2013; Vanderploeg et al., 2010).

Based on this timeline, it would be easy to hypothesize that the most dramatic changes in the Lake Michigan nearshore zone likely occurred between the 1980s and 1990s following the initial introduction of zebra mussels and their colonization of the nearshore zone. However, the magnitude of the changes in the lake offshore since the year 2000 have undoubtedly had an influence on the nearshore zone due to nearshore-offshore mixing. In order to accurately identify mechanisms for nearshore change, nearshore chlorophyll *a* and silica concentrations were also compared to those measured throughout the Lake Michigan southern basin from 1983 to 2013 so that nearshore and offshore specific mechanisms could be identified.

2.2 Methods

Parameters included in the nearshore zone analysis were: chlorophyll *a* concentration, dissolved silica concentration, turbidity, and secchi depth. Additional, nearshore water quality parameters of interest, such as total and dissolved phosphorus, were excluded based on limited data availability and/or inconsistent data reporting. Data from 1980 to 2013 were provided by the Milwaukee Metropolitan Sewerage District (MMSD) which collects and maintains water quality data for the Milwaukee, Menomonee, and Kinnickinnic Rivers, Milwaukee Harbor, and the nearshore waters around Milwaukee, WI. Data from two MMSD nearshore stations north of Milwaukee Harbor (NS-7 and NS-8) were used for this analysis (Fig. 2.1) and include depths of approximately 10 m and 30 m. The lake bottom in this region is characterized by a mix of rock, sand, clay, and silt sediments. Analysis was limited to these two stations to avoid any spatial biases due to spatially and temporally inconsistent sampling across all of the MMSD nearshore monitoring stations (Fig. 2.1) between 1980 and 2013. These stations

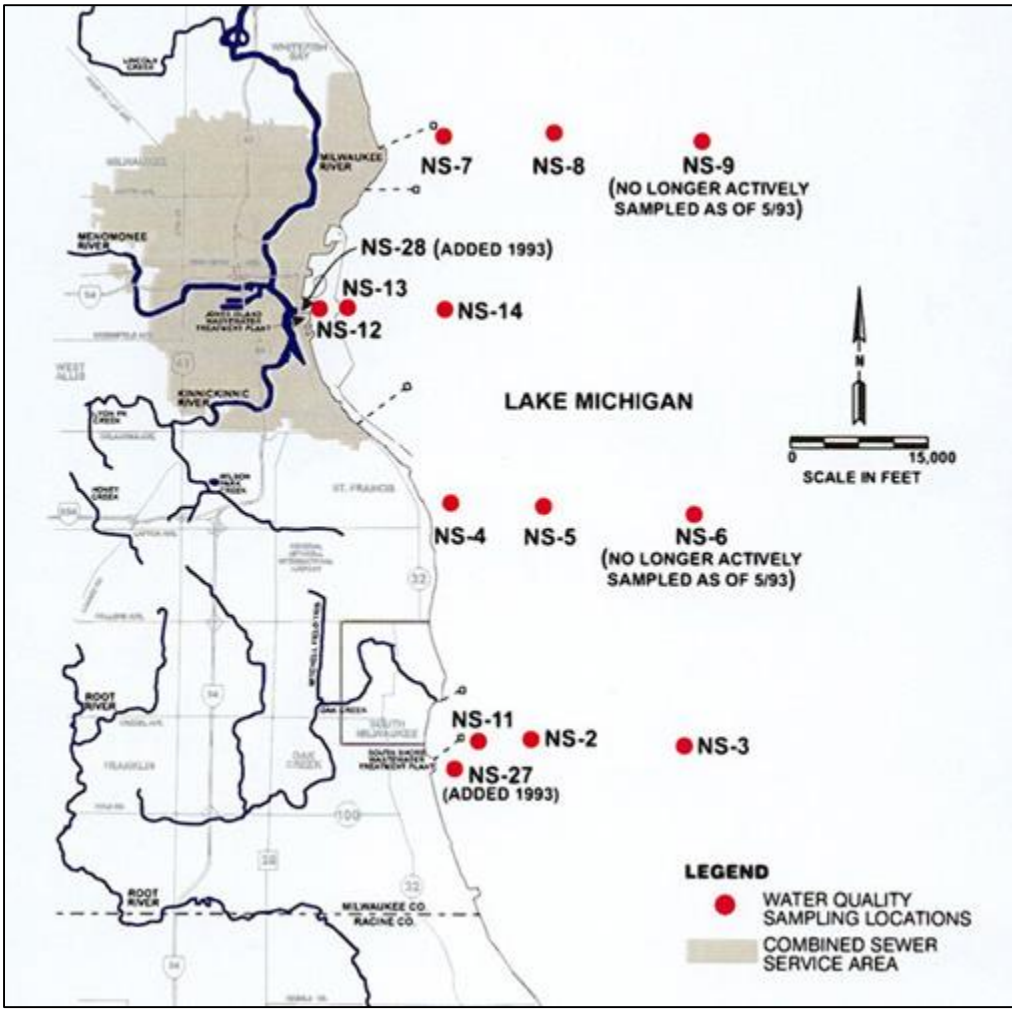


Figure 2.1: Map of the Milwaukee, WI and the Lake Michigan nearshore zone with MMSD monitoring stations indicated with red dots and labeled. NS-7 and 8 were included in this study of historical nearshore water quality parameters. This map was modified from its original version which was provided by MMSD.

were also chosen for their distance from tributary and point source loading sources which may introduce variability directly associated with river loading and may not reflect the full seasonal status of the nearshore. Data for a given year was only included if it represented 4 or more individual samples representing at least two sampling days in a given year. Figure 2.2 presents the number of chlorophyll *a* samples collected by MMSD during each month and grouped by decade (1980s, 1990s, and 2000s). Sampling occurred fairly uniformly from May through October with very few samples collected during April and November. More samples were collected during the 2000s than in the previous two decades.

A full list of MMSD measurement methods is available on the University of Wisconsin Milwaukee WaterBase webpage (<http://www.waterbase.glwi.uwm.edu/mmsd/documentation.html>). Briefly, MMSD nearshore chlorophyll *a* concentrations were measured fluorometrically using the method 10200H in “Standard Methods for the Examination of Water and Wastewater” of the American Public Health Association (20th edition, 1998). Dissolved silica concentration measurements, reported as SiO₂ (mg L⁻¹) and presented here as μmol Si L⁻¹, were made colorimetrically using method 370.1 in “Methods of Chemical Analysis of Water and Wastes” (USEPA, EPA-600/4-79-020), (<http://nepis.epa.gov/Exe/ZyPURL.cgi?Dockey=30000Q10.TXT>). Turbidity measurements were made using method 2130B also in “Standard Methods for the Examination of Water and Wastewater”.

The nearshore data were analyzed on decadal, annual and seasonal scales. Annual means were calculated as the mean of all data from individual years. Seasonal

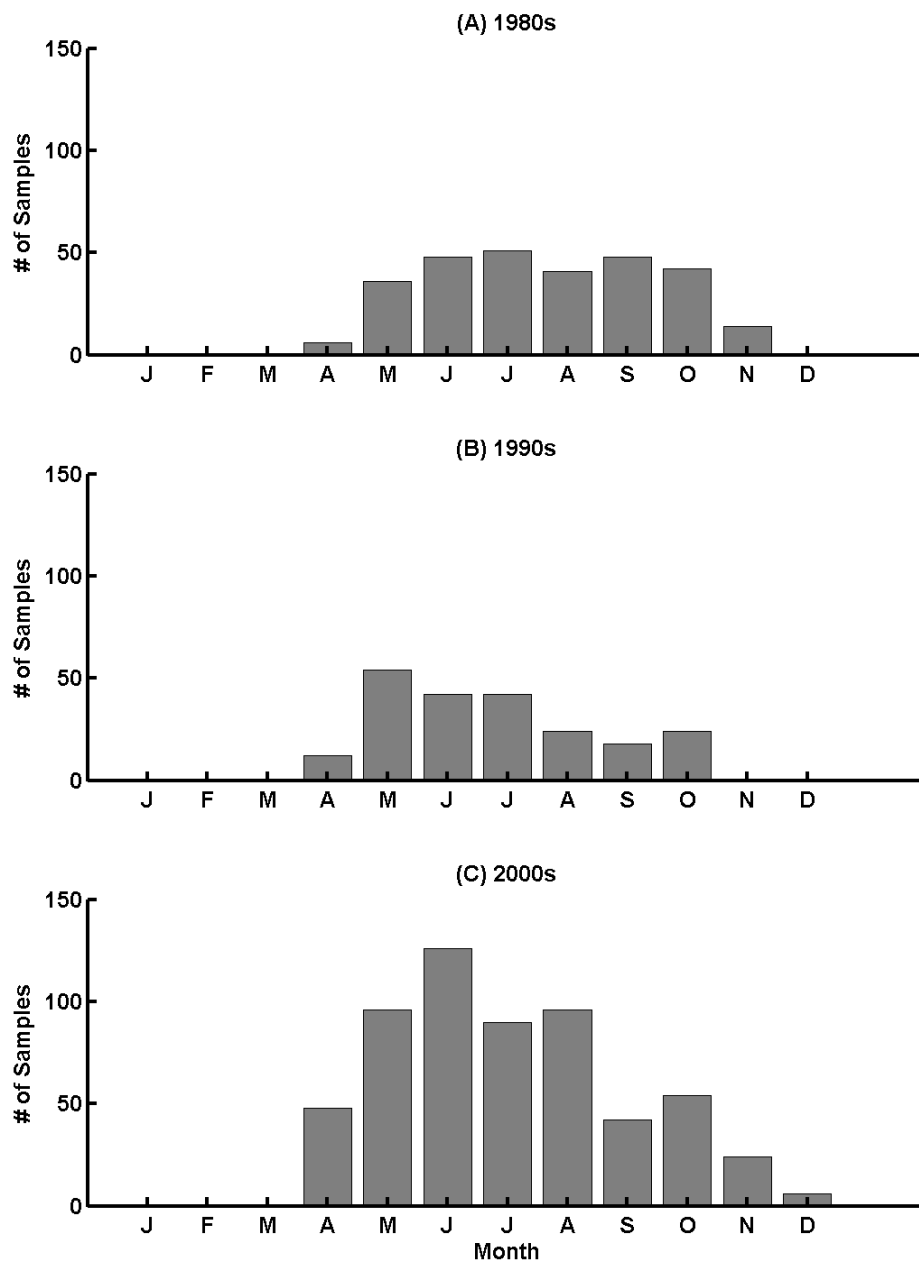


Figure 2.2: Number of chlorophyll *a* samples collected during each month and decade by the Milwaukee Metropolitan Sewerage District at nearshore monitoring stations 7 and 8.

comparisons were done by grouping the data into the three decades (1980s, 1990s, and 2000s) and then averaging over each spring, summer, and fall month (May through October) providing three, monthly mean time series representing each decade.

Confidence intervals displayed as error bars on annual and monthly means represent the 95% confidence interval of the mean and were calculated using two sided, student's t-tests using the MATLAB statistical toolbox (version R2014a). Polynomials, both linear and cubic, were fit to annual mean time series using MATLAB and were used to interpret long term trends. Boxplots of decade grouped data show the mean, median, the 25th and 75th percentile range, and the maximum and minimum range (calculated as 1.5 times the 25th and 75th percentile range representing 99% of the data and excluding outliers).

Analyses of variance tests (ANOVAs) were conducted on decade grouped data using MATLAB to test the null hypothesis that decade groups were sampled from populations with equal means. The ANOVAs assumed normally distributed samples and that decade populations had equal variances. The null hypothesis was rejected at $p < 0.05$. A Welch's t-test (a two sample t-test, assuming unequal variances) was used to test the null hypothesis of equal means for decade groups using MATLAB. The t-statistic was calculated as:

$$t = \frac{\bar{x} - \bar{y}}{\sqrt{\frac{S_x^2}{n} + \frac{S_y^2}{m}}} \quad (1)$$

where over bars indicate sample means of x and y samples, S_x and S_y are the sample standard deviations, and n and m are the sample sizes of x and y respectively. The null hypothesis of equal means was rejected at $p < 0.05$.

Nearshore seston can have high concentrations of both organic and inorganic particulate material due to variable primary productivity and regular sediment resuspension events. The nearshore chlorophyll *a* to turbidity ratio (Ch:Tb) indicates the relative proportion of phytoplankton in nearshore seston. The chlorophyll *a* to secchi depth ratio (Ch:Sd) indicates the influence of phytoplankton on water clarity. Together the two ratios provide valuable information on the trophic status of the nearshore zone. These ratios were calculated by dividing individual sample pairs based on matching collection time and depth. Confidence intervals on ratio monthly means were calculated as for parameter means.

Lake Michigan offshore chlorophyll *a* concentrations from 1983 to 2013 were obtained from the Environmental Protection Agency (EPA) central data exchange, Great Lakes Environmental Database (http://www.epa.gov/greatlakes/monitoring/data_proj/glenda/#query). The data included southern basin spring and summer monitoring locations at depths greater than 50 m (stations MI 11, 17, 18, 19, 23, and 27). Annual means, linear regressions, boxplots, and confidence intervals were calculated the same as for the nearshore data. Methods for sample collection and measurement are described by Mida et al. (2010) and are available in the EPA, R/V Peter Wise Lake Guardian Standard Operating Procedures Manual (http://www.epa.gov/greatlakes/monitoring/sop/index.html#Chapter_2). From 1983 to 1993 dissolved silica concentrations were reported as SiO₂ (mg L⁻¹) and from 1996 to 2013 they were reported as mg Si L⁻¹. For consistency and for comparison with nearshore data, dissolved silica is presented as μmol Si L⁻¹. Figure 2.3 presents the number of individual chlorophyll *a* samples collected by the EPA throughout the year for each

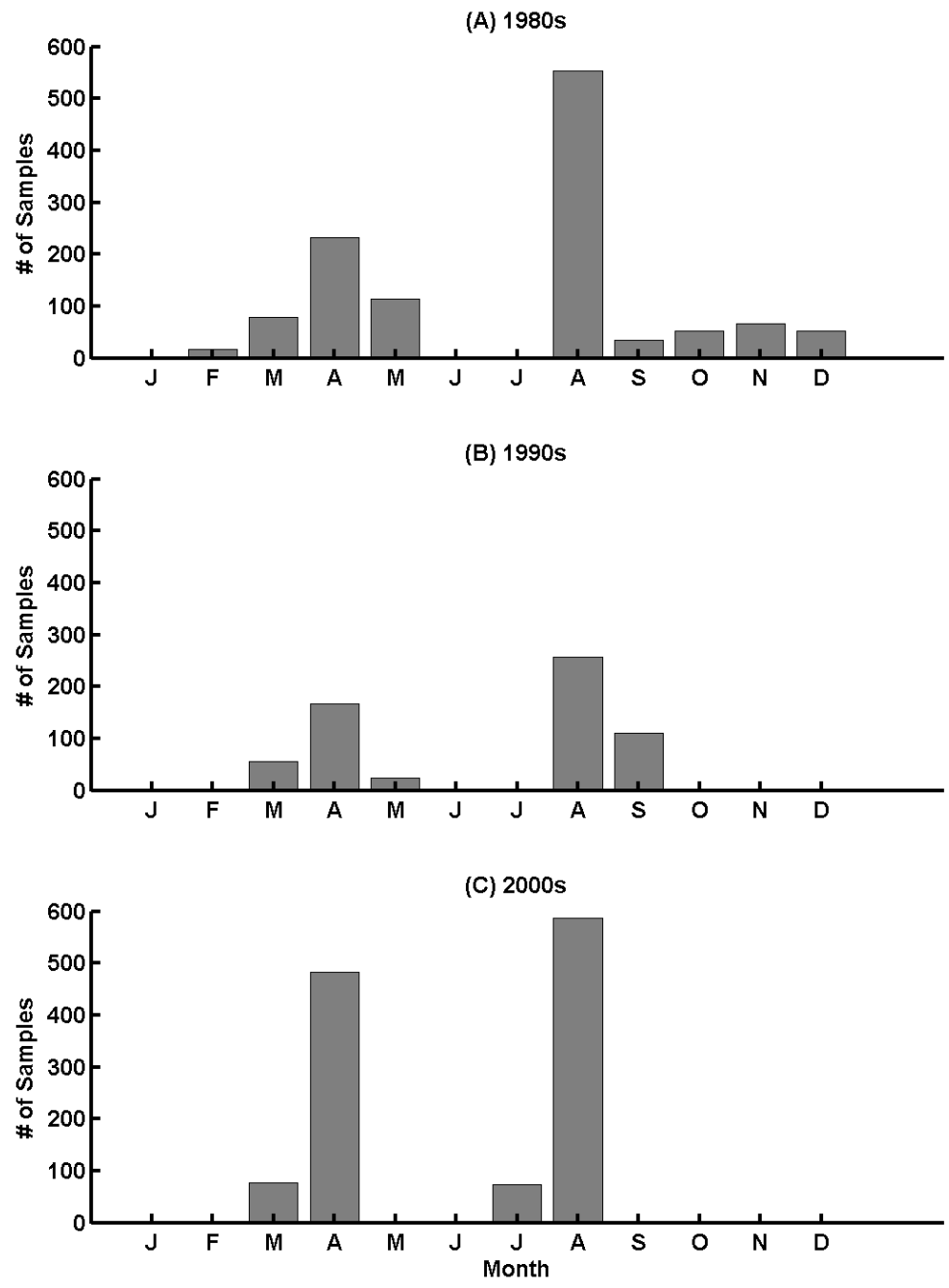


Figure 2.3: Number of chlorophyll *a* samples collected during each month and decade by the EPA during offshore monitoring cruises at Lake Michigan southern basin stations: MI 11, 17, 18, 19, 23, and 27.

decade. Sampling cruises occurred several times a year throughout the 1980s and early 1990s while regular spring and summer monitoring cruises were conducted in April and August. During the 2000s sampling was limited primarily to the spring and summer monitoring cruises. The larger number of samples compared to that collected by the MMSD (Fig. 2.2) reflects the larger number of southern basin monitoring stations included in the analysis as well as the number of depths sampled at each station.

2.3 Results

2.3.1 Analysis of Nearshore Data

All four water quality parameters: chlorophyll *a* concentration, silica concentration, turbidity, and secchi depth, changed significantly from the 1980s through the 2000s. Figure 2.4 displays the annual means, as well as the linear and cubic fits for all four parameters. Chlorophyll *a* concentration decreased from more than $3 \mu\text{g L}^{-1}$ in the early 1980s to less than $1 \mu\text{g L}^{-1}$ after 2010 (Fig. 2.4A). Nearshore silica concentration increased from less than $15 \mu\text{mol Si L}^{-1}$ in the late 1980s to more than $25 \mu\text{mol Si L}^{-1}$ after 2005 (Fig. 4B). There was substantial variability in turbidity data prior to 1999 with annual means between 0.5 and 2 NTU. Following the year 2000, turbidity data was much more consistent with annual means below 1 NTU. Secchi depth was between 3 and 6 m between 1980 and the late 1990s, and increased to between 6 and 10 m during the 2000s.

Each parameter was fit with both a linear and a cubic polynomial to allow for comparison of linear and non-linear changes across decades (1980s, 1990s, and 2000s, Fig. 2.2). Both the linear and cubic fits for chlorophyll *a* concentration annual means correlated similarly well indicating chlorophyll *a* concentration has declined steadily

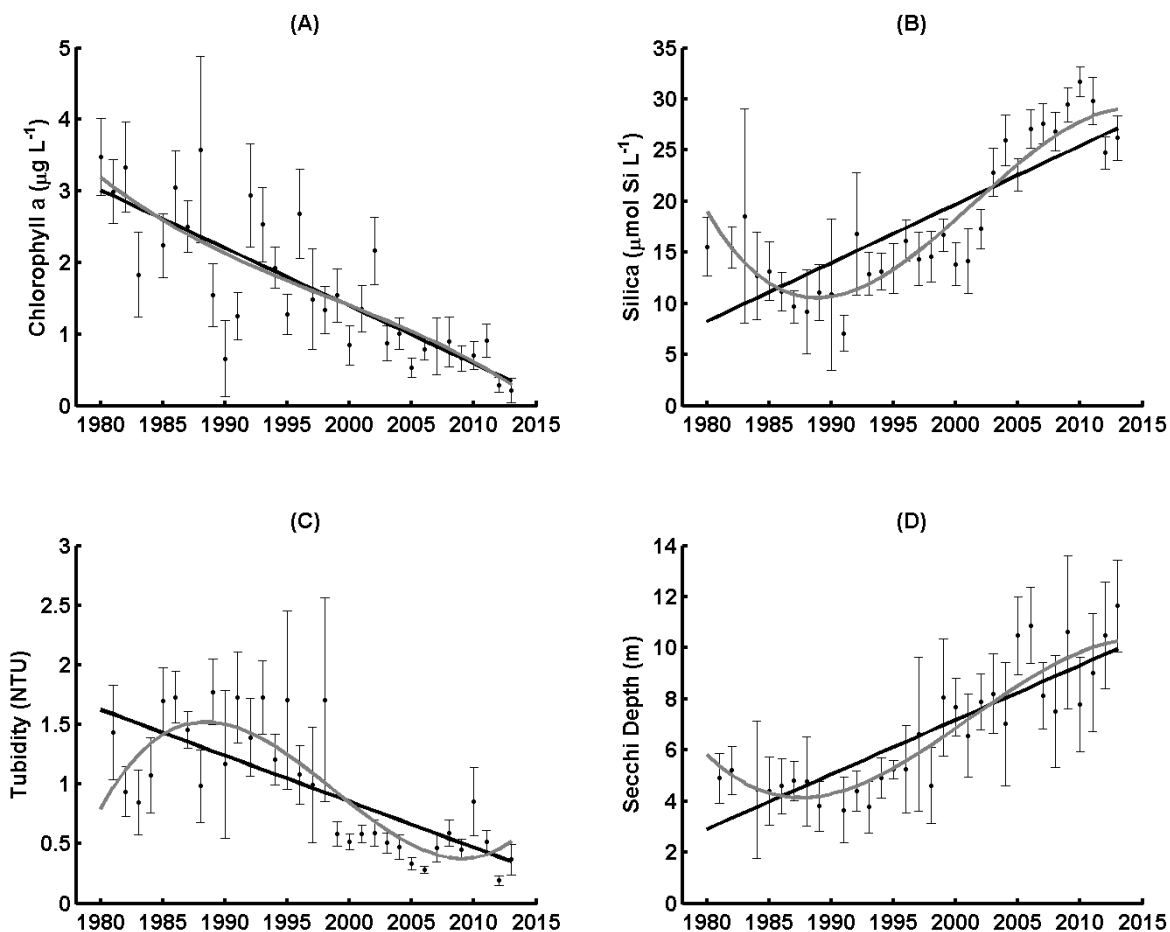


Figure 2.4: A) Chlorophyll *a* concentration, B) silica concentration, C) turbidity, and D) secchi depth annual means. Error bars indicate the 95% confidence interval of the annual mean. Linear regressions of the means from 1980 to 2013 are shown for each parameter as black lines. The slope, R^2 , and p values for each linear regression are: A) $m = -0.081$, $R^2 = 0.65$, $p < 0.001$, B) $m = 0.572$, $R^2 = 0.64$, $p < 0.001$, C) $m = -0.039$, $R^2 = 0.52$, $p < 0.001$, D) $m = 0.213$, $R^2 = 0.72$, $p < 0.001$. The cubic polynomial fit for each parameter annual means is shown as a gray line with R^2 and p values: A) 0.65, $p < 0.001$ B) 0.86, $p < 0.001$ C) 0.68, $p < 0.001$ and D) 0.81, $p < 0.001$.

from 1980 to 2013 (Fig. 2.4A). There was a marked improvement in correlation from the linear fit to the cubic fit for silica concentration ($R^2 = 0.64$ to 0.86), turbidity ($R^2 = 0.52$ to 0.68), and secchi depth ($R^2 = 0.72$ to 0.81), (Fig. 2.4 B, C and D). The improved correlation of the cubic polynomial for silica, turbidity, and secchi depth indicates that these three parameters have changed at variable rates between 1980 and 2013. This change is qualified by the concavity of the cubic curve which highlights the change in trend over time. There is a consistent inflection point, a change in concavity of the cubic polynomial, between the years 2000 and 2005 for all three parameters suggesting a period of rapid change.

This regression comparison is purely qualitative. To analyze the time change of each parameter across decades more quantitatively, the total distribution of each parameter for each decade was calculated (Fig. 2.5). There was a clear, steady decline in chlorophyll *a* across decades (Fig. 2.5A) while silica concentration (Fig. 2.5B), turbidity (Fig. 2.5C), and secchi depth (Fig. 2.5D) do not change between the 1980s and the 1990s and then change dramatically between the 1990s and the 2000s. The percent change in decade means for each parameter is provided in Table 2.1. A one way ANOVA ($\alpha = 0.05$) was used to test the null hypothesis that all decade samples are drawn from populations with the same mean. The results of the ANOVA tests for all four parameters showed a significant variation between decade groups compared to each decade's own variation ($p < 0.001$ for all four parameters) indicating a significant difference between at least two decade means for all four parameters. A Welch's t-test was conducted post-hoc to compare the decade means for each parameter directly. There was a significant difference between all of the chlorophyll *a* decade means while there was only significant

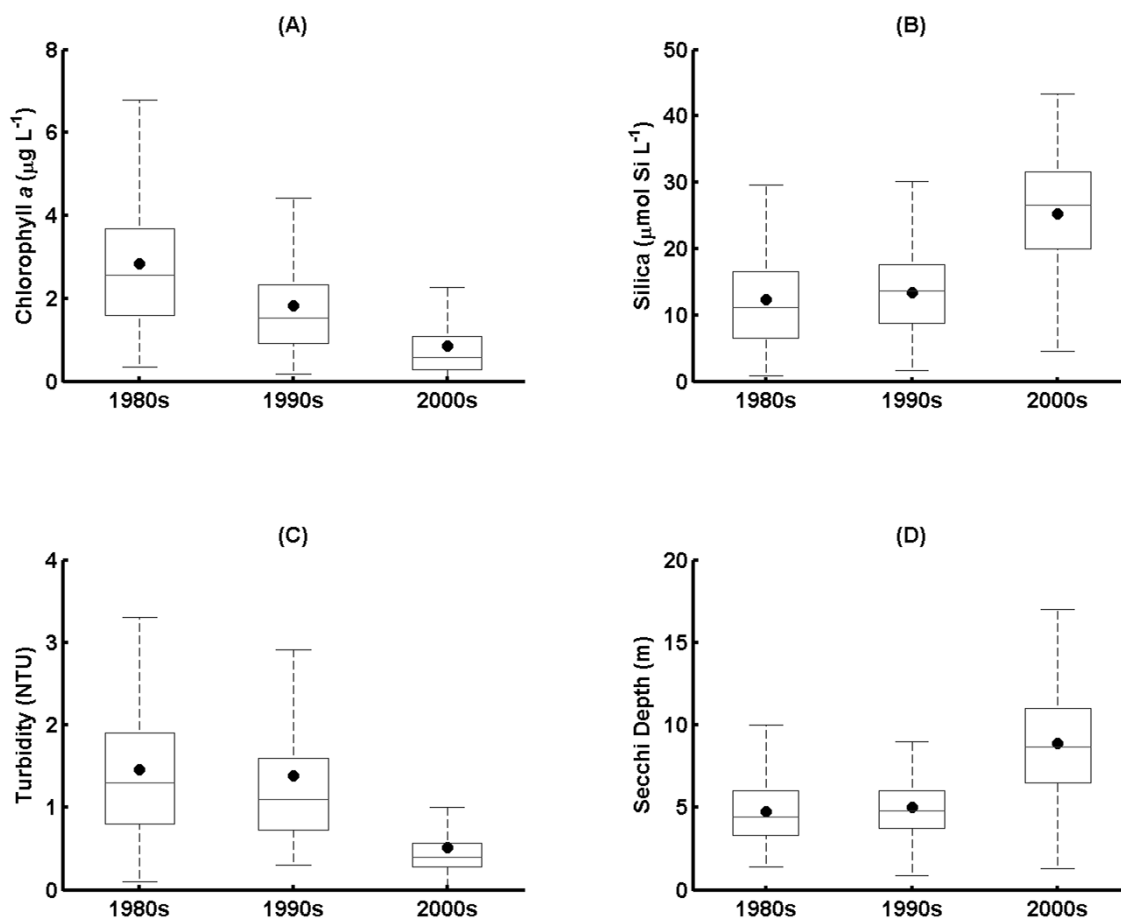


Figure 2.5: A) Chlorophyll *a* concentration, B) silica concentration, C) turbidity, and D) secchi depth decade distributions. The mid line is the decade median and the dot is the decade mean. The rectangle indicates the 25th and 75th percentile of the decade distribution while the dashed whiskers indicate 1.5 times the 25th and 75th percentile range representing the maximum and minimum values with outliers removed.

Table 2.1: Percent change in decadal means for each nearshore parameter. Negative values indicate a percent decrease between the labeled decades, and positive values indicate a percent increase between the labeled decades.

Parameter (units)	1980s to 1990s	1990s to 2000s	1980s to 2000s
Chlorophyll <i>a</i> ($\mu\text{g L}^{-1}$)	-36	-53	-70
Silica ($\mu\text{mol Si L}^{-1}$)	8	89	105
Turbidity (NTU)	-5	-63	-65
Secchi Depth (m)	6	77	87

differences between the 1990s and 2000s and 1980s and 2000s for silica, turbidity, and secchi depth (Table 2.2).

The changes between each decade were strikingly apparent when the four parameters were grouped by decade and month (Figure 2.6). If the 95% confidence intervals (error bars) of monthly means overlapped in Figure 2.6, it was concluded that a null hypothesis of equal means could not be rejected at the 5% level. If confidence intervals did not overlap in Figure 2.6, the null hypothesis was rejected and means were assumed to be significantly different. The consistent decline in chlorophyll *a* observed in annual and decadal means was observed primarily in May, June, and October with no significant change in concentration during July, August, and September (Fig. 2.6A). Changes in the seasonal pattern of chlorophyll *a* concentration were also apparent. There was a shift from a significant season low chlorophyll *a* concentration in the summer during the 1980s to a significant season high chlorophyll *a* concentration in the summer during the 2000s. There was no significant variation in chlorophyll *a* through the spring, summer, and fall in the 1990s.

Very little if any change in silica (Fig. 2.6B), turbidity (Fig. 2.6C), and secchi depth (Fig. 2.6D) occurs between months during the 1980s and 1990s. The only significant decadal change in these three parameters occurs between the 1990s and the 2000s with little if any segregation of this change by month or season. There was a shift in the seasonal pattern of silica concentration from little or no significant change through the spring, summer, and fall seasons during the 1980s and 1990s to a trend with a significant decrease in silica between May and June, as well as between May and August.

Table 2.2: Results of Welch's t-tests for nearshore decadal means. For each parameter sample, the mean (standard deviation), t-statistic (degrees of freedom), test result, and the test p value are presented. A test result of 1 indicates a rejection of the null hypothesis of equal means at the 5% confidence level and a result of 0 indicates that the null hypothesis could not be rejected at the 5% confidence level. The results are presented so that the listed t-test is between the decade column and the following decade from left to right, where the test results under the 2000s are between the 1980s and 2000s.

Parameter	Decade:	1980s	1990s	2000s
Chlorophyll <i>a</i> ($\mu\text{g L}^{-1}$)	Mean (SD)	2.84 (1.61)	1.82 (1.2)	0.85 (0.97)
	t-stat (DF)	8.15 (500)	10.65 (324)	19.29 (389)
	Test Result	1	1	1
	p-value	< 0.01	< 0.01	< 0.01
Silica ($\mu\text{mol L}^{-1}$)	Mean (SD)	12.35 (7.34)	13.36 (6.01)	25.26 (8.07)
	t-stat (DF)	-1.61 (451)	-21.89 (457)	-22.72 (537)
	Test Result	0	1	1
	p-value	0.11	< 0.01	< 0.01
Turbidity (NTU)	Mean (SD)	1.46 (0.9)	1.39 (1.15)	0.51 (0.51)
	t-stat (DF)	0.78 (402)	10.84 (248)	16.13 (351)
	Test Result	0	1	1
	p-value	0.44	< 0.01	< 0.01
Secchi Depth (m)	Mean (SD)	4.77 (1.88)	5.03 (2.02)	8.90 (3.61)
	t-stat (DF)	-0.89 (145)	-11 (224)	-13.04 (297)
	Test Result	0	1	1
	p-value	0.37	< 0.01	< 0.01

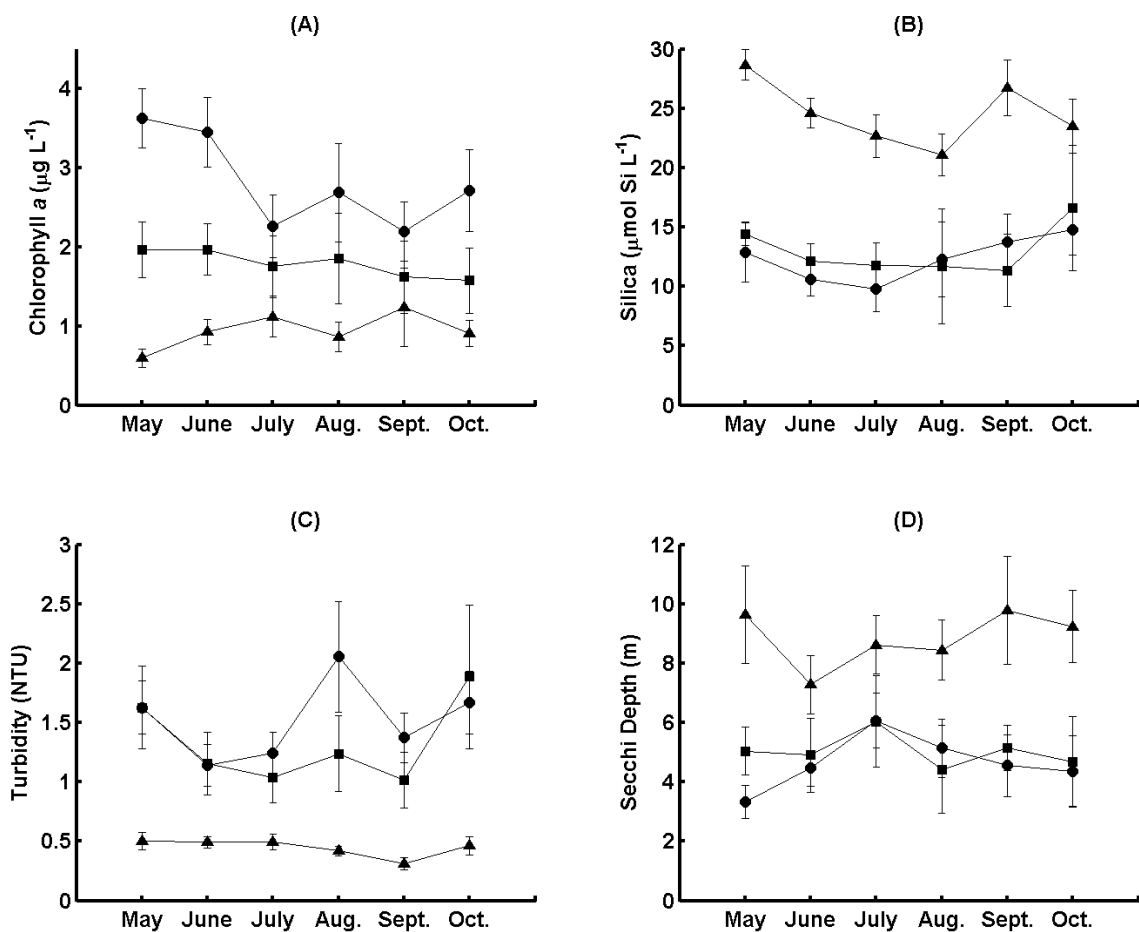


Figure 2.6: Chlorophyll *a* concentration (A), silica concentration (B), turbidity (C), and secchi depth (D) monthly means sorted by decade. Error bars represent the 95% confidence intervals of the monthly means represented by: circles for the 1980s, squares for the 1990s, and triangles for the 2000s.

Ch:Tb and Ch:Sd ratios were calculated and grouped into monthly, decade means (Figure 2.7). During the spring and early summer in the 1980s the nearshore water column was relatively productive with high Ch:Tb and Ch:Sd ratios in May, June, and July. As the summer progresses into August and September, the 1980s nearshore becomes clearer and less productive with simultaneously decreasing Ch:Tb and Ch:Sd ratios. The nearshore becomes less productive during May in the 1990s with a marked although not significant decline in both Ch:Tb and Ch:Sd ratios. There was a significant decline in Ch:Tb and Ch:Sd ratios in June between the 1980s and 1990s. Both ratios tend to stay relatively constant throughout the year during the 1990s unlike the previous decade. During the 2000s, the spring continues to have low productivity as the Ch:Sd ratio declines significantly further from the 1980s level. The Ch:Tb ratio during the 2000s remains the same as that of the 1990s during the spring and summer, but increases significantly from the 1990s through September and October indicating a consistent increase in fall primary production. The 2000s Ch:Sd ratio is significantly lower than that of the 1980s and 1990s in May and October, but not significantly different through the summer.

2.3.2 Nearshore versus Offshore Trends

In order to adequately compare the nearshore to the offshore, much of the same offshore data analyzed in the literature (e.g. Mida et al., 2010) was reanalyzed for direct comparison with nearshore data. Figure 2.8 presents the offshore annual means, linear and cubic fits of annual mean times series, and decadal distributions of chlorophyll *a* concentration for the Lake Michigan southern basin offshore pelagic from 1983 to 2013. Data is presented as all available data from offshore southern basin stations (Fig. 2.8A

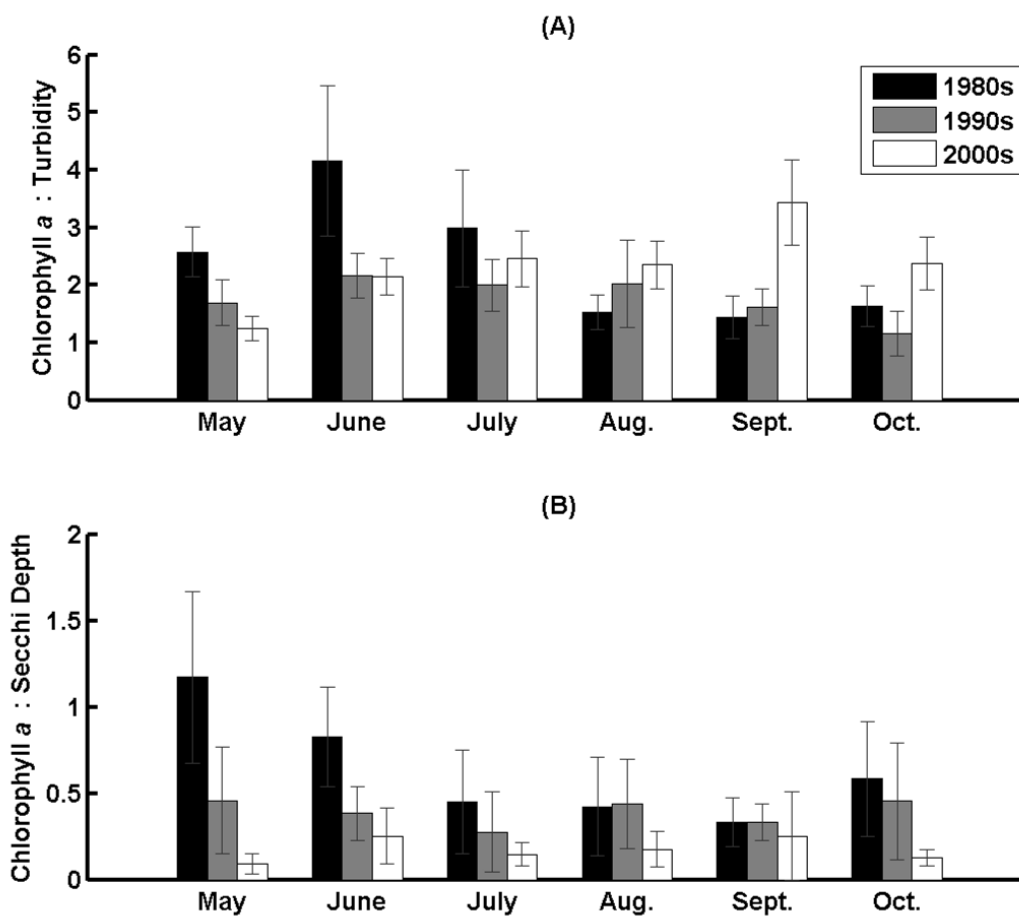


Figure 2.7: Ratios of chlorophyll *a* concentration ($\mu\text{g L}^{-1}$) to A) turbidity (NTU), and B) secchi depth (m). Black bars represent the 1980s, gray bars the 1990s, and white bars the 2000s. Error bars indicate the 95% confidence interval of the decade month ratio mean.

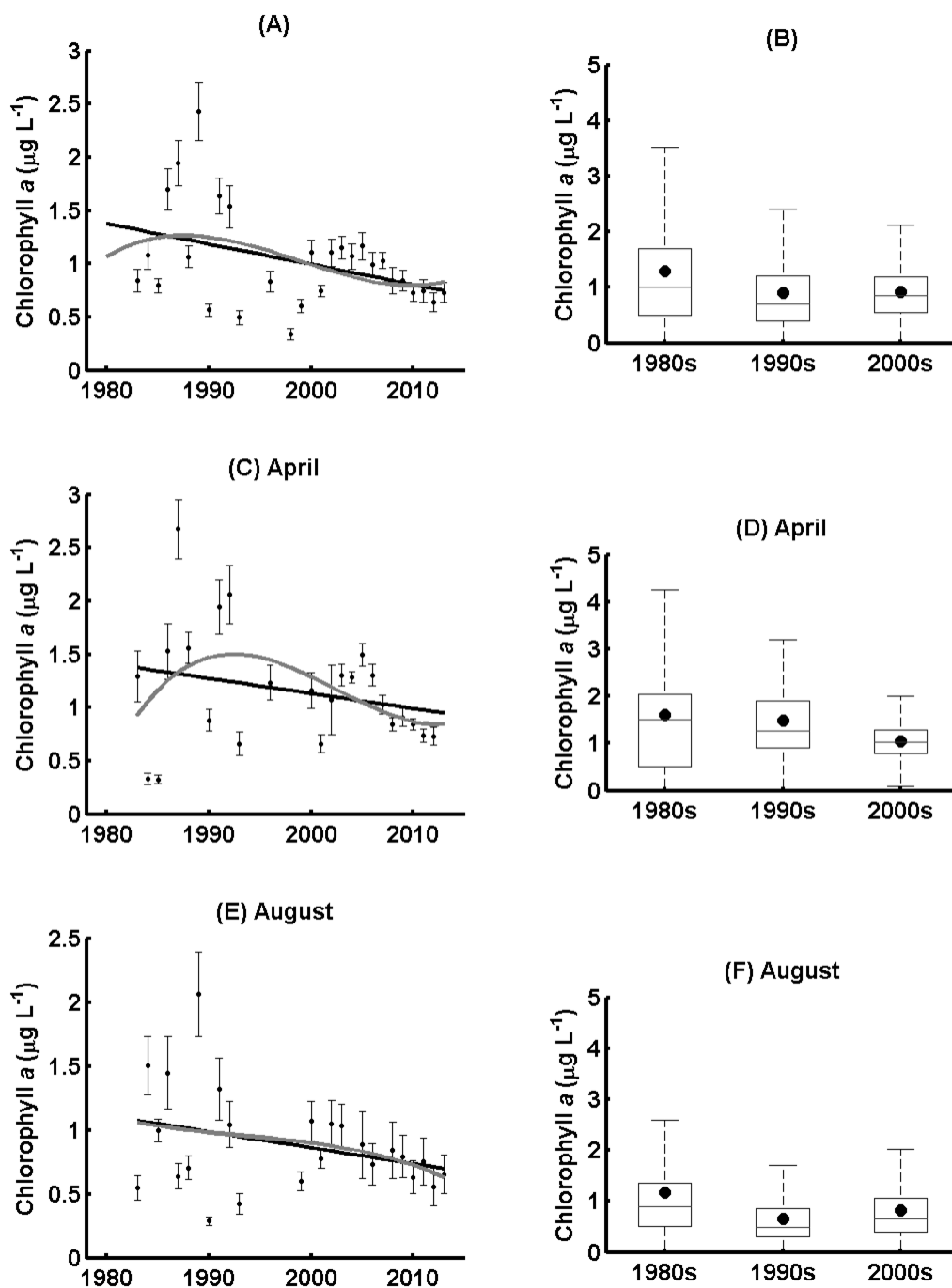


Figure 2.8: Lake Michigan, southern basin, offshore depth averaged chlorophyll *a* concentration collected by the EPA: A and B include all available data, C and D include April data only, and E and F include August data only. A, D, and E are presented the same as in Fig. 4 where the linear fit R^2 and p values are: A) $R^2 = 0.15$, $p = 0.04$; C) $R^2 = 0.06$, $p = 0.24$; and D) $R^2 = 0.10$, $p = 0.13$, and the cubic R^2 and p values are A) $R^2 = 0.17$, $p = 0.03$; C) $R^2 = 0.17$, $p = 0.04$; and D) $R^2 = 0.11$, $p = 0.12$. B, D and F are presented the same as in Fig. 2.5.

and B), and that for the spring (C and D) and summer EPA monitoring cruises (E and F) conducted in April and August respectively. Data are presented for all three categories due to the shift from nearly year round sampling during the 1980s to that limited to April and August sampling during the 2000s (Fig. 2.3). A weak yet significant decreasing linear trend in offshore chlorophyll *a* concentration for all available data was found (Fig. 2.8A; $R^2 = 0.15$, $p = 0.04$), however, there was not a significant trend in either the April or August data alone. The results of one way ANOVAs of decade groups (Fig. 2.8B, D, and F) suggested there was a significant difference between at least two of the three decade means. The results of post-hoc, Welch's t-tests indicated there were significant differences between all decade means except for spring between the 1980s and 1990s ($p = 0.28$), and summer between the 1990s and the 2000s ($p = 0.57$).

Figure 2.9 presents the silica concentration in the same format as Fig. 2.8. A significant increasing linear trend for all three offshore silica data sets was found (Fig. 2.9). The results of one way ANOVAs of decade groups suggested there was a significant difference between at least two of the three decade means and post-hoc Welch's t-tests indicated that all decades had significantly different means with the exception of the summer between the 1980s and the 1990s ($p = 0.09$). These results generally agree with other studies of the Lake Michigan offshore which have included these data and other data collected in the Lake Michigan, southern basin, pelagic (Barbiero et al., 2002; Fahnenstiel et al., 2010b; Mida et al., 2010).

The nearshore chlorophyll *a* concentration has decreased at a faster rate than in the offshore (Fig. 2.10). Nearshore chlorophyll *a* concentrations have declined to the point where, during the 2000s, the nearshore and offshore concentrations were nearly

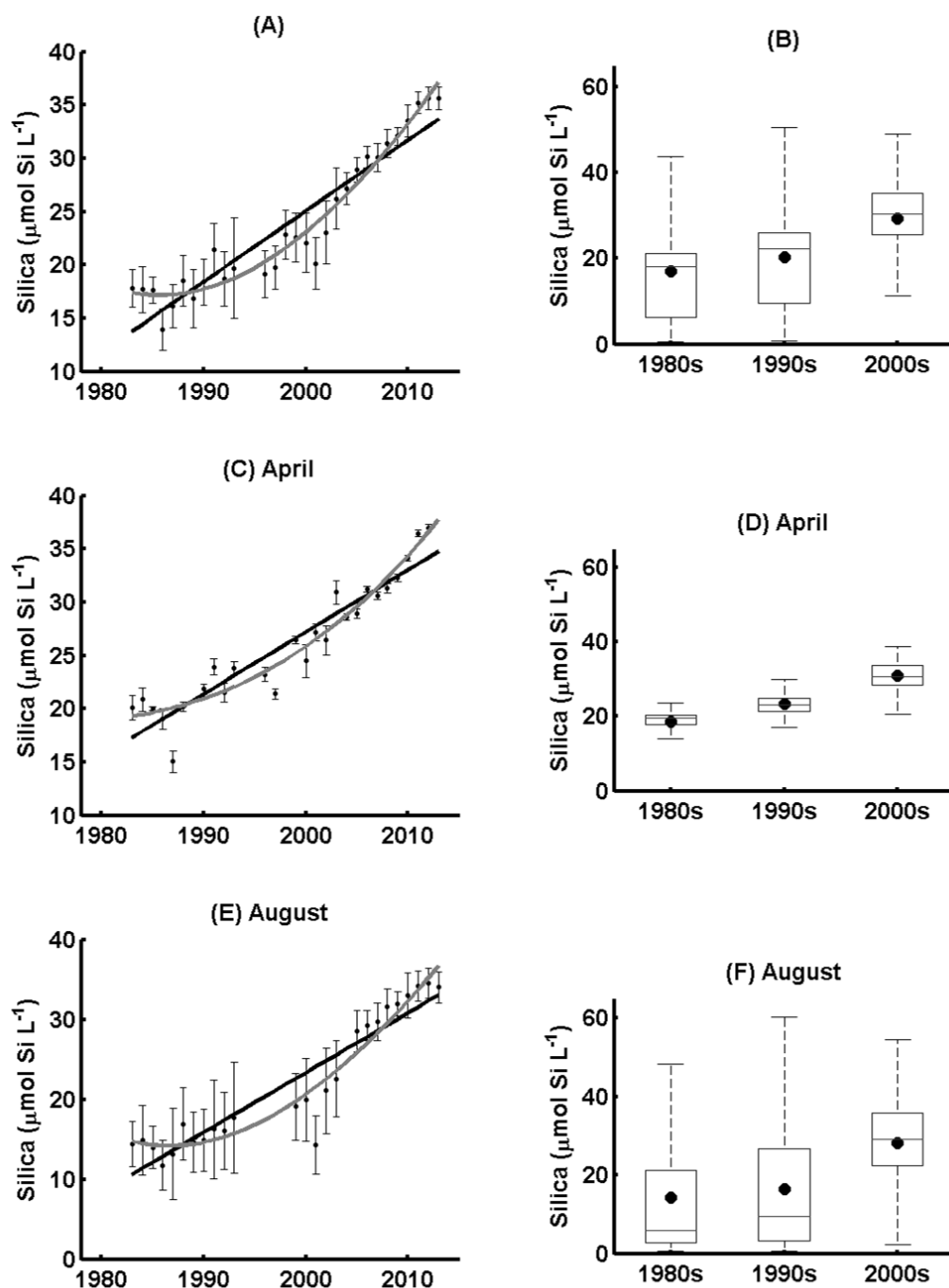


Figure 2.9: Lake Michigan, southern basin, offshore depth averaged silica concentration collected by the EPA where: A and B include all available data; C and D include April data only; and E and F include August data only. A, D, and E are presented the same as in Fig. 4 where the linear fit R^2 and p values are: A) $R^2 = 0.88$, $p < 0.001$, C) $R^2 = 0.88$, $p < 0.001$, D) $R^2 = 0.86$, $p < 0.001$ and the cubic fit R^2 and p values are A) $R^2 = 0.95$ ($p < 0.001$), C) $R^2 = 0.92$ ($p < 0.001$), D) $R^2 = 0.92$ ($p < 0.001$) for the cubic polynomials. B, D and F are presented the same as in Fig. 5.

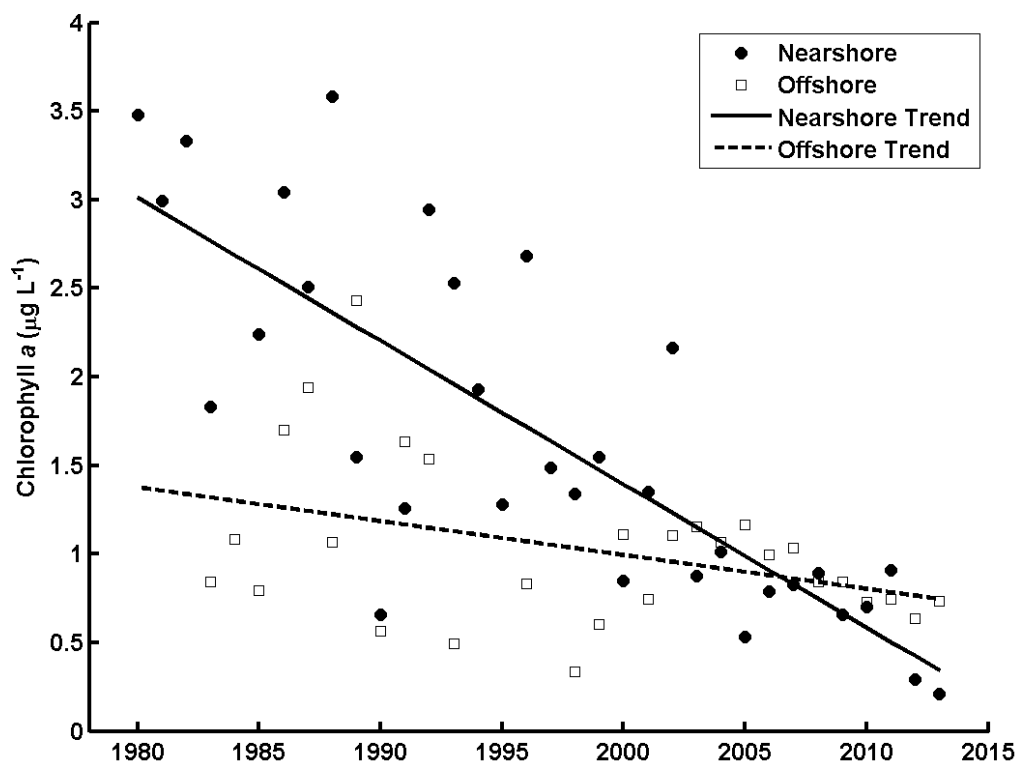


Figure 2.10: Nearshore and offshore chlorophyll a concentration annual means and linear regressions of the annual means. Both nearshore ($R^2 = 0.65$, $p < 0.001$) and offshore ($R^2 = 0.15$, $p = 0.04$) linear trends are significant.

equal. Figure 2.11 presents the chlorophyll *a* and silica concentrations in the nearshore and in the offshore for each decade during the spring (May for the nearshore and April for the offshore) and summer (August for both regions). During the 1980s spring, the nearshore zone had a significantly greater chlorophyll *a* concentration than in the offshore (Fig. 2.11A). During the 2000s spring, there was a significantly lower chlorophyll *a* concentration in the nearshore than in the offshore (Fig. 2.11A). During the summer, the nearshore zone had a significantly greater chlorophyll *a* concentration than the offshore until the 2000s when they became statistically equal (Fig. 2.11B).

Offshore spring silica concentrations were significantly greater than those in the nearshore for all three decades (Fig. 2.11C), but were not in the summer during the 1980s and 1990s (Fig. 2.11D). Summer silica concentrations during the 2000s were significantly greater in the offshore than in the nearshore, unlike the previous two decades. Figure 2.12 compares the nearshore and offshore spring and summer chlorophyll *a* and silica concentrations across the three decades. The difference between spring and summer silica concentration in each region provides a rough estimate of the silica utilization (Mida et al., 2010; Schelske, 1985). In the nearshore there was no significant difference between spring and summer silica concentrations (Fig. 2.12C). During the 2000s, there was significantly less silica in the summer than in the spring in the nearshore (Fig. 2.12C). There were significant declines in silica between spring and summer in the offshore during all three decades, however, the magnitude of this change decreased from the 1980s and 1990s to the 2000s. Table 2.3 lists the mean silica concentration for each regions spring and summer for each decade along with the decade mean silica utilization estimate. Silica utilization in the nearshore during the 2000s

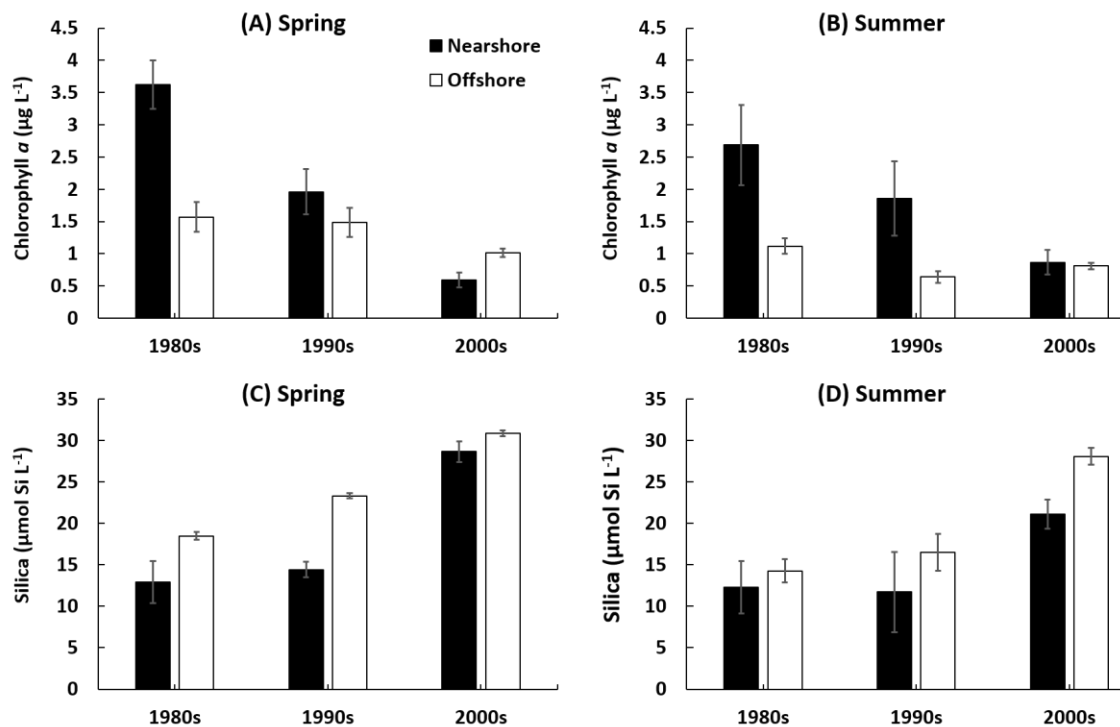


Figure 2.11: Depth and decade mean chlorophyll *a* and silica concentrations in the nearshore (black bars) and offshore (white bars). Spring (A and C) indicates samples taken in May for the nearshore and April for the offshore, and summer (B and D) indicates samples take in August for both the nearshore and offshore.

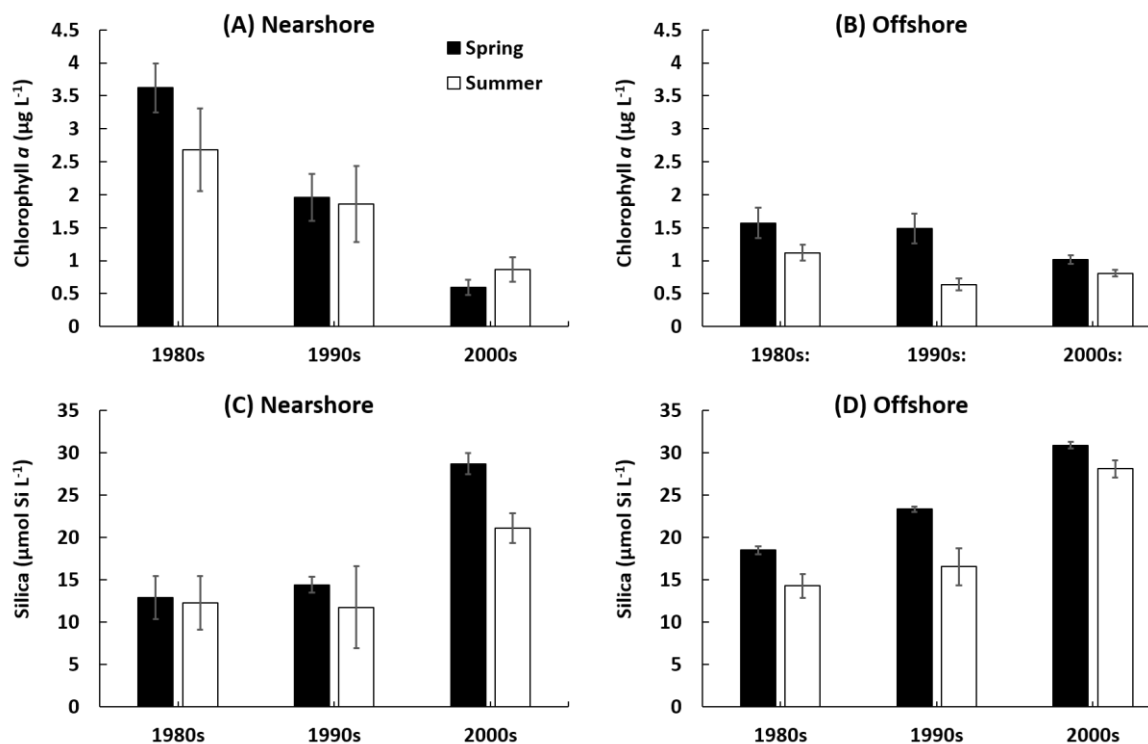


Figure 2.12: Nearshore (A and C) and offshore (B and D) chlorophyll a and silica concentrations during spring (black bars) and summer (white bars) in the 1980s, 1990s, and 2000s. Error bars indicate the 95% confidence interval of the decade mean. Spring is represented by the month of May in the nearshore and April in the offshore. Summer is represented by the month of August for both the nearshore and offshore.

Table 2.3: Mean silica concentration ($\mu\text{mol Si L}^{-1}$) for the nearshore spring (May) and summer (August) and offshore spring (April) and summer (August) along with 95% confidence intervals of each mean (CI) and estimated silica utilization ($\mu\text{mol Si L}^{-1}$) in the nearshore and offshore calculated as the difference between spring and summer mean concentrations.

Nearshore Silica ($\mu\text{mol Si L}^{-1}$)	Spring		Summer		Mean Silica Utilization ($\mu\text{mol Si L}^{-1}$)
	Mean	95% CI	Mean	95% CI	
1980s	12.89	2.55	12.30	3.16	0.60
1990s	14.42	0.94	11.73	4.84	2.69
2000s	28.68	1.25	21.09	1.77	7.58
Offshore Silica ($\mu\text{mol Si L}^{-1}$)	Spring		Summer		Mean Silica Utilization ($\mu\text{mol Si L}^{-1}$)
	Mean	95% CI	Mean	95% CI	
1980s	18.49	0.48	14.27	1.39	4.22
1990s	23.33	0.33	16.53	2.22	6.80
2000s	30.87	0.38	28.08	1.00	2.78

increased to levels similar to the offshore during the 1980s and 1990s while silica utilization in the offshore during the 2000s dropped to levels similar to the nearshore in the 1990s.

2.4 Discussion and Conclusions

The Lake Michigan nearshore zone has experienced similar changes as the lake offshore over the last three decades. The nearshore water column has become significantly clearer with a 65% decrease in nearshore turbidity and an 87% increase in secchi depth between the 1980s and 2000s (Fig. 2.5C and D, and Table 2.2) with the majority of this change occurring between the 1990s and the 2000s. Chlorophyll *a* concentration has declined steadily since the 1980s, with most of this change occurring in the spring and fall, while silica concentration has significantly increased between the 1990s and the 2000s with no change between the 1980s and the 1990s (Fig. 2.5A and B, and Table 2.2). Chlorophyll *a* concentrations in the nearshore were significantly greater than in the offshore until the 2000s when they became less than or equal to those of the offshore. Nearshore spring silica concentrations were lower than in the offshore and were not statistically different during the summer until the 2000s.

The decline in nearshore chlorophyll *a* concentration between the 1980s and 1990s is likely associated with the invasion of *Dreissenia polymorpha*, or zebra mussel, in the late 1980s and early 1990s and the introduction of the massive filtering capacity to the lake nearshore zone (Fleischer et al., 2001; Nalepa et al., 2010). The continuation of this trend makes sense as the zebra mussel thrived in the nearshore until it was displaced by *Dreissena bugensis*, or quagga mussel, in the early 2000s (Karatayev et al., 2014; Nalepa et al., 2010). It is interesting that there were significant declines in chlorophyll *a*

concentration across all decades with no significant change in water clarity or silica concentration until the 2000s. Changes in the nearshore zone can be associated with either allochthonous loading of organic and inorganic material, with changes within the nearshore ecosystem itself, such as the introduction of dreissenid mussels, or with changes in the lake offshore which regularly mixes with the nearshore (Rao and Schwab, 2007). These three factors, and combinations of the three, are discussed as to their potential influence on the Lake Michigan nearshore zone over the last three decades with a focus on the 1990s and 2000s due to the dramatic changes between these two decades.

There has been a slow yet steady decline in total phosphorus loading to Lake Michigan since 1980 (Dolan and Chapra, 2012). A dramatic decrease in local total phosphorus loading may have caused the observed increase in water clarity and silica concentration owing to a sharp decline in phytoplankton production and silica uptake. Figure 2.13A presents the Lake Michigan southern basin total phosphorus load from 1994 to 2008 using data from Dolan and Chapra (2012). There was no statistically significant trend in southern basin total phosphorus loading between 1994 and 2008. Figure 2.13B presents the total and total dissolved phosphorus loading from the Milwaukee, Menomonee, and Kinnickinnic Rivers calculated using MMSD monthly concentrations collected from the confluence of the three rivers at the Milwaukee Harbor (Figure 2.1, NS-28) and US Geological Survey daily discharge rates for the same location. Total annual loads revealed no significant trend between 1995 and 2009 (Fig. 2.13B). Without a drastic, or even consistent, change in nutrient or particulate loading to the southern basin, or the Milwaukee region, it is unlikely that allochthonous input caused the observed nearshore changes between the 1990s and 2000s.

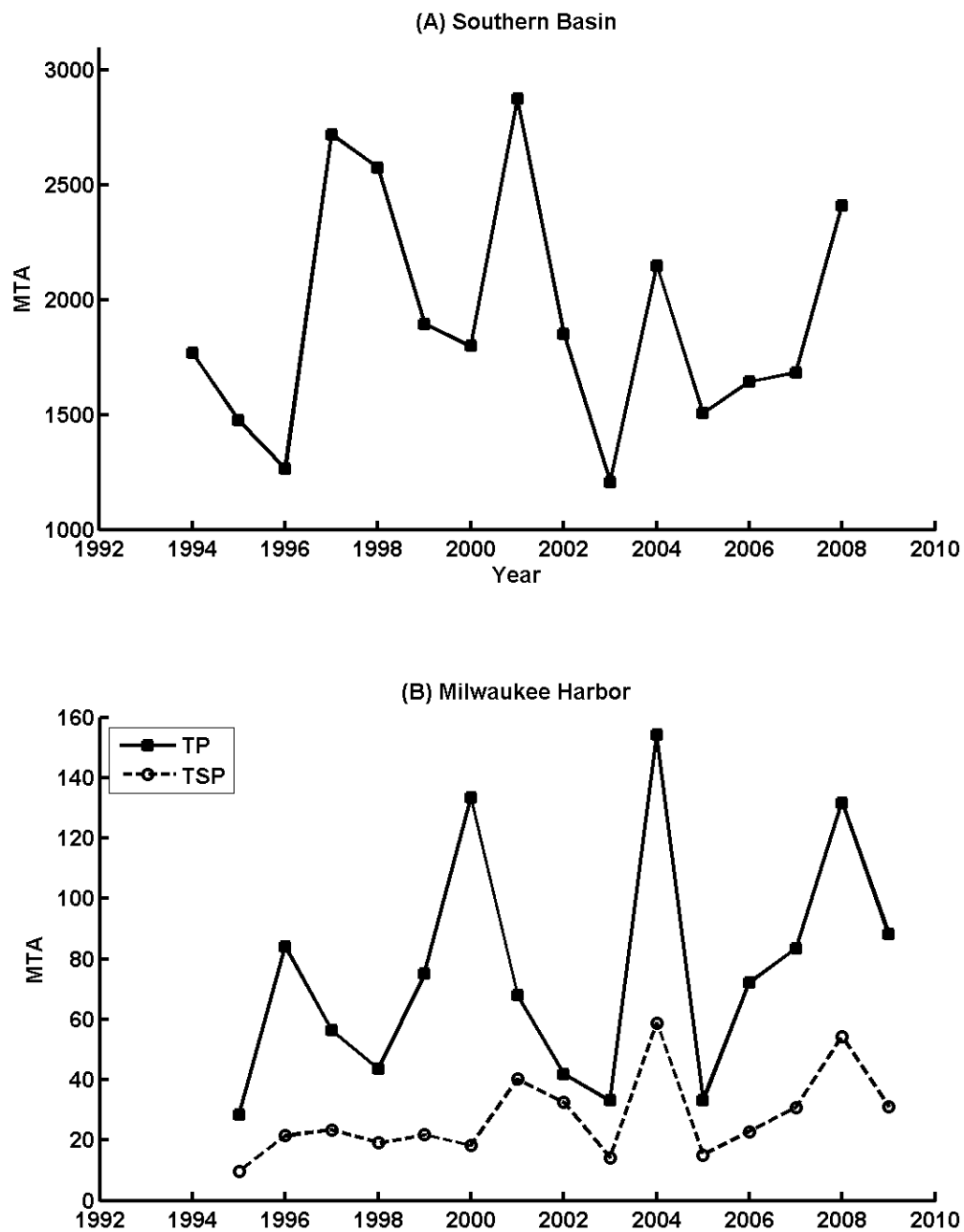


Figure 2.13: Lake Michigan southern basin total phosphorus loading in metric tons per annum (from Chapra and Dolan 2012) (A), and total and total soluble phosphorus loading from the Milwaukee, WI river confluence in the inner harbor in metric tons per annum (B).

Quagga mussel densities in the lake nearshore during the 2000s were similar to those of zebra mussels in the 1990s (Bunnell et al., 2009a; Fleischer et al., 2001; Nalepa et al., 2010). Differences in clearance rates between the zebra and quagga mussel species may be to blame for the observed nearshore changes following the invasion of the quagga mussel in the 2000s. Tang et al. (2014) found that quagga mussel clearance rates in Saginaw Bay, Lake Huron were similar to zebra mussels during the 1990s agreeing with similar results found by Baldwin et al. (2002) where no significant difference between species clearance rates was found. In contrast, Diggins (2001) found that quagga mussels had significantly higher, 37%, clearance rates than zebra mussels. Selective grazing differences may have played a role in the observed nearshore changes, however, Tang et al. (2014) attributes the observed differences in selective grazing between zebra and quagga mussels, at least in part, to the phytoplankton composition in regions studied. Little information is available on the dreissenid density, biomass, and mussel size distribution changes in the Lake Michigan nearshore zone, particularly at depths less than 10m, between the 1990s and the 2000s. Larger or smaller mussel sizes influence species specific grazing (Tang et al., 2014) and increased winter resiliency (Baldwin et al., 2002) possibly resulting in higher spring grazing patterns in the 2000s which may have changed the nearshore phytoplankton community resulting in the observed changes in water clarity and silica concentration. Without more information on the changes in nearshore dreissenid population, it seems likely, that changes in the Lake Michigan offshore, attributable to the quagga mussel filtering after their expansion into the offshore (Fahnenstiel et al., 2010b; Mida et al., 2010; Pothoven and Fahnenstiel, 2013;

Vanderploeg et al., 2010), may be, at least partially responsible for the observed changes in the nearshore between the 1990s and the 2000s.

Hecky et al. (2004) hypothesized that nearshore dreissenid mussels would cause a nearshore phosphorus shunt, limiting transport of phosphorus to the lake offshore and stripping particulate material from the lake offshore as water passes through the nearshore zone. Phosphorus could be stored in dreissenid tissue, *Cladophora* biomass, and within mussel ejecta in nearshore sediments (Hecky et al., 2004). Bootsma and Liao (2013) showed that nearshore quagga mussel populations are capable of clearing enough of the nearshore water column to cause a consistent flux of particulate material from the offshore to the nearshore using a 2D hydrodynamic model with a constant mussel filtering rate and a constant particulate concentration at the model offshore boundary. Bocaniov et al. (2014) modified the hydrodynamic-ecological model (ELCOM-CAEDYM) to include dreissenid mussels in Lake Erie. Their modeling study produced results which supported the nearshore shunt hypothesis and suggested that mussels have greater impacts on the shallow nearshore than in the deeper offshore. Their results also showed that advection through high mussel density regions directly influences downstream concentrations. With peak mussel densities in Lake Michigan shifting from 40 m to 80 m depth during the 2000s (Bunnell et al., 2009a) it is likely that the expansion of dreissenids into the mid-depth regions of Lake Michigan (Malkin et al., 2012; Vanderploeg et al., 2010) has caused significant effects to both the nearshore and the offshore.

There was an increase in lake wide, spring silica concentration through the last three decades (Fig. 2.9C and D), an indicator of whole lake silica stores (Conway et al.,

1977; Schelske, 1985). The lake offshore summer silica concentration has also increased significantly, but only between the 1990s and the 2000s indicating a decline in spring and summer diatom silica uptake and production (Mida et al., 2010). The sharp increase in nearshore silica concentration between the 1990s and the 2000s (Fig. 2.6B) may be attributable to the change in offshore silica which has only become consistently higher throughout the spring and summer during the 2000s. The increase in offshore summer silica and the decline in seasonal silica utilization (Table 2.3) has been attributed to decreased TP loading and lake oligotrophication (Barbiero et al., 2002) as well as the loss of the spring diatom bloom which has been attributed to profundal quagga mussel filtering (Kerfoot et al., 2010; Mida et al., 2010; Vanderploeg et al., 2010).

Silica utilization increased in the lake nearshore zone between the 1990s and 2000s after being insignificant in the 1980s and 1990s (Fig. 2.11A and Table 2.3). This cannot be attributed to changes in offshore silica utilization which has decreased over the same period (Table 2.3). The nearshore had very low chlorophyll *a* concentrations throughout the 2000s (Fig. 2.6A) and very clear and low turbidity water (Fig. 2.6C and D). High *Cladophora* diatom epiphyte populations have been documented in areas with high *Cladophora* biomass in Lake Ontario (Malkin et al., 2009), and it has been found that benthic algae in Lake Michigan nearshore may be secondarily silica limited (Carrick and Lowe, 2007). It has been shown that *Cladophora* growth potential in the Lake Michigan nearshore zone has increased 50% due to recent changes in water clarity and nutrient availability (Auer et al., 2010; Dayton et al., 2014) and, in the region studied here, *Cladophora* biomass has been reported as high as 250 gDW m⁻² within the last decade (Bootsma, 2009). The nearshore increase in silica utilization between the 1990s

and the 2000s did not likely occur in the nearshore water column, rather, it occurred in the nearshore benthos associated with the increase in nearshore benthic production and silica demand. Benthification and benthic-pelagic coupling can be associated with dreissenid mussels and their ability to increase water clarity and light intensity in the near bottom layer allowing for greater benthic production (Higgins et al., 2014).

The resurgence of nuisance *Cladophora* growth in the nearshore zones of the Great Lakes has been studied in detail (Auer et al., 2010; Higgins et al., 2008b, 2005b) and has been attributed to water column clearing and the increase in benthic nutrients associated with mussel phosphorus recycling (Auer et al., 2010; Dayton et al., 2014; Malkin et al., 2008; Ozersky et al., 2009). Two validated models for *Cladophora* growth and phosphorus uptake and storage are available for use in studying the influence of *Cladophora* on lake ecosystem dynamics (Higgins et al., 2005a; Malkin et al., 2008; Tomlinson et al., 2010). To our knowledge, no study has included a *Cladophora* growth model in a dynamic phosphorus model to assess the coupled influence of both dreissenid mussels and *Cladophora* on the nearshore and lake wide ecosystem. The analysis of the Lake Michigan nearshore and offshore in this study suggests that dreissenid mussels are playing an important role in how both the nearshore and offshore have changed over the last three decades. These changes have led to a dramatic shift in the nearshore and the nearshore-offshore relationship leading to the resurgence of nearshore *Cladophora* which may be dependent on the lake's declining offshore primary producer population. This subject should be considered a top research priority for Great Lakes ecosystem scientists and modelers.

CHAPTER 3

MODELING NEARSHORE PHOSPHORUS DYNAMICS

Abstract:

A one dimensional, vertical, three layer model was constructed to evaluate the influence of dreissenid quagga mussels (*Dreissena rostriformis bugensis*) on phosphorus dynamics in the Lake Michigan nearshore. Mussel grazing, phosphorus excretion and egestion in the nearshore near bottom layer were simulated using a model developed based on observations of mussel excretion and respiration. Growth of *Cladophora* algae was simulated using an existing model validated for Lake Michigan. The model was driven by observed temperature, surface PAR, and hydrodynamics. The model did an adequate job simulating dissolved and particulate phosphorus concentrations as well as *Cladophora* biomass in the Lake Michigan nearshore zone near Milwaukee, WI during the late spring, summer and fall of 2013. The model was sensitive to both mussel grazing rate and light extinction parameterizations. After comparing a realistic model simulation with a test scenario simulation where mussel density were set to zero, it was determined that nearshore mussels support observed, nuisance level, *Cladophora* biomasses during the summer and a 150% increase in areal, domain total phosphorus. Due to nearshore-offshore mixing, mussel grazing and phosphorus recycling along with *Cladophora* phosphorus storage forced the nearshore zone to act as a sink for Lake Michigan, pelagic phosphorus through the spring and summer. The nearshore zone acted as a source of phosphorus to the lake during the late summer and fall due to the detachment and sloughing of *Cladophora*. Future research is needed to adequately validate nearshore,

vertical turbulent mixing in order to better evaluate its role in nearshore phosphorus dynamics in the presence of dreissenid mussels and *Cladophora* algae.

3.1 Introduction

Invasive dreissenid mussels (zebra, *Dreissena polymorpha* and quagga, *Dreissena rostriformis bugensis*) have changed energy and nutrient cycles in the Laurentian Great Lakes. Declines in Lake Michigan primary productivity, the near loss of macroinvertebrates such as *Diporeia*, and declines in deep water fishes abundance have all been attributed, at least in part, to mussel grazing of phytoplankton (Bunnell et al., 2013, 2009b; Fahnenstiel et al., 2010b; Madenjian et al., 2002; Mida et al., 2010; Nalepa et al., 2009; Vanderploeg et al., 2010, 2002). Lake wide declines in total phosphorus concentration have occurred faster than what would be expected based on decreases to phosphorus loading, a possible artifact of mussel water column filtering (Chapra and Dolan, 2012; Mida et al., 2010). The resurgence of *Cladophora* algae (*C. glomerata*) in the Lake Michigan nearshore zone to nuisance levels not observed since phosphorus controls were instituted in the 1980s has been tied to these trends (Auer et al., 2010; Bootsma, 2009). *Cladophora* detachment, known as sloughing, and shoreline accumulation, degrades beach quality, supports pathogenic organisms hazardous to human health, clogs water intake pipes at the cost of millions of dollars annually, and may be linked to avian botulism outbreaks (Auer et al., 2010; Chun et al., 2013; Verhougstraete et al., 2010). Interestingly, offshore fish communities have begun to show an increasingly nearshore stable isotope signature which may be a result of sloughed *Cladophora* advection offshore, where it can enter the pelagic food web (Turschak et al., 2014). This finding indicates that the Lake Michigan nearshore zone

may be playing a more important role in lake energy pathways particularly following the recent declines in offshore primary production particularly during the spring bloom (see Chapter 1).

Hecky et al. (2004) hypothesized that mussel populations in the nearshore zones of the Great Lakes are effectively trapping phosphorus both directly through sediment accumulation of mussel waste (biodeposits) and indirectly by promoting *Cladophora* uptake and storage of phosphorus. It was further hypothesized that this nearshore phosphorus storage has played a major role in the changes observed in lake offshore food webs. Cha et al. (2011) showed that mussels in the inner Saginaw Bay have likely decreased phosphorus loading into Lake Huron by 60% through phosphorus retention. Chapra and Dolan (2012) show that the effective settling velocity of most of the Great Lakes has increased substantially since the dreissenid mussel invasion in 1990, increasing lake wide phosphorus retention. Although the Chapra and Dolan (2012) mass balance model does not resolve the Great Lake nearshore zones, it is clear that the nearshore may play an important role in producing these results (Bocaniov et al., 2014; Bootsma and Liao, 2013). To date there have been no published biogeochemical modeling studies that fully account for the effects of dreissenid mussels on carbon and nutrient dynamics due to the lack of nearshore *Cladophora* growth in model simulations (Auer et al., 2010; Pauer et al., 2011).

The scale and complexity of an aquatic biogeochemical model must balance any increase in model accuracy with the computational cost of that complexity, including the utility of the model for conducting sensitivity analyses and test scenario simulations, and the availability of data for adequate model validation (Robson, 2014). The computational

expense of simulating the finer scale nearshore environment within a larger lake domain is often impractical and leads to the use of coarse mass balance models such as that used by Cha et al. (2011) for Saginaw Bay, or complex, nested, 3D models such as that implemented by Leon et al. (2012) for a nearshore study area in Lake Ontario. None of the biogeochemical modeling studies on the Great Lakes have explored the nearshore zone while including both dreissenid mussels and *Cladophora* algae, despite the fact that these two components likely represent dominant phosphorus pathways in the Great Lakes nearshore zones (Bocaniov et al., 2014; Bootsma et al., 2012; Leon et al., 2012; Pauer et al., 2011). The goal of this research was to construct a useful biogeochemical model for the nearshore zone of Lake Michigan. The model has a 1D column framework with three vertical layers and simulates phosphorus fluxes between the dominant phosphorus pools and pathways in the Lake Michigan nearshore zone. The model will be referred to here as the nearshore phosphorus flux model (NPFM).

The NPFM was used to address the influence of nearshore dreissenid mussel particulate phosphorus grazing on the storage and fluxes of phosphorus in the Lake Michigan nearshore zone based on the 2013 late spring, summer and fall seasons at a nearshore monitoring station. First, the model was used to simulate the nearshore environment, the accuracy of which was evaluated against observations. Second, the model was used to simulate a test scenario where quagga mussels were removed from the model framework, so that by comparison of the two scenarios, the influence of dreissenid mussels on nearshore phosphorus dynamics could be evaluated. Results of this comparison suggest that quagga mussels are increasing nearshore total phosphorus during the summer leading to a net sink for pelagic phosphorus during this time of year.

3.2 Data Collection and Sampling Methods

Data from two monitoring stations in the nearshore zone of Lake Michigan located in 9 and 20 m of water approximately 1 and 2 km east of Shorewood, WI and 6 km north of Milwaukee Harbor (Fig. 3.1) were used for model input and validation. The 9m station has a rocky benthic habitat which supports a dense quagga mussel population of up to 5500 individuals per square meter and a thick *Cladophora* mat which reaches standing crops of over 100 grams of dry weight per square meter (gDW m⁻²) in the late summer, a biomass which is well above the nuisance level of 50 gDW m⁻² cited by Auer et al. (2010). The 9m station is located at latitude and longitude: N 43° 05.737' and W 87° 51.866'. The 20m station is located at latitude and longitude: N 43° 06.079' and W 87° 50.996'.

During the 2013 summer and fall seasons an extensive data set was collected at both stations. Water temperature was measured with temperature strings suspended in the water column with data collected every hour at 1m intervals at the 20m station. Water current profiles were measured at the 20m station using a down facing, buoy mounted, Acoustic Doppler Current Profiler (ADCP) producing profiles every 30 minutes at 2m depth bins for most of the 2013 season. Currents at the 9m station were retrieved from the NOAA, Great Lakes Coastal Forecasting System (GLCFS) and Great Lakes Observing System (GLOS) point inquiry tool (<http://glos.us/data-tools/point-query-tool-glcfs>). The GLCFS model “nowcast” data was used as it represents model simulations of the observed conditions rather than forecasted conditions. The NOAA GLCFS is a modified version of the Princeton Ocean Model which has been shown to accurately represent currents in Lake Michigan (Beletsky et al., 2006). Surface wave height and wave period

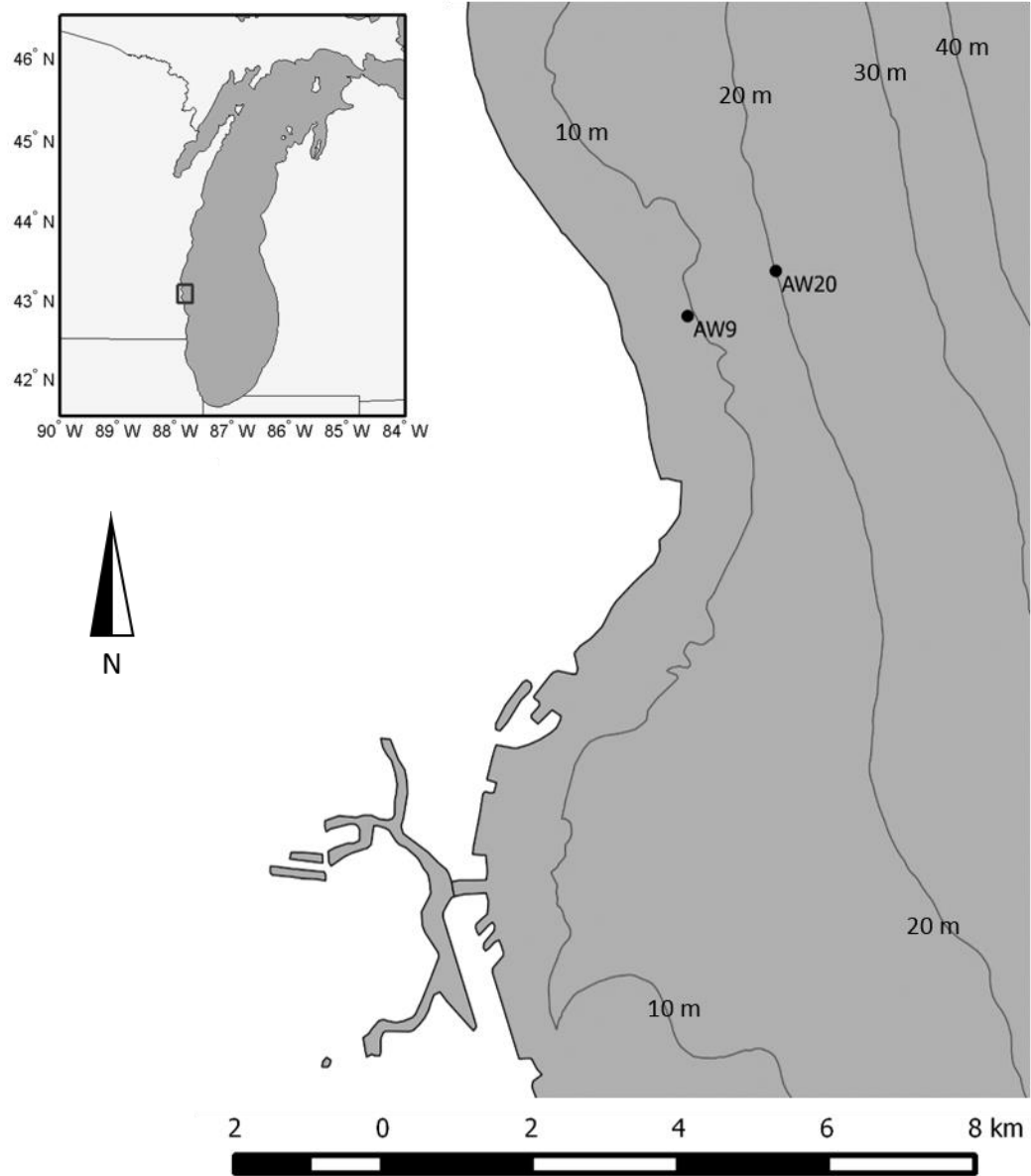


Figure 3.1: Map of Lake Michigan near Milwaukee, WI. The 9m monitoring station is labeled AW9 and the 20m monitoring station is labeled AW20. Depth contours are labeled and shown every 10m. The Milwaukee Harbor break-wall is not shown.

data were also collected from the GLCFS nowcast archive. The NOAA GLERL-Donelan wave model has been shown to accurately represent observations (Hawley et al., 2004).

Grab samples of water were taken at 2 and 8 m depth at the 9 m station, and 2, 10, and 18 m, depth at the 20m station at approximately bi – weekly intervals as weather allowed, from May through November 2013. Water samples were collected with a 4 L Niskin bottle and transferred to a clean, and lake water rinsed, 4 L Nalgene bottle which was immediately stored on ice. Within 24 hours the water samples were filtered in the lab through a Whatman GF/F filter. PP, total dissolved phosphorus (TDP), and soluble reactive phosphorus (SRP) were measured using the methods described by Stainton et al. (1977). *Cladophora* was collected by SCUBA diver at the 9 m station once per month and analyzed as described by Tomlinson et al. (2010) for Lake Michigan, with the exception that samples were collected in triplicate rather than quadruplicate. Triplicate mussel samples were collected by SCUBA diver at the 9 m station following the same method as for *Cladophora* and were returned to the laboratory where they were sorted by size classes between 5 mm and 30 mm and counted providing monthly mussel densities and size distributions. For a more detailed description of sampling and measurement methods see Appendix A.

Two sets of triplicate sediment traps were deployed at the 9m station. The traps were suspended using a spherical plastic float at 4m and 8m depths attached to a line anchored to the lake bottom using 125 pounds of weight. Each trap tube was 1m in length and had a diameter of 0.09m. The bottom of each trap tube was equipped with a removable cup which was removed and replaced when sediment samples were collected by SCUBA diver approximately once per month from July to November 2013. For each

deployment period, 5 mL of liquid chloroform was added to each trap for sample preservation. Sample cups were sealed and stored on ice until reaching the laboratory. In the laboratory, particulates were allowed to settle while the samples were stored in a refrigerator, after which, the surface water was decanted and the remaining sediment freeze dried. PP measurements were made by homogenizing individual samples with a mortar and pestle, followed by digestions and analysis for soluble reactive P (Stainton et al. 1977). For measured values and detailed analysis methods see Appendix A.

3.3 Model Description

The NPFM consists of three vertical layers: two water column layers (upper and lower water column) each set at 4.5m thick, and a near-bottom layer (NBL) set at 20 cm thick. The NBL is set at 20 cm in order to incorporate the height of the near bottom layer and to balance computation time with the time scale required to simulate dynamics within a thin near bottom layer using a controlled volume approach with an explicit, forward differencing discretization scheme (Chapra, 1997). The horizontal domain of the model is 1 km in the east-west (x) and north-south (y) directions. This horizontal scale is chosen because of the distance between the 9m and 20m stations where water measurements were taken. It is assumed that, while in reality a 1 km east to west domain would result in a change in depth from 6m to 14m in the vicinity of the 9m station, that the entire model domain is approximately 9.2 m deep reflecting that of the 9m station. The model has a time step of 20 seconds which is required to prevent numerical instability given the scale of the near bottom layer.

The model is driven by 5 independent variables: water temperature, surface PAR, horizontal current, and surface wind-wave height and period. The model simulates 12

dependent variables (Fig. 3.2) which are listed and described in Table 3.1. There are 17 phosphorus fluxes calculated by the model (listed in Table 3.2) consisting of those between model layers, between phosphorus pools, and at the model domain boundaries (Fig. 3.2). Model constants are listed in Table 3.3 with their description, value, and units. For more information regarding the constants associated with *Cladophora*, see Tomlinson et al., (2010) and Canale and Auer, (1982). The phosphorus mass balance equations for the model variables (Table 3.1) are:

$$V_U \frac{d}{dt} PP_U = J_{VWPP} A_X + J_{HPP} A_Z - J_{SW} A_X \quad (1)$$

$$V_L \frac{d}{dt} PP_L = J_{VBPP} A_X + J_{HPP} A_Z + J_{SW} A_X - J_{VWPP} A_X - J_{SB} A_X \quad (2)$$

$$V_B \frac{d}{dt} PP_B = J_{RES} A_X + J_{SB} A_X - J_{VBPP} A_X - J_{SD} A_X - J_{MG} A_X \quad (3)$$

$$\frac{d}{dt} S_D = J_{VBPP} - J_{RES} + J_{ME} \quad (4)$$

$$V_U \frac{d}{dt} DP_U = J_{VWDP} A_X + J_{HDP} A_Z \quad (5)$$

$$V_L \frac{d}{dt} DP_L = J_{VBDP} A_X - J_{VWDP} A_X + J_{HDP} A_Z \quad (6)$$

$$V_B \frac{d}{dt} DP_B = J_{MX} A_X - J_{VBDP} A_X - J_{CU} A_X \quad (7)$$

where V is the volume of the model layer in m³ and subscripts: U, L, and B indicate upper water column, lower water column, and near bottom layers respectively. A_X and A_Z represent the area (m²) of the horizontal (x and y) faces of the model layers and the vertical (y and z) face of the eastern model boundary for the upper and lower water column layers. The fluxes (*J* terms) are listed and described in Table 3.2.

The NPFM does not include water column and sediment fluxes between the DP and PP pools. These fluxes would represent uptake of DP by phytoplankton,

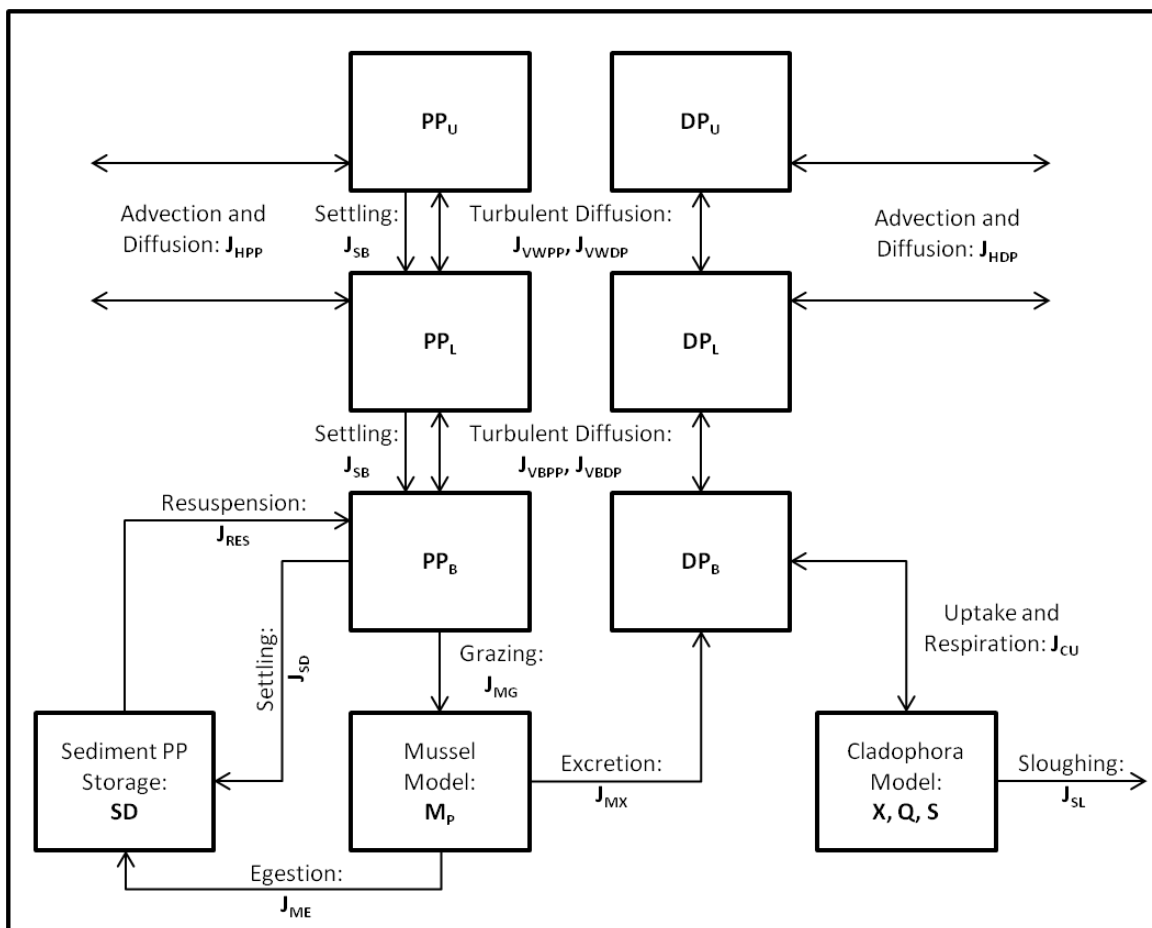


Figure 3.2: Schematic diagram of the model variables and phosphorus fluxes

Table 3.1: List of model variables, their units and description.

Variable	Units	Description
DP _U	$\mu\text{g L}^{-1}$	Upper water column dissolved phosphorus concentration
DP _L	$\mu\text{g L}^{-1}$	Lower water column dissolved phosphorus concentration
DP _B	$\mu\text{g L}^{-1}$	Near bottom layer dissolved phosphorus concentration
PP _U	$\mu\text{g L}^{-1}$	Upper water column particulate phosphorus concentration
PP _L	$\mu\text{g L}^{-1}$	Lower water column particulate phosphorus concentration
PP _B	$\mu\text{g L}^{-1}$	Near Bottom layer particulate phosphorus concentration
X	g DW m^{-2}	<i>Cladophora</i> areal biomass as dry weight
Q	mg P gDW^{-1}	<i>Cladophora</i> biomass specific tissue phosphorus content
S	mg P m^{-2}	<i>Cladophora</i> areal stored particulate phosphorus
S _D	mg P m^{-2}	Areal sediment stored particulate phosphorus
I	$\mu\text{E m}^{-2} \text{s}^{-1}$	PAR in the near bottom layer
M _P	$\text{L m}^{-2} \text{s}^{-1}$	Mussel volumetric water pumping rate

Table 3.2: List of model phosphorus fluxes, with units of $\text{mg P m}^{-2} \text{s}^{-1}$, and their description.

Flux	Description
J_{VWPP}	Vertical flux of particulate phosphorus between the upper and lower water column layers
J_{VWDP}	Vertical flux of dissolved phosphorus between the upper and lower water column layers
J_{VBPP}	Vertical flux of particulate phosphorus between the near bottom layer and the lower water column layer
J_{VBDP}	Vertical flux of dissolved phosphorus between the near bottom layer and lower water column layer
J_{HPPU}	Horizontal flux of particulate phosphorus between the upper water column layer and the domain wall
J_{HDPU}	Horizontal flux of dissolved phosphorus between the upper water column layer and the domain wall
J_{HPPL}	Horizontal flux of particulate phosphorus between the lower water column layer and the domain wall
J_{HDPL}	Horizontal flux of dissolved phosphorus between the lower water column layer and the domain wall
J_{CU}	Net <i>Cladophora</i> dissolved phosphorus uptake flux
J_{SL}	<i>Cladophora</i> sloughing flux of tissue as particulate phosphorus
J_{MG}	Mussel particulate phosphorus grazing flux
J_{MX}	Mussel dissolved phosphorus excretion flux
J_{ME}	Mussel particulate phosphorus egestion flux
J_{SW}	Downward flux of particulate phosphorus between the upper and lower water column layers due to settling
J_{SB}	Downward flux of particulate phosphorus between the lower water column layer and the near bottom layer due to settling
J_{SD}	Total flux of particulate phosphorus to the sediment storage pool ($J_{\text{SB}} + J_{\text{ME}}$)
J_{RES}	Vertical flux of particulate phosphorus from the sediment storage pool to the near bottom layer due to wind-wave driven resuspension

Table 3.3: Model constants listed with their description, value used during model simulations, and their units.

Constant	Description	Value	Units
L_{\max}	Maximum <i>Cladophora</i> sloughing rate	0.176	day ⁻¹
vs	Particulate phosphorus settling rate	0.5	m day ⁻¹
τ_w	Benthic shear stress threshold for resuspension and sloughing	0.4	N m ⁻²
ks	Effective Nikuradse sand roughness length for mussels	0.025	m
l_a	Height of the <i>Cladophora</i> mat above the lake bottom	0.10	m
ex	Dreissenid mussel phosphorus recycling efficiency	0.80	
μ_{\max}	Maximum <i>Cladophora</i> growth rate	1.53	day ⁻¹
Q_0	Minimum <i>Cladophora</i> tissue phosphorus quota	0.05	P as %DW
X_{\max}	Maximum <i>Cladophora</i> biomass density	800	gDW m ⁻²
ρ_{\max}	Maximum <i>Cladophora</i> phosphorus uptake rate	4.5	%P day ⁻¹
K_C	Half saturation constant for <i>Cladophora</i> phosphorus uptake	125	μ P L ⁻¹
R_{\max}	Maximum <i>Cladophora</i> respiration rate	0.23	day ⁻¹
T_{opt}	Optimum water temperature for <i>Cladophora</i> sloughing	17	°C
M_1	Mussel pumping model scaling factor	0.633	
M_2	Mussel pumping model exponential constant	0.074	
α	Light extinction model scaling factor	0.2394	
β	Light extinction model power constant	0.2848	

rem mineralization of PP to DP, recycling of PP to DP by the microbial community and consumers, etc. (Chen et al., 2002). Due to limitations in available data for comparison, it is seen as impractical to include all of the additional parameterizations needed to account for these fluxes. However, this should not substantially influence model results as these water column and sediment fluxes are likely small in comparison to those associated with the large quagga mussel and *Cladophora* biomasses observed during the summer and fall simulation period at the 9m station (Hecky et al., 2004). Estimates of P uptake by phytoplankton and *Cladophora* based on observed areal biomasses of each and uptake kinetic parameters derived from the literature suggest that P uptake by phytoplankton is less than 10% that of *Cladophora*. The model also does not differentiate between dissolved organic phosphorus (DOP) and soluble reactive phosphorus (SRP) and therefore labels dissolved phosphorus, generically, DP.

3.3.1 Horizontal Advection and Diffusion

Currents in the Lake Michigan nearshore during the stratified period are generally parallel to shore (Boyce, 1974; Rao and Murthy, 2001; Rao and Schwab, 2007). Kinetic energy spectra in Lake Huron and Lake Ontario show two clearly distinct coastal boundary layers in the nearshore region of both lakes (Murthy and Dunbar, 1981; Rao and Murthy, 2001; Rao and Schwab, 2007). The frictional boundary layer (FBL) is closest to shore and extends outward to approximately 2 km where the shore line and bottom friction influence the flow. The inertial boundary layer (IBL) extends several kilometers further offshore from the FBL and represents the transition zone between shore parallel flow and the cross shore energy due to internal wave oscillations.

The 9 m deep nearshore monitoring station, 1 km from shore, likely rests inside the FBL and is subject to predominantly shore parallel currents. The station is approximately 6 km north of the nearest tributary (Fig. 3.1), the Milwaukee harbor, which is contained by a sea wall, and the flow into it from the Milwaukee, Menomonee, and Kinnikinnick rivers. Although harbor PP and DP plumes periodically influence the monitoring station during large loading events, this source is not included for simplicity and is subject of ongoing research. It was assumed that the primary source of DP and PP to the 1-D model column was through the domain offshore boundary. The offshore boundary conditions were set as the DP and PP concentrations measured at the 20m station. Concentrations measured at 2m (upper water column) and 10m depths (lower water column), were linearly interpolated to match the model time. The boundary flux of DP and PP was calculated using the 9m station cross shore current velocity, where the 2m velocity is used for the upper water column and the 7m velocity is used for the lower water column. The boundary fluxes of PP and DP were calculated as:

$$J_{HPU} = |u_U|(P_{OU} - P_U) \quad (8)$$

$$J_{HPL} = |u_L|(P_{OL} - P_L) \quad (9)$$

where P represents either DP or PP in the upper water column (U) or lower water column (L), u is the cross shore current velocity in the upper water column (U) or lower water column (L), and P_O represents the boundary (offshore) concentration of DP or PP in the upper water column (U) or lower water column (L). This boundary flux method assumes that all of the offshore (eastward) velocity is compensated by onshore (westward) velocity providing a water mass balance at each time step. Effectively, the model boundary conditions provide horizontal turbulent diffusion between the nearshore and the

offshore and the absolute value of the cross shore current velocity represents the turbulent diffusion velocity.

3.3.2 Vertical Turbulent Diffusion

Vertical turbulent diffusion is considered the dominant process by which DP and PP is mixed between the upper and lower model layers and the NBL, and is critical to accurate simulation of mussel grazing rates as well as the flux of dissolved P, excreted by mussels, to the water column (Ackerman et al., 2001; L. Boegman et al., 2008; Bootsma and Liao, 2013; Dayton et al., 2014; Edwards et al., 2005). The vertical diffusion coefficient between the upper and lower water column layers (D_{VW}) is dependent on the two primary sources of turbulent kinetic energy in the nearshore water column: vertical current shear (dU/dz , where U is the total current velocity), and the vertical density gradient. The length scale method employed by Boegman et al. (2008) to simulate turbulent diffusion over zebra mussel beds in Lake Erie was used to calculate D_{VW} based on the measured current and temperature profiles of the top 9 m at the 20m station, used as a surrogate for that at the 9m station where current profiles were not available,

$$D_{VW} = \frac{\kappa l^2}{2P_r} \sqrt{\left(\frac{\partial u}{\partial z}\right)^2 + \left(\frac{\partial v}{\partial z}\right)^2} e^{-cR_i} \quad (10)$$

where, κ is the Von Karman constant equal to 0.41, l is the turbulent length scale in meters which is arbitrarily set to the model layer thickness as in Boegman et al. (2008), P_r is the Prandtl number, u and v are the cross shore, and along shore current velocities in $m\ s^{-1}$ respectively, c is constant equal to 1.5, and R_i is the Richardson number. R_i was calculated as

$$R_i = N^2 / [(\partial u / \partial z)^2 + (\partial v / \partial z)^2] \quad (11)$$

where N is the stability frequency, calculated as $N = \sqrt{-g / \rho_0 (\partial \rho / \partial z)}$, where g is the gravity constant, 9.81 m s^{-2} , and ρ is the water density in kg m^{-3} . The mean D_{VW} for the 2013 season was $0.002 \text{ m}^2 \text{ s}^{-1}$ which is within the expected range for surface waters (Chapra, 1997). Since the 20m station data is used as a surrogate for the 9m station, the depth average is used so that mixing between the upper and lower water column is represented no matter the depth of minimum turbulent diffusivity. D_{VW} was linearly interpolated to the model time step from the 30 min measurement interval.

Turbulent diffusion between the NBL and the lower water column, D_{VB} , was calculated assuming the law of the wall applied, and that the NBL is within the log layer (Liao et al. 2009),

$$D_{VB} = \kappa u_* z \quad (12)$$

where, κ is the von Karman constant, u_* is the friction velocity, and z is the height above the lake bottom, or the thickness of the NBL. The friction velocity is calculated by solving the equation for the log layer over an algal mat for u_* from Escartín and Aubrey (1995),

$$u_* = \frac{u_z \kappa}{\ln(30(z - l_a) / k_s)} \quad (13)$$

where u_z is the maximum of either the horizontal current measured at 1m above the lake bottom or the calculated wind wave benthic orbital velocity calculated as in Schwab et al. (2006). The effective Nikuradse sand roughness length, k_s , is set to the average length of mussels, 25 mm, which covers nearly all of the hard substrate at the nearshore monitoring

station, and the height of the benthic algal mat, l_a , is set to a constant half the thickness of the near bottom layer, 10 cm. The season average D_{VB} , $3.34 \text{ cm}^2 \text{ s}^{-1}$, was considerably lower than the water column average, and was in the expected range (Chapra, 1997). The well-mixed threshold for the NBL is $20 \text{ cm}^2 \text{ s}^{-1}$ which is exceeded for brief periods during high wave events. For numerical stability, D_{VB} is capped at the well mixed threshold. The vertical flux of phosphorus between the model layers is calculated as:

$$J_{VWP} = \frac{D_{VW}}{dz_W} (P_U - P_L) \quad (14)$$

$$J_{VBP} = \frac{D_{VB}}{dz_B} (P_L - P_B) \quad (15)$$

where P can represent either DP or PP in the upper water column (U), lower water column (L) or near bottom layers (B), D_{VW} and D_{VB} are the water column, and near bottom vertical turbulent diffusion coefficients respectively, and dz_W and dz_B are the thicknesses of the water column and near bottom layers respectively.

3.3.3 The Mussel Model

The mussel component of the NPFM simulates the areal mussel clearance rate ($\text{L m}^2 \text{ s}^{-1}$), as well as grazing, excretion and egestion phosphorus fluxes. Clearance rate is calculated as a function of the local mussel density, length distribution, and water temperature based on empirical relationships (Bootsma, 2009; Ozersky et al., 2009; Tyner, 2013; Vanderploeg et al., 2010). When the benthic shear stress is large enough to force sediment resuspension (proceeding section) mussel grazing is set to zero as it has been shown that mussel clearance, ingestion, and assimilation rates exponentially decline when exposed to high concentrations of inorganic sediment (Madon et al., 1998). Mussel

grazing is the product of the areal clearance rate, in $\text{m}^3 \text{m}^{-2} \text{s}^{-1}$, and the NBL PP concentration, in mg m^{-3} , where $J_{MG} = M_P \cdot PP_B$. Mussel DP excretion and PP egestion are calculated assuming a recycling efficiency of 80% (Berg et al., 1996). Mussels excrete DP (J_{MX}) into the NBL while mussel egested PP (J_{ME}) goes into the sediment PP storage pool, S_D (Fig. 3.2). Mussel internal phosphorus content is not included in the NPFM as it is assumed to be at steady state (Padilla et al., 1996).

Tyner (2013) measured the respiration rate of quagga mussels collected from the Lake Michigan nearshore zone at 4 different water temperatures (4, 10, 15, 20 °C) and produced a model for mussel respiration as a function of temperature. Tyner (2013) used respiration rates, R ($\text{mg O}_2 \text{mgDW}^{-1} \text{hr}^{-1}$), to estimate carbon grazing rates, G ($\text{mg C mgDW}^{-1} \text{hr}^{-1}$), by multiplying R by a factor of 0.337 mg C consumed to 1 mg O_2 respired, where $G = 0.337R$. The 0.337 factor was derived from the mussel caloric demand for respiration and a conversion factor for phytoplankton calories per mg C (Tyner 2013). To calculate mussel volumetric pumping, M_p ($\text{L mgDW}^{-1} \text{hr}^{-1}$), G is divided by the average, available organic carbon concentration (mg C L^{-1}) provided during the laboratory experiments. Estimated pumping rates were compared with temperature (Fig. 3.3), and the relationship was fitted according to the van't Hoff model:

$$M_p = M_1 e^{M_2 \cdot T} \quad (\text{mL mgDW}^{-1} \text{hr}^{-1}) \quad (16)$$

where M_1 and M_2 are provided in Table 3.3, and T is in °C ($R^2 = 0.98$ and $p = 0.009$).

Accounting for mussel density and applying correction factors for size distribution and length to mass distribution based on the work of Bootsma (2009), a mussel areal clearance rate ($\text{L m}^{-2} \text{hr}^{-1}$) was calculated by integrating over the 25 mussel length classes, $LC = 5$ to 30 mm,

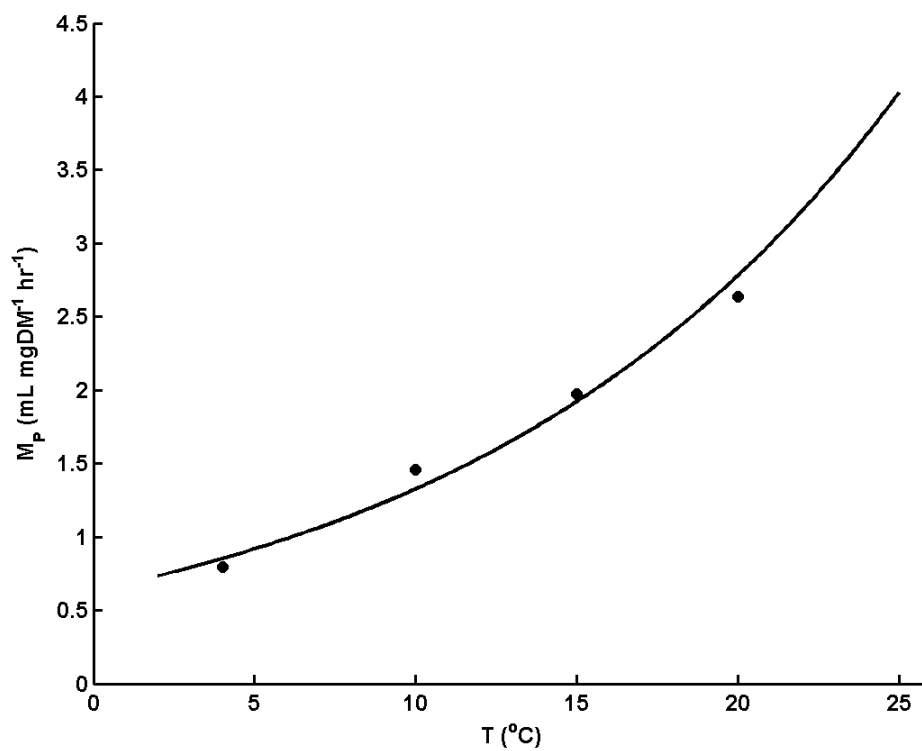


Figure 3.3: Mussel volumetric pumping rate as a function of temperature based on the results of Tyner (2013). The equation of best fit is $M_P = 0.633e^{0.074T}$, where $R^2 = 0.98$ ($p = 0.01$).

$$M_p(t) = \sum_{LC=5}^{30} [(M_1 e^{M_2 \cdot T}) \cdot M_D(t) \cdot M_L(LC, t) \cdot (2.174(LC)^{0.7411})] \quad (17)$$

where $M_D(t)$ is the mussel areal density (number of mussels m^{-2}) at time t , and $M_L(LC, t)$ is the measured mussel length distribution across the 25 length classes, LC , at time t . The last term in Eq. 4 represents the combined correction factors for length distribution and length to mass distribution from Bootsma, (2009). Mussel pumping rates calculated with this model are slightly lower than those determined by Bootsma et al. (2012) but are in good agreement with those found by Vanderploeg et al. (2010) for profundal morph quagga mussels.

3.3.4 Light Extinction and Light at Depth

The details of the *Cladophora* component of the NPFM are presented in detail by Tomlinson et al. (2010) and will not be repeated here, however, the treatment of PAR at depth needs to be addressed in some detail due to the critical relationship between mussel particulate grazing, water column light extinction, and the dependence of *Cladophora* growth on PAR at depth (Auer et al., 2010; Bootsma, 2009; Higgins et al., 2006). Measurements taken at the School of Freshwater Sciences rooftop approximately 6 km south of the 9m monitoring station provided a continuous surface PAR dataset for 2013 and 2014. An internal light extinction algorithm was employed so that PAR at depth is calculated based on water column particulate phosphorus concentration (as a surrogate for water clarity) and surface PAR. As part of our 2013 and 2014 field campaigns, measurements of bottom PAR and regular profiles of PAR and PP (representing total seston PP) were conducted at the 9m station. Light extinction coefficients were calculated based on surface and bottom PAR measurements and the Beer Lambert Law. A

functional, linear, relationship was observed (Fig. 3.4) between depth averaged water column PP concentrations ($\mu\text{g L}^{-1}$) and the measured light extinction coefficient, K_e (m^{-1}),

$$K_e = \alpha[PP] + \beta \quad (18)$$

where α and β are listed in Table 3. The observed relationship between PP and K_e , although adequate for the NPFM domain, should not be considered a universal model for Lake Michigan. This K_e model is limited by the scope of the NPFM in that the NPFM does not differentiate between different particulate species and their individual influences on K_e , and does not include water column colored dissolved organic matter.

3.3.5 Sediment Accumulation and Resuspension

The NPFM simulates accumulation and storage of settled PP (S_D) based on water column vertical turbulent diffusion, PP settling fluxes, and mussel PP egestion flux. Settling rate is set at a constant 0.5 m day^{-1} representing the mean value of the sinking rates used by Chen et al. (2002) for phytoplankton and detritus from multiple studies. It is assumed that the S_D pool is empty at the beginning of the model simulation, reflecting the high mixing and resuspension rates in the spring isothermal conditions. Resuspension of sediment PP is driven by surface wind-waves based on the method of Schwab et al. (2006). Based on linear wave theory, the benthic shear stress (N m^{-2}) is calculated as a function of wave height and wave period:

$$\tau_w = \rho \sqrt{v} \frac{W_H (2\pi/W_T)^{3/2}}{2 \sinh(k \cdot h)} \quad (19)$$

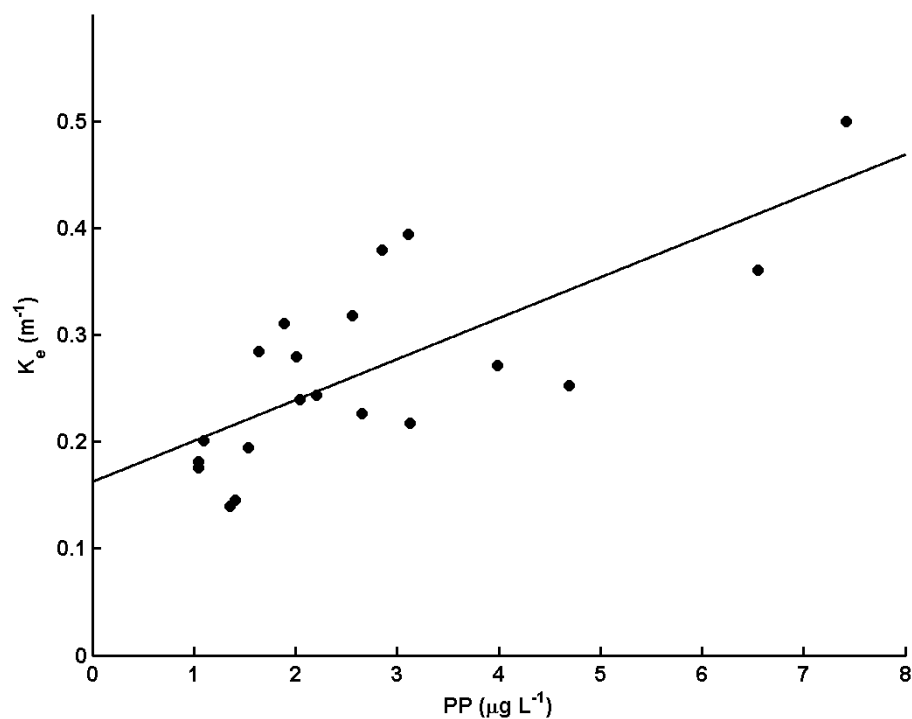


Figure 3.4: Light extinction coefficient (K_e) as a function of the depth averaged particulate phosphorus concentration (PP) at the Lake Michigan nearshore 9m monitoring station. Measurements were taken during the 2013 and 2014 monitoring seasons. The dots represent measured values of K_e and PP and the solid line represents the best fit linear regression of the data, where $K_e = 0.0383[\text{PP}] + 0.162$, and $R^2 = 0.55$ ($p < 0.01$).

where ρ is the water density, ν is the water viscosity, W_H is the wave height in m, W_T is the wave period in seconds, k is the wave number, and h is the water column depth in m.

Wave number is calculated as: $k = 2\pi/\lambda$ where λ is wave length in m,

$$\lambda = g \left(\frac{W_T^2}{2\pi} \right) \left(\tanh(\omega^2 W_H / g) \right)^{2/3} \quad (20)$$

where ω is the wave frequency calculated as $2\pi/W_T$, and g is the gravity constant (Fenton and McKee, 1990). Schwab et al. (2006) report a benthic shear stress threshold of 0.4 N m^{-2} for fine grain sediment resuspension in Lake Michigan near Chicago, IL. Whenever this wave driven benthic shear stress threshold is exceeded, sediment PP is immediately moved to the NBL where it becomes available to mix upward into the water column.

Sediment traps are included in the model for comparison with monitoring station sediment trap measurements. Model simulated sediment traps are located at the model layer interfaces, 4.5 m below the surface and 9 m below the surface. Sedimentation into the sediment pool accounts for the flux of PP due to settling, turbulent diffusion as well as the flux of PP from mussels as egested waste. Mussel grazing and P recycling transforms a large amount of the PP settling into the NBL to DP which can be taken up by *Cladophora* or mixed into the water column above. The model simulated bottom sediment trap only accounts for the PP which settles or mixes into the near bottom layer and does not include mussel grazing and egestion as there were no mussels in the sediment traps deployed at the 9m station.

3.3.6 The *Cladophora* Sloughing Algorithm

The physical and biological controls of *Cladophora* sloughing are not well understood. Canale and Auer (1982) calculated sloughing as a function of biomass and

wind speed representing the influence of benthic shear stress on *Cladophora* detachment. Their sloughing model is based on experiments where *Cladophora* detachment was measured *in situ* and sloughing rate was calibrated based on the relationships between mass loss, biomass, and wind speed. Higgins et al. (2005) revised the Canale and Auer (1982) sloughing algorithm with parameters specific to a Lake Erie monitoring station. Higgins et al. (2008) presents a revised model for *Cladophora* sloughing based on algal canopy, self-shading which produces a metabolic imbalance between the canopy top and base. Over time the effect of self shading produces weakening at the algal substrate attachment point leading to detachment and sloughing events (Higgins et al., 2006). The influence of self-shading was shown for stations in shallow water (0 to 4 m), but Higgins et al. (2008) discuss how the influence of self-shading may not apply in deeper water (7 to 10m). Tomlinson et al. (2010) simulated sloughing as an empirically derived function of temperature, employing a minimum and optimal temperature threshold for sloughing. Their model included of a depth dependent correction factor to account for the wind-wave bottom shear stress.

It is proposed that, as for sediment resuspension, *Cladophora* sloughing is influenced by wind-wave driven benthic shear stress and that any metabolic influence of temperature and self-shading generate sloughing under the influence of hydrodynamic detachment and resuspension (Flindt et al., 2007; Graba et al., 2012; Henry and Myrhaug, 2013). The sloughing algorithm of Tomlinson et al. (2010) is modified to account for this process by removing the minimum temperature and adding a benthic shear stress threshold. The *Cladophora* sloughing algorithm used in the NPFM was,

$$SL = \begin{cases} 0 & T < T_{opt} \text{ \& } \tau_w < \tau_{opt} \\ L_{max} & T \geq T_{opt} \\ L_{max} & \tau_w \geq \tau_{opt} \end{cases} \quad (21)$$

where SL is the *Cladophora* sloughing rate (day^{-1}), L_{max} is the maximum observed sloughing rate (0.176 day^{-1}) reported by Canale and Auer (1982), T is the water temperature ($^{\circ}\text{C}$), T_{opt} is the optimum temperature for *Cladophora* sloughing (20°C as in Tomlinson et al. 2010), τ_w is the wave driven benthic shear stress (N m^{-2}), and τ_{opt} is the benthic shear stress threshold for *Cladophora* detachment which is assumed to be equal to that of sediment resuspension, 0.4 N m^{-2} . It is assumed that sloughed *Cladophora* leaves the model domain. It is difficult to know the fate of sloughed *Cladophora*, however, it is clear that substantial amounts accumulate on beaches (Auer et al., 2010) while some can be advected offshore (Turschak et al., 2014) or accumulates in nearshore depositional areas (Tyner, 2013).

3.4 Model Simulation Results

The NPFM is used to simulate the 2013 summer and fall seasons at the 9m station. All model time series, with the exception of bottom PAR, are shown averaged over three hour intervals. Input variables are shown in Figure 3.5, including bottom water temperature, cross-shore current velocity, surface wind-wave height, the calculated turbulent diffusion coefficient between the upper and lower water column layers, and the calculated turbulent diffusion coefficient between the lower water column and the NBL. Initial conditions are set to equal measurements taken the day before the start of the model simulation period (2013 day number 149, or May 29, 2013). Model simulation output is validated against measured bottom PAR (collected during the early summer

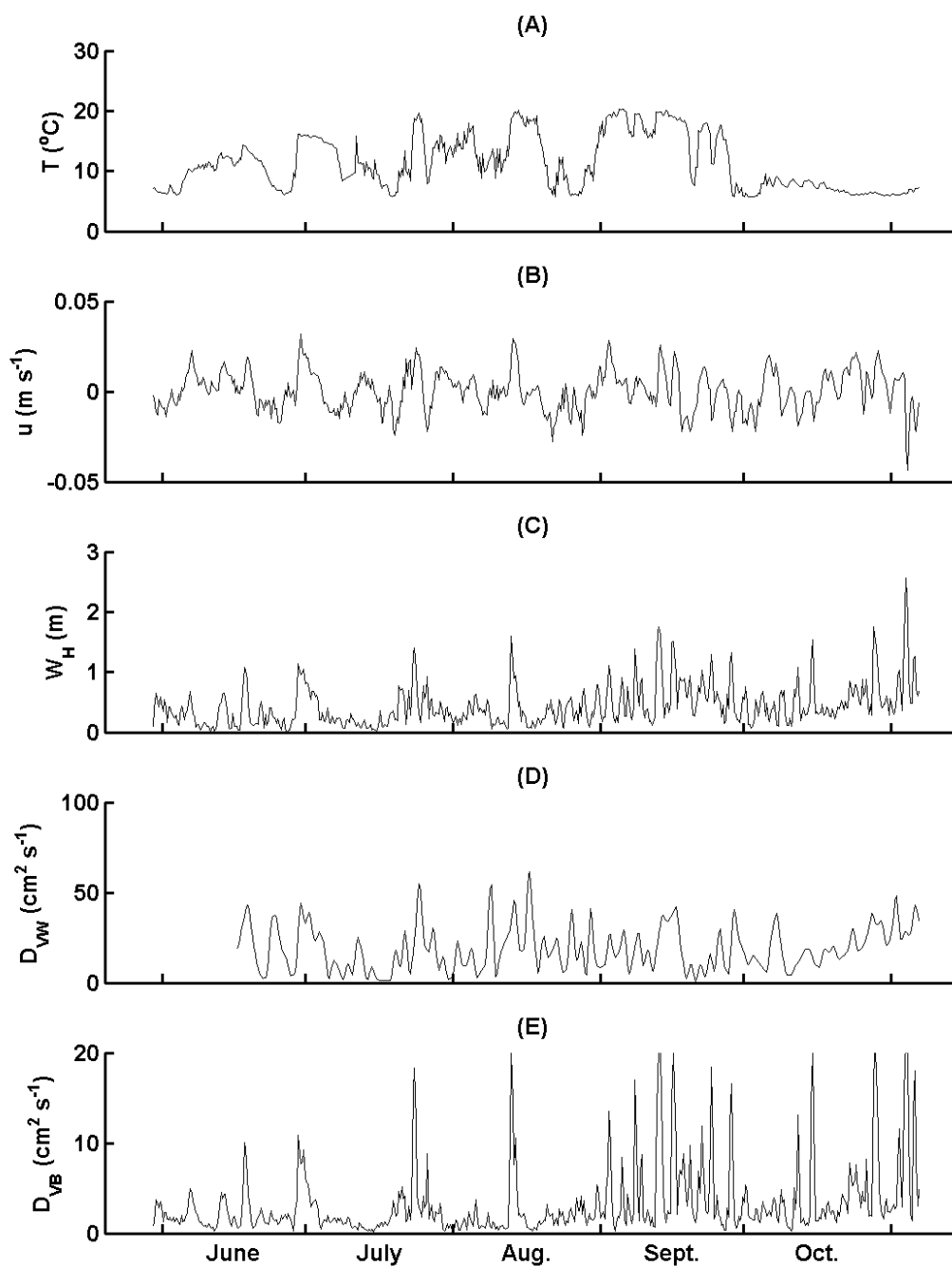


Figure 3.5: Model input variables: A) bottom water temperature, B) east – west current velocity, where negative values are towards the west from the east, C) surface wind-wave height, D) water column turbulent diffusion coefficient, and E) near-bottom turbulent diffusion coefficient. The x-axis is the consistent for all subplots and is shown below E.

only), 2m and 8m PP and SRP, *Cladophora* biomass, *Cladophora* tissue phosphorus content, and sediment trap derived sediment accumulation rates for the surface and bottom layers.

Model simulated bottom PAR is compared to the measured near bottom PAR collected at the 9m station from late May to late June 2013 (Fig. 3.6). Due to equipment failure, near bottom PAR was not measured after June 2013. The model does an adequate job simulating the NBL light conditions with a statistically significant positive correlation ($R^2 = 0.42$, $p < 0.01$) between the modeled and measured PAR values (Table 3.4). The error resulting from the K_e -PP model (Fig. 3.6 and Table 3.4) is associated with both error in the simulated PP concentration (Fig. 3.7) as well as the error in the observed K_e -PP relationship (Fig. 3.4).

Model output DP and PP for all three model layers are presented in Figure 3.7. The NPFM does a good job simulating the temporal pattern in observed DP and PP with a few periods of divergence. The DP concentration is over estimated by the model during August and October when SRP concentrations were below detection and set to zero. The model underestimates the PP concentration in August, and slightly over estimates the PP concentration in the later part of October. Near bottom DP concentrations (Fig. 3.7C) are not substantially different from the lower water column (Fig. 3.7B). NBL PP concentrations (Fig. 3.7F) are generally lower than the over lying water column (Fig. 3.7D and E) with the exception of sediment resuspension events which fill the NBL with sediment stored PP causing short term spikes in the NBL PP concentration.

Model simulated and observed 2013 *Cladophora* biomass, tissue P content, and areal stored PP are presented in Figure 8. Simulated *Cladophora* biomass (Fig. 3.8A) and

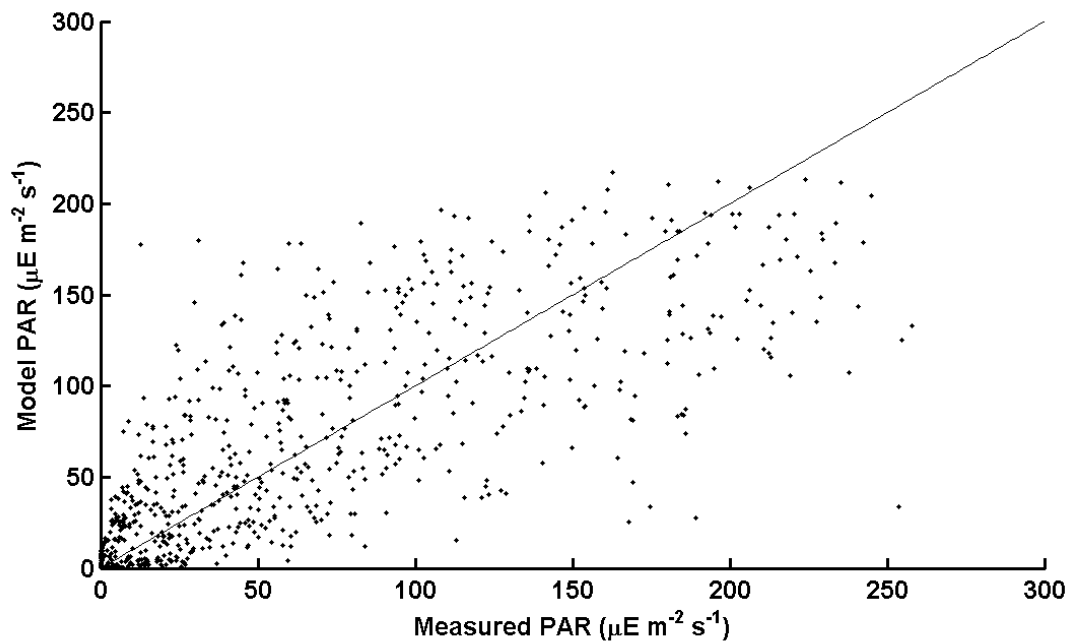


Figure 3.6: The model simulated near bottom PAR compared to the measured near bottom PAR at the 9m monitoring from May 30, 2013 - July 13, 2013. The solid line represents the perfect fit while the model vs. observed $R^2 = 0.47$ ($p < 0.001$).

Table 3.4: Model variables and their accuracy metrics calculated based on measurements taken at the 9m monitoring station. Error is calculated as the mean relative error as in Eq. 9.

Variable	Season R²	p value	Error · 100%	# of Observations
I	0.42	< 0.01	66 %	562
DP _U	0.73	< 0.01	309 %	13
DP _L	0.85	< 0.01	62 %	13
PP _U	0.02	0.70	47 %	13
PP _L	< 0.01	0.97	47 %	13
X	0.41	0.36	47 %	4
Q	0.82	0.10	46 %	4
S	< 0.01	0.99	93 %	4

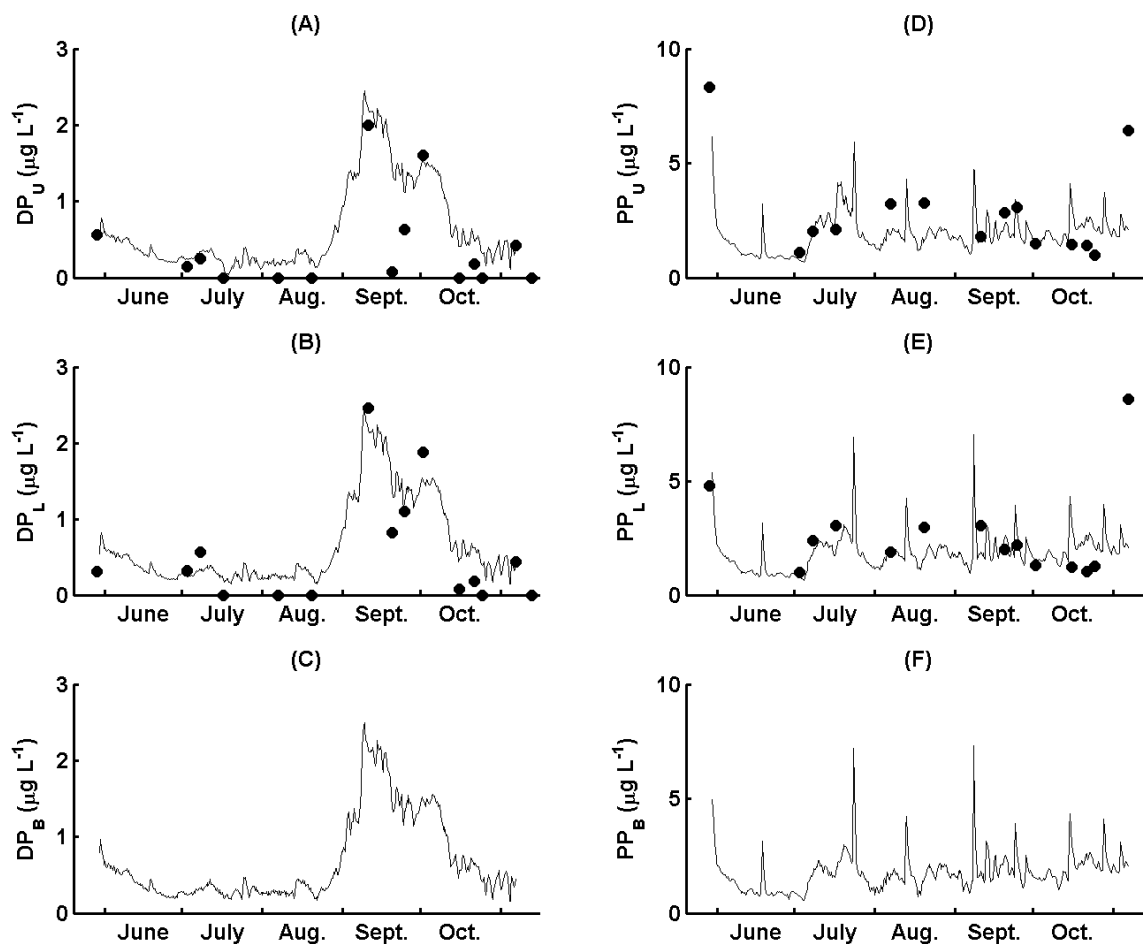


Figure 3.7: Model phosphorus simulation results (lines) and measured values at the 9m monitoring station (dots): A) upper layer dissolved phosphorus; B) lower layer dissolved phosphorus; C) NBL dissolved phosphorus; D) upper layer particulate phosphorus; E) lower layer particulate phosphorus; and F) NBL particulate phosphorus.

tissue P content (Fig. 3.8B) follow the observed seasonal trends reasonably well. Simulated biomass is lower than observed in early July and greater than observed in early August. *Cladophora* tissue phosphorus content is generally overestimated through the simulation period (Fig. 3.8B). Model simulated *Cladophora* areal stored phosphorus (Fig. 3.8C) follows observations reasonably well, however it over estimates stored PP in early August through mid-September. *Cladophora* growth is slightly lower than observed through June, but the observed season peak biomass of 129 ± 30 gDW m⁻² is reached in mid-July (Fig. 3.8A). The model slightly underestimates *Cladophora* fall regrowth in October and November (Fig. 3.8A).

Table 3.4 summarizes the goodness of fit and mean relative error of water column phosphorus and *Cladophora* variables. Goodness of fit is represented by the correlation coefficient (R^2) for the modeled daily average values compared to measured values. Mean relative error, or simply the error, is calculated as:

$$\text{Error} = \frac{1}{N} \sum_{n=1}^N [(x(n) - x'(n))/x(n)] \quad (22)$$

where x and x' represent the observed and modeled variable, and N is the total number of observations, n , of x . There was little agreement between the two quality metrics across the simulated variables. Model simulated and observed bottom PAR has a significant correlation ($R^2 = 0.42$, $p < 0.01$) with a fairly high error (66%). Empirical and simulated DP (Fig. 3.7A and B) were significantly correlated ($R^2 = 0.73, 0.85$, $p = < 0.01$ for the upper and lower water column and $n = 13$), but the error was high (309% and 62%). Water column PP (Fig. 3.7D and E) did not correlate with the 13 observations at all, but both the upper and lower water column layers had an acceptable error (47% and 47%).

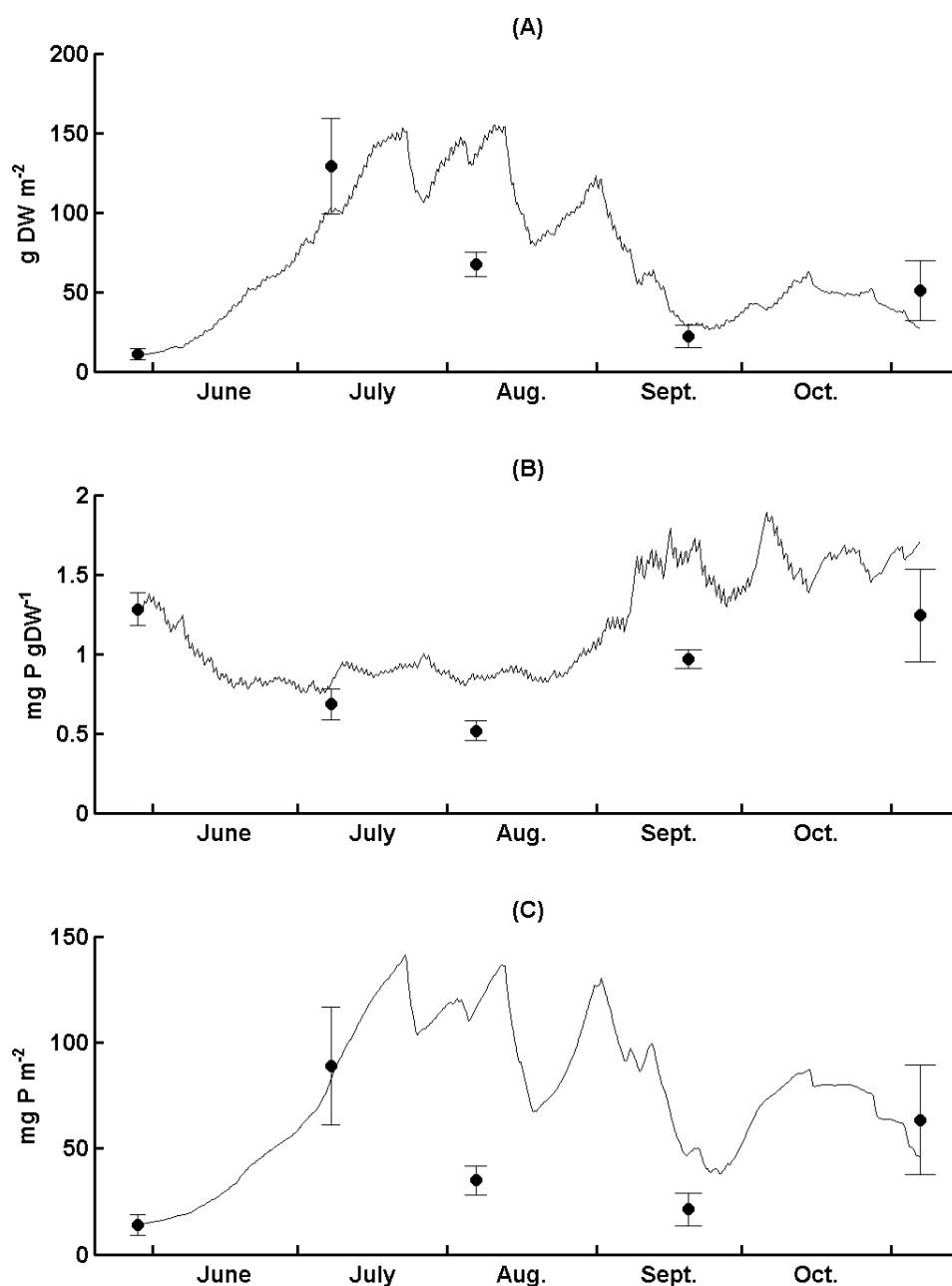


Figure 3.8: A) Model simulated (line) and measured (dots) Cladophora biomass; B) Model simulated (line) and measured (dots) Cladophora tissue phosphorus content; and C) model simulated (line) and measured (dots) Cladophora areal phosphorus storage. Dots and error bars represent the mean and \pm the standard deviation of triplicate samples.

Cladophora biomass (Fig. 3.8A) did not significantly correlate with the 4 observations, but had an acceptable error (47%). *Cladophora* tissue phosphorus content (Fig. 3.8B) correlated reasonably well with observations ($R^2 = 0.82$, $p = 0.10$), and had an acceptable error (46%). *Cladophora* areal stored phosphorus (Fig. 8C) did not correlate well with observations and had high error (93%).

Evaluation of these model accuracy metrics requires context. The fact the NPFM simulates, DP, PP, and *Cladophora* biomass within reasonable limits of measured values should be seen as a success. This is the first attempt at incorporating dreissenid mussels and *Cladophora* into a nearshore dynamic P model within a simple 1-D column. When these results are compared to those of other biogeochemical modeling studies in the literature, the NPFM model accuracy is generally close to average (Arhonditsis and Brett, 2004).

3.4.1 Mussel Grazing and Excretion

Mussel model volumetric pumping rate and mussel grazing flux of PP is shown in Figure 9. Mussel pumping rates (Fig. 3.9A) range from 0.4 and 1.4 L mussel⁻¹ day⁻¹ and mussel grazing rates (Fig. 3.9B) range from 0 to 1.8 mg PP m⁻² hr⁻¹. Figure 3.8C presents the net, mussel-*Cladophora* DP excretion-uptake flux in the NBL. This was calculated as the sum of mussel excreted DP and *Cladophora* DP uptake in the NBL. There were a few periods where mussel DP excretion was less than the *Cladophora* DP uptake flux (negative values). These periods between August and October coincided with upwelling events, indicated by sharp decreases in temperature to unseasonably cold levels (Fig. 3.5A), reducing mussel pumping and therefore grazing and DP excretion in the model. Through most of the simulation period the mussel-*Cladophora* complex was a net source

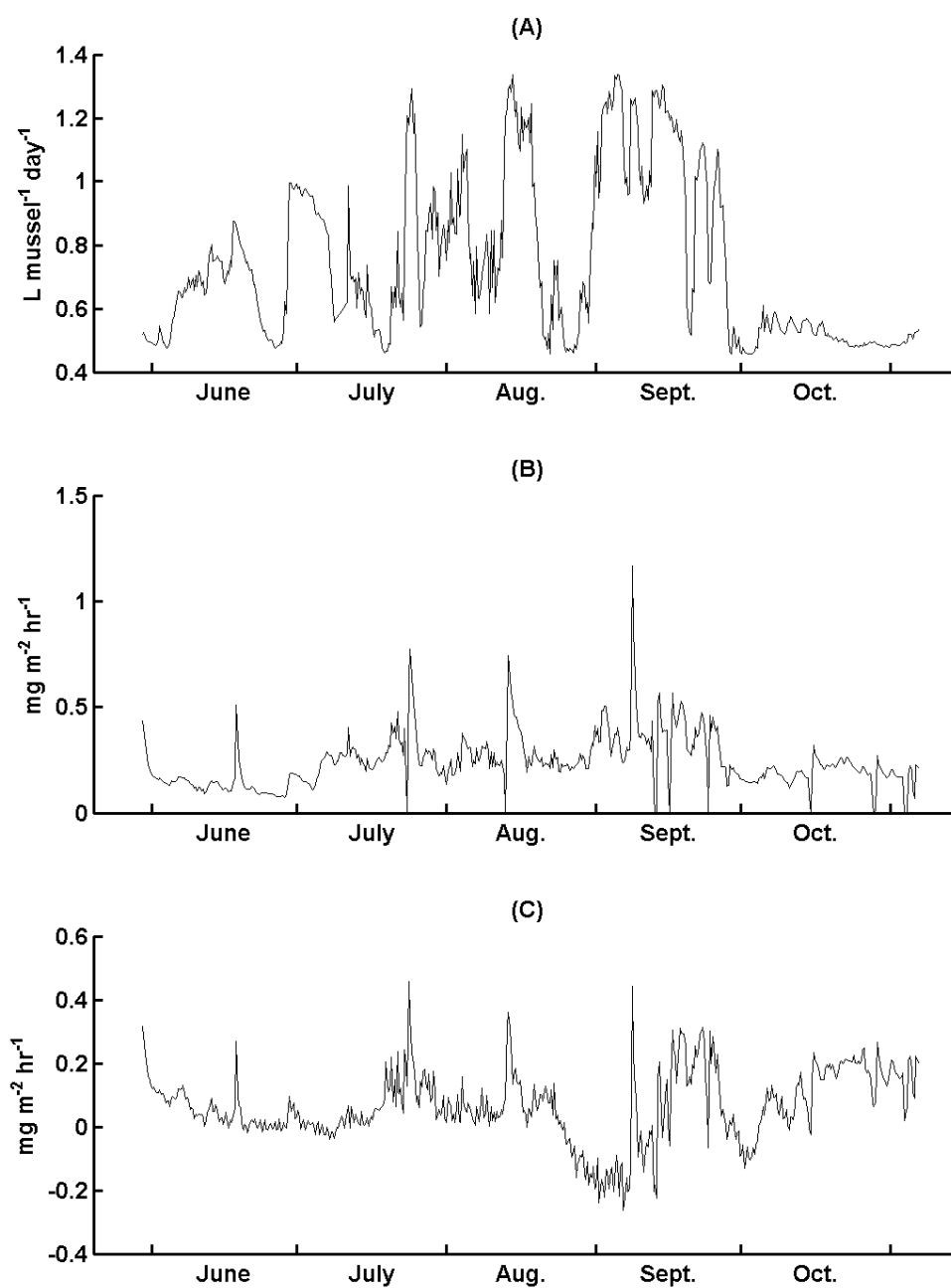


Figure 3.9: Model simulated mussel volumetric pumping rate (A), mussel grazing phosphorus flux (B), and the net dissolved phosphorus flux due to mussel excretion and *Cladophora* uptake ($J_{MX} - J_{CU}$) (C). Positive values indicate mussel DP excretion surpasses *Cladophora* DP uptake and negative values indicate mussel excretion is less than *Cladophora* uptake.

of DP to the NBL indicating mussel excretion supported *Cladophora* growth through most of the simulation. Bootsma (2009) presented mussel excretion measurements made with benthic chamber incubations at the same 9m station simulated in this study, during the spring, summer, and fall of 2007 and 2008. Measured mussel SRP excretion fluxes ranged from 0.1 to 1 mg m⁻² hr⁻¹ agreeing with the mussel DP excretion flux range simulated by the NPFM providing confidence in the mussel component of the NPFM.

3.4.2 Sedimentation and Resuspension

Simulated, sediment trap PP accumulation is compared with sediment trap measured PP accumulation during three collection periods in 2013: 1) July 11th through August 7th, 2) August 7th through September 20th, and 3) September 20th through November 7th (Fig. 3.10). The upper simulated sediment trap collected 157.2, 114.7, and 120.0 mg P m⁻² during the three collection periods respectively, while the actual, top sediment traps collected a mean of 4.96 ± 0.12 , 46.08 ± 3.93 , and 41.88 ± 1.14 mg P m⁻² during the three collection periods, where \pm indicates the standard deviation of triplicate samples (Fig. 3.10A). The model simulated bottom sediment trap collected 209.2, 383, and 286.5 mg P m⁻² during the three periods while the actual, bottom sediment traps collected a mean of 39.09 ± 1.49 , 193.44 ± 17.55 , 122.16 ± 50.21 mg P m⁻² during the three collection periods (Fig. 3.10B). Sediment trap derived sedimentation rates (mg P m⁻² day⁻¹) were calculated by dividing the total accumulated PP by the duration of each collection period. The upper, simulated, sedimentation rates for the three collection periods were 5.73, 2.57 and 2.5 mg P m⁻² day⁻¹, while the observed, upper sedimentation rates were 0.18 ± 0.01 , 1.05 ± 0.09 , 0.87 ± 0.02 mg P m⁻² day⁻¹. The bottom, simulated, sedimentation rates for the three collection periods were 7.73, 8.69 and 5.97 mg P m⁻²

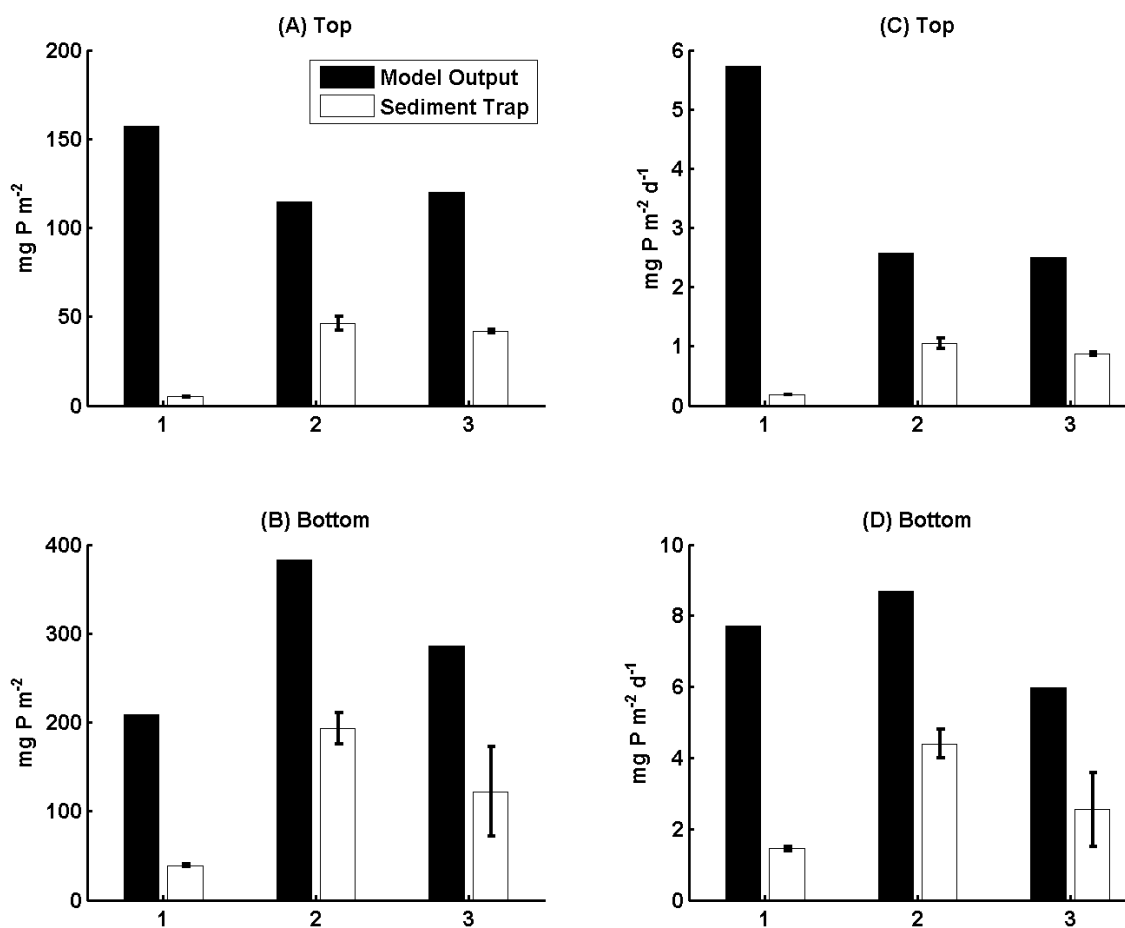


Figure 3.10: Sediment trap (white bars) with model simulated sediment trap (black bars) accumulated particulate phosphorus (top A, bottom B) and sediment trap particulate phosphorus accumulation rate (top C, bottom D) for deployment periods 1) July 11 – August 7, 2013, 2) August 7 – September 20, 2013, and 3) September 20 – November 7, 2013. Error bars on empirical sediment traps represent the standard deviation of triplicate traps at each depth. Note the difference scales on each graph.

day⁻¹, while the observed, bottom sedimentation rates were 1.45 ± 0.06 , 4.40 ± 0.40 , 2.54 ± 1.05 mg P m⁻² day⁻¹.

The model simulated sediment PP storage pool is presented in Figure 3.11A. Ignoring resuspension events, sediment accumulation in the sediment storage pool occurred at a mean rate of 1.77 mg P m⁻² day⁻¹ and at a maximum rate of 154.9 mg P m⁻² day⁻¹. The periodic loss of accumulated sediment (Fig. 3.11A) is caused by wave driven resuspension events which force all of the accumulated sediment into the NBL where it is able to mix with the overlying water column. The accuracy of simulated resuspension events is evaluated by comparing model simulated NBL PP concentration to water turbidity measured near the bottom at the 9m monitoring station. Turbidity was measured from early August through November (Fig. 3.11B) using a YSI sonde suspended a few inches from the lake bottom on a tripod. The model captures the major resuspension events well, as indicated by the matching peaks in PP and turbidity in Figure 3.11B.

3.4.3 Nearshore – Offshore Phosphorus Exchange

The change in domain areal total phosphorus through the simulation is accounted for by the ending net total phosphorus input through the boundaries. The difference between the starting and ending domain areal total phosphorus due to the cumulative boundary input and output is 6.78 mg of phosphorus m⁻², where domain total phosphorus is calculated as the sum of simulated areal water column PP, DP, sediment stored PP, and areal *Cladophora* stored phosphorus. These phosphorus pools are presented in Figure 3.12A where total suspended phosphorus accounts for both PP and DP in all three model layers. *Cladophora* stored phosphorus represents the largest pool of phosphorus in the model domain during July and August reaching a peak of 141.3 mg P

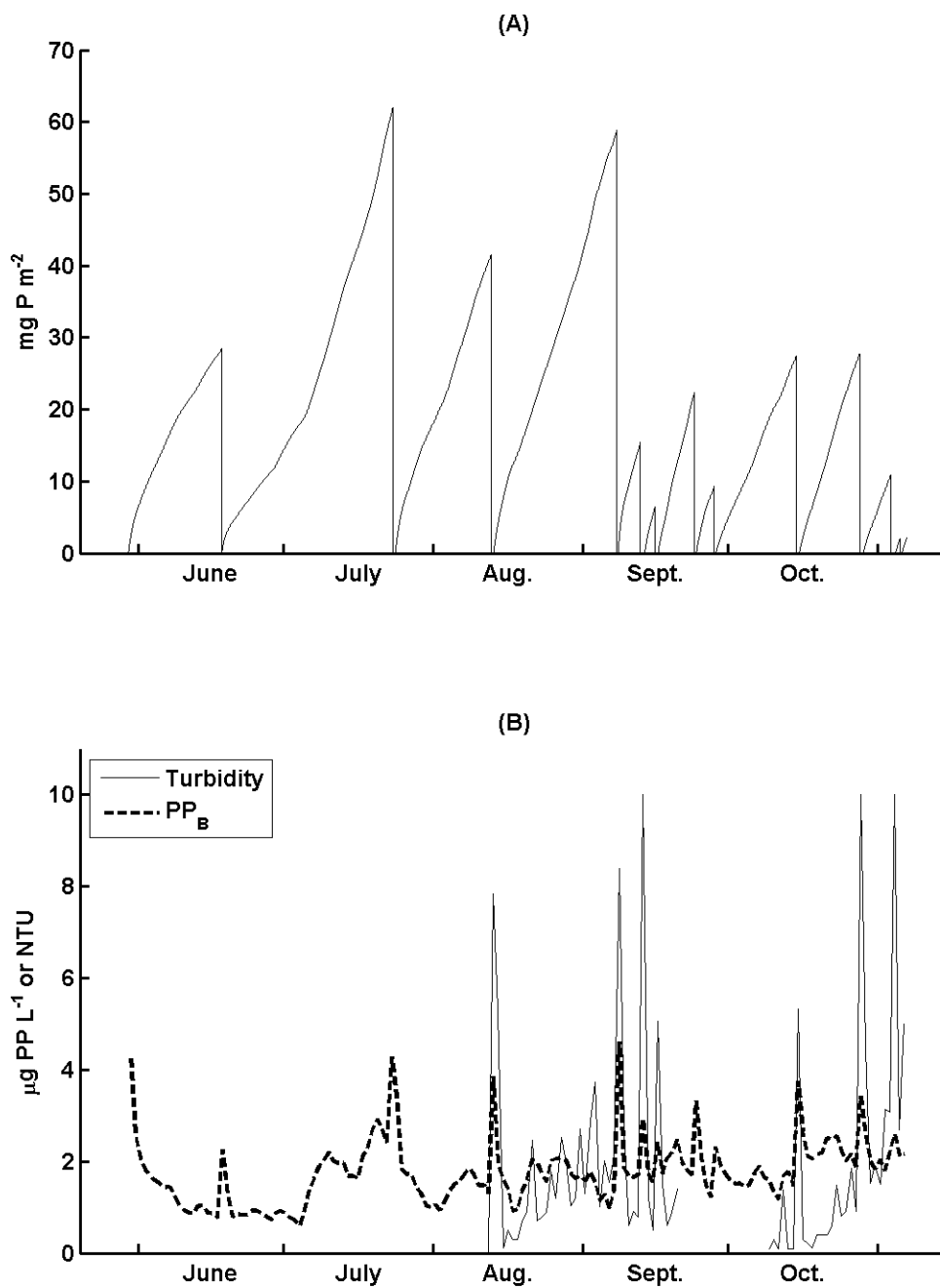


Figure 3.11: A) Model simulated areal sediment stored particulate phosphorus concentration, and B) model simulated near-bottom particulate phosphorus concentration (dashed line) and measured bottom turbidity (solid line).

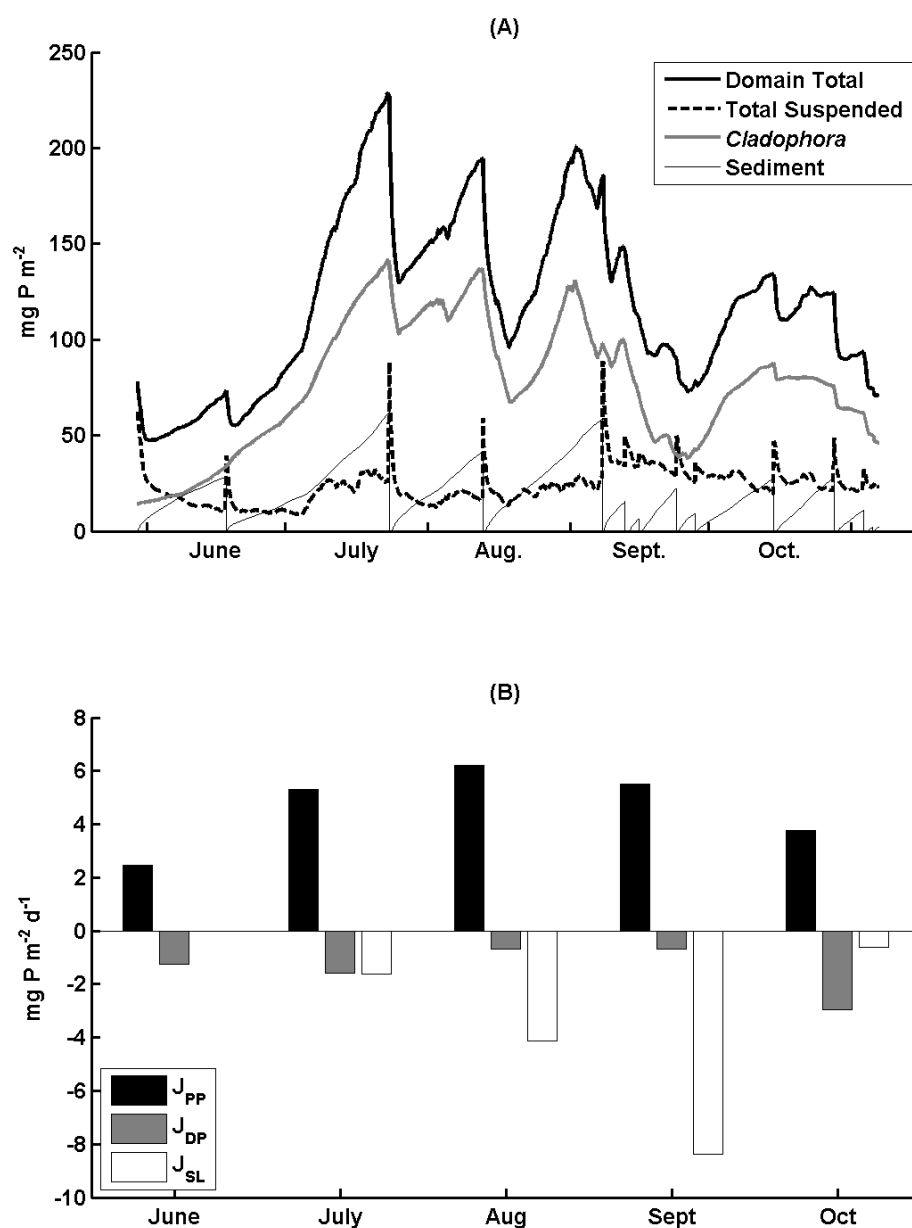


Figure 3.12: A) Model simulated phosphorus budget including total domain phosphorus, total suspended phosphorus, *Cladophora* stored phosphorus, and sediment stored phosphorus; B) monthly average horizontal particulate (J_{PP}) dissolved (J_{DP}) and sloughed *Cladophora* (J_{SL}) fluxes into (positive) and out of (negative) the nearshore zone.

m^{-2} , more than twice the season sediment stored PP peak of 62 mg P m^{-2} and 52.5 mg P m^{-2} larger than the total suspended phosphorus peak of 88.8 mg P m^{-2} .

The cross shore current velocity and the gradient between the offshore boundary concentration (set to that measured at the 20m station) and the domain DP and PP concentrations determined the horizontal flux of PP and DP into and out of the two water column layers. The model domain was a net sink for PP and a net source of DP throughout the 2013 summer (Fig. 3.12B). During August, the nearshore demand for PP was greatest with a monthly mean flux of $6.21 \text{ mg P m}^{-2} \text{ d}^{-1}$. The greatest output of DP occurred in October with a mean flux of $2.96 \text{ mg P m}^{-2} \text{ d}^{-1}$. *Cladophora* flux out of the model domain was substantial in late summer and early fall with a season peak in September of $8.35 \text{ mg P m}^{-2} \text{ d}^{-1}$. Fluxes reported here are calculated as the mean of fluxes through the offshore boundary ($\text{mg P m}^{-2} \text{ d}^{-1}$) integrated over the layer depth (4.5m) and divided by the horizontal area of the domain (1000m x 1000m).

Waples and Klump (2013) used thorium-234 as a tracer to calculate cross-shore fluxes of particulate organic carbon (POC) in the nearshore of Lake Michigan in the region of our nearshore monitoring station for one week periods during March, April and May 2000. They calculated fluxes in the range of -8.4 to $+272 \text{ mmol C m}^{-2} \text{ day}^{-1}$ for periods between March and May based on a nearshore ^{234}Th budget and $^{234}\text{Th}/^{238}\text{U}$ disequilibria. Multiplying the monthly mean fluxes of PP in Figure 3.12B by a seston C:P mass ratio of 80, 207 molar, (Chen et al. 2002; Bootsma et al. 2012) and converting to molar units, produces cross shore fluxes of particulate carbon in the range of 16.32 to $41.37 \text{ mmol carbon m}^{-2} \text{ day}^{-1}$. The season average of daily mean cross shore particulate carbon fluxes was $29 \text{ mmol carbon m}^{-2} \text{ day}^{-1}$ with a maximum of $112.2 \text{ mmol C m}^{-2} \text{ day}^{-1}$

and minimum of $-174.6 \text{ mg P m}^{-2} \text{ day}^{-1}$, where positive values indicate a flux from offshore to nearshore and negative values indicated a flux from nearshore to offshore. There was a large range in cross shore fluxes due to the cumulative influence of rapidly changing current velocity (Fig. 3.5B), nearshore PP concentration (Fig. 3.7D), and nearshore resuspension events (Fig. 3.11). Considering this variability, the fact that our model calculated cross shore particulate fluxes within a reasonable range of those calculated by Waples and Klump (2013) during short periods, provides confidence in the models ability to represent nearshore-offshore mass exchange.

3.4.4 Model Sensitivity Tests

Evaluating the sensitivity of biogeochemical model output to input parameters is critical for a complete understanding of model and system dynamics and model accuracy. A sensitivity analysis can help identify parameters which have a large impact on simulation output and may help guide interpretation of model output and direct further research focused on the uncertainty of those parameters (Cariboni et al., 2007). The sensitivity of the NPFM output to model constant parameters was evaluated by comparing the variation in model output to a range of variability in the model constants. Model outputs evaluated in the sensitivity tests were mean and maximum *Cladophora* biomass (Fig. 3.8A) and mean boundary, or nearshore-offshore, dissolved and particulate phosphorus fluxes (Fig. 3.12B). These variables were chosen for their significance to the primary questions and hypotheses addressed in this study: do dreissenid mussels support *Cladophora* growth in the nearshore zone of Lake Michigan, and how do dreissenid mussels impact nearshore phosphorus storage and fluxes? It is clear that *Cladophora* biomass is the single largest pool of phosphorus in the nearshore domain (Fig. 3.12),

therefore, analysis of the response of mean and maximum *Cladophora* biomass and nearshore-offshore fluxes of phosphorus provides an efficient analysis of the model output key to the questions of this study. There were 17 constants used in the model simulations (Table 3.3). The sensitivity analysis excluded the 26 polynomial coefficients used to calculate light and temperature multipliers in the *Cladophora* model (Tomlinson et al., 2010). To our knowledge, no thorough sensitivity analysis of *Cladophora* model parameters has been conducted. The last 7 constants in Table 3 represent critical biological parameters used to calculate *Cladophora* growth and therefore are assumed to provide an adequate representation of *Cladophora* model sensitivity.

A local, “one-at-a-time” sensitivity analysis method was used to compare the variation in model output to perturbation in model constant values (Cariboni et al., 2007). Variation, or response, V , of an output variable, X , based on the perturbation of a constant is defined here as:

$$V_X(t) = \frac{(\overline{X_S(t)} - \overline{X(t)})}{\overline{X(t)}} \quad (23)$$

where the subscript S indicates output variable X for a specific parameter perturbation simulation, and the over-bars indicate mean values in time, t . The response of each output variable was evaluated by comparing the calculated variation of the output variable (Eq. 23) against the perturbation in the tested parameter. For the 2013 simulation period the NPFM was run with each of the 17 model constants independently varied from -50% to +50% at a 10% interval from their original, base simulation, values. In total, 187 model simulations were conducted producing 11 different sets of output variables per constant tested. The values of constants for perturbation percentages: -50, -30, -10, 0, 10,

30, and 50% are listed in Table 3.5 (± 20 and 40% perturbations are excluded for brevity).

The response matrix for mean *Cladophora* biomass, mean, net nearshore-offshore PP flux and mean, net nearshore-offshore DP flux are presented in Table 3.6. Listed values represent those calculated using Eq. 23 and zero values indicate no response to the parameter perturbation. All of the model parameters associated with the *Cladophora* model (μ_{\max} , Q_0 , X_{\max} , ρ_{\max} , K_C , R_{\max} , L_{\max} , T_{opt}) produced high degrees of variation in both mean *Cladophora* biomass and boundary DP flux, with many parameters producing variation in the state variable that was substantially higher than the parameter perturbation. Parameters used to calculate dreissenid mussel grazing, excretion, and egestion (M_1 , M_2 , ex) as well as the two parameters used to calculate light extinction (α , and β) also produce notable variation in these same model outputs. Boundary PP flux was not responsive to perturbations in *Cladophora* growth parameters, but was moderately responsive to mussel clearance rate and phosphorus recycling parameters (M_1 , M_2 , and ex). All three model outputs tested (Table 3.6) were not sensitive to settling rate (vs), benthic shear stress threshold (τ_w), and the height of the algal mat above the lake bottom (l_a), indicating the mussel grazing and phosphorus recycling and *Cladophora* growth and phosphorus uptake played a greater role in nearshore phosphorus dynamics.

Extensive laboratory and field measurements were conducted in the 1980s to produce the Great Lakes *Cladophora* Model (Auer and Canale, 1982; Auer et al., 1982). The model was calibrated and confirmed in the 1980s based on observations made in Lake Huron (Canale and Auer, 1982b) and revisions to the model were made by Tomlinson et al. (2010) with further model calibration and confirmation based on newly

Table 3.5: Model constant parameters and their sensitivity analysis perturbation values ranging from -50% of the value used to +50% of the value used in the base model simulation. The $\pm 20\%$ and 40% perturbation values are not included. The center column with perturbation 0 lists the constant values used in the base simulation. See Table 3 for constant descriptions and units.

Constant Ref. # and Symbol		Percent Perturbation						
		-50	-30	-10	0	10	30	50
1	vs	0.25	0.35	0.45	0.5	0.55	0.65	0.75
2	τ_w	0.2	0.28	0.36	0.4	0.44	0.52	0.6
3	M_1	0.3165	0.4431	0.5697	0.633	0.6963	0.8229	0.9495
4	M_2	0.037	0.0518	0.0666	0.074	0.0814	0.0962	0.111
5	ks	0.0125	0.0175	0.0225	0.025	0.0275	0.0325	0.0375
6	l_a	0.05	0.07	0.09	0.1	0.11	0.13	0.15
7	ex	0.4	0.56	0.72	0.8	0.88	1.04	1.2
8	α	0.01915	0.02681	0.03447	0.0383	0.04213	0.04979	0.05745
9	β	0.081	0.1134	0.1458	0.162	0.1782	0.2106	0.243
10	μ_{\max}	0.765	1.071	1.377	1.53	1.683	1.989	2.295
11	Q_0	0.025	0.035	0.045	0.05	0.055	0.065	0.075
12	X_{\max}	400	560	720	800	880	1040	1200
13	ρ_{\max}	2.25	3.15	4.05	4.5	4.95	5.85	6.75
14	K_C	62.5	87.5	112.5	125	137.5	162.5	187.5
15	R_{\max}	0.115	0.161	0.207	0.23	0.253	0.299	0.345
16	L_{\max}	0.088	0.1232	0.1584	0.176	0.1936	0.2288	0.264
17	T_{opt}	8.5	11.9	15.3	17	18.7	22.1	25.5

Table 3.6: Sensitivity test response matrix for mean *Cladophora* biomass, mean, net boundary particulate phosphorus flux, and mean, net boundary dissolved phosphorus flux. The percent constant perturbation is listed at the top of the table and values below indicate the variation response calculated as Eq. 23 associated with each model constant parameter.

Model Response Variable	Constant Parameter	Percent Perturbation						
		-50	-30	-10	0	10	30	50
Mean <i>Cladophora</i> Biomass	vs	-0.0026	-0.0014	-0.0004	0	0.0003	0.0008	0.0016
	τ_w	-0.2203	-0.0804	-0.0154	0	0.0208	0.0409	0.0492
	M_1	-0.5295	-0.2882	-0.0862	0	0.0903	0.2466	0.3765
	M_2	-0.2813	-0.1798	-0.0634	0	0.0666	0.2102	0.3648
	ks	-0.2814	-0.1801	-0.0636	0	0.0669	0.2117	0.3682
	l_a	-0.2814	-0.1802	-0.0637	0	0.067	0.2119	0.3686
	ex	-0.5643	-0.3839	-0.1421	0	0.1533	0.492	0.8659
	α	0.6277	0.3631	0.1094	0	-0.104	-0.292	-0.4581
	β	1.6842	1.1088	0.3568	0	-0.3061	-0.7642	-0.929
	μ_{\max}	-0.2477	0.1118	0.0968	0	-0.1339	-0.514	-0.8393
	Q_0	1.5316	0.7809	0.2219	0	-0.189	-0.4804	-0.6744
	X_{\max}	0.7365	0.5675	0.1917	0	-0.1766	-0.4661	-0.6658
	ρ_{\max}	0.5338	0.3968	0.131	0	-0.1203	-0.3231	-0.4783
	K_C	0.3689	0.2003	0.0613	0	-0.0567	-0.1582	-0.2464
	R_{\max}	0.7037	0.3983	0.1252	0	-0.1175	-0.3283	-0.5046
	L_{\max}	1.7873	0.9141	0.2515	0	-0.2013	-0.4813	-0.6514
T_{opt}	-0.2347	-0.4333	-0.3293	0	-0.2013	-0.4813	-0.6514	
Mean, Net PP Flux	vs	0.0054	0.0033	0.0011	0	-0.0011	-0.0033	-0.0055
	τ_w	-0.0979	-0.0394	-0.0105	0	0.0056	0.0265	0.0327
	M_1	-0.4899	-0.2732	-0.0859	0	0.0779	0.2368	0.3685
	M_2	-0.2951	-0.1856	-0.0646	0	0.067	0.2076	0.3547
	ks	-0.2971	-0.187	-0.0651	0	0.0677	0.2097	0.3586
	l_a	-0.2973	-0.1871	-0.0652	0	0.0677	0.2099	0.3592
	ex	-0.6583	-0.4294	-0.1544	0	0.1649	0.5222	0.907
	α	0	0	0	0	0	0	0
	β	0	0	0	0	0	0	0
	μ_{\max}	0	0	0	0	0	0	0
	Q_0	0	0	0	0	0	0	0
	X_{\max}	0	0	0	0	0	0	0
	ρ_{\max}	0	0	0	0	0	0	0
	K_C	0	0	0	0	0	0	0
	R_{\max}	0	0	0	0	0	0	0
	L_{\max}	0	0	0	0	0	0	0
T_{opt}	0	0	0	0	0	0	0	

Table 3.6
cont.

Mean, Net DP Flux	vs	0.0109	0.0063	0.002	0	-0.002	-0.0056	-0.0096
	τ_w	-0.0163	-0.0184	-0.0202	0	-0.0147	0.0126	0.0155
	M_1	-0.3365	-0.19	-0.0715	0	0.0329	0.1454	0.2345
	M_2	-0.1825	-0.1094	-0.0364	0	0.0364	0.1066	0.1742
	ks	-0.1869	-0.1118	-0.0371	0	0.0371	0.1085	0.1769
	l_a	-0.1872	-0.112	-0.0372	0	0.0372	0.1087	0.1773
	ex	-0.5328	-0.3164	-0.102	0	0.1024	0.305	0.4853
	α	-0.6848	-0.4155	-0.1335	0	0.1335	0.3884	0.6353
	β	-1.5689	-1.1465	-0.4263	0	0.4142	1.1683	1.4468
	μ_{\max}	0.4105	-0.0896	-0.109	0	0.1701	0.7333	1.3136
	Q_0	-1.3189	-0.7965	-0.2601	0	0.2473	0.6825	1.0112
	X_{\max}	-0.6984	-0.5822	-0.2214	0	0.2281	0.6571	0.9951
	ρ_{\max}	-0.168	-0.243	-0.1042	0	0.1133	0.3437	0.5581
	K_C	-0.7795	-0.4097	-0.1222	0	0.1108	0.3042	0.4671
	R_{\max}	-1.1983	-0.675	-0.2115	0	0.1982	0.5532	0.8484
	L_{\max}	-1.7371	-1.0708	-0.3372	0	0.2943	0.7437	1.0386
T_{opt}	-0.5892	0.0547	0.1597	0	0.2943	0.7437	1.0386	

collected observations in Lake Michigan. The role that *Cladophora* plays in the nearshore zone, however, appears to be dependent, to a high degree, on the *Cladophora* model parameters. It is recommended that further research into the uncertainty associated with these parameters continue, such as those revisions made by Tomlinson et al. (2010), because small changes in model parameters (e.g. 10% as shown in Table 3.6), may have a large impact on how *Cladophora* and phosphorus are simulated and understood in a dynamic nearshore environment.

This is the first attempt to utilize the *Cladophora* model within a dynamic phosphorus model (Auer et al., 2010; Dayton et al., 2014; Tomlinson et al., 2010). It is therefore important to highlight that the sensitivity analysis demonstrated the major role *Cladophora* plays in the nearshore zone. The coincident sensitivity of *Cladophora* biomass and cross-shore DP boundary flux to the same model parameters (Table 3.6) illustrates that a large, mean *Cladophora* biomass greatly impacted nearshore dissolved phosphorus concentrations and nearshore-offshore DP fluxes. This was dependent on the presence and impact of dreissenid mussel PP grazing and DP excretion as it was shown previously that dreissenid mussels excrete enough DP to support *Cladophora* DP uptake in the near bottom layer (Fig. 3.9D) and that *Cladophora* biomass and nearshore-offshore DP flux was sensitive to mussel grazing and P recycling parameters (Table 3.6).

There is some uncertainty associated with the both the light extinction parameterization used in the NPFM (Eq. 18 and Fig. 3.4 and 3.6), and the ratio of mussel excretion to egestion of grazed PP. Light extinction parameters influence *Cladophora* biomass by directly limiting *Cladophora* growth rate, controlling cross-shore DP flux through the resulting change in *Cladophora* DP uptake. Improvements to light extinction

parameterization may be dependent on model complexity as additional water column constituents likely influence light attenuation. Light extinction could be included as an empirical model input, however, the goal of the current study is to identify the influence of dreissenid mussels on *Cladophora* and phosphorus in the nearshore, and mussels directly impact water clarity through their filtering activity (Cecala et al., 2008; Higgins and Vander Zanden, 2010; Vanderploeg et al., 2010). Future modeling efforts may require improved light extinction parameterizations which still incorporate the influence of dreissenid mussel filtering on water transparency.

The ratio of mussel P excretion to egestion was based on observations made in laboratory and field studies (Baldwin et al., 2002; Berg et al., 1996). Additional research is clearly needed to develop uncertainty constraints and improved parameterization of mussel nutrient recycling efficiency, particularly for identifying the differences between zebra and quagga mussel congeners (Bootsma and Liao, 2013). The mussel model incorporated in the NPFM includes parameterization of the influence of water temperature, mussel density, and size distribution. More complex dreissenid mussel metabolism models have been used in studies of other lakes (Bocaniov et al., 2014; Madenjian, 1995; Schwalb et al., 2013). Adding model complexity with substantial uncertainty in biological parameterizations can make it very difficult to fully understand the ecosystem as well as the limitations of the model (Arhonditsis and Brett, 2004; Cariboni et al., 2007). Refining the dreissenid mussel, and in particular quagga mussel, metabolism and phosphorus excretion and egestion models should be a research priority as these parameterizations have a major impact on simulated nutrient dynamics.

When parameters controlling mussel clearance rate were decreased by 50%, mean *Cladophora* biomass declined 28 to 56% from the base simulation (Figure 3.13A). When these same parameters were increased 50%, mean *Cladophora* biomass increased between 36 and 87%. Similarly, cross-shore DP flux varied between -18 and -53%, and between +17% and +49% for 50% decreases increases in parameter values respectively (Figure 3.13B). Cross-shore PP flux varied between -30% and -65% and between +36% and +90% (Figure 3.13C). This sensitivity analysis indicated that reducing or removing mussels from the model framework in test scenario simulations would dramatically influence the state of the nearshore zone by substantially reducing *Cladophora* biomass and cross-shore phosphorus fluxes. Results of a simulation test scenario should be put into the context of this sensitivity analysis, however, as uncertainty in any of the previously highlighted parameters will contribute uncertainty to conclusions.

3.4.5 Dreissenid Mussel Test Scenario

The NPFM was used to test the hypothesis that nearshore quagga mussels are trapping phosphorus in the nearshore zone of Lake Michigan (Hecky et al., 2004). This hypothesis was tested by conducting a simulation test scenario where mussel density was set to zero. The output of this “no mussel” test scenario was compared to the “realistic” environment simulated previously, allowing for quantification of the specific changes in the nearshore environment attributable to mussels. The no-mussel test scenario simulation produced a nearshore zone which was essentially a conduit for phosphorus,

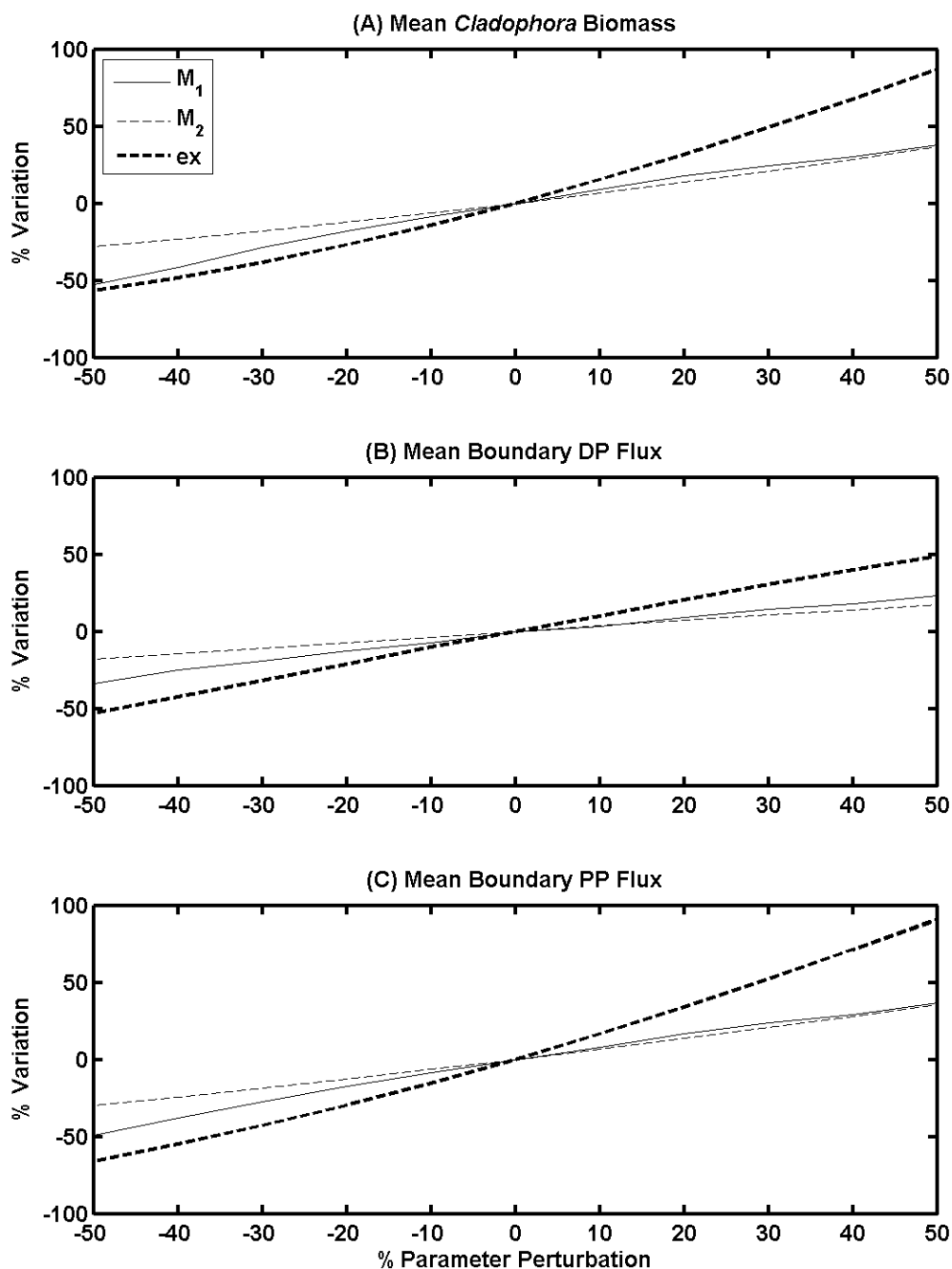


Figure 3.13: Response variation of model simulated A) mean *Cladophora* biomass, B) mean, net boundary, or cross-shore, dissolved phosphorus flux, and C) mean, net boundary particulate phosphorus flux as a function of perturbations of the mussel model parameters M_1 , M_2 , and ex (see Table 3 for parameter descriptions and units) from -50% to +50% of the base simulation values (see Table 6 for specific response variation values). The horizontal axis is the same in all three figures and is labeled beneath C.

except for the trapping of PP by sedimentation and reintroduction by resuspension. Figure 3.14 presents the same output as Figure 3.12, but for the no mussel simulation. Peak domain total phosphorus decreased from 229 mg P m⁻² with mussels to 98.6 mg P m⁻² without. Maximum *Cladophora* stored phosphorus dropped dramatically from 141.6 mg P m⁻² with mussels to 33.2 mg P m⁻². The mean boundary fluxes of PP and DP (Fig. 3.14B) decreased substantially and reversed direction during June and September and June through September respectively. These changes indicate that the nearshore would be a source of phosphorus to Lake Michigan without mussels in every month except August. Whether or not the nearshore zone would be a source of P to the offshore without mussels is dependent on initial and boundary conditions which remained the same as for the realistic simulation. The drastic reduction and reversal in boundary, or nearshore-offshore P fluxes indicates the major role dreissenid mussels play in the nearshore zone.

Table 3.7 lists the percent change in mean model variables from the no mussel scenario to the realistic simulation representing the likely changes in the nearshore zone associated with the invasion and establishment of dreissenid mussels. These results show that mussels at observed densities cause there to be 37% more areal dissolved phosphorus, 21% less areal particulate phosphorus, 19% higher bottom PAR, 2.5 times as much *Cladophora* biomass with 4 times the seasonal *Cladophora* peak biomass. The presence of mussels also cause sedimentation rates to increase by a factor of 4.5 in the lower water column, and by 76% in the upper water column. Mussels also increase sediment stored areal PP by 72%. Model domain total phosphorus, accounting for suspended total phosphorus, *Cladophora* stored phosphorus, and sediment stored phosphorus, increased 145% due to mussels. These results provide substantial evidence

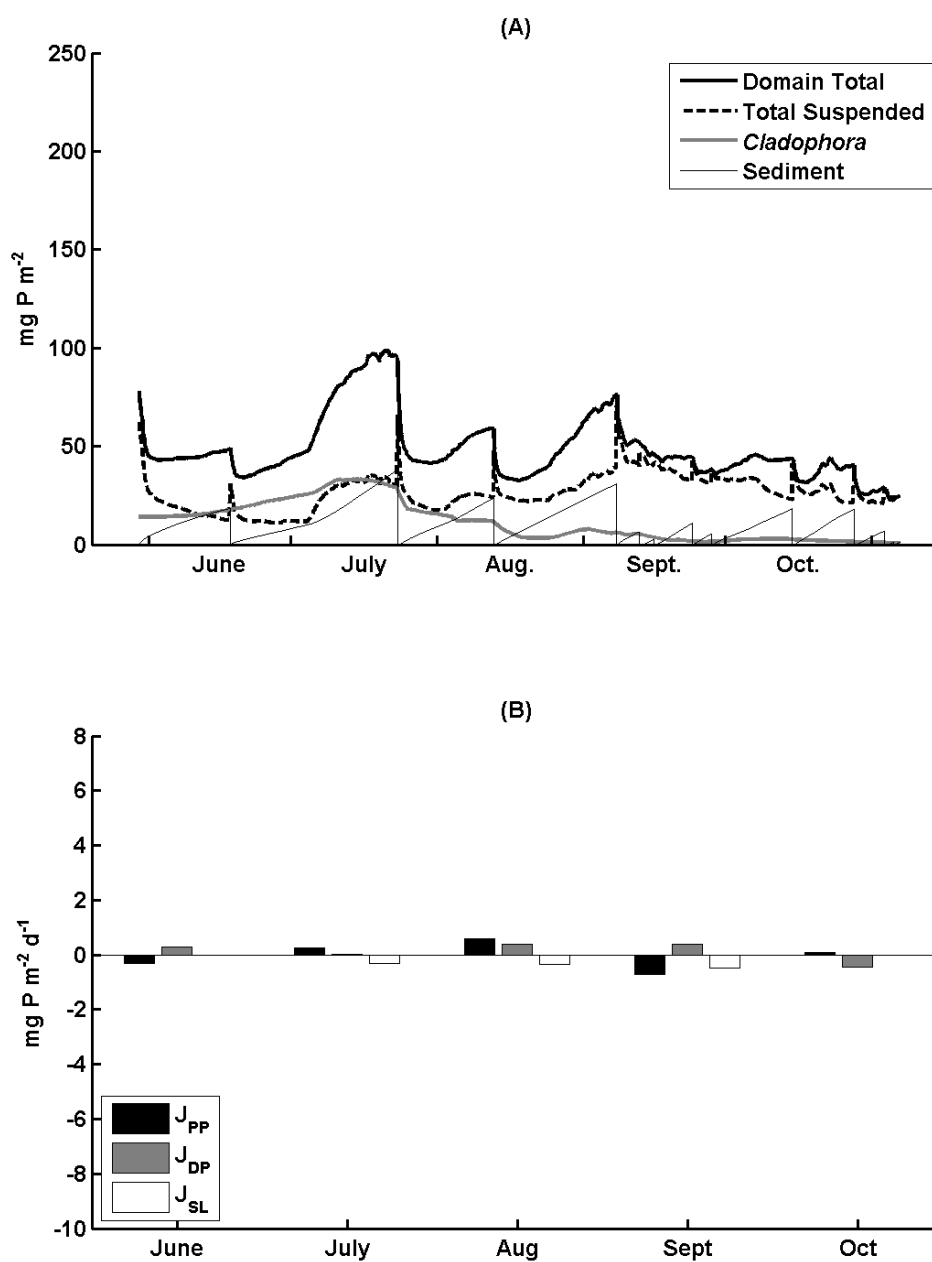


Figure 3.14: A) Model simulated phosphorus budget including all simulated phosphorus pools for the no mussel test scenario, and B) monthly average horizontal particulate (J_{PP}) dissolved (J_{DP}) and sloughed *Cladophora* (J_{SL}) fluxes into (positive) and out of (negative) the nearshore zone for the no mussel test scenario.

Table 3.7: The influence of mussels on the Lake Michigan nearshore zone calculated based on the differences between simulations with and without mussels. Positive values indicate an increase from the no mussel to mussel simulation and negative values indicate a decrease from the no mussel to the mussel simulation.

Modeled Parameter	Change Due to Nearshore Mussels
Areal water column dissolved phosphorus	37 %
Areal water column particulate phosphorus	-21 %
Sediment stored particulate phosphorus	76 %
Near bottom PAR	19 %
Summer Maximum <i>Cladophora</i> biomass	248 %
Summer Mean <i>Cladophora</i> biomass	399 %
Upper Water Column Sedimentation Rate	76 %
Lower Water Column Sedimentation Rate	446 %
Sedimentation Rate	72 %
Domain total phosphorus	145 %

for the validity of the nearshore shunt hypothesis proposed by Hecky et al. (2004) and agree with other modeling studies of Great Lake nearshore areas (Bocaniov et al., 2014; Cha et al., 2011).

3.5 Discussion and Conclusions

By comparing two simulations of the nearshore phosphorus flux model, one reflecting the current nearshore rocky environment, and another with mussels removed, it is clear that quagga mussels have both a direct and an indirect effect on nearshore P dynamics. Mussel grazing and P egestion in the form of feces and pseudofeces results in the accumulation of particulate P in the benthos, while mussel recycling of dissolved P, along with water clarification, promotes *Cladophora* growth and the retention of P in *Cladophora* tissue through late summer. The net result of this system is to produce a sink for offshore Lake Michigan phosphorus and a 145% greater, average domain total phosphorus concentration when mussels are present than when they are not. This result can be extrapolated to basin scale to estimate the influence of nearshore mussels on Lake Michigan as a whole.

Using the 2 km resolution Lake Michigan bathymetry grid, used for the NOAA, GLERL-Donelan wave model (Hawley et al., 2004) the area of the Lake Michigan southern basin less than 15 m deep is estimated to be $2.24 \times 10^9 \text{ m}^2$. Using a rough estimate of 12% of the lake nearshore covered in rocky substrate (Waples et al., 2005) reduces the area of nearshore zone associated with dreissenid mussels to $2.68 \times 10^8 \text{ m}^2$. The NPFM predicts an approximate total domain phosphorus increase of 150 mg P m^{-2} from May 30 to July 23, 2013. If all of the phosphorus accumulated in the nearshore zone is sourced from the Lake Michigan offshore pelagic and that phosphorus is assumed to be

permanently lost from the offshore, such as in the form of sloughed *Cladophora* accumulation and burial on beaches, than there would be a loss of 40 metric tons of phosphorus from the lake offshore to the nearshore each summer.

Multiplying the mean, southern basin, total phosphorus concentration (calculated using depth averaged measurements collected by the EPA aboard the Lake Guardian during their spring monitoring cruises on Lake Michigan from 2006 to 2012) by an estimated volume of the Lake Michigan southern basin: 2324 km³ (Chapra and Dolan, 2012), produces an estimated 7000 metric tons of phosphorus in the Lake Michigan southern basin with an approximate range of 5500 to 8500 metric tons. The average southern basin total phosphorus load from 1994 to 2008 was estimated to be 1921 metric tons per year (Dolan and Chapra, 2012). The impact of rocky nearshore areas covered with dreissenid mussels and *Cladophora* algae, therefore, represents only 2.1% of the river TP loading to the lake and only 1% of the 2006 to 2012 variation in annual mean TP mass. If the net flux of phosphorus from the offshore to the nearshore is extended to the entire nearshore zone, rather than the estimated 12% associated with rocky substrate, the nearshore removes 335 metric tons of phosphorus from the offshore which is 17% of the mean annual load and 11% of the inter-annual variability. Although the NPFM provides evidence supporting the nearshore shunt hypothesis, this analysis indicates that the influence of the nearshore is small compared to the total loading to the lake and the inter-annual variability of basin total phosphorus. The colonization of dreissenid quagga mussels in the Lake Michigan profundal zone and their expansion to large densities there (Karatayev et al., 2014; Nalepa et al., 2010; Vanderploeg et al., 2010) may have played a more important role in the observed changes in the Lake Michigan offshore zone than

the nearshore shunt during this period (Chapra and Dolan, 2012; Mida et al., 2010; Pothoven and Fahnenstiel, 2013).

The cross shore phosphorus fluxes calculated by the NPFM are dependent on model domain P concentration, the observed P concentration at the 20m station and the cross shore current velocity. The assumption that any cross shore flow must be replaced with the opposite flow somewhere in the along shore direction to maintain a water mass balance in the nearshore leads to the cross shore current velocity effectively becoming a horizontal exchange coefficient. Under this assumption, the cross shore advection equation (Eq. 8 and 9) can be roughly equated with a horizontal diffusion equation,

$$|u| \frac{\partial P}{\partial x} \approx \frac{\partial}{\partial x} D_H \frac{\partial P}{\partial x} \quad (24)$$

where, u is the cross shore current velocity (m s^{-1}), x is the cross shore length scale (1000 m) and D_H is a horizontal turbulent diffusion coefficient ($\text{m}^2 \text{s}^{-1}$). Multiplying the absolute value of the cross shore current velocity range (~ 0 to 0.05 m s^{-1}) by the cross shore length scale of the model ($dx = 1000 \text{ m}$) produces a range of D_H values: ~ 0 to $50 \text{ m}^2 \text{s}^{-1}$ with a median of $7.7 \pm 7 \text{ m}^2 \text{s}^{-1}$. Using the unstructured grid, 3D Finite-Volume Coastal Ocean Model (FVCOM) with a large eddy simulation approach, Bootsma and Liao (2013) found mean simulated horizontal diffusion coefficients for the Lake Michigan nearshore during August 2009 on the order of 0.1 to $0.3 \text{ m}^2 \text{s}^{-1}$. Based on offshore dye experiments, the horizontal diffusivity in the epilimnion of Lake Ontario was found to be on the order of $10 \text{ m}^2 \text{s}^{-1}$ for 1 km diffusion scales (Murthy, 1976). These measurements compared well with similar measurements in the ocean (Okubo, 1971). Horizontal diffusivity in the nearshore zone of Lake Geneva, Switzerland was found to be in the

range of 0.01 to 1 m² s⁻¹ using current measurements and the integral time scale approach (Lemmin, 1989). Colbert and Hammond (2007) used a 2D model of surface water radium to evaluate cross shore transport in the coastal zone of San Pedro Bay, CA. The mean horizontal diffusivity for summer time conditions was 1.4 ± 0.4 m² s⁻¹, and it was found that horizontal diffusivity increases with distance from shore. A cross shore increase in cross shore mixing is likely to occur in the Great Lakes as well due to the structure of the nearshore boundary layer and the transition from alongshore currents closer to shore to oscillating currents associated with internal waves further offshore (Murthy and Dunbar, 1981). Further research on the importance of upwelling events on cross shore transport relative to horizontal eddy transport may provide needed insight into cross shore transport in the Great Lakes as it has in other coastal upwelling systems such as the California Current System along the US west coast (Combes et al., 2013). The mean, effective diffusion rate in the NPFM for the 2013 season is higher, but on the same order of magnitude as direct measurements or calculated horizontal diffusivities in Lake Michigan and other lake and coastal environments. Application of the NPFM in a lake wide, 3D hydrodynamic model would likely provide accurate cross shore P flux estimates due to the inclusion of spatially variable diffusion and advection as well as inclusion of depth and along shore biological heterogeneity.

Additional observational work is required to fully understand the influence of nearshore vertical turbulent mixing on the nearshore ecosystem. Attention should be paid to the influence of currents and wave orbital motions on mixing rates and the influence of benthic roughness properties such as rocky topography and *Cladophora* mat roughness. It is assumed that mussel shell length is the dominant factor influencing near bottom

roughness, however, the *Cladophora* mat may also play an important, if not dominant role in near bottom diffusivity (Dodds et al., 2014; Escartín and Aubrey, 1995; Nepf, 2012). *Cladophora* mat height changes throughout the season based on *Cladophora* growth, sloughing, and senescence (Depew et al., 2011) and will likely have a variable influence on near bottom mixing throughout the summer. Without validation of the model vertical diffusion parameters it is not clear whether mixing is simulated at the correct rate. Near-bottom mixing has been shown to substantially influence *Cladophora* phosphorus uptake at short time scales and is critical to the accurate simulation of the nearshore environment (Bootsma and Liao, 2013).

Near bottom turbulent mixing coefficients for a nearshore zone in northeastern Lake Michigan were calculated using near-bottom profiles of SRP by Dayton et al., (2014). Turbulent diffusion coefficients were found to be on the order of 1×10^{-5} to 1×10^{-3} $\text{cm}^2 \text{s}^{-1}$ during calm periods, coincident with large SRP gradients in a 30 cm near the bottom layer, and diffusion coefficient of $1 \text{ cm}^2 \text{s}^{-1}$ during turbulent conditions. This range is substantially lower than the near bottom turbulent diffusion coefficient calculated in this study (Fig. 3.5E) with a season mean of $\sim 3 \text{ cm}^2 \text{s}^{-1}$ and values rarely below $0.1 \text{ cm}^2 \text{s}^{-1}$. Liao et al., (2009) used particle imaging velocimetry technology at the Lake Michigan bottom near the 9m monitoring station to measure particle motion and calculated a turbulent mixing profile on Sept. 7, 2007. Their observations indicated that the turbulent diffusivity was on the order of $1 \text{ cm}^2 \text{s}^{-1}$ at 5 cm above the lake bottom during moderate current and wave conditions. Turbulent diffusion above mussel beds has been found to be approximately $1 \text{ cm}^2 \text{s}^{-1}$ on average in shallow marine systems (Petersen et al., 2013; Saurel et al., 2013), as well as within algal mats studied in the lab under

realistic current conditions (Escartín and Aubrey, 1995). Agreement with these studies provides confidence in the near bottom turbulent diffusion coefficient range used in the NPFM, however, direct, site specific, validation is still necessary to fully quantify the relationships between near bottom mixing, SRP concentration, mussel grazing, excretion, and *Cladophora* SRP uptake in the near bottom layer.

A simple test scenario using the NPFM was conducted to determine the influence of vertical mixing on *Cladophora* biomass in the nearshore near bottom layer. The vertical diffusivity used to calculate vertical phosphorus fluxes between the bottom model layer and the lower water column layer were set to a range of constant values from $10 \text{ cm}^2 \text{ s}^{-1}$ to $0.001 \text{ cm}^2 \text{ s}^{-1}$ in two cases. In the first case, the constant diffusivities were applied to both particulate phosphorus and dissolved phosphorus vertical flux calculations and the second case they were applied to dissolved phosphorus alone and the vertical particulate phosphorus flux calculation retained the original calculated diffusivity values used in the base simulation. Model simulated maximum *Cladophora* biomass for the 2013 simulation period was compared between the two series of test scenarios (Figure 3.15). When the constant vertical diffusivity range was applied to just DP and not PP the NPFM predicted that maximum *Cladophora* biomass would go up with decreasing vertical mixing reflecting the accumulation of near bottom DP due to mussel excretion and little dilution with the over lying water column. In contrast, when the diffusivity range was applied to both DP and PP, the maximum *Cladophora* biomass declined with decreased vertical mixing. Based on previous modeling studies it was thought that *Cladophora* biomass would increase when vertical mixing decreases, as shown the first

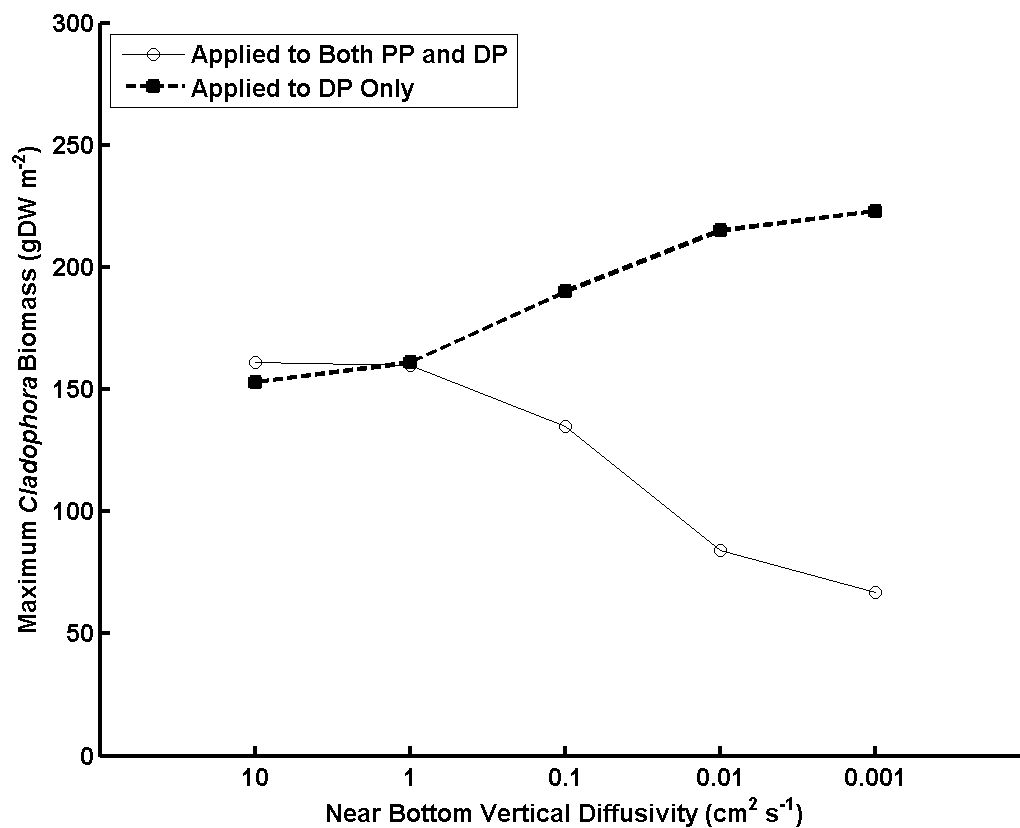


Figure 3.15: Maximum *Cladophora* biomass simulated using constant vertical diffusivities for the calculation of vertical fluxes of particulate phosphorus (PP) and dissolved phosphorus (DP) between the bottom layer and the lower water column layer. The constant diffusivities were applied to both PP and DP (white circles and line) and DP alone (black squares and dashed line). In the latter case, the base simulation diffusivity was used to calculate PP fluxes.

scenario (Bootsma and Liao, 2013). This simple model experiment demonstrates the importance of vertical mixing controlling the delivery of food, in the form of particulate phosphorus, to the near bottom layer. When mussels run out of food during long periods of low mixing, their phosphorus excretion rate declines (Bootsma and Liao, 2013; Johengen et al., 2013) reducing phosphorus available for *Cladophora* in the near bottom layer and in turn reducing *Cladophora* growth. In addition, under low mixing conditions mussels are not able to clear the water column of particulate material and increase light at the bottom, further limiting *Cladophora* growth. The results of this analysis indicate that there may be an ideal vertical mixing rate and duration of this mixing rate in the nearshore near bottom layer which supports *Cladophora* growth at maximum levels. Interestingly, the maximum *Cladophora* biomass simulated using the 10 and 1 $\text{cm}^2 \text{s}^{-1}$ constant diffusivities in both scenarios (Fig. 3.15) were very similar to the base model simulation ($\sim 157 \text{ gDW m}^{-2}$, Fig. 3.8A) which had a mean diffusivity of $\sim 3 \text{ cm}^2 \text{ s}^{-1}$ between the bottom layer and lower water column layer. This suggests more work is needed to understand the influence of the duration of mixing rates on *Cladophora* growth. The near bottom SRP gradients observed by Dayton et al. (2010) and their estimates of the duration for which these periods last in the Lake Michigan nearshore zone would substantially influence *Cladophora* growth further highlighting the importance of this subject for future observational and modeling research. It is clear that the application of a model of the nearshore zone incorporating dreissenid mussels and *Cladophora* is a useful and necessary tool for identifying and quantifying the critical relationship between vertical mixing, mussel phosphorus recycling and *Cladophora* growth.

There are a several possible reasons why the model over predicts sediment accumulation and sedimentation rate when compared to sediment trap observations. First, vertical mixing rates may have been too high during brief or prolonged periods allowing particles to mix through the vertical layers more rapidly than in reality. Because the simulated sediment traps were calculated as the accumulated PP passing through the vertical layer boundaries, enhanced vertical mixing may have resulted in high simulated “sedimentation” rates. Second, using sediment traps in the nearshore zone likely produces low biased measurements of particle accumulation rates as periodically strong nearshore currents will bow the suspended sediment trap apparatus down current causing limited particle collection (Buesseler et al., 2007). Third, algal growth on the sediment traps themselves may have interfered with particle collection reducing sediment accumulation in the sediment traps relative to that which may have occurred around the traps.

To our knowledge, this is the first attempt to simulate the effects of dreissenid mussels and *Cladophora* on nearshore phosphorus dynamics. Although the model accuracy metrics and sensitivity tests for the 2013 summer and fall simulation suggest there is scope for model improvement, the majority of the state variable output is well within the top 50th percentile of the accuracy values of aquatic biogeochemical models reported by Arhonditsis and Brett (2004), giving us confidence that the model can be used to explore mechanisms controlling nearshore nutrient and energy dynamics, even if at a general level. Further simulations of different nearshore environments with variable benthic habitat and hydrodynamics would help to fine tune and validate the model. Improvements to model accuracy could be made by adding complexity to sediment dynamics, including microbial and invertebrate impacts on sediment phosphorus fluxes.

Accounting for water column biological processes may also lead to improved model accuracy, although it is unlikely to alter the general conclusions reached here. This model can easily be incorporated into 3D biogeochemical models of Lake Michigan (e.g. Pauer et al., 2011) which would help to assess the effect of nearshore processes, including mussel grazing and *Cladophora* growth, on the lake as a whole.

CHAPTER 4

MODELING LAKE MICHIGAN NEARSHORE CARBON DYNAMICS

Abstract:

A dynamic carbon and phosphorus model was used to simulate the Lake Michigan nearshore ecosystem near Milwaukee, WI. The model was a 9.2 m deep, single box model that simulated water column dissolved phosphorus, particulate carbon in the form of phytoplankton and particulate detritus, dissolved inorganic carbon (DIC), *Cladophora* algae, and quagga mussels (*Dreissena bugensis*). The model allows for CO₂ exchange across the air-water interface and the horizontal exchange of particulate material, dissolved phosphorus and DIC between the nearshore and offshore zones. Model simulation output accuracy was evaluated against measurements taken at a monitoring station in the model simulation domain. The model was shown to adequately simulate surface water *p*CO₂, dissolved phosphorus, particulate carbon concentrations, *Cladophora* biomass, *Cladophora* tissue phosphorus content, and benthic areal phosphorus storage through the 2013 summer and fall seasons. Model error was attributed to the simplicity of the hydrodynamic framework of the model. In agreement with empirical observations, model simulations indicate that the nearshore zone is net autotrophic due to the high, net production of benthic *Cladophora* associated with their high tissue C:P ratio, mussel recycled phosphorus and water column clearing increasing light at depth. Phytoplankton production was found to be nearly insignificant in comparison to that of *Cladophora* and *Cladophora* production regularly surpassed mussel respiration. The influence of dreissenid mussels on nearshore algal dynamics was evaluated by comparing model output under scenarios with and without quagga mussels.

In the absence of mussels, mean *Cladophora* biomass decreased 89% and mean phytoplankton concentration increased 49%, and net growth rates for *Cladophora* and phytoplankton both decreased. Model results suggest that mussels support a net autotrophic nearshore ecosystem in Lake Michigan during the summer, with the majority of the primary production occurring in the nearshore benthos.

4.1 Introduction

The pelagic zone of Lake Michigan has become clearer and less productive over the last three decades (Fahnenstiel et al., 2010b; Mida et al., 2010), changes which have been attributed to the filter feeding of dreissenid mussels (Higgins and Vander Zanden, 2010; Kerfoot et al., 2010; Vanderploeg et al., 2010). There have been similar changes in the Lake Michigan nearshore zone (Chapter 1), where productivity has shifted from the water column to the benthos with the recent resurgence of *Cladophora* in the near bottom layer (Auer et al., 2010; Higgins et al., 2005b). Increased *Cladophora* growth in the nearshore zone is attributed to both nearshore and offshore dreissenid mussels and their ability to increase water clarity while also increasing available phosphorus (Chapters 1 and 2).

The shift in nearshore production from the water column to the benthos represents a major change in the autotrophic structure of the nearshore (Higgins et al., 2014; Lowe and Pillsbury, 1995; Malkin et al., 2010; Zhu et al., 2006). In Lake Ontario during the summer, *Cladophora* has become the dominant primary producer in nearshore with areal rates equal to or greater than nearshore phytoplankton (Malkin et al., 2010). Davies and Hecky (2005) showed that littoral benthic photosynthesis rates on rocky strata associated with *Cladophora* and dreissenid mussels in the Lake Erie nearshore were among some of

the highest in freshwater lakes and likely surpass pelagic rates in generally eutrophic Lake Erie. In addition, *Cladophora* can exude large amounts of its fixed carbon as dissolved organic carbon (DOC) and may enhance heterotrophic, microbial production in the nearshore (Wyatt et al., 2014a; Wyatt et al., 2014b). Recent evidence in Lake Michigan has shown that nearshore energy subsidies may subsidize the pelagic food web, partially offsetting the decreasing pelagic primary production (Turschak et al., 2014). Based on a meta-analysis of studies focused on invasive dreissenid mussels, Higgins and Vander Zanden (2010) showed that the systematic impact of dreissenid mussels is to shift nutrient and energy flow in lakes from pelagic to littoral, benthic pathways. The growth and production rates of *Cladophora* in the nearshore zones of the Great Lakes provides clear evidence of this shift and the possible influence of dreissenid mussels on lake autotrophic structure (Higgins et al., 2014).

Nutrient enrichment and foodweb structure of freshwater lakes has been shown to influence the carbon flux between the lake and the atmosphere (Cole et al., 2000; Schindler et al., 1997). Although the direct influence of dreissenid mussels on the Lake Michigan foodweb remains a matter of correlation and coincidence (Bunnell et al., 2013, 2009b; Fahnenstiel et al., 2010a), the observed shift in the nearshore zone from the dominance of water column to benthic energy pathways suggests that a large population of filter feeders in the Great Lakes may dramatically change lake carbon cycling. As a predominantly oligotrophic system (Mida et al., 2010), with declining allochthonous phosphorus input (Dolan and Chapra, 2012) the Lake Michigan carbon cycle as a whole could be similar to that of Lake Superior which has been considered net heterotrophic (Atilla et al., 2011; Biddanda et al., 2001; Urban et al., 2005). The ability of dreissenid

mussels to rapidly filter the nearshore water column, increase light penetration, and efficiently recycle phosphorus in the near bottom layer indicates that they are capable of increasing lake primary production (Cecala et al., 2008; Higgins et al., 2014) suggesting that their net influence on the nearshore trophic status is a function of the sum of their own, heterotrophic, respiration and the primary production they support.

With the goal of quantifying the influence of dreissenid mussels on nearshore energy and nutrient dynamics in Lake Michigan, the nearshore phosphorus flux model (presented in Chapter 2) was modified to include carbon dynamics, here referred to as the nearshore carbon and phosphorus model (NCPM). Based on the studies conducted in Lake Ontario and Lake Erie (Davies and Hecky, 2005; Malkin et al., 2010), it was hypothesized that *Cladophora* production is much larger than that of phytoplankton in the nearshore zone of Lake Michigan and that dreissenid mussel water column clearing and phosphorus recycling has created a net autotrophic, nearshore ecosystem due to their support of *Cladophora* growth in the near bottom layer and the ability of *Cladophora* to grow with a high tissue C:P ratio (Bootsma et al., 2012; Higgins et al., 2008b; Malkin et al., 2010).

4.2 Data Collection and Sampling Methods

During the spring, summer, and fall of 2013 air and surface water $p\text{CO}_2$ were measured using an autonomous CO_2 monitoring system mounted on a buoy moored in a region of the Lake Michigan nearshore zone dominated by rocky substrate (bottom depth = 9 m). Air and water from approximately 1m above and 0.5m below the water surface were sampled for 10 minutes every hour. The mean of each 10 minute measurement period provided an hourly $p\text{CO}_2$ time series for air and water. Lake water was sampled

using 0.25 inch plastic tubing that was insulated with foam pipe insulation to prevent temperature change during sampling. Water was pumped through the CO₂ system and returned to the lake using a peristaltic pump. Within the CO₂ system water passed through a gas equilibrator with a semi permeable, gas membrane (Mini Modules Membrane Contractors, item: G543, batch: P0106404 – 1L.7475). Air in the equilibrator head space was pumped in the opposite direction of the water flow with an electric air pump and followed a closed loop through the system to allow for 95% equilibration in 90 seconds. CO₂ partial pressure, normalized to 1 atmosphere, was measured using a LICOR (LI-820) CO₂ infrared gas analyzer. Water temperature was measured using an in-line thermistor. The flow speed of water through the CO₂ system was monitored during operation. For periods during which flow speeds dropped below normal levels either due to system malfunction or water intake clogging the data was not included in analyses. Air was desiccated before entering the LICOR to prevent IR light absorption due to water vapor. Measurements were remotely downloaded from a CR10X data logger using radio communication with the buoy. For further collection and analysis methods along with raw data collected at the 9m station during 2013 see Appendix A. Aqueous CO₂ concentrations were calculated from partial pressure measurements using Henry's Law,

$$[CO_2] (mol L^{-1}) = K_H (mol L^{-1} atm^{-1}) \cdot pCO_2(atm) \quad (1)$$

where K_H is Henry's constant. Measured pCO_2 values were corrected for atmospheric pressure by multiplying by the ratio of measured atmospheric pressure to 1 atm = 101325 pa. The pK_H was calculated as the best fit polynomial function of temperature based on data presented in Stumm and Morgan (1981) for freshwater,

$$pK_H = 8 \cdot 10^{-5}T^2 + 0.0165T + 1.1082 \quad (2)$$

where T is the water temperature at the lake surface in °C. Two YSI sondes were deployed at the 9m station, one suspended in the water 1 m below the surface and the other suspended just above the lake bottom on a tripod, to measure water temperature every half hour. Sonde measured temperatures were used as inputs for the NCPM.

A CO₂ monitoring system, similar to that deployed on the 9m station buoy, was deployed aboard the vessel of the opportunity, the Lake Express Car Ferry, throughout its 2013 cruise season. The ferry docks in the southern portion of the Milwaukee Harbor and conducts regular lake crossings to Muskegon, MI where it enters the Muskegon channel and docks in Muskegon Lake (Figure 4.1). The CO₂ system is programmed to monitor the ferry's speed and location using a GPS mounted on the ferry's starboard, stern rail. Water sampling began after the ferry reached a speed of 12 knots which put the ferry offshore of the Milwaukee Harbor breakwall and the Muskegon Lake channel, minimizing harbor and river water sampling. Water samples were collected from the ferry's sea chest which, at speed, is quickly refreshed with surface lake water allowing for accurate measurements of surface water $p\text{CO}_2$ and virtually no change in water temperature. The ferry CO₂ system was regularly calibrated using the same method as the buoy CO₂ system, although little or no drift during deployment was observed.

Dissolved phosphorus (DP) and particulate phosphorus (PP) concentrations were measured at both the 9m and 20m monitoring stations as described in Chapter 2.

Chlorophyll a ($\text{Chl } a$) and particulate carbon (PC) concentrations were also measured at the 9m and 20m stations using the same, bulk water sampled for DP and PP . Water samples were filtered through ash free Whatman GF/F filters. $\text{Chl } a$ sample filters were stored frozen and in the dark until being analyzed fluorometrically. Filters used to

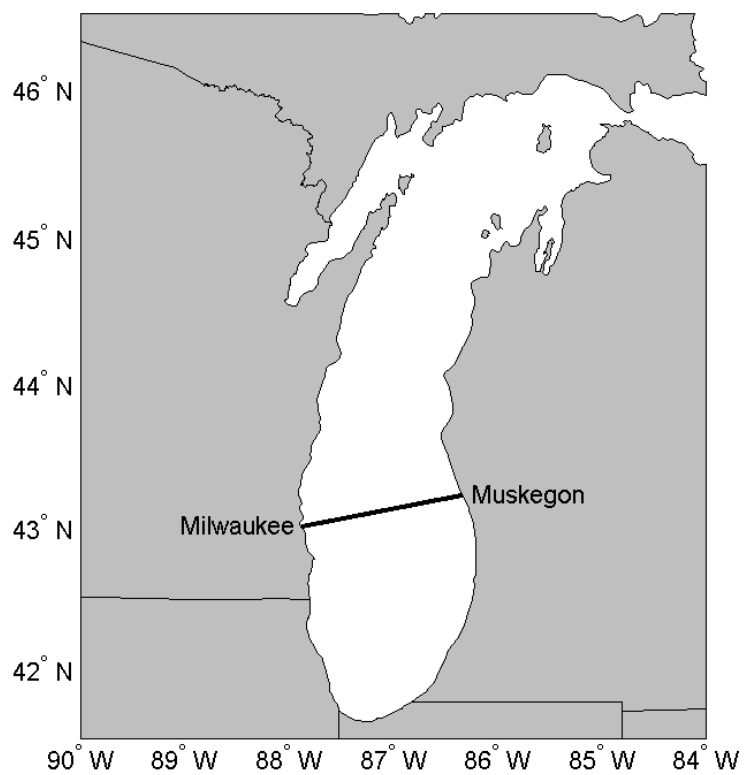


Figure 4.1: Map of Lake Michigan and the Lake Express Car Ferry route (black line) from Milwaukee, WI to Muskegon, MI as labeled.

measure particulate carbon were dried in desiccators and folded into 30 mm tin disks. Sample carbon content was measured by Washington State University Stable Isotope Core Laboratory in Pullman, WA. For a detailed description of the methods used to measure phosphorus, Chl *a*, and PC concentrations see Appendix A.

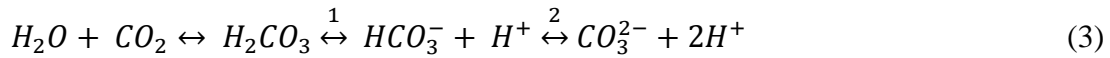
4.3 Model Description

The NCPM was used to simulate the 2013 summer and fall seasons as in Chapter 2. The accuracy of model output was evaluated against measurements taken at the 9m station, while initial and boundary conditions were determined using measurements from the 20m station. Model test simulations were conducted to evaluate model parameterizations and simplifying assumptions, as well as to test the influence of dreissenid mussels on nearshore carbon and phosphorus dynamics. The NCPM consists of a single nearshore, 1D box model, which was run with a time step of 2 hours. Not including vertical stratification and mixing may add error to the nearshore model simulation as vertical mixing rates have been shown to influence both dreissenid mussel clearance rates (Ackerman et al., 2001; L. Boegman et al., 2008; Edwards et al., 2005), and near bottom nutrient gradients associated with mussel soluble reactive phosphorus (SRP) excretion (Dayton et al., 2014). This potential error will be discussed and evaluated based on comparison between the NCPM and NPFM output.

The box model has a horizontal scale of 1000 m and a vertical depth of 9.2 m. As in Chapter 2, the horizontal cross shore scale of the model domain results in a depth change from 6 to 14 m. For simplicity it is assumed that the domain depth is a constant 9.2m. The NCPM water column was based on the nutrient, phytoplankton, zooplankton, and detritus (NPZD) model used by Chen et al. (2002) for the Lake Michigan pelagic.

The model excludes zooplankton, bacteria, and silica dynamics due to the lack of data and parameterizations for these variables in the nearshore of Lake Michigan. The NCPM conceptual diagram (Figure 4.2) illustrates the fluxes and pools of carbon and phosphorus simulated by the model. The model state variables are listed and described in Table 4.1.

The NCPM calculated the DIC equilibrium as:



$$DIC = CO_2 + HCO_3^- + CO_3^{2-} \quad (4)$$

where it is assumed that $CO_2 + H_2CO_3 \approx CO_2$ due to the rapid disassociation of H_2CO_3 (Stumm and Morgan, 1981). The equilibrium relationships based on Eq. 3 were:

$$K_1 = \frac{[H^+][HCO_3^-]}{[CO_2]} \quad (5)$$

$$K_2 = \frac{[H^+][CO_3^{2-}]}{[HCO_3^-]} \quad (6)$$

where K_1 and K_2 are the equilibrium constants for the equilibrium reactions 1 and 2 in Eq. 2, and pK_1 and pK_2 were calculated as the best fit polynomial function of water temperature based on data presented in Stumm and Morgan (1996) for freshwater,

$$pK_1 = 8 \cdot 10^{-7}T^3 + 0.0002T^2 - 0.0133T + 6.5791 \quad (7)$$

$$pK_2 = 0.0001T^2 - 0.0146T + 10.625 \quad (8)$$

where T is the water temperature in °C. To solve the system of Eqs. 4-6 it is assumed that the lake alkalinity (Alk) is constant where,

$$Alk = [HCO_3^-] + 2[CO_3^{2-}] - [H^+] + [OH^+] \quad (9)$$

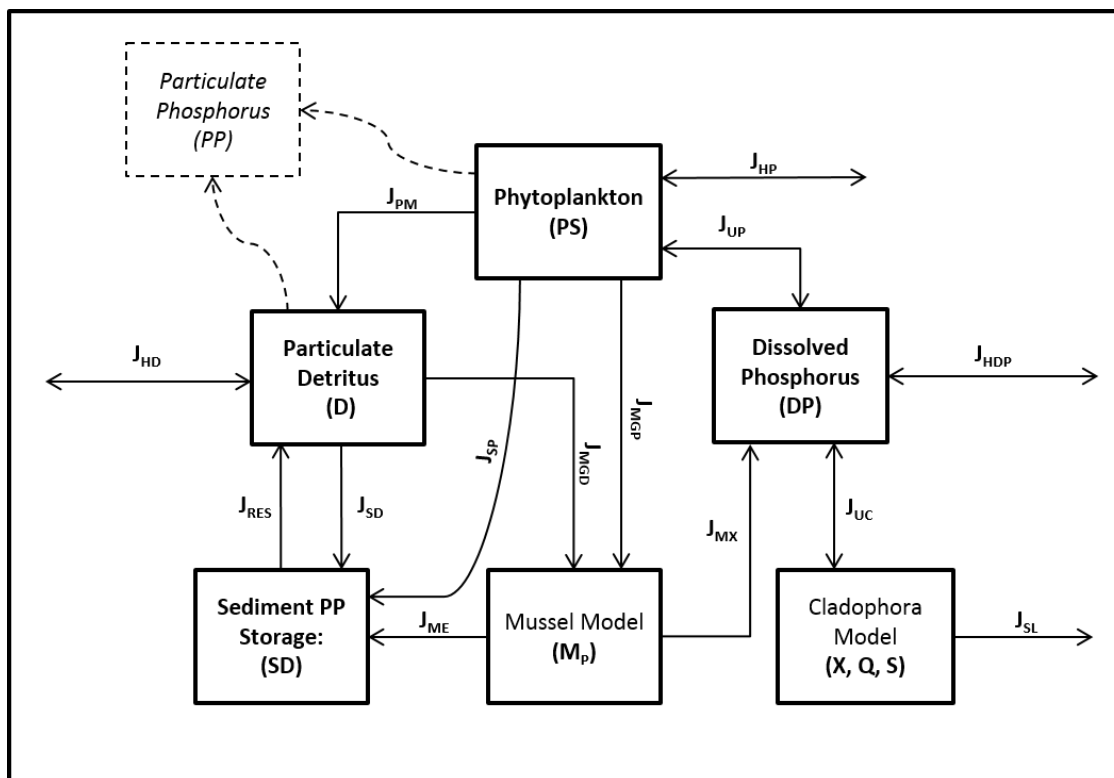


Figure 4.2: Conceptual diagram of the NCPM showing pools of particulate carbon and dissolved phosphorus and fluxes of carbon and phosphorus. Particulate phosphorus is calculated as the sum of suspended particulate carbon pools: phytoplankton and particulate detritus. DIC and the influence of biology on DIC is not shown.

Table 4.1: Model carbon and phosphorus variables, their units, and descriptions.

Variable:	Units:	Description:
PS	$\mu\text{mol C L}^{-1}$	Phytoplankton concentration
D	$\mu\text{mol C L}^{-1}$	Suspended particulate detritus concentration
DIC	mol C L^{-1}	Dissolved inorganic carbon concentration
SD	mmol C m^{-2} and mg P m^{-2}	Sediment stored detritus
DP	$\mu\text{g P L}^{-1}$	Dissolved phosphorus concentration
PP	$\mu\text{g P L}^{-1}$	Suspended particulate phosphorus concentration
Mp	$\text{L mussel}^{-1} \text{d}^{-1}$	Mussel clearance rate
X	gDW m^{-2}	<i>Cladophora</i> biomass
Q	mg P gDW^{-1}	<i>Cladophora</i> tissue phosphorus content
S	mg P m^{-2}	<i>Cladophora</i> stored phosphorus

The alkalinity of Lake Michigan water received from an intake pipe located at 20m depth approximately 1 km south of the 20m station has been measured by Milwaukee Water Works since the late 1980s. Data collected between 1987 and 1999 are available through the Waterbase website managed by the School of Freshwater Sciences at UW-Milwaukee (<http://www.waterbase.glwi.uwm.edu/linnwood/>). The median alkalinity for the 1987 to 1999 period, measured as the concentration of CaCO₃, (converted using the relationship: 1 meq L⁻¹ = 50 mg CaCO₃ L⁻¹; Wetzel, 2001), was 2.22 meq L⁻¹ with a consistent annual range of 2.1 to 2.4 meq L⁻¹. The constant Alk used in the NCPM model is set to the 2.22 meq L⁻¹ median value.

Any CO₂ flux from, or to, the atmosphere or biota represents a change in total DIC (Eq. 3 and 4) so that the mass balance of DIC is:

$$V \frac{d}{dt} DIC = J_{HDIC} A_X + J_{AWC} A_Z + J_{MXC} A_Z + J_{PC} A_Z + J_{CC} A_Z \quad (10)$$

where V is the volume of the model domain (1000m x 1000m x 9.2m), A_X is the area of the vertical face between the model domain and the lake offshore (1000m x 9.2m), A_Z is the horizontal area of the model domain (1000m x 1000m), and the sources and sinks of each variable (the fluxes indicated by J terms) are listed and described in Table 4.2. With Alk and DIC known at each model time step, a quartic equation can be solved (Stumm and Morgan, 1981) to obtain [CO₂]. For simplicity, an iterative approach was used to determine the hydrogen ion concentration, [H⁺], associated with any change in DIC, eliminating the need to solve the quartic equation. The technique determined the [H⁺] for the next time step based on 20,000 evenly spaced [H⁺] values, or guesses, between 0.5 and 3 times the previous [H⁺] value. The new [H⁺] was chosen as the value which

Table 4.2: Carbon and phosphorus fluxes calculated by the model, their units, and descriptions.

Flux Variable:	Units:	Description:
J _{HP}	mmol C m ⁻² s ⁻¹	Boundary, cross shore flux of phytoplankton
J _{HDP}	mg P m ⁻² s ⁻¹	Boundary, cross shore flux of dissolved phosphorus
J _{HD}	mmol C m ⁻² s ⁻¹	Boundary, cross shore flux of suspended particulate detritus
J _{PM}	mmol C m ⁻² s ⁻¹	Phytoplankton mortality flux to detritus
J _{UP}	mg P m ⁻² s ⁻¹	Net phytoplankton dissolved phosphorus uptake flux
J _{MGP}	mmol C m ⁻² s ⁻¹	Mussel phytoplankton grazing flux
J _{MGD}	mmol C m ⁻² s ⁻¹	Mussel detritus grazing flux
J _{MX}	mg P m ⁻² s ⁻¹	Mussel dissolved phosphorus excretion flux
J _{ME}	mg P m ⁻² s ⁻¹	Mussel detritus egestion flux to sediment
J _{SD}	mmol C m ⁻² s ⁻¹	Suspended particulate detritus settling flux
J _{SP}	mmol C m ⁻² s ⁻¹	Phytoplankton settling flux
J _{RES}	mmol C m ⁻² s ⁻¹	Resuspension flux of sediment stored detritus
J _{UC}	mg P m ⁻² s ⁻¹	Net <i>Cladophora</i> dissolved phosphorus uptake flux
J _{SL}	mg P m ⁻² s ⁻¹	<i>Cladophora</i> sloughing flux
J _{HDIC}	mmol C m ⁻² s ⁻¹	Boundary, cross shore flux of DIC
J _{AWC}	mmol C m ⁻² s ⁻¹	Boundary, air-water flux of CO ₂
J _{MXC}	mmol C m ⁻² s ⁻¹	Mussel respiration CO ₂ flux
J _{PC}	mmol C m ⁻² s ⁻¹	Net phytoplankton photosynthesis and respiration CO ₂ flux
J _{CC}	mmol C m ⁻² s ⁻¹	Net <i>Cladophora</i> photosynthesis and respiration CO ₂

minimized the error between the Alk guesses and the known constant Alk, where the Alk guesses were calculated by simultaneously solving Eq. 4 to 9,

$$[CO_2] = \gamma_0 DIC_{t+1} \quad (11)$$

$$[HCO_3^-] = \gamma_1 DIC_{t+1} \quad (12)$$

$$[CO_3^{2-}] = \gamma_2 DIC_{t+1} \quad (13)$$

where the subscript (t+1) indicates DIC at the next model time step calculated as Eq. 10,

and

$$\gamma_0 = \frac{[H^+]^2}{[H^+]^2 + K_1[H^+] + K_1K_2} \quad (14)$$

$$\gamma_1 = \frac{K_1[H^+]}{[H^+]^2 + K_1[H^+] + K_1K_2} \quad (15)$$

$$\gamma_2 = \frac{K_1K_2}{[H^+]^2 + K_1[H^+] + K_1K_2} \quad (16)$$

where K_1 and K_2 are calculated using Eqs. 7 and 8 (Stumm and Morgan, 1981).

The air-water flux of CO_2 was calculated using the bulk method,

$$J_{AWC} = k \cdot \sigma \cdot (pCO_{2,air} - pCO_{2,water}) \quad (17)$$

where k is the air-water CO_2 piston velocity, also known as the transfer velocity, σ is the solubility coefficient for CO_2 in freshwater which was calculated as a function of water temperature as in Wanninkhof (1992), and $pCO_{2,air}$ and $pCO_{2,water}$ are the air and water CO_2 partial pressures respectively. The air-water CO_2 transfer velocity has been studied in detail and has been a matter of debate in terms of its parameterization, the techniques used to determine those parameters, and the applicability of different parameterizations in

different aquatic and marine environments (Ho et al., 2011; Upstill-Goddard, 2006; Vachon and Prairie, 2013; Wanninkhof et al., 2009). In the nearshore zone of Lake Michigan it is critical to choose a k model that adequately represents the nature of the turbulent air-water interface due to fetch limiting conditions when wind is offshore. The baseline model used in the NCPM was the commonly used wind speed parameterization from Wanninkhof (1992):

$$k_1 = 0.31U_{10}^2 \cdot (Sc/600)^{-1/2} \text{ (cm hr}^{-1}\text{)} \quad (18)$$

where U_{10} is the wind speed at 10m above the surface in m s^{-1} , and Sc is the Schmidt number which is normalized to that of freshwater at 20°C (600). Sc was calculated for freshwater as a function of water temperature as in Wanninkhof (1992). Wind speed was measured by the 9m station buoy at a height of 3m above the water surface. To avoid the complexity of calculating the 10m wind speed, the calculation of which involves calculating the surface drag coefficient which is a function of surface waves and near surface atmospheric temperature gradients (Foreman and Emeis, 2010; Mahrt et al., 2003; Vickers and Mahrt, 2006), wind speed was collected from a NOAA maintained meteorological station 5.5 km south of the 9m station with an anemometer located at approximately 10 m above the water surface (<http://www.glerl.noaa.gov/metdata/mil/>).

To evaluate the effect of using k_1 on model accuracy, a test scenario was conducted with an additional k model from the literature. The bi-parameter model of Zhao and Xie (2010) includes both wind speed and wave height in a modified wind-sea Reynolds number parameterization,

$$k_2 = \min \left\{ \begin{array}{l} 6.81(U_{10}H_s)^{0.63} \\ 0.75(U_{10}^{1.89}) \end{array} \right\} \cdot (Sc/600)^{-1/2} \text{ (cm hr}^{-1}\text{)} \quad (19)$$

where min indicates that the minimum of the two calculated k values is used, U_{10} is the 10m wind speed in m s^{-1} , and H_S is significant wave height in m. Significant wave height implicitly accounts for fetch in that for offshore wind, regardless of magnitude, wave height will likely be small within a short distance from shore (Schilder et al., 2013; Vachon and Prairie, 2013). When wind is from the offshore, fetch is long and waves may become fully developed. In the Zhao and Xie (2010) model, k_2 , was shown to agree with other wind-based k models at different wave ages, including k_1 , and approaches a quadratic dependence on wind speed as the sea state becomes fully developed. The greatest diversion between the two occurs when wind speed is high and in the offshore direction producing small wave heights.

Suspended particulate carbon was simulated in the form of a single phytoplankton class (PS), suspended particulate detritus (D), and particulate detritus stored in the sediment (SD):

$$V \frac{d}{dt} PS = J_{HP}A_X + J_{UP}A_Z - J_{PM}A_Z - J_{MGP}A_Z - J_{SP}A_Z \quad (20)$$

$$V \frac{d}{dt} D = J_{HD}A_X + J_{PM}A_Z + J_{RES}A_Z - J_{MGD}A_Z - J_{SD}A_Z \quad (21)$$

$$\frac{d}{dt} SD = J_{SP} + J_{SD} + J_{ME} - J_{RES} \quad (22)$$

where V , A_X , and A_Z are the same as described previously and all of the J terms are listed and described in Table 4.2. Dissolved phosphorus (DP) is simulated as in the NPFM (Chapter 2) with the added interaction of phytoplankton uptake and respiration (J_{UP}) in the water column,

$$V \frac{d}{dt} DP = J_{HDP}A_X + J_{MX}A_Z - J_{UP}A_Z - J_{UC}A_Z \quad (23)$$

Particulate phosphorus was calculated based on the suspended particulate carbon concentration (PS + D) using a constant C:P mass ratio of 80 (207 molar) (Chen et al., 2002). A constant C:P ratio for both phytoplankton and particulate detritus is used for simplicity and the influence of this assumption on model accuracy is discussed. The value of 207 molar is close to the average of values found for suspended particulates, mussel feces, and sediment at a nearby 20m monitoring station south of the model domain in the nearshore of Lake Michigan (Bootsma et al., 2012; and analysis of unpublished data). Phytoplankton production is calculated as the net increase in phytoplankton carbon based on growth and respiration, excluding mortality. Phytoplankton growth is calculated as in Chen et al. (2002),

$$J_{UP} = V_{max}^{PS} \cdot \left(\frac{DP}{K_P + DP} \right) \cdot f(I) \cdot PS - r \cdot PS \quad (24)$$

where V_{max}^{PS} is the maximum growth rate of phytoplankton, DP is the dissolved phosphorus concentration, K_P is the half saturation constant for phytoplankton DP uptake, and $f(I) = e^{-K_e Z}$ where K_e is the light extinction coefficient calculated as a function of PP as in Chapter 2, Z is half the domain depth (4.6m), and r is the constant phytoplankton respiration rate used by Bierman and Dolan (1981). See Table 4.3 for model constants and parameters, their units, and descriptions.

Cladophora biomass, phosphorus uptake, tissue content, and areal storage were modeled as in Chapter 2 using the Great Lakes *Cladophora* Model (Tomlinson et al., 2010). *Cladophora* net production was calculated as the change in *Cladophora* stored carbon, estimated as a constant 30% of *Cladophora* dry biomass (Malkin et al., 2010), at each model time step, excluding sloughed biomass. The change in *Cladophora* biomass

Table 4.3: Model constants and parameters, their value, units, and descriptions.

Constant	Value	Units	Description
C:P	80 (207)	gC/gP (M)	Carbon to phosphorus ratio for phytoplankton
C:Chla	27	gC/gChla	Carbon to chlorophyll <i>a</i> ratio for phytoplankton
V_{max}^P	1.4	day ⁻¹	Maximum phytoplankton growth rate
K_P	3.1	μg P L ⁻¹	Half saturation constant for phytoplankton phosphorus uptake
r	0.05	day ⁻¹	Phytoplankton respiration rate
α_P	0.01	day ⁻¹	Phytoplankton mortality rate
L_{max}	0.176	day ⁻¹	Maximum <i>Cladophora</i> sloughing rate
vs	0.5	m day ⁻¹	Particulate phosphorus settling rate
τ_w	0.4	N m ⁻²	Benthic shear stress threshold for resuspension and sloughing
ex	0.80	---	Dreissenid mussel phosphorus and carbon recycling efficiency
μ_{max}	1.53	day ⁻¹	Maximum <i>Cladophora</i> growth rate
Q_0	0.05	P as %DW	Minimum <i>Cladophora</i> tissue phosphorus quota
X_{max}	800	gDW m ⁻²	Maximum <i>Cladophora</i> biomass density
ρ_{max}	4.5	%P day ⁻¹	Maximum <i>Cladophora</i> phosphorus uptake rate
K_C	125	μg P L ⁻¹	Half saturation constant for <i>Cladophora</i> phosphorus uptake
R_{max}	0.23	day ⁻¹	Maximum <i>Cladophora</i> respiration rate
T_{opt}	17	°C	Optimum water temperature for <i>Cladophora</i> sloughing
τ_{opt}	0.4	N m ⁻²	Benthic shear stress threshold for <i>Cladophora</i> detachment
M_1	0.633	---	Mussel pumping model scaling factor
M_2	0.074	---	Mussel pumping model exponential constant
α	0.2394	---	Light extinction model scaling factor
β	0.2848	---	Light extinction model power constant

was calculated as the net sum of growth, respiration and sloughing. Sloughing was excluded from the calculation of *Cladophora* production as it does not represent a change in carbon based on population photosynthesis or respiration.

It is assumed, as in the NPFM, that mussel biomass is at steady state, and that although it likely represents a major pool of carbon and phosphorus, at daily to monthly time scales the changes in the size of this pool are small relative to other fluxes in the nearshore zone. Quagga mussels were included the same way as in the NPFM with the added component of mussel respiration which was calculated assuming the same carbon recycling efficiency as phosphorus (0.80), where 80% of carbon consumed is respired as CO₂ and 20% is egested as particulate detritus into the sediment storage pool, *SD*. The same mussel carbon and phosphorus recycling efficiencies were used primarily to maintain the assumption of a constant particulate C:P ratio (excluding *Cladophora*) within the model. Analysis of unpublished data collected at a nearby 20m monitoring station south of the model domain during the study of Bootsma et al., (2012), however, suggests that this assumption may be valid. Based on replicate samples from September 10, 2009, the mean (\pm standard deviation) C:P ratios of mussel feces, 138 ± 4 molar, and of particulates suspended in the near bottom layer, 156 ± 10 molar, were not statistically different (two variable t-test, $p = 0.21$). This indicates that mussels recycled carbon and phosphorus at similar rates. In Chapter 2 it was found that the NPFM model was sensitive to the phosphorus recycling efficiency value and that further research is required to increase confidence in this value. To allow for comparison between Chapter 2 model output and that simulated with the NCPM, the 0.8 recycling efficiency value is retained.

Horizontal mass fluxes across the eastern model boundary were calculated as in Chapter 2 using depth averaged cross-shore current velocity. Depth average current velocity for the model domain was obtained from the Great Lakes Coastal Forecasting System nowcast in the Great Lakes Observing System archive (<http://glos.us/data-tools/point-query-tool-glafs>). DIC boundary concentrations were calculated using the $p\text{CO}_2$ time series measured aboard the Lake Express Car Ferry (Fig. 4.3). $p\text{CO}_2$ values were chosen as those closest to the 20 m isobath along the ferry's path which was approximately on the longitude line: W $87^\circ 51'$ (-87.85), 10 km south of the 20m station (Fig. 4.4). DIC was calculated from $p\text{CO}_2$ by calculating $[\text{CO}_2]$ (Eq. 1) and using the iterative approach described previously for solving Eq. 4-6 using the same constant Alk as the nearshore domain. Measured DP , PP , and Chl a from the 20m station were used to calculate the DP , PS , and D boundary concentrations. The boundary PS concentration was calculated using measured Chl a concentrations from the 20m station and a constant C:Chl a mass ratio of 27 representing the mean of those used by Chen et al. (2002) and White et al. (2012). The boundary D concentration was calculated as the difference between the PS concentration and the measured 20m station, surface PC concentration. The mean PC:Chl a mass ratio at the 9m and 20m stations during 2013 was 163.9. Comparison of this value to that of phytoplankton (27) indicates that particulate detrital carbon concentration was substantially larger than that of phytoplankton in the nearshore domain.

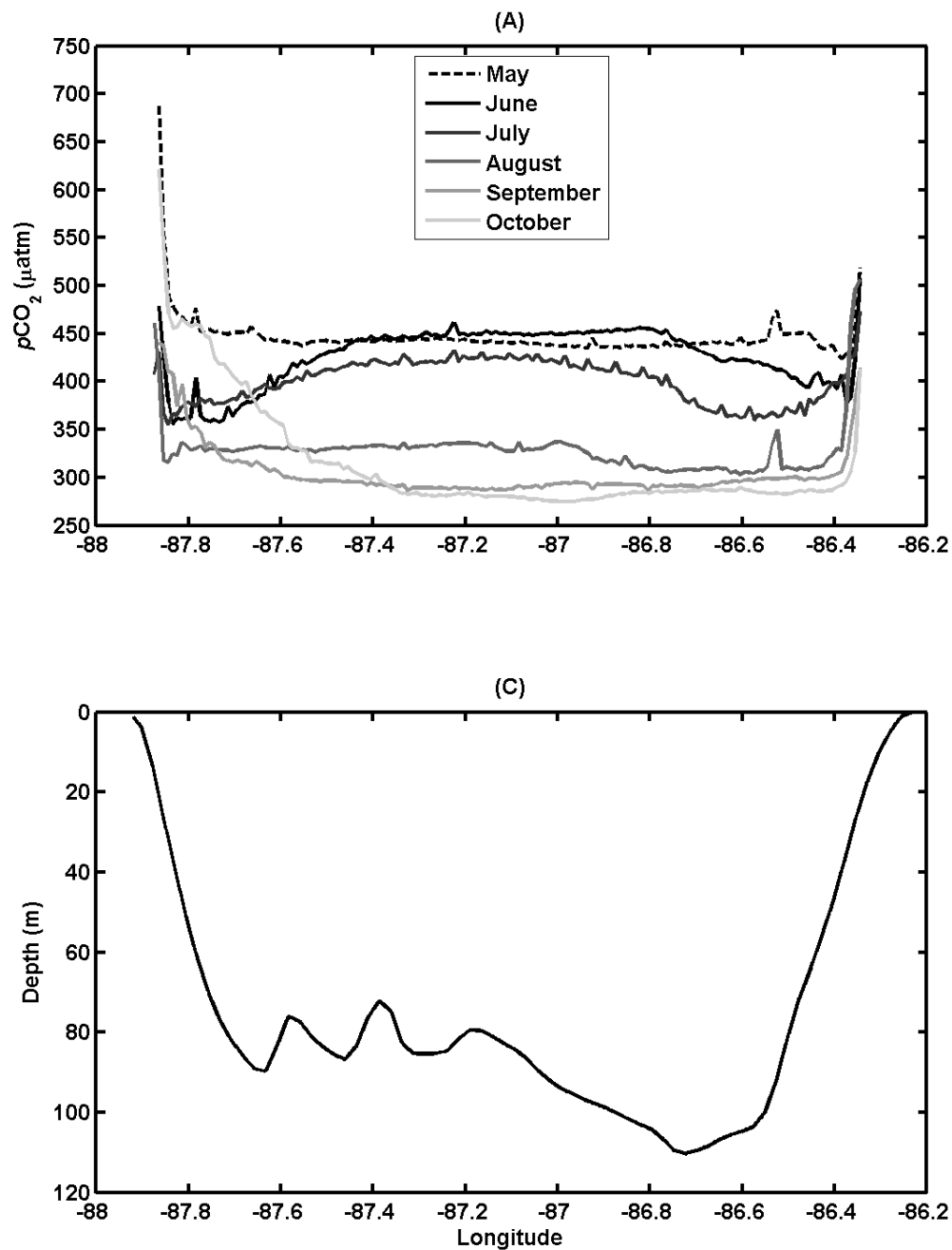


Figure 4.3: A) Transects (Fig 1) of monthly mean, Lake Express measured, $p\text{CO}_2$ (μatm) for May through October from Milwaukee, WI (W 87.9) to Muskegon, MI (W 86.3) where negative longitude values indicate $^\circ\text{W}$. B) The approximate depth along the lake transect.

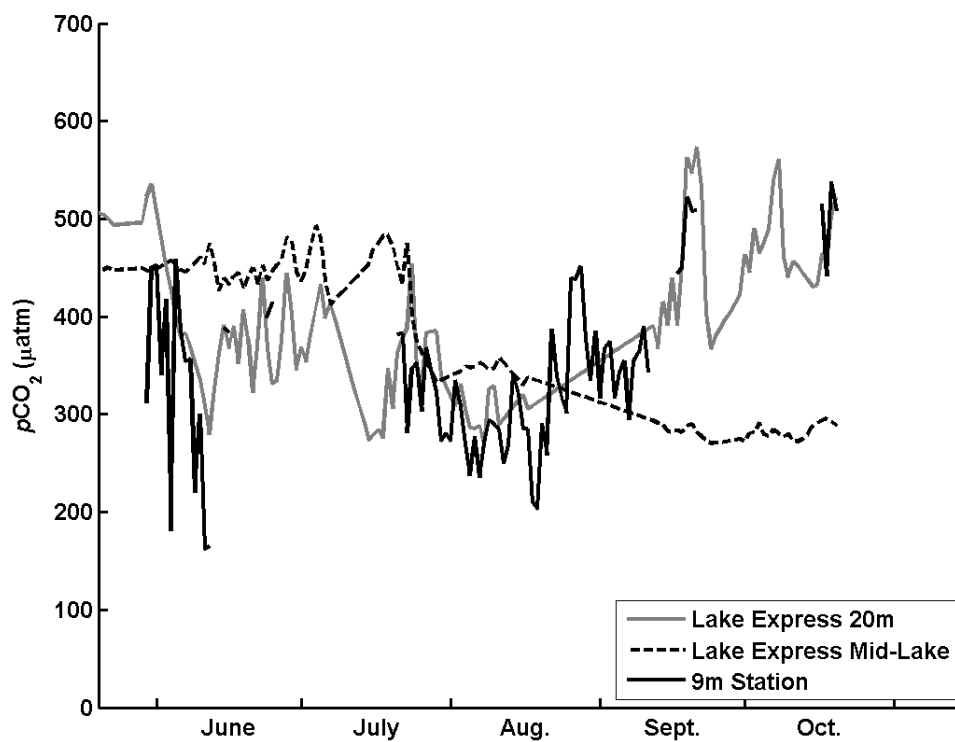


Figure 4.4: Mean daily ferry measured and 9m station buoy measured $p\text{CO}_2$. Gaps in the 9m station time series represent data which was removed due to system malfunction or occurred during system maintenance. Gaps in the Lake Express data are filled by linear interpolation between gap end points and occur in mid-July and late August through early September.

4.4 Model Simulation Results

4.4.1 Model Output and Accuracy

The NCPM was used to simulate the spring, summer, and fall of 2013. Model input variables are shown in Figure 4.5, including water temperature (A), surface PAR (B), depth averaged east-west current velocity representing the cross-shore current velocity (C), surface wave height (D), and the 10m wind speed (E). Wave heights at the nearshore station were variable with periods of calm and short periods with waves as high as 2 m. Wave heights generally increased through the simulation period and were greater during September and October than in June, July, and August. Wind speed was variable throughout the simulation period with a range of 0 to 14 m s⁻¹. Strong wind events matched large wave events, however, there were several periods where wind speed was high and wave heights were relatively small.

The NCPM simulated surface $p\text{CO}_2$ measured at the 9m station reasonably well (Fig. 4.6). In situ measurements during the first half of June (Fig. 4.6A) showed an increasing surface $p\text{CO}_2$ and then a steady draw down with large daily variation. By June 8th, surface $p\text{CO}_2$ was consistently below atmospheric saturation which was approximately 400 μatm . The model did a reasonable job following the overall trend through June although it underestimated the CO_2 draw down after June 8th. A substantial diel cycle was produced by the model, but its amplitude was lower than that of the empirical data. Through July (Fig. 6B), August (Fig. 4.6C), and September (Fig. 4.6D) the model produced a large diel CO_2 cycle which was similar to that observed in measured $p\text{CO}_2$. The overall trend in data available during July was captured remarkably well by the model while during August and September the model generally

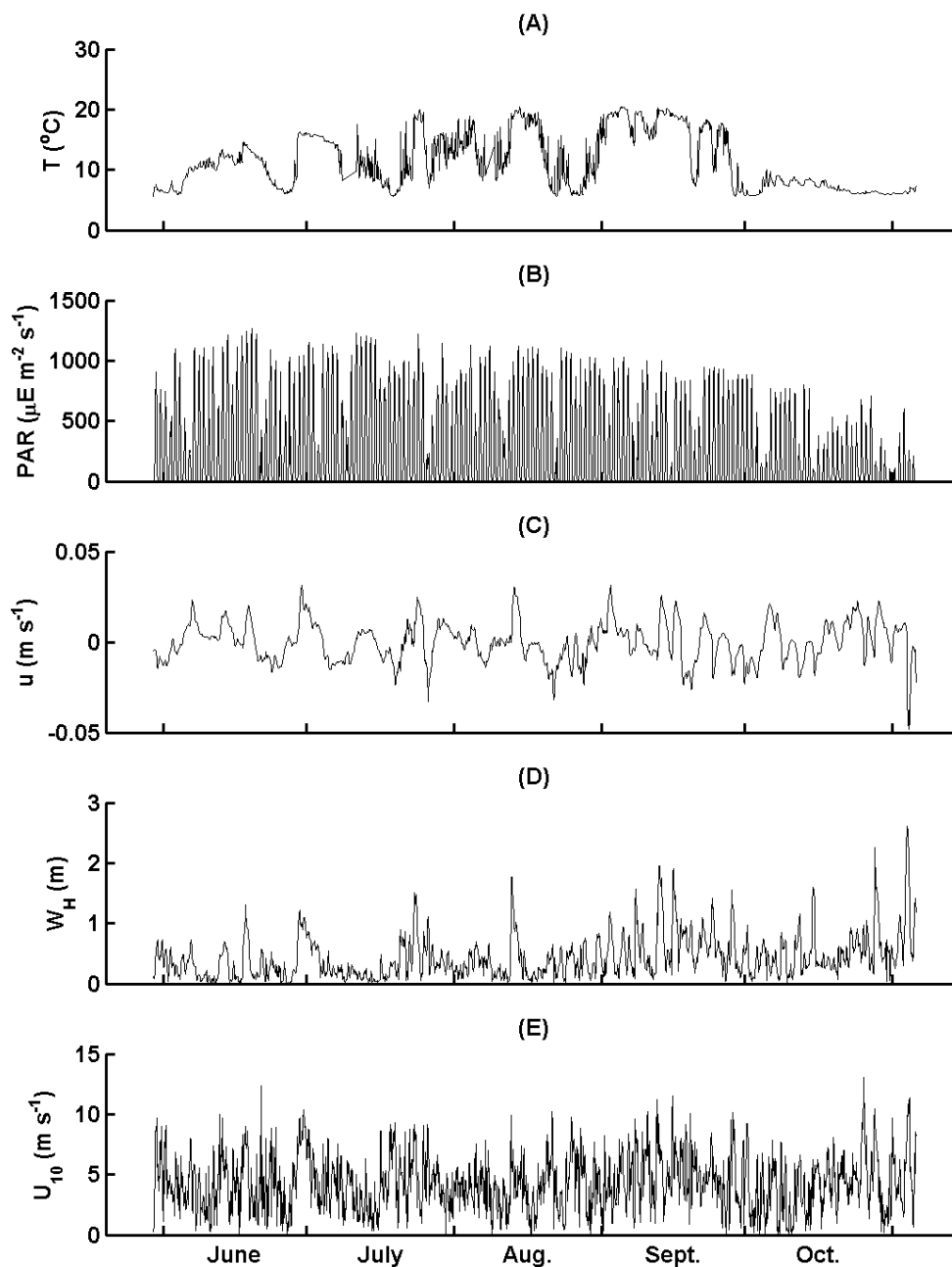


Figure 4.5: Model input variables: A) water temperature, B) surface PAR, C) depth averaged, east – west current velocity, where negative values are towards the west from the east, D) surface wind-wave height, and E) the wind speed at $\sim 10\text{m}$ above the lake surface. The x-axis is identical for all subplots and is shown below E.

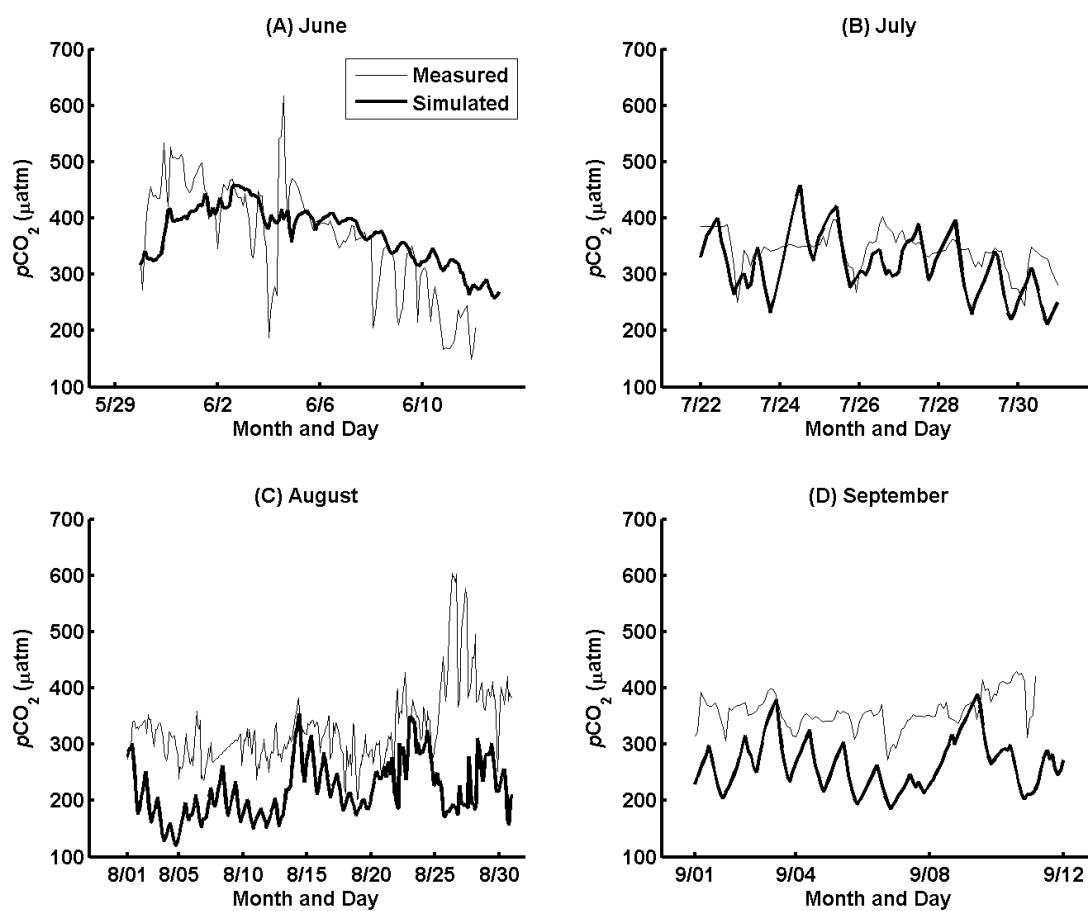


Figure 4.6: Measured (thin black line) and simulated (thick black line) nearshore $p\text{CO}_2$ for each month of the simulation period when $p\text{CO}_2$ measurements at the 9m station were available during June – September as labeled.

underestimates measured $p\text{CO}_2$, with error up to more than 400 μatm for brief period in lake August.

Accurate simulation of nearshore primary production, and importantly *Cladophora* production, is heavily dependent on accurate PAR at depth (Auer et al., 2010). Model simulated maximum daily, bottom PAR is compared to that measured at the 9m station during June and early July in Figure 4.7. The model does an adequate job reproducing the benthic light climate with some variation associated with the combined error in simulated PP concentration and in the $K_e - PP$ model (see the discussion of the K_e model in Chapter 2). Figure 4.8 presents the depth averaged measured values for *DP* (A), *PP* (B), *Chl a* (C), and *PC* (D) concentration at the 9m station along with the model simulation output for each variable. *DP* was over-estimated throughout the simulation period except for the two peaks in September and October which were underestimated (Fig. 4.8A). *PP* was generally underestimated by the model until October when the simulated values compared very well with observations (Fig. 4.8B). *Chl a* concentration was simulated within the measured range of values, however temporal fluctuations of *Chl a* were not captured well (Fig. 4.8C). The simulated *PC* concentration was close to measured *PC* values although slightly underestimated through the summer until October when the *PC* concentration was slightly over estimated (Fig. 4.8D).

Cladophora biomass, tissue phosphorus content, and areal stored phosphorus were simulated fairly well by the model (Fig. 4.9) with results similar to those in Chapter 2. In Chapter 2, the NPFM contained three vertical layers with mixing between them controlled by turbulent diffusivity. The NCPM is a simple well mixed reactor model, therefore, differences between the NPFM and the NCPM simulated *Cladophora* are

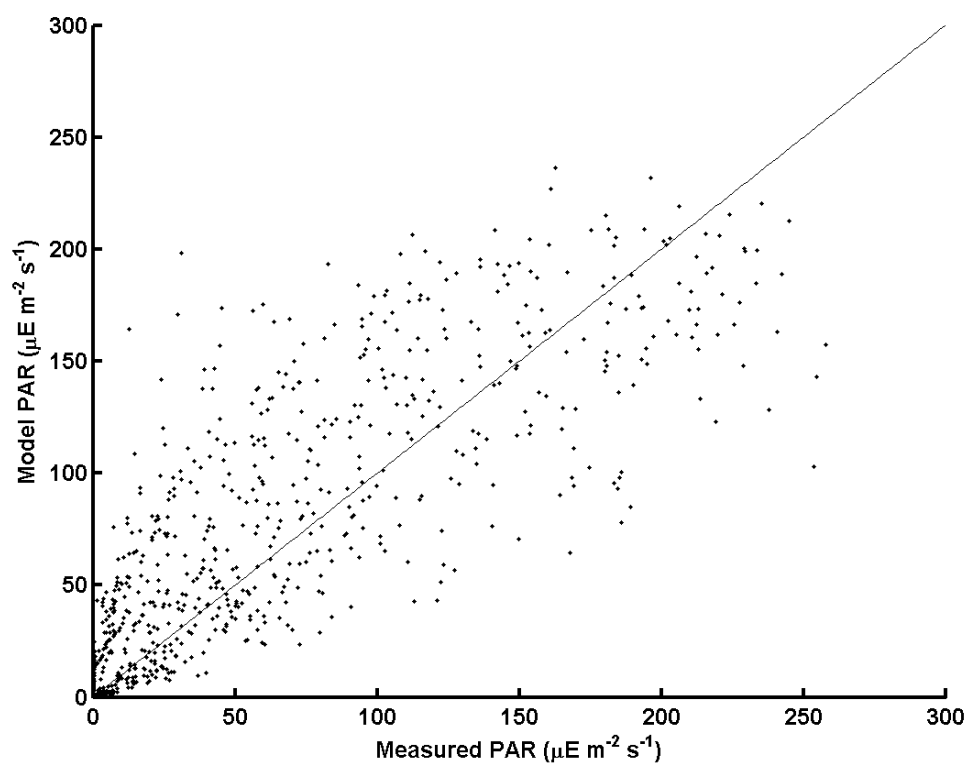


Figure 4.7: Model simulated versus measured daily maximum PAR (dots) at the bottom of the 9m station. The black line is the one to one, best fit line.

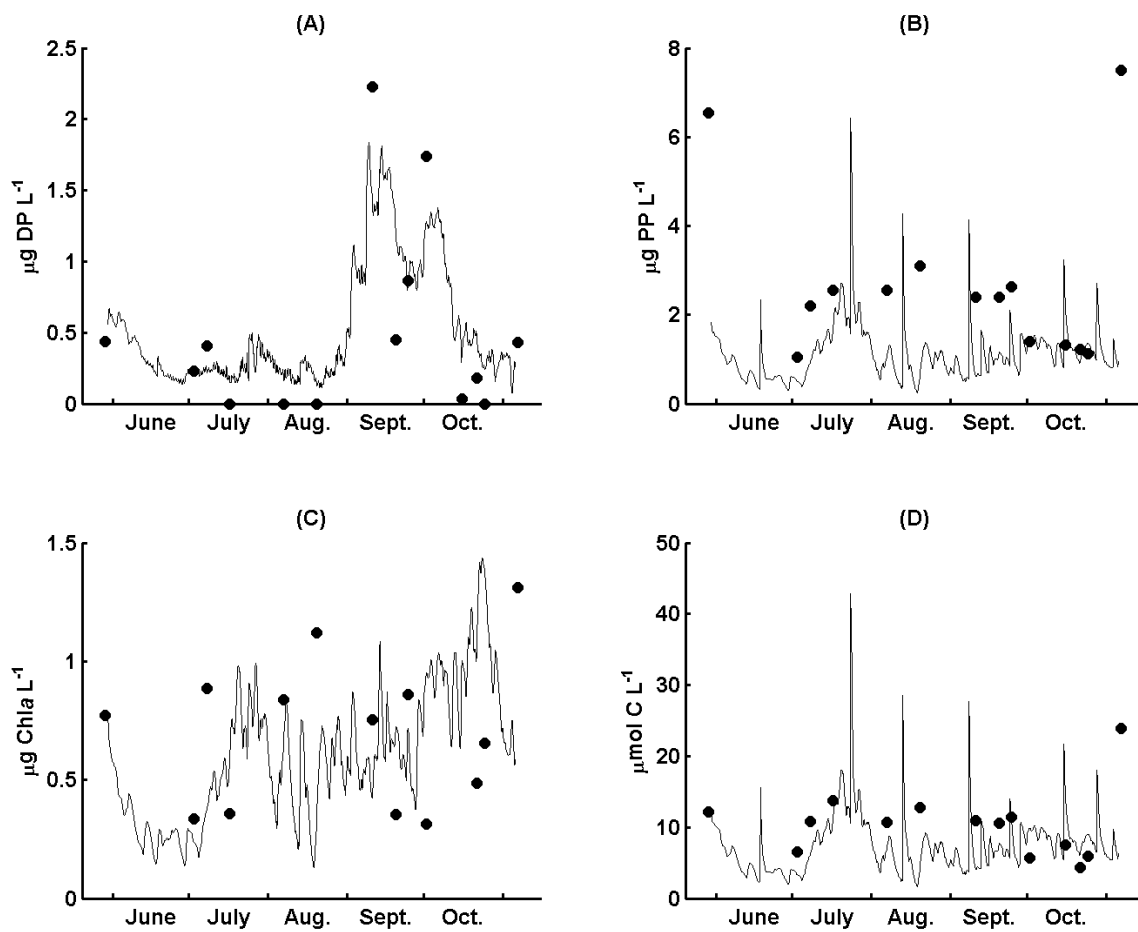


Figure 4.8: Measured (dots) and model simulated (black lines) dissolved phosphorus (A), particulate phosphorus (B), chlorophyll *a* (C), and particulate carbon (D) concentrations.

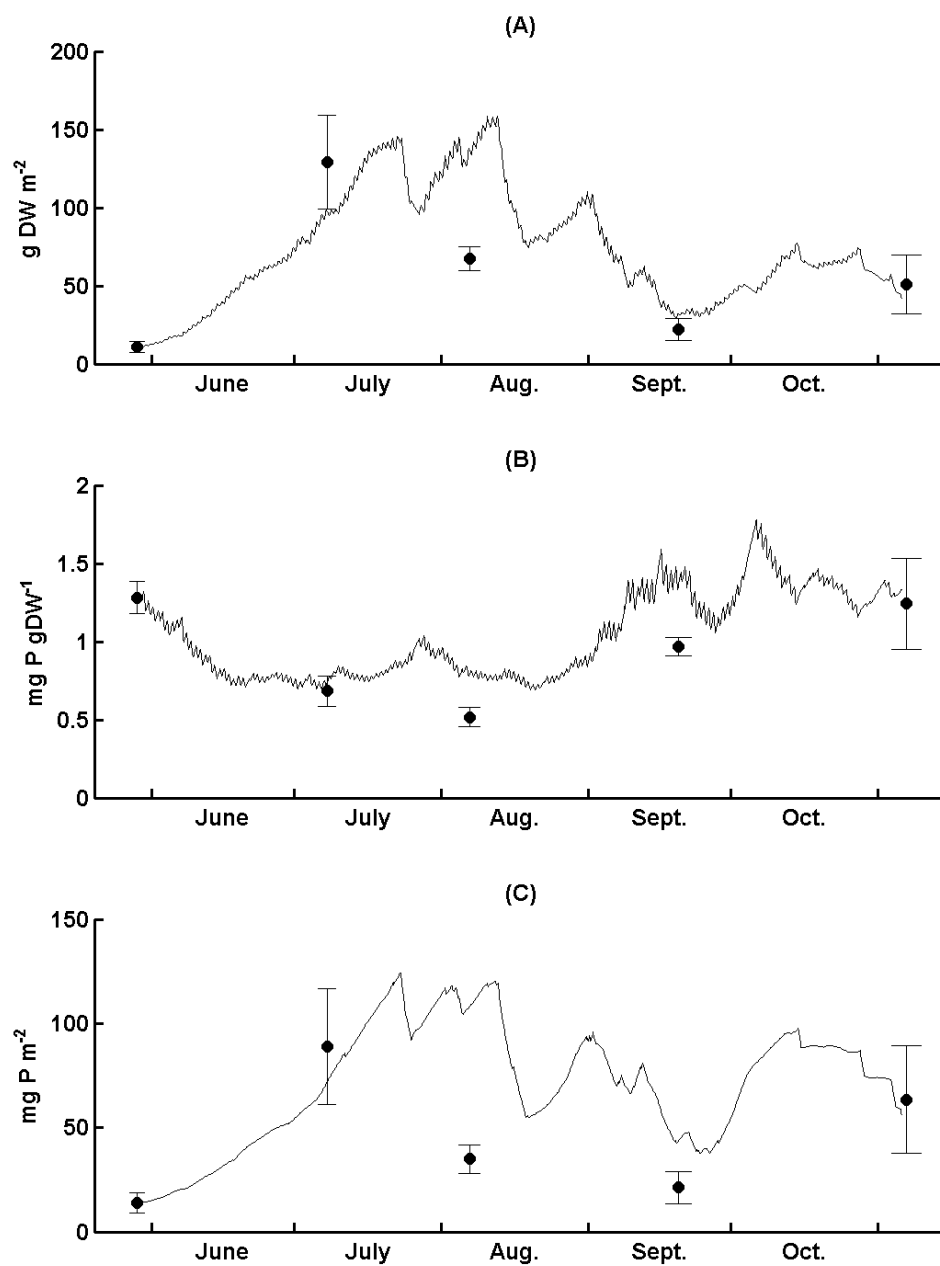


Figure 4.9: Measured (dots) and model simulated (black lines) *Cladophora* biomass (A), tissue phosphorus content (B), and areal stored phosphorus (C). Error bars represent one standard deviation of triplicate samples.

controlled by the influence of vertical mixing on light extinction, and PAR at depth, and DP availability. Early summer *Cladophora* growth was slightly underestimated by the NCPM (Fig. 4.9A), however, the season maximum biomass (158 gDW m⁻²) and late summer decline in *Cladophora* biomass were accurately reproduced in July through September. Biomass was overestimated in August and September, but was accurate in early November capturing the fall *Cladophora* regrowth, which has also been observed in other Great Lakes (Malkin et al., 2010). Tissue phosphorus content was simulated accurately, matching all measurements except those in August and September when the model over estimated tissue phosphorus (Fig. 4.9B). Areal *Cladophora* stored phosphorus (Fig. 4.9C) was accurately predicted through July, over estimated by the model in August and September, and accurate again in early November following the trend in simulated biomass.

Mussel volumetric pumping rate, was calculated the same as in Chapter 2 (Fig. 4.10A), and ranged from 0.4 to 1.4 L mussel⁻¹ day⁻¹. Based on measured mussel densities, mean of 5500 mussels m⁻², and length distributions the mean simulated mussel PP grazing flux was 0.16 mg PP m⁻² hr⁻¹ and the maximum was 1.24 mg PP m⁻² hr⁻¹ (Fig. 4.10B). The net near bottom DP flux, calculated as the sum of the net *Cladophora* DP uptake flux and the mussel DP excretion flux, varies between -0.5 and 1 mg DP m⁻² hr⁻², where negative values indicate a net DP uptake by the benthic community. The season mean, net, near bottom DP flux was 0.012 mg DP m⁻² hr⁻¹ indicating that, on average, mussels excretion of DP was greater than DP uptake by *Cladophora*.

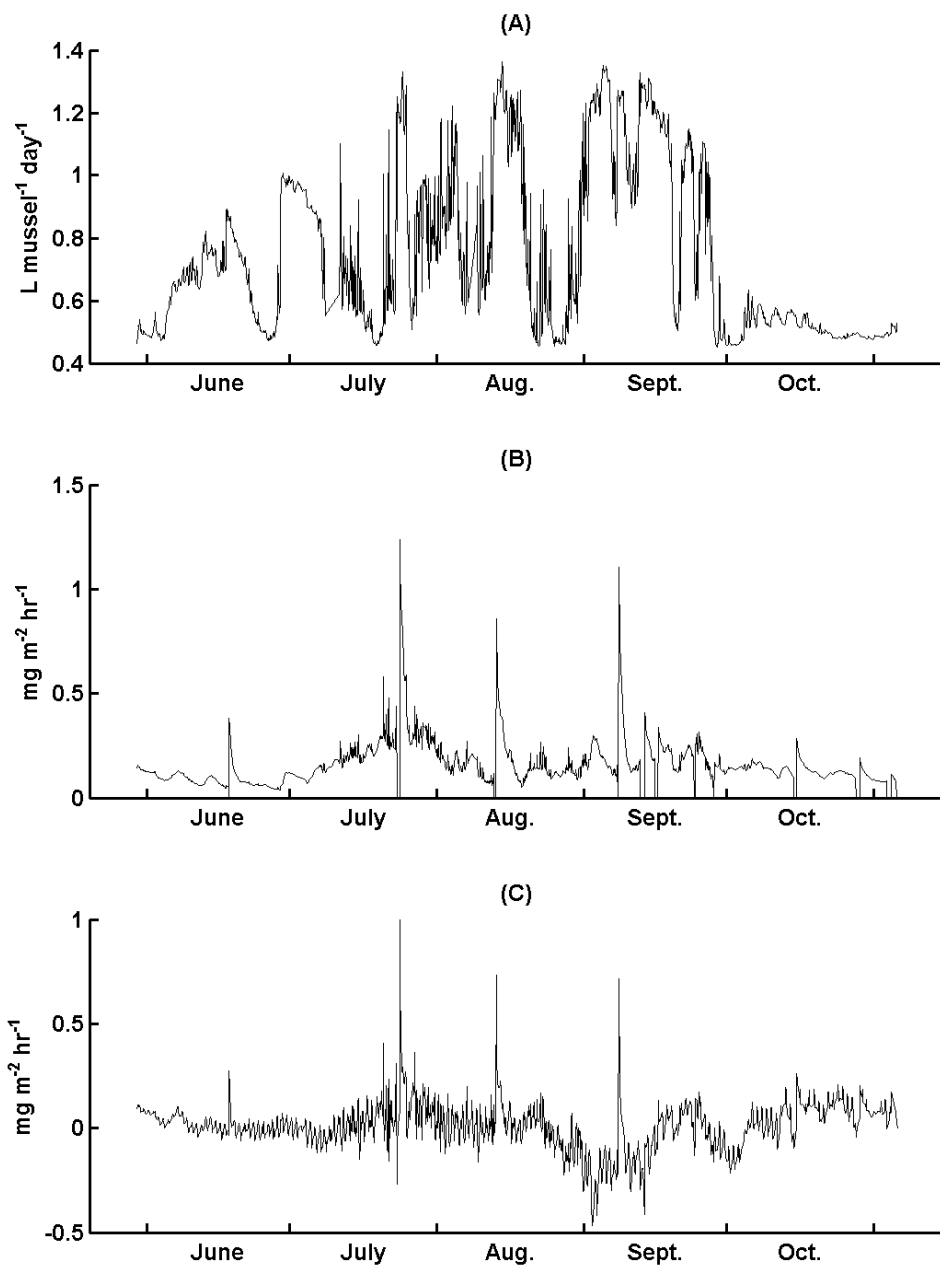


Figure 4.10: Model simulated mussel volumetric pumping rate (A), mussel particulate phosphorus grazing flux (B), and the net near bottom dissolved phosphorus flux due to mussel excretion and *Cladophora* uptake ($J_{MX} - J_{CU}$) (C). Positive values indicate mussel DP excretion surpasses *Cladophora* DP uptake and negative values indicate mussel excretion is less than *Cladophora* uptake.

The NCPM accuracy for the 2013 simulation was evaluated by calculating the correlation coefficient (R^2) and the mean error between measured parameters and their simulated values for each matching day and time:

$$\text{Error} = \frac{1}{N} \sum_{n=1}^N [(x(n) - x'(n))/x(n)] \quad (26)$$

where N is the total number of observations for each parameter, and x and x' represent the measured and modeled values respectively. The accuracy metrics for $p\text{CO}_2$, maximum daily near bottom PAR (I), *PP*, *DP*, *PC*, *Cladophora* biomass (X), *Cladophora* tissue phosphorus content (Q), and *Cladophora* stored phosphorus are presented in Table 4.4. Measurements of *PP*, *DP*, *PC*, X, S, and Q were compared to model daily average values while $p\text{CO}_2$ was compared to the matching time of each measurement, and I was compared to model simulated daily maximum near bottom PAR.

Model simulated $p\text{CO}_2$ was significantly correlated with observations ($R^2 = 0.30$, $p < 0.001$) and had remarkably little error (25%). Bottom PAR was significantly correlated with observations ($R^2 = 0.55$, $p < 0.001$), however the mean error was high (72%). Accuracy metrics for *PP*, *DP*, X, Q, and S were similar to those found in Chapter 2, with little agreement between correlation and mean error. *DP* was significantly correlated with observations ($R^2 = 0.76$, $p < 0.001$), however, mean error was exceptionally high (185%). *PP*, *PC*, X, Q, S were all not significantly correlated with observations, but mean error was acceptable for *PP* (41%), X (47%), and Q (29%). *PC*, calculated as the sum of phytoplankton (*PS*) and particulate detritus (*D*) carbon, was not well simulated according to accuracy metrics, however, visual comparison of model

Table 4.4: Model accuracy metrics for listed model variables calculated based on measurements taken at the 9m monitoring station. Error is calculated as the mean relative error as in Eq. 26.

Variable	Season R²	p value	Error · 100%	# of Observations
<i>p</i> CO ₂	0.30	< 0.001	27 %	1156
I	0.55	< 0.001	72 %	561
DP	0.76	< 0.001	185 %	12
PP	< 0.01	0.95	41 %	12
PC	0.01	0.77	91 %	12
X	0.32	0.43	47 %	4
Q	0.74	0.14	29 %	4
S	< 0.01	0.96	87 %	4

output to observations suggests the model does an acceptable job of reproducing measured *PC* (Fig. 4.8D).

4.4.2 The Nearshore Carbon Budget and Nearshore-Offshore Exchange

Model domain carbon pools include DIC, suspended particulates (phytoplankton and detritus), and benthic particulates (*Cladophora* and sediment) (Fig. 4.11A). There is a large size range among these carbon pools so the logarithm (base 10) of each areal, molar concentration is displayed in Figure 4.11A. Phytoplankton represent the smallest carbon pool with a mean and maximum areal concentration of 12.55 and 29.75 mmol C m⁻², nearly an order of magnitude less than model simulated suspended detritus which had a mean and maximum concentration of 56.83 and 381.85 mmol C m⁻² respectively. This was expected due to the order of magnitude larger mean *PC:Chl a* observed in nearshore domain in 2013 than that for phytoplankton. Phytoplankton, areal carbon concentrations fall within the range reported by Fahnenstiel et al. (2010) for the lake offshore surface layer in 2007-2008. Sediment stored particulate carbon ranged from zero, following resuspension events, to a maximum of 296.73 mmol C m⁻² with a mean of 88.06 mmol C m⁻². *Cladophora* stored carbon is nearly 2 orders of magnitude greater than phytoplankton stored carbon with a mean of 1,846.8 mmol C m⁻² and a maximum of 3,961.5 mmol C m⁻². DIC is the single largest pool of carbon in the 9.2m deep nearshore zone on an areal basis, with a mean concentration of 20.22 mol C m⁻² (note the change in units).

Daily and monthly mean carbon fluxes across the offshore boundary and the air-water interface are presented in Figure 4.12. Except for resuspension events, the nearshore was a sink for suspended particulate carbon in the form of phytoplankton and

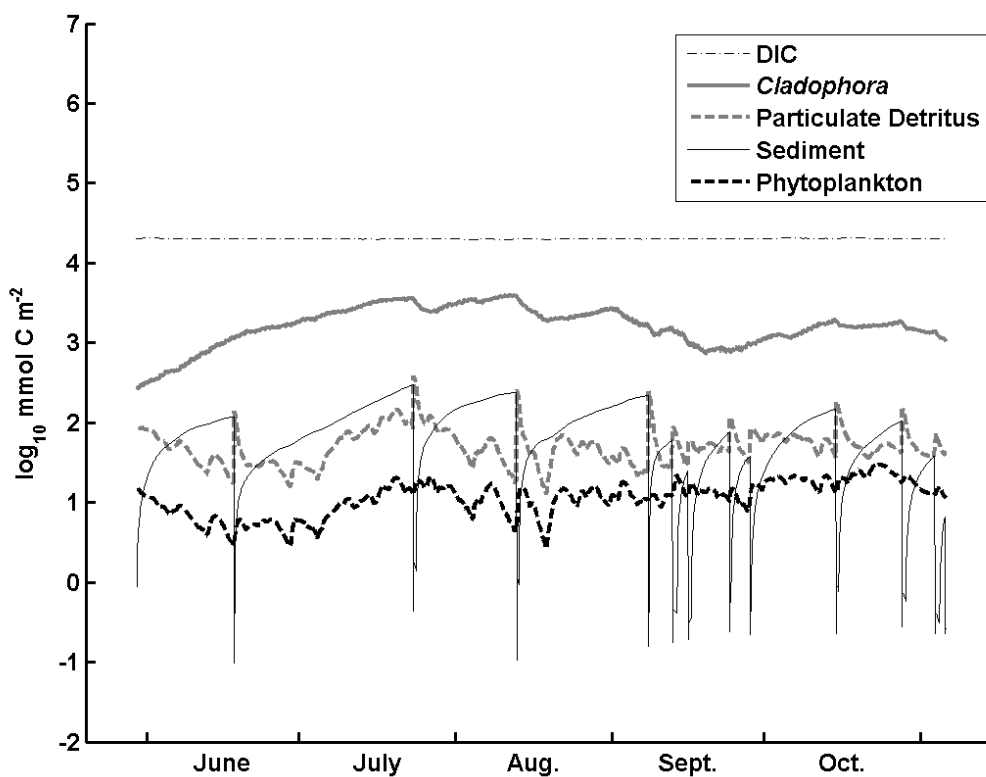


Figure 4.11: The \log_{10} of each model areal carbon pool including DIC, *Cladophora*, particulate detritus, sediment, and phytoplankton for the model domain of depth 9.2m.

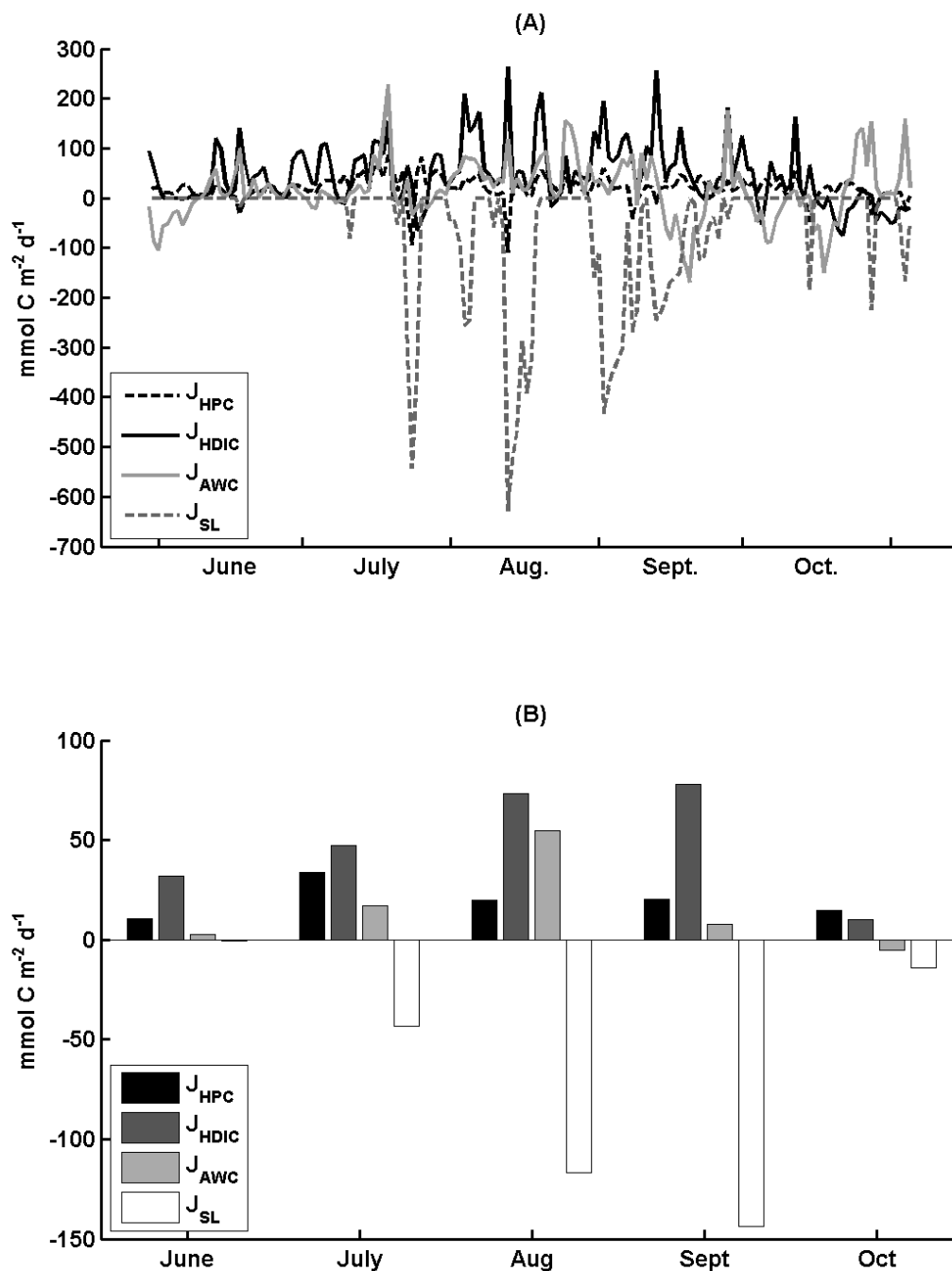


Figure 4.12: A) Daily mean carbon fluxes through the model boundaries including: nearshore-offshore suspended particulate carbon (J_{HPC}), nearshore-offshore DIC (J_{HDIC}), CO_2 through the air-water interface (J_{AWC}), and nearshore-offshore sloughed *Cladophora* (J_{SL}). B) Monthly mean carbon boundary fluxes listed the same as in A. Negative values indicate a flux out of the model domain to either the offshore or the atmosphere and positive values indicate flux into the model domain from the offshore or the atmosphere.

detritus. Resuspension events cause a brief period of nearshore to offshore *PC* flux (Fig. 4.12A). The mean flux of *PC* from the offshore was $19.96 \text{ mmol C m}^{-2} \text{ d}^{-1}$ and ranged from a minimum of $10.70 \text{ mmol C m}^{-2} \text{ d}^{-1}$ in June to a maximum of $33.88 \text{ mmol C m}^{-2} \text{ d}^{-1}$ in July (Fig. 4.12B). The nearshore was also a sink for DIC, including both DIC flux through the offshore boundary, and the air-water interface, with means of 48.12 and $15.39 \text{ mmol C m}^{-2} \text{ d}^{-1}$ respectively. DIC flux across the nearshore-offshore interface ranged from a minimum of $10.05 \text{ mmol C m}^{-2} \text{ d}^{-1}$ in October, to a maximum of $78.13 \text{ mmol C m}^{-2} \text{ d}^{-1}$ in September (Fig. 4.12B). Air-water CO_2 flux ranged from -5.38 to $54.83 \text{ mmol C m}^{-2} \text{ d}^{-1}$ in October and August respectively, where negative flux values indicate CO_2 evasion to the atmosphere. The uptake of carbon within the nearshore results in the accumulation of nearshore carbon, primarily as *Cladophora* tissue (Fig. 4.11) and the eventual loss of carbon as sloughed *Cladophora* tissue (Fig. 4.12). *Cladophora* sloughing flux represents the largest monthly mean flux of carbon throughout the season with values in August and September of 116.63 and $143.77 \text{ mmol C m}^{-2} \text{ d}^{-1}$ respectively.

Figure 13A presents the mean daily, net production by *Cladophora* and phytoplankton, and respiration by dreissenid mussels. As phytoplankton represent a very small proportion of the domain carbon budget (Fig. 4.11), it was no surprise that phytoplankton net production was very small compared to *Cladophora* and mussels, with a mean of $0.37 \text{ mmol C m}^{-2} \text{ d}^{-1}$, compared to that of *Cladophora*, $70.64 \text{ mmol C m}^{-2} \text{ d}^{-1}$, and mussel respiration, $20.56 \text{ mmol C m}^{-2} \text{ d}^{-1}$. The domain net production is controlled by *Cladophora* photosynthesis and respiration. Periods of net respiration (negative carbon fluxes in Fig. 4.12A) match periods of sediment resuspension and high detrital

concentrations in the water column (see “Sediment” in Fig. 4.11) which limits light penetration and photosynthesis by *Cladophora* at the lake bottom. The monthly mean carbon fluxes associated with *Cladophora* and phytoplankton production and mussel respiration are shown in Figure 4.13B. *Cladophora* net production increases through the year to a peak in August of $104.03 \text{ mmol C m}^{-2} \text{ d}^{-1}$, and then decreases again through October. There was no significant trend in mussel respiration which had a peak in monthly mean in July of $29.67 \text{ mmol C m}^{-2} \text{ d}^{-1}$.

4.4.3 Air-Water CO₂ Transfer Velocity Parameterization

The effect of the air-water CO₂ transfer velocity parameterization on model accuracy was tested by comparing model accuracy metrics calculated from model output using two different transfer velocity parameterizations from the literature. The Wanninkhof (1992) model, k_1 , is a wind dependent model and varies with the square of the wind speed (Eq. 18). The Zhao and Xie (2010) model, k_2 , is a wind and wave height dependent model (Eq. 19). Figure 4.14A compares k_1 and k_2 directly illustrating the strong correlation between the two models ($R^2 = 0.64$, $p < 0.001$) and the difference between them through the model simulation. The mean difference between the two models is 3.4 cm hr^{-1} and the maximum difference is 21 cm hr^{-1} . The k_2 parameterization predicts higher k values at lower wind speeds than the k_1 parameterization through a range of wave heights, however, there was no discernable difference in $p\text{CO}_2$ R^2 or mean error between model output using k_1 and k_2 .

The cumulative CO₂ flux across the air-water interface calculated using both k models is presented in Figure 4.14B. Negative, cumulative flux indicates a net loss of CO₂ from the water to the atmosphere and positive values indicate a net uptake of CO₂

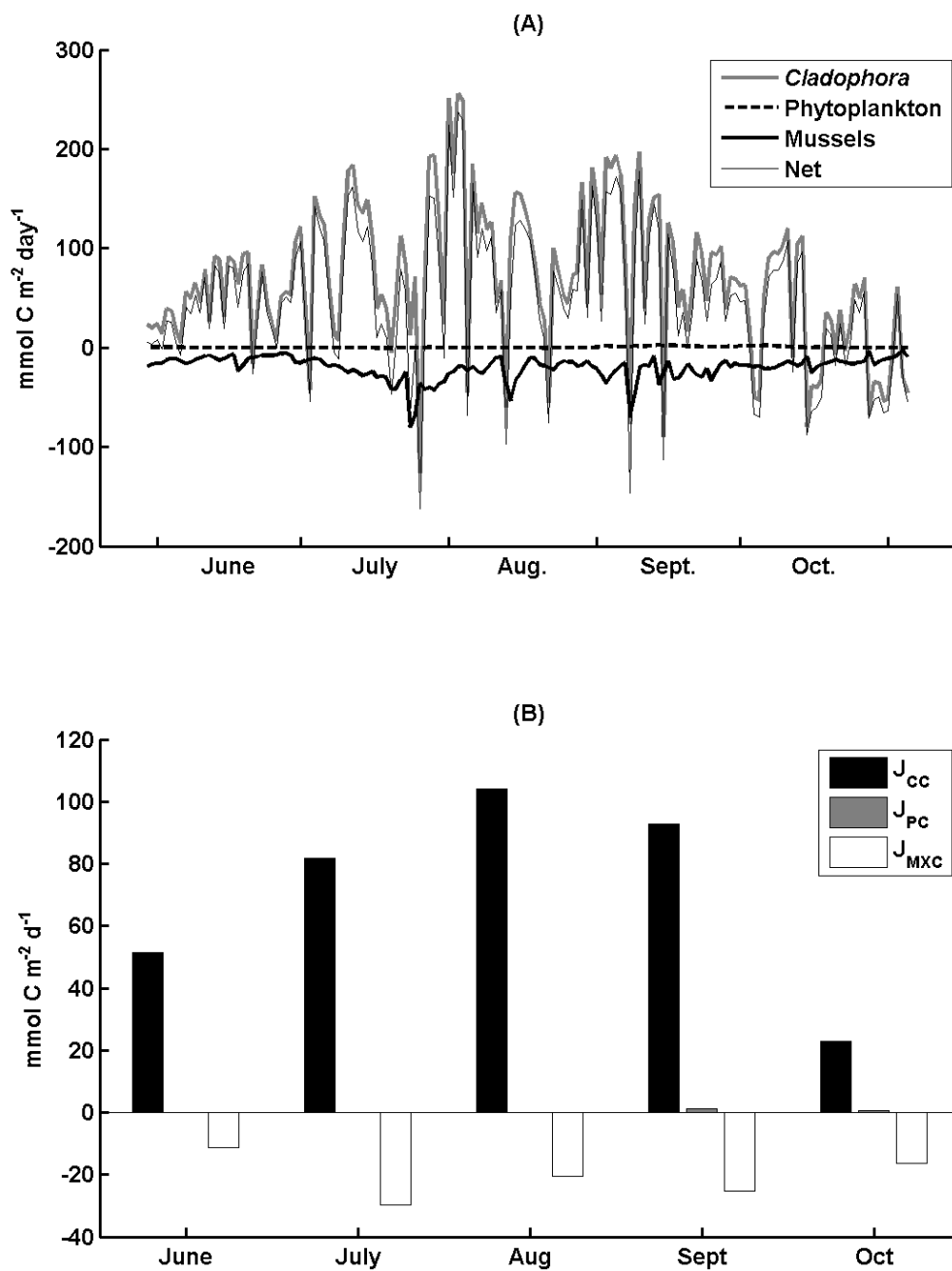


Figure 4.13: A) Mean simulated daily, net carbon fluxes associated with *Cladophora*, phytoplankton, dreissenid mussels, and community (net) production, where negative values indicate respiration and positive values indicate photosynthesis. B) Monthly means of simulated net carbon fluxes associated with *Cladophora* (J_{CC}) and phytoplankton (J_{PC}) net production, and dreissenid mussel respiration (J_{MXC}).

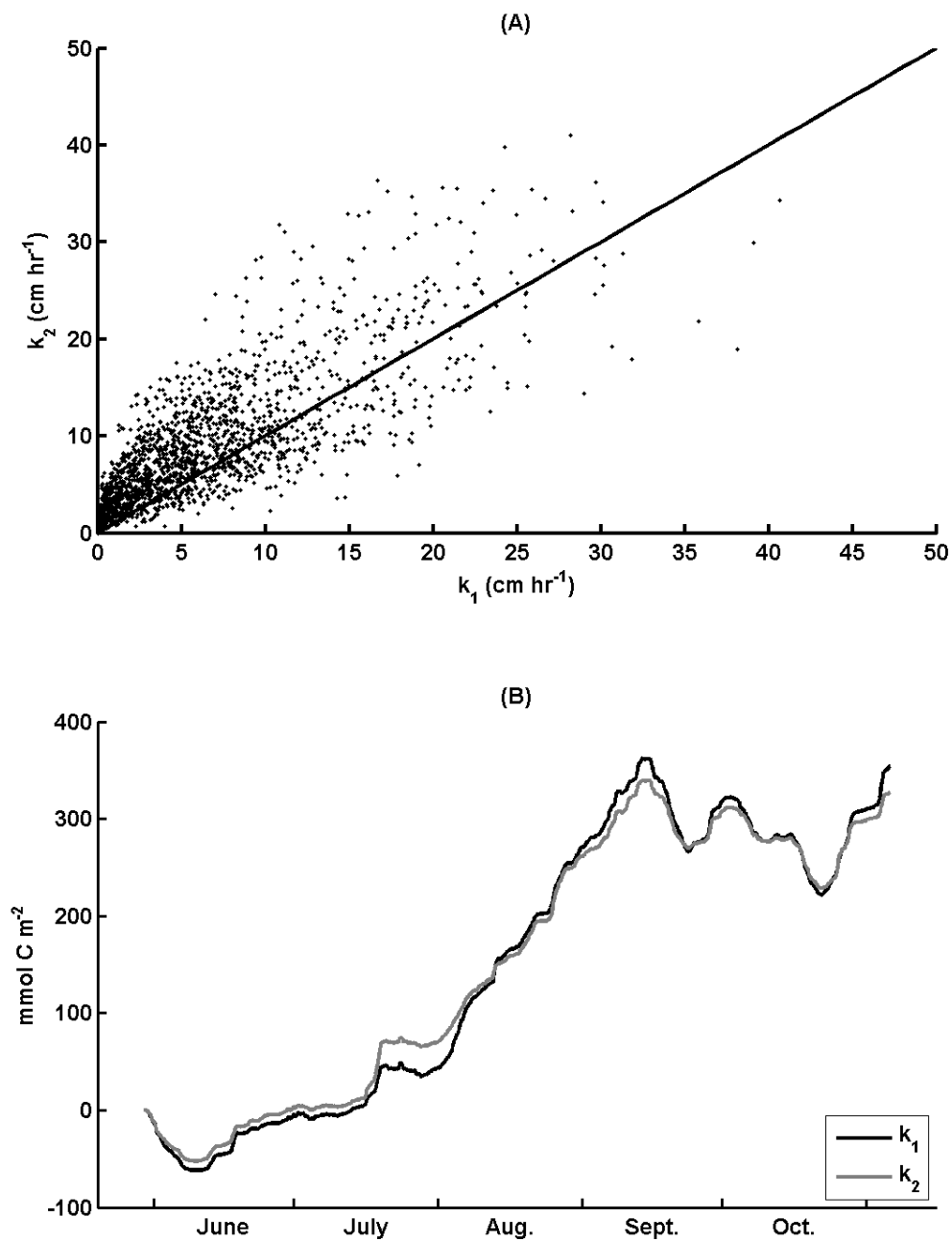


Figure 4.14: Air-water CO₂ transfer velocity model comparison (A) where k_1 represents the parameterization of Wanninkhof (1992) and k_2 represents the parameterization of Zhao and Xie (2010). B) Cumulative sum of the air-water CO₂ flux associated with transfer velocity models: k_1 and k_2 .

from the atmosphere. The trend in the cumulative CO₂ flux is controlled by the air-water CO₂ gradient which is dependent on primary production and respiration, but the difference between the two cumulative CO₂ flux curves represents the influence of the two *k* parameterizations. There was a mean difference of 10.25 mmol C m⁻² over the simulated period. The influence of the *k* parameterization was surprisingly modest considering the impact of local fetch limitation on surface turbulence.

4.4.4 Test Scenario 1 - No Dreissenid Mussels

As in Chapter 2, a test scenario was conducted with no dreissenid mussels included in the model domain. A comparison of the carbon budgets and fluxes between model simulations with and without mussels allows for the quantification of their impact on nearshore carbon and phosphorus dynamics. When mussels were removed from the model, water clarity decreased 18%, dissolved phosphorus decreased 15%, phytoplankton concentration increased 49%, suspended detritus concentration increased 48%, total water column particulate carbon concentration increased 48%, sediment stored carbon decreased 67%, *Cladophora* biomass decreased 76% with a 68% decrease in maximum biomass, and *Cladophora* stored phosphorus decreased 81%. *Cladophora* stored carbon becomes a much smaller component, yet still the largest single portion of the nearshore carbon budget in June, July and August. By September, the amount of carbon in *Cladophora*, detritus, and sediment was similar, with regular resuspension events controlling sediment and suspended detritus carbon storage.

Figure 4.15 presents the nearshore-offshore carbon fluxes (the same as in Figure 4.12) for the no mussel test scenario. Without mussels the magnitude of the boundary fluxes is substantially less in the offshore to nearshore direction with resuspension events

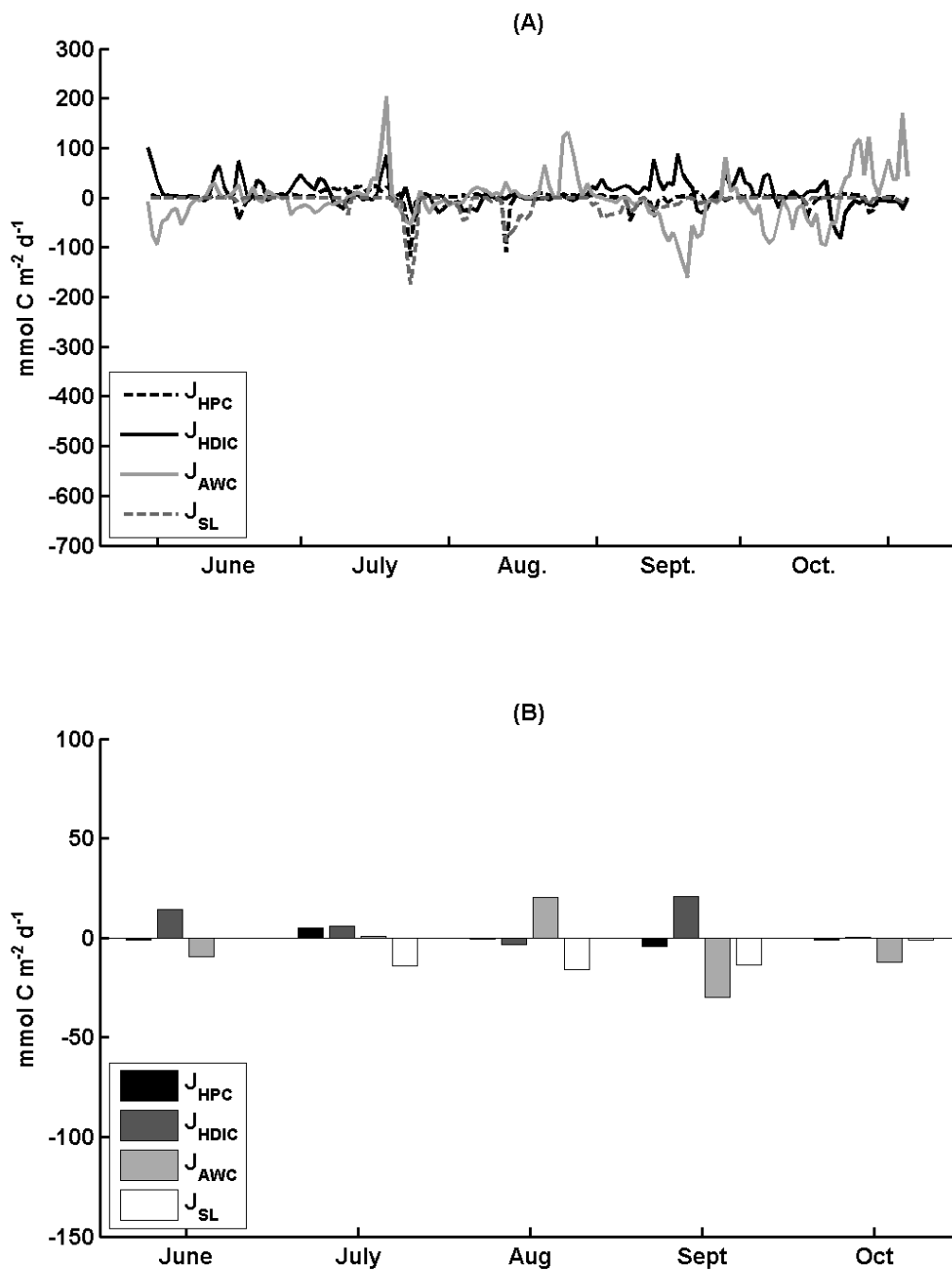


Figure 4.15: Carbon fluxes in Figure 12, for the no dreissenid mussel test scenario. The y-axis scales are the same as in Figure 12 for direct comparison.

causing similar fluxes from the nearshore to the offshore (Fig. 15A). The flux of particulate carbon across the nearshore-offshore boundary reverses direction from the base simulation in every month except July, indicating that the nearshore was a net source of PC to the offshore in the absence of mussels (Fig. 4.15B). During July, when the nearshore was a sink of PC to the offshore, the calculated flux dropped by $29 \text{ mmol C m}^{-2} \text{ d}^{-1}$, or 86%, when mussels were removed. In the absence of mussels, the nearshore is a source of CO_2 to the atmosphere during June, September, and October. When mussels are present, the nearshore is only a source of CO_2 to the atmosphere in October. The nearshore-offshore DIC flux reversed direction in the absence of mussels during August and declined $40 \text{ mmol C m}^{-2} \text{ d}^{-1}$ on average throughout the year.

Domain primary production decreased substantially when mussels were removed from the model (Fig. 4.16). *Cladophora* mean, net production decreased $63 \text{ mmol C m}^{-2} \text{ d}^{-1}$, or 89% from the base simulation and phytoplankton mean, net production decreased $0.12 \text{ mmol C m}^{-2} \text{ d}^{-1}$, or 32%. Phytoplankton production is a function of the calculated growth and respiration (Eq. 24). Net growth rate was calculated as the ratio of production ($\text{mmol C m}^{-2} \text{ d}^{-1}$), the sum of growth and respiration, to areal biomass (mmol C m^{-2}) for both *Cladophora* and phytoplankton and was averaged over each month (Fig. 4.17). These biomass specific, net growth rates for *Cladophora* and phytoplankton populations decreased during every month when mussels were not present in the model simulation. During June, phytoplankton net growth rates changed from positive in the presence of mussels, to negative in the absence of mussels, while in July through October the net growth rates were of the same sign, but declined. The smallest change for both *Cladophora* and phytoplankton was during September. During both September and

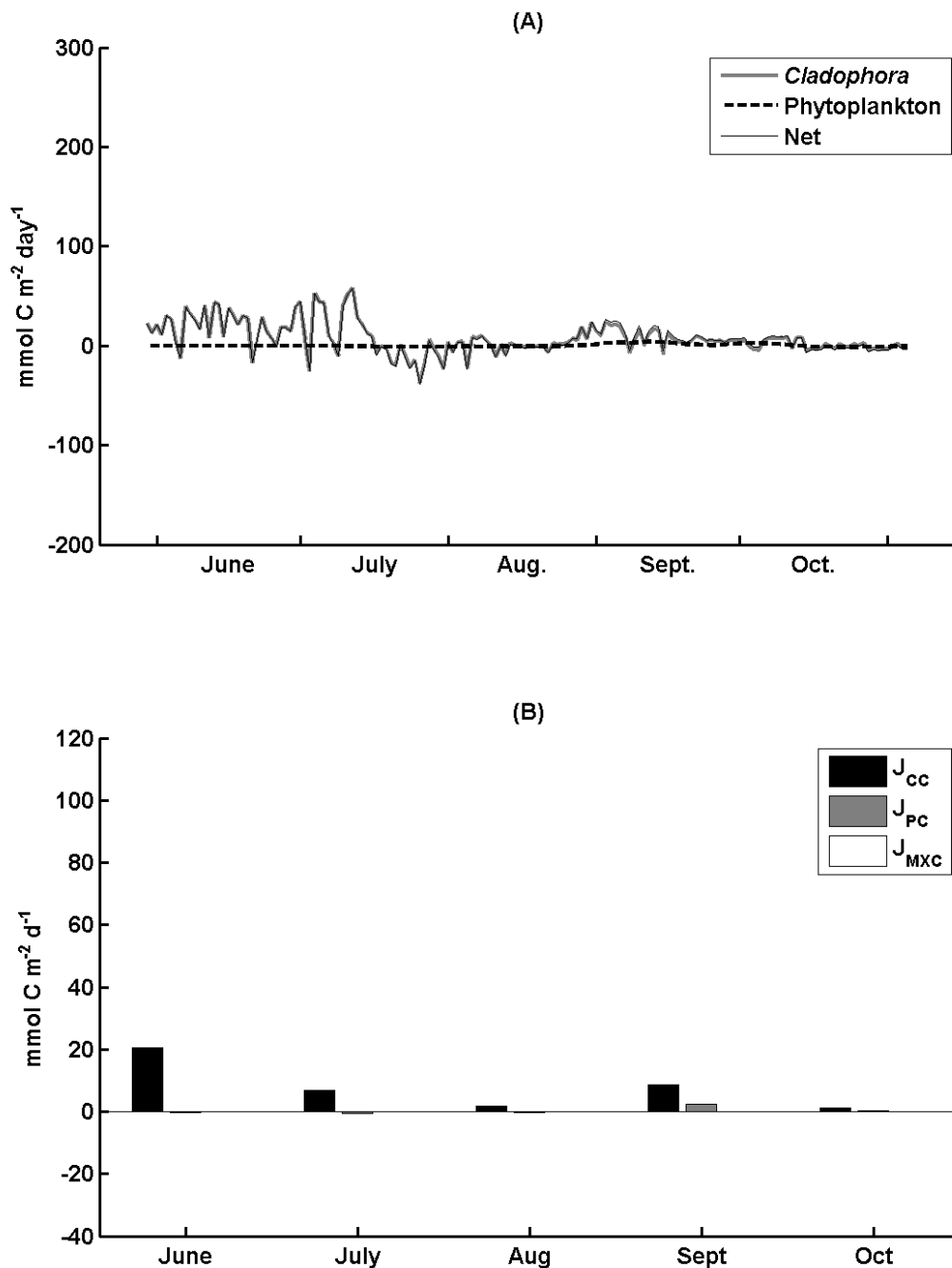


Figure 4.16: Mean daily carbon fluxes (A) and mean monthly carbon fluxes (B) associated with *Cladophora*, and phytoplankton production, as in Figure 13, for the no mussel test scenario. Y-axis scales are the same as in Figure 12 for direct comparison.

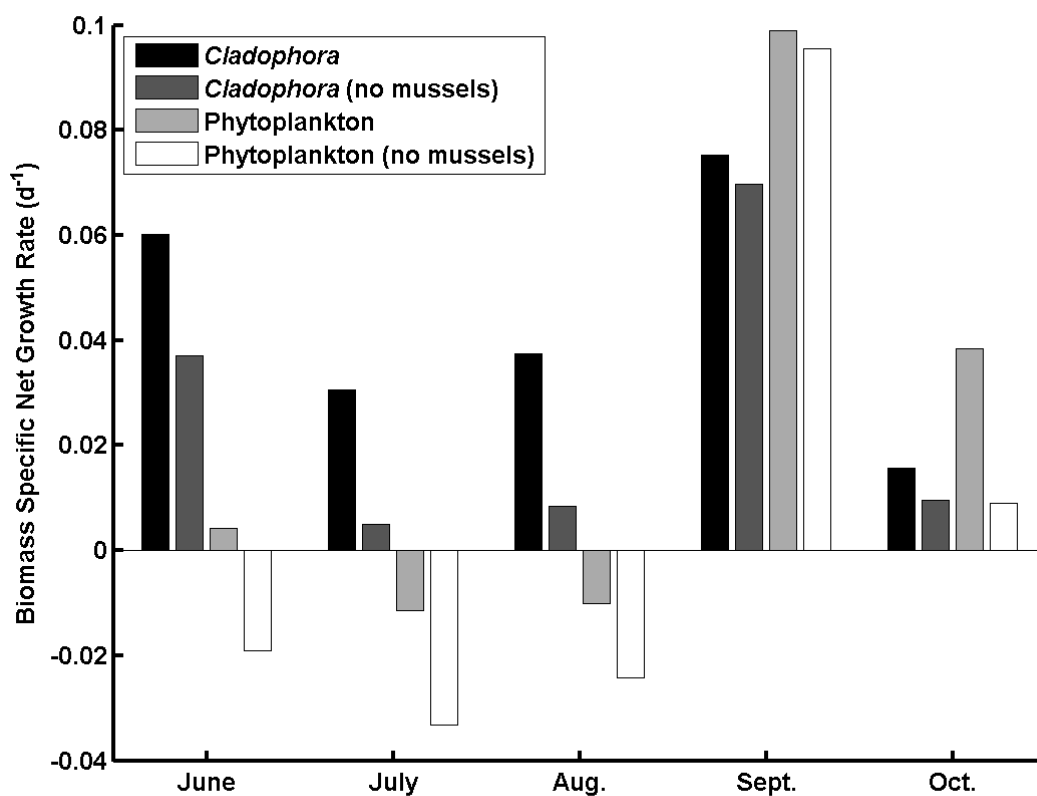


Figure 4.17: Comparison of monthly mean, biomass specific, net growth rates for *Cladophora* and phytoplankton for model simulations with and without mussels (labeled: no mussels). Rates are calculated as the ratio of net production in $\text{mmol C m}^{-2} \text{d}^{-1}$ to areal biomass in mmol C m^{-2} .

October, phytoplankton had a higher biomass specific net growth rate than *Cladophora* for both simulation scenarios. The lower *Cladophora* and phytoplankton population, biomass specific, net growth rates in the absence of mussels reflects the 15% decrease in dissolved phosphorus and the 18% decrease in available light. *Cladophora* maintain positive net growth rates during the same period that phytoplankton had negative net growth due to the higher sensitivity of phytoplankton to phosphorus availability. *Cladophora* are able to store large quantities of phosphorus when available phosphorus concentrations are high and utilize it for growth when available phosphorus is limiting (Auer et al., 2010; Canale and Auer, 1982a; Tomlinson et al., 2010).

4.4.5 Test Scenario 2 - Variable Alkalinity

In order to calculate the DIC constituents at each model time step a constant lake alkalinity was assumed, 2.22 meq L⁻¹, based on the median value of over a decade of alkalinity measurements collected in the vicinity of the nearshore domain. Alkalinity is dependent on the precipitation and dissolution of CaCO₃ following periods of rapid CO₂ draw down associated with photosynthesis, mixing of water masses, or from chemical changes in the water column such as calcium uptake (Barbiero et al., 2006; Lejart et al., 2012; Wetzel, 2001). To test the effect of the assumed constant lake alkalinity on model accuracy, several test scenarios were conducted with different constant alkalinity values and with variable alkalinity. The first two scenarios were conducted with constant alkalinity values higher and lower than the initial chosen value of 2.22 meq L⁻¹, representing a reasonable maximum, 2.3, and minimum, 2.14, based on the range of the observed values in the Lake Michigan nearshore. The second set of test scenarios was conducted with changing alkalinity so that alkalinity either declined or increased linearly

through the simulation period from 2.3 to 2.14 meq L⁻¹, or vice versa, or oscillated on a diel cycle with a mean of 2.22 meq L⁻¹. Offshore DIC and [H⁺] boundary conditions calculated as daily mean values from *p*CO₂ data collected aboard the Lake Express Car Ferry were recalculated for each alkalinity scenario except for the diel alkalinity cycle scenario. For this scenario, boundary DIC values were left the same as in the base simulation with alkalinity held constant at 2.22 meq L⁻¹ presenting the mean value of the diel cycle.

The only test scenario to improve the accuracy of simulated *p*CO₂ was the linear decreasing alkalinity scenario. The R² value of the model simulation improved from 0.30 in the baseline simulation to 0.34 (*p* < 0.001) in the test scenario, while mean error improved from 27% to 25%. These improvements were very modest and may not represent significant improvement in model accuracy. Although it did not improve accuracy of the model simulation, the diel alkalinity cycle test scenario produced interesting results. The diel cycle was calculated using a cosine curve with a period of 24 hours and an amplitude of 0.01 meq L⁻¹ and a mean of 2.22 meq L⁻¹, where the daily maximum alkalinity was at midnight and the daily minimum was at noon representing precipitation of CaCO₃ during the day associated with the biological driven, diel CO₂ cycle. Although the daily change in alkalinity was small, the model produced a larger diel *p*CO₂ amplitude than simulated in the baseline simulation (Fig. 4.18). Based on the definition of alkalinity (Eq. 9) and the DIC equilibrium (Eq. 3 and 4) it was expected that a diel alkalinity cycle would reduce the diel *p*CO₂ amplitude compared to the base simulation. Model boundary conditions allowed for the nearshore domain to mix with water with a constant alkalinity and associated DIC. The net result of this system was to

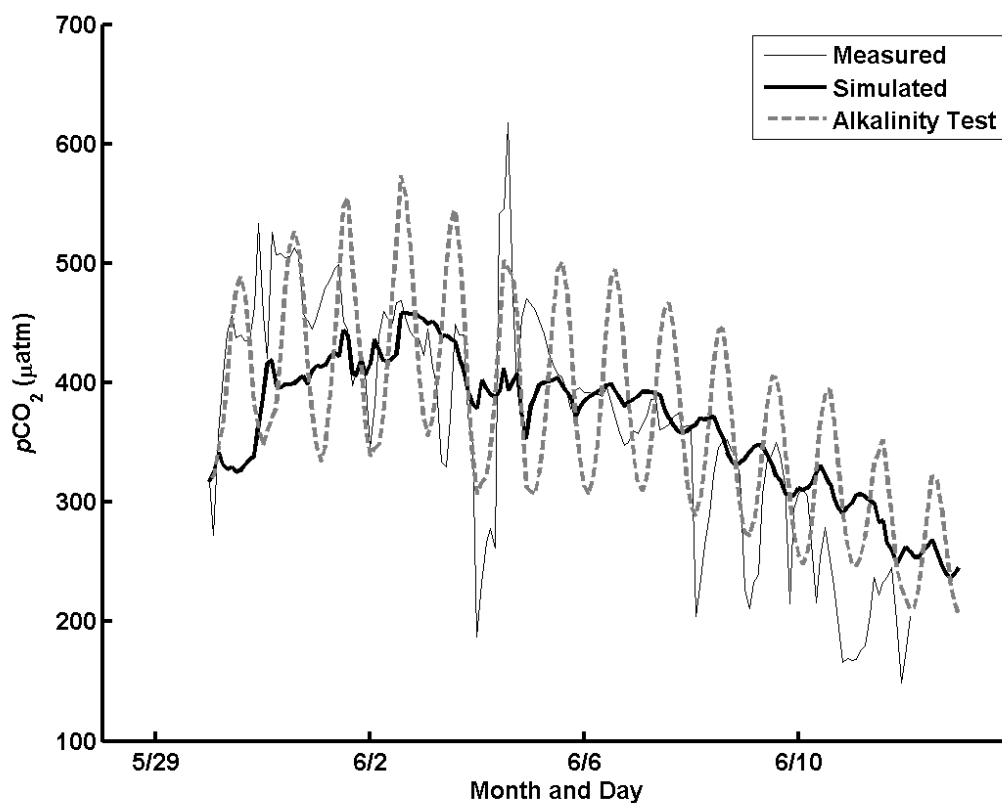


Figure 4.18: Comparison of model $p\text{CO}_2$ output for the period of June 2013 when $p\text{CO}_2$ observations were available. The alkalinity test represents the test scenario where alkalinity was set to a constant diel cycle represented by a cosine curve with a mean of 2.22 meq L^{-1} , a range of $\pm 0.01 \text{ meq L}^{-1}$ and daily maximums at midnight and minimums at noon.

produce a larger $p\text{CO}_2$ diel cycle within the model domain. If this result accurately reflects the true environment it could explain some of the variation in diel cycle magnitudes observed in the nearshore zone which was not captured by the model. For example, the decrease and increase in observed $p\text{CO}_2$ on June 4-5, 2013 (Fig. 4.17) was simulated better with the diel alkalinity cycle than without. This event could have been caused by a local change in alkalinity and mixing with surrounding waters with different alkalinity and DIC concentrations.

4.5 Discussion

4.5.1 Model Accuracy and Production

The accuracy of the NCPM was evaluated against measured $p\text{CO}_2$ (Fig. 4.6), dissolved phosphorus (Fig. 4.8A), particulate carbon (Fig. 4.8D), and *Cladophora* biomass and tissue phosphorus content (Fig. 4.9). Although the NCPM does an adequate job simulating the 2013 summer and fall season, there were periods where *PP* and *PC* were severely underestimated and the NCPM captured little if any of the measured trends in *Chl a* concentration. Model simulated concentrations of suspended particulates are likely underestimated due to the lack of vertical mixing in the model. It has been shown that vertical mixing rates can lead to a near bottom concentration boundary layer over mussel beds limiting the influence of mussel clearance rates on water column particulate concentrations (Ackerman et al., 2001; L. Boegman et al., 2008; Edwards et al., 2005; Zhang et al., 2008). In Chapter 2, it was shown that although the simulated vertical gradient in *PP* was small, under the influence of turbulent vertical mixing rates found in the nearshore zone, there was a lower *PP* concentration in the near bottom layer than in the surface layer. Mean error for simulated *PP* in the surface and bottom layers in

Chapter 2 was 47% while the mean error for simulated *PC*, here, was 91% indicating the importance of vertical mixing to model accuracy.

The initial particulate detritus concentration in the water column was calculated as the difference between the initial Chl *a* concentration and the measured total *PC* concentration. Suspended particulate detritus consists of different organic and inorganic materials associated with plankton and resuspended sediments (Hecky et al., 2004; Waples et al., 2005). Model simulated detritus was assumed to have the same C:P ratio as phytoplankton. Error associated with the lack of range in the model-simulated detrital C:P ratio may have contributed to the large errors in simulated PP and PC concentrations. In addition to inorganic detrital matter such as sands and clays, organic detritus such as mussel bio-deposits and other consumer waste may play a role in this source of error. It was assumed that mussel egested particulate detritus had the same C:P ratio as consumed particulates. The difference in mussel carbon and phosphorus recycling efficiency (Baldwin et al., 2002; Bootsma et al., 2012), as well as selective grazing of particulates with different C:P ratios (Baldwin et al., 2002; Tang et al., 2014), will likely alter waste deposit C:P ratios and influence suspended particulate C:P ratios after resuspension events.

It was not surprising that the model did not simulate observed trends in nearshore Chl *a*. The model utilizes a constant C:Chl *a* ratio from the literature and does not take into consideration fluctuations in phytoplankton Chl *a* associated with photo-adaptation when light levels are not at optimal levels for photosynthesis (Fennel et al., 2006; White and Matsumoto, 2012). Water samples were collected at different times of the day, often between mid-morning and early afternoon. During these periods, PAR was high and

photo-adaptation could have influenced measured chlorophyll concentrations. The fact that model Chl *a* values are within the range of measured values is considered a positive result and provides confidence in the model simulated phytoplankton biomass.

On visual comparison of the simulated and measured $p\text{CO}_2$ (Fig. 4.6) it is clear that the model captures some of the long term trends and the diel cycles associated with photosynthesis and respiration at the 9m station. There were periods, however, where the model diverged from observations to the point where, as was the case in late August (Fig 4.6C), $p\text{CO}_2$ was underestimated by as much as 400 μatm . The most important source of this error is likely due to the model not resolving direct advection of high CO_2 water from the lake hypolimnion during upwelling events. Upwelling events were common in the simulation area in 2013, particularly in August, and are shown in Figure 4.5A as periods where water temperatures rapidly drop below average. During August, upwelling events closely match periods of large error in simulated $p\text{CO}_2$ (Fig. 4.5A and 4.6C). The DIC boundary conditions were calculated using surface $p\text{CO}_2$ data (Fig. 4.4) and, therefore, do not fully resolve the full influence of upwelling events on the nearshore. Very little information is available in the literature for a thorough discussion of carbon advection during upwelling events in the Great Lakes. The regular occurrence of upwelling likely plays an important role in the late summer model error. Other possible, although likely smaller, sources of error could be from the model overestimating primary production or underestimating community respiration due to the lack of a microbial community and other heterotrophic consumers in the model. Also, the model could have underestimated air-water CO_2 renewal rates due to the hydrodynamic transfer velocity calculated for that boundary. It was shown by comparing two different air-water CO_2

transfer velocity parameterizations from the literature that reasonable variation in air-water transfer velocity does not substantially impact the accuracy of model output so this did not likely influence model error at levels observed in Figure 4.6.

Phytoplankton photosynthesis and respiration was simulated based on a modified method from Chen et al. (2002), *Cladophora* photosynthesis and respiration was determined using the Great Lakes *Cladophora* model of Tomlinson et al. (2010), and mussel respiration was determined using a mass balance technique assuming an 80% carbon recycling efficiency, with clearance and grazing rates calculated as a function of temperature based on the work of Tyner (2013). Table 4.5 summarizes the monthly mean, net, production and respiration values for phytoplankton, *Cladophora*, and mussels. The simulated nearshore zone is clearly autotrophic with monthly mean community, net production rates ranging from 7.5 mmol C m⁻² d⁻¹ in October to 83.5 mmol C m⁻² d⁻¹ in August, and benthic community production ranges from 6.7 mmol C m⁻² d⁻¹ in October to 83.6 mmol C m⁻² d⁻¹ in August. These monthly mean, benthic values are within the range of benthic production found in the eastern basin of Lake Erie in the late 1990s based on *in situ* ΔO₂ and ΔDIC measurements (Davies and Hecky, 2005).

Biomass specific, net production rates (Fig. 4.19) were calculated as the ratio of model simulated *Cladophora* net production (mg C m⁻² d⁻¹) to *Cladophora* biomass (gDW m⁻²) for comparison with the same rates reported by Malkin et al. (2010) in the western nearshore zone of Lake Ontario. Malkin et al. (2010) measured *Cladophora* production rates *in situ* using benthic chambers and the ΔpCO₂ method, and also simulated *Cladophora* production using the *Cladophora* Growth Model (Higgins et al., 2005a; Malkin et al., 2008). The biomass specific production rates simulated by the

Table 4.5: Model calculated net, monthly mean, production and respiration for phytoplankton, *Cladophora*, and mussels as well as the net, monthly mean, nearshore community production, and the net benthic community production, calculated as the sum of *Cladophora* net production and mussel respiration only. Negative values indicate net respiration and positive values indicate net production. Units for all values are $\text{mmol C m}^{-2} \text{d}^{-1}$.

Month of 2013	Net Mean Phytoplankton Production	Net Mean <i>Cladophora</i> Production	Mean Mussel Respiration	Net Community Production	Net Benthic Production
June	0.057	51.552	-11.292	40.317	40.260
July	-0.136	81.713	-29.672	51.905	52.041
August	-0.105	104.031	-2.405	83.521	83.626
September	1.3	92.91	-25.167	69.042	67.743
October	0.738	23.001	-16.288	7.459	6.72

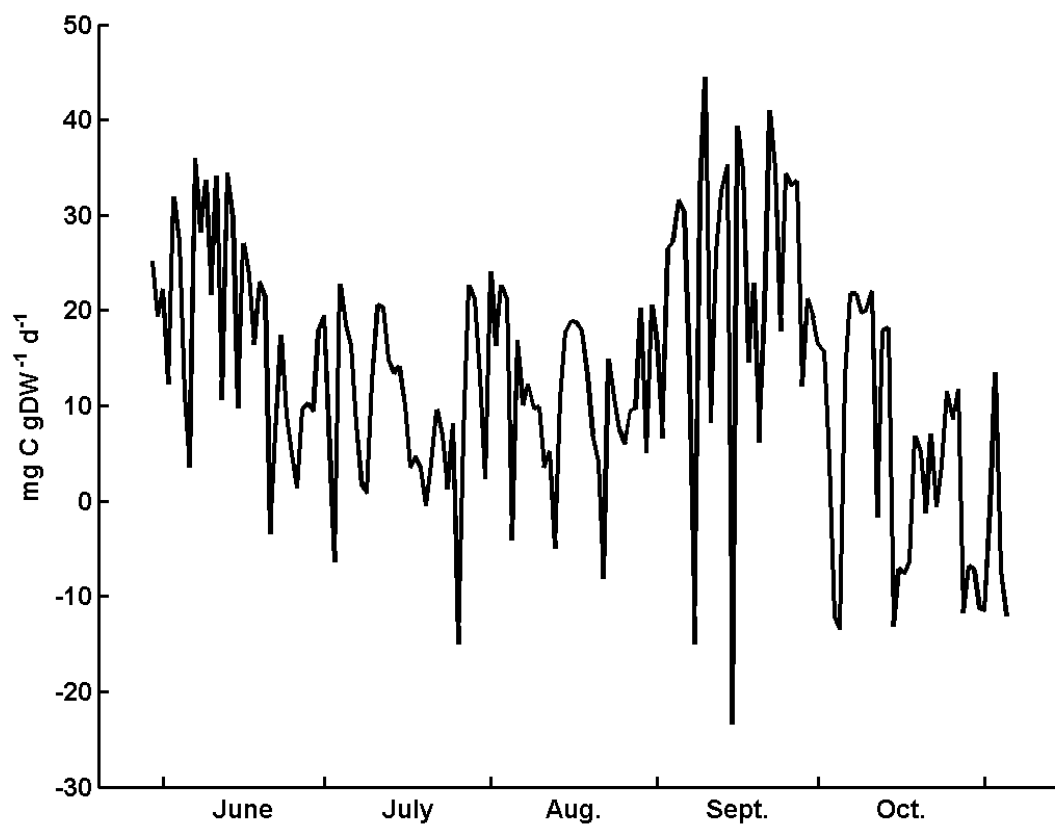


Figure 4.19: Biomass specific, *Cladophora* net production calculated as the ratio of daily mean *Cladophora* net production and daily mean *Cladophora* biomass.

NCPM were remarkably similar to both measured and model simulated values found by Malkin et al. (2010) both in terms of magnitude, ranging from -20 to +50 mg C gDW⁻¹ d⁻¹, and in seasonal trend, with a peak in June, a minimum in July and August, and a peak again in September (Fig. 4.19). The depth of *Cladophora* production measured and simulated by Malkin et al. (2010) was considerably shallower (2 m) than that of the domain simulated here (10 m). Malkin et al. (2010) report daily, net phytoplankton production rates at 10m depth of -673 to 660 mg C m⁻² d⁻¹, while rates simulated by the NCPM for the 9m station ranged from -1.64 to 15.6 mg C m⁻² d⁻¹, indicating that phytoplankton were much more abundant in the studied region of Lake Ontario than that of Lake Michigan here. The ability of *Cladophora* to grow at a depth of 10m in Lake Michigan at rates similar to *Cladophora* at 2m depth in Lake Ontario is not surprising due to the difference in phytoplankton abundance and, therefore, water clarity between Lake Michigan and Lake Ontario.

Although the magnitude of *Cladophora* production was simulated at reasonable levels, biomass was simulated low through June and into early July, and was overestimated in August and September (Fig. 4.9A). These errors appear modest in terms of the seasonal biomass range (Auer et al., 2010), but they may account for at least some of the underestimated CO₂ draw down in June (Fig. 4.6A), and the overestimated CO₂ draw down in September (Fig. 4.6D). Error in the NCPM simulation of *Cladophora* biomass and production may be due to the lack of vertical structure in the NCPM. The near bottom dreissenid mussel, *Cladophora* complex produces an interesting system under the control of vertical mixing. If mixing is very high than mussels have access to a constantly renewed source of food, and their excreted phosphorus is diluted into the water

column reducing *Cladophora* access (Dayton et al., 2014). High mixing allows mussels to clear the water column faster potentially increasing light penetration needed for *Cladophora* growth. If mixing is very low than mussels do not have access to as much food, a result of plankton depletion in the near bottom boundary layer due to their own grazing (L. Boegman et al., 2008; Zhang et al., 2008), while the concentration of mussel excreted phosphorus increases, increasing *Cladophora* access. Low mixing also impacts light penetration as less of the water column is cleared of particulate matter by mussels causing light penetration to decrease. When low mixing conditions persist, mussel excretion will eventually decline due to the lack of food, and *Cladophora* phosphorus uptake will deplete near bottom available phosphorus, a process which will be effected by light intensity. This interplay between mixing, mussel food supply, bottom light intensity, mussel P excretion, and *Cladophora* growth may cause there to be a mixing intensity which produces the maximum *Cladophora* biomass based on an optimal balance between light levels and P supply for growth (see discussion in Chapter 3).

Without stratification in the NCPM, *Cladophora* could be under estimated in the spring and summer when mixing is low and overestimated in the late summer and fall when mixing is high (Fig. 4.5D). To test this hypothesis, the output of the NPFM from Chapter 2 was compared to that of the NCPM. Both models simulated the same domain and region of Lake Michigan during the summer and fall of 2013. The NPFM incorporates vertical structure and stratification between the 20cm thick near bottom layer and the between the upper and lower halves of the water column. Figure 4.20 presents the difference between the NCPM and NPFM bottom PAR, dissolved phosphorus, and *Cladophora* biomass output. Negative values in Figure 4.20 indicate

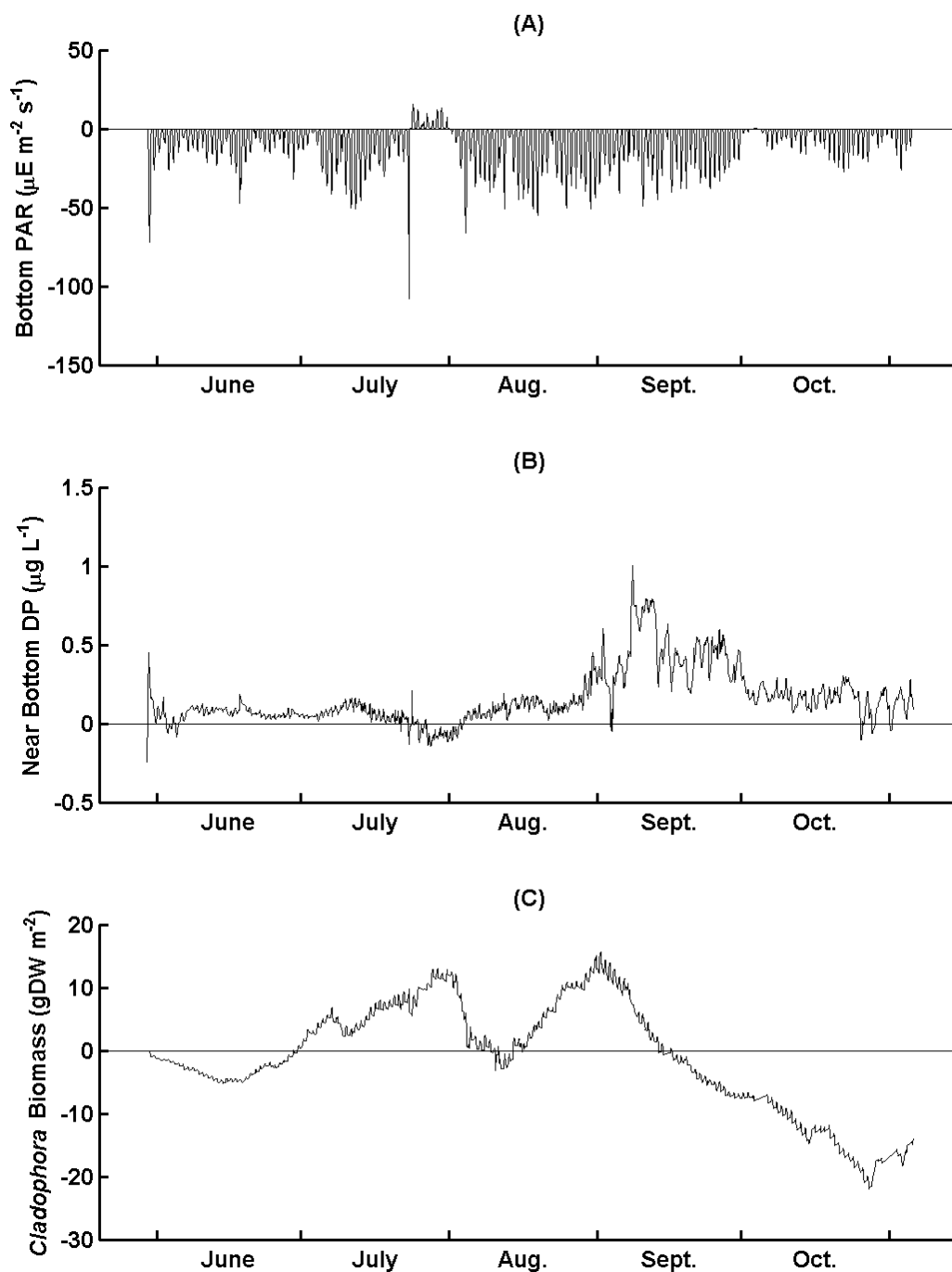


Figure 4.20: The difference between the NPFM and NCPM simulated bottom PAR (A), dissolved phosphorus in the near bottom layer (B), and *Cladophora* biomass (C). Values were calculated as: NPFM – NCPM so that negative values indicate periods where the NPFM produced output which was lower than the NCPM and positive values indicate periods where the NPFM produced output which was higher than the NCPM.

periods where the NPFM produced output which was lower than the NCPM and positive values indicate periods where the NPFM produced output which was higher than the NCPM. NPFM, with stratification, produces lower output values than the NCPM, which is well mixed, and the positive values indicate periods where the NPFM produces higher output values than the NCPM. Throughout the simulation, the influence of stratification was to decrease bottom PAR (Fig. 4.20A) and increase near bottom dissolved phosphorus concentration (Fig. 4.20B). The net result of these impacts and, therefore, of vertical mixing rates was to produce lower *Cladophora* biomass in June and increase biomass in July, increase biomass at the end of August and beginning of September, and lower biomass in through the fall (Fig. 4.20C). The lack of vertical structure in the NCPM may be responsible for the simulated $p\text{CO}_2$ error during the first several days of September (Fig. 4.6D) as *Cladophora* production was likely overestimated during this period. The results of the comparison between the NPFM and the NCPM suggest that any error in *Cladophora* production during mid-June was not likely associated with mixing, although it is possible that the NPFM did not fully represent the vertical mixing dynamics of the nearshore zone (see discussion in Chapter 2). Both models underestimated *Cladophora* biomass by the beginning of July suggesting that model simulated PAR or near bottom DP was not simulated perfectly in either simulation.

Areal phytoplankton production and phytoplankton carbon concentration in the offshore zone of Lake Michigan during 2007 and 2008 was reported by Fahnenstiel et al. (2010). The NCPM estimated a mean phytoplankton carbon content of $1.36 \mu\text{mol C L}^{-1}$ ($16.37 \text{ mg C m}^{-3}$) which agrees with mean surface layer values found by Fahnenstiel et al. (2010) between the spring isothermal mixing period and the mid-stratification period (~5

to 30 mg C m^{-3}). Phytoplankton production measured at the offshore stations in 2007 and 2008 ranged from 16.67 to $83.33 \text{ mmol C m}^{-2} \text{ d}^{-1}$, with peak values measured in July. If these values are converted to volumetric units based on an approximate depth of 100 m for the two sampling stations, then production rates ranged from approximately 0.17 to $0.83 \text{ mmol C m}^{-3} \text{ d}^{-1}$. If the values reported for phytoplankton in Table 5 are converted to volumetric units for the model domain, they range from -0.014 to $0.13 \text{ mmol C m}^{-3} \text{ d}^{-1}$. The range of these values is lower than that reported by Fahnenstiel et al. (2010) although similar in magnitude at the high and low ends of each range. The difference between the two production estimates is likely due to production in the deep chlorophyll layer (DCL) during the stratified period in the lake offshore and the increased mussel predation in the nearshore due to the shallower depth. DCL Chl *a* concentrations in 2011 were nearly double those observed in the model domain in 2013 (Pothoven and Fahnenstiel, 2013). The general agreement between the two ranges accounting for the difference in phytoplankton abundance between the two regions provides confidence in the model estimated phytoplankton production.

Lake Michigan is oligotrophic and has been shown to be approaching the trophic level of Lake Superior (Mida et al., 2010). As an oligotrophic system, it is likely that bacterial metabolism plays a role in the lake carbon cycle (Biddanda et al., 2001). Biddanda and Cotner (2002) show that the carbon flux through bacteria ranges from 12.5% to 76.5% of primary production in the Lake Michigan southern basin based on measurements made at stations in the nearshore and offshore during the winter and summer of 1999 and 2000. If bacterial production is on the same order of magnitude as phytoplankton primary production, it is unlikely that bacteria would substantially

influence the nearshore carbon budget as phytoplankton were shown to be nearly insignificant when compared to *Cladophora* and mussels (Fig. 4.11 and 4.13).

Cladophora have been shown to exude relatively large amounts of dissolved organic carbon when under stress (Wyatt et al., 2014a; Wyatt et al., 2014b), and with high particulate detrital concentrations in the model domain (Fig. 4.11) it is possible that a large microbial community, able to utilize these sources of carbon, could be sustained in the nearshore water column and benthos.

Other heterotrophic consumers may influence the nearshore carbon cycle as well, and their exclusion from the NCPM may have contributed, in part, to the model error. Benthic invertebrates such as amphipods and chironomids may be in high abundance due to increased sediment nutrients associated with mussel egested material and changes to benthic habitat (González and Downing, 1999; Higgins and Vander Zanden, 2010; Tyner, 2013; Vanderploeg et al., 2002). The invasive round goby is also found in high abundance in the Lake Michigan nearshore (Vanderploeg et al., 2002) and may play a part in the benthic carbon cycle (Pennuto et al., 2012; Wilson et al., 2006). Future work should focus on the magnitude and role of bacteria and higher trophic level consumers in the nearshore carbon cycle to determine if inclusion of these components might result in more accurate simulation of C and P dynamics.

4.5.2 The Nearshore Trophic Structure and Dreissenid Mussels

The results of the NCPM simulation and test scenario with no mussels suggest that dreissenid mussels play a critical role in supporting primary production in the Lake Michigan nearshore zone. With mussels present at mean densities of 5500 individuals m^{-2} , *Cladophora* net production rates are on the order of 100 $\text{mmol C m}^{-2} \text{d}^{-1}$ in July and

August, nearly two orders of magnitude greater than phytoplankton (Fig. 4.13). Mussel grazing limits the phytoplankton biomass and reduces the residence time of phytoplankton in the nearshore capping production. When mussels were removed from the model simulation, *Cladophora* mean, net production dropped 89%. Interestingly, biomass specific, net growth rates of both *Cladophora* and phytoplankton decreased in the test scenario from the base simulation (Fig. 4.17) suggesting that the mussels stimulate water column phytoplankton growth in addition to benthic *Cladophora* growth even though they limit biomass due to grazing. These findings reinforce results of other studies where the influence of dreissenid mussels on the phytoplankton community was modeled. Bierman et al. (2005) found that selective feeding and phosphorus recycling rates could allow increased blue green algae production in Saginaw Bay, Lake Huron. Zhang et al., (2008) and Zhang et al. (2011) concluded that mussel phytoplankton grazing in Lake Erie was limited by a concentration boundary layer in the lake near bottom layer and that even though phytoplankton abundance declined, non-edible phytoplankton abundance increased due to selective feeding and the increase in available nutrients associated with mussel phosphorus recycling.

The no mussel test scenario predicted that areal *Cladophora* production without mussels present was still substantially larger than that of phytoplankton although the *Cladophora* biomass decreased 76% and phytoplankton biomass increased 49%. *Cladophora* tissue C:P ratios have been observed to be more than twice that of phytoplankton in Lake Michigan and other Great Lakes (Bootsma et al., 2012; Higgins et al., 2008b; Malkin et al., 2010) indicating that *Cladophora* is able to produce substantially more biomass for the same amount of available phosphorus than

phytoplankton. In the NCPM *Cladophora* net production is calculated as the change in biomass based on the *Cladophora* model calculated growth and respiration and assuming 30% of biomass is carbon as presented by Higgins et al. (2008) and Malkin et al. (2010). The *Cladophora* model calculated the amount of phosphorus in *Cladophora* tissue based on phosphorus uptake and respiration (Tomlinson et al., 2010) producing a time variable *Cladophora* C:P ratio throughout the 2013 model simulation. The NCPM simulated *Cladophora* C:P ratios were between 451 and 1091 molar with a mean of 799 molar. Model simulated *Cladophora* C:P ratios were twice the 300 to 450 range measured by Bootsma et al. (2012), but within the 630 to 1557 molar range measured in Lake Ontario by Malkin (2007). The *Cladophora* C:P ratios simulated by the NCPM indicate that *Cladophora* production may be an important part of nearshore primary production even when biomass is below nuisance levels. However, the NCPM no mussel test scenario likely over-estimates *Cladophora* production during July, August, and September due to the lack of model vertical structure (Fig. 4.20C). Without stratification in the NCPM, *Cladophora* were able to access the entire water column dissolved phosphorus pool, which, although *DP* was 15% less in the test scenario due to the lack of mussel phosphorus recycling, allowed greater *Cladophora* growth than would be possible in a stratified environment. If *Cladophora* growth was lower in the no mussel test scenario, than phytoplankton production would likely increase due to the lack of competition for limited dissolved phosphorus resources in the model domain.

The NCPM no mussel test scenario had lower offshore to nearshore PC fluxes than the mussel scenario, with months where the mean boundary PC flux direction was reversed (Fig. 12 and 15). If phytoplankton concentration was higher in the nearshore

when mussels were not present, then horizontal fluxes would consistently be in the nearshore to offshore direction, opposite of what was observed when mussels were present. These results agree with the hypotheses made in Chapter 1. During the 1980s nearshore Chl *a* concentration was higher on average than in the offshore, but by 2005, the annual mean nearshore to offshore Chl *a* concentration gradient was weak to non-existent. It is reasonable to assume that phytoplankton production played a much greater role in the nearshore carbon and phosphorus cycles when mussels were not present than they do today.

Mussels appear to produce a shift in nearshore primary production from the water column to the benthos, as observed in other studies (Higgins and Vander Zanden, 2010; Higgins et al., 2014), while supporting a net autotrophic nearshore zone. *Cladophora* C:P ratios simulated by the NPCM ranged from 2 to 5 times that of phytoplankton which was assumed to be a constant 207 molar. The model also assumed that mussel recycling maintained the constant seston C:P ratio in excreted and egested waste. Added model complexity may improve how the influence of mussel recycling on nearshore stoichiometry is simulated, however, at a general level the NPCM simulation output indicated that mussel recycling of phytoplankton supports high *Cladophora* growth rates by increasing available phosphorus and light at depth. *Cladophora* was able to utilize these resources to support production at levels higher than phytoplankton and mussels due to the stoichiometric limits of *Cladophora*. Even though dreissenid mussels in the Lake Michigan nearshore zone represent a massive population of heterotrophic consumers, the net influence of their grazing and recycling activity is to support a net autotrophic nearshore ecosystem due to their co-location in the nearshore bottom layer

with *Cladophora* which, as a primary producer with a high tolerance for limited available phosphorus can grow at high rates when supported by mussel water column clearing and phosphorus recycling.

4.6 Conclusions

Using a 1D box model of the Lake Michigan nearshore carbon and phosphorus dynamics, it was found that grazing and nutrient recycling by dreissenid mussels supported high *Cladophora* production, which in combination with high *Cladophora* C:P ratios resulted in a net autotrophic nearshore during the summer. Model accuracy compared to measurements was acceptable, with the primary source of error likely associated with the lack of vertical structure, which precluded the influence of turbulent vertical mixing on the near bottom layer. Mussels force nearshore primary production to be primarily benthic due to their ability to keep phytoplankton crop at low concentrations, clear the water column, and recycle phosphorus, increasing its availability to *Cladophora*. Phytoplankton production was a very small component of the nearshore carbon cycle and was found to be insignificant when compared to that of *Cladophora* a result of both mussel grazing and the ability of *Cladophora* to grow at a high rate with a C:P ratio. Mussels increased both *Cladophora* and phytoplankton growth rates, even though phytoplankton abundance was kept in check by mussel grazing and nearshore-offshore mixing. The findings of this modeling study suggest that dreissenid mussels play a critical role in engineering nearshore, biological energy pathways, supporting the findings and hypotheses of other recent studies (Higgins and Vander Zanden, 2010; Higgins et al., 2014; Turschak et al., 2014). The coupling of the NCPM with a more complex hydrodynamic framework or 3D hydrodynamic model may improve nearshore model

accuracy. Coupling with whole-lake biophysical models will help to elucidate the relative importance of nearshore carbon and nutrient dynamics to the lake as a whole.

CHAPTER 5

SYNTHESIS AND CONCLUSIONS

This is the first study to use a computer model to simulate the carbon and phosphorus dynamics of the Lake Michigan nearshore zone associated with both dreissenid mussels and *Cladophora* algae. The Nearshore Phosphorus Flux Model and the Nearshore Carbon and Phosphorus Model were shown to accurately represent the phosphorus and carbon pools at a 9m deep nearshore station north of Milwaukee, WI showing promise for further application in other Great Lakes. By comparing realistic model output with simulation test scenarios, performed with mussels removed from the model domains, the influence of dreissenid mussels on *Cladophora* growth and nearshore carbon and phosphorus storage and fluxes was identified and quantified. It was found that dreissenid mussels increase nearshore phosphorus and carbon storage primarily by supporting *Cladophora* growth during the summer. In addition, the results of this study indicate that mussels produce a consistent flux of particulate material from the lake offshore to the nearshore and a regular flux of dissolved phosphorus from the nearshore to the offshore. Although there is room for model improvement in the form of improved parameterizations and increased hydrodynamic complexity, highlighting important areas of future research, the results of this study represent an important step forward in our understanding of the Lake Michigan nearshore ecosystem under the influence of dreissenid mussels.

By analyzing a long term data set of water quality parameters collected in the nearshore zone of Lake Michigan near Milwaukee, WI, it was found that the Lake Michigan nearshore has experienced changes similar to those in the Lake Michigan

pelagic over the last three decades (Evans et al., 2011; Fahnenstiel et al., 2010b; Mida et al., 2010) with declining phytoplankton abundance, and increasing water clarity.

Nearshore chlorophyll *a* concentrations were larger than those of the offshore in the 1980s and 1990s and have decreased steadily and at a faster rate than in the offshore between 1980 and 2013 resulting in a nearly uniform, annual mean concentration of chlorophyll *a* in the nearshore and offshore. The results of comparing test simulations where mussels were not included with realistic simulations with mussels included at recently observed densities indicate that nearshore dreissenid mussels produce a consistent flux of particulate phosphorus and carbon from the offshore to the nearshore. Although some of this demand may be provided by tributary and non-point source inputs in some areas of Lake Michigan, in general, the nearshore mussel community relies heavily on offshore sources of particulate organic material to survive (Bootsma, 2009; Malkin et al., 2012). Incorporation of nearshore mussels into 3-D biogeochemical simulations of Lakes Erie and Simcoe demonstrated the important role of advection of water masses over dense mussel colonies on whole lake production (Bocaniov et al., 2014; Schwalb et al., 2015). Including nearshore dreissenid mussels and *Cladophora* growth in 3-D biogeochemical simulations of Lake Michigan will help to improve our understanding of the role of dreissenid mussels and *Cladophora* on whole lake phosphorus dynamics and energy pathways.

Dreissenid quagga mussels have had a dramatic impact on the Lake Michigan nearshore zone through both their ability to filter the nearshore water column, thereby increasing light penetration, and their ability to recycle phosphorus from particulate to dissolved available forms. The net result of these effects is to support the growth of

Cladophora algae at nuisance levels in the nearshore, near bottom layer. It could be argued that offshore quagga mussels play a major role in producing nearshore water quality conditions through the so called “mid-depth sink” and nearshore-offshore exchange (Vanderploeg et al., 2010). Evidence of this process was highlighted in Chapter 2 as dramatic changes in water clarity and nearshore silica concentration occurred coincident with the expansion of quagga mussels offshore, in contrast to the minimal change that occurred when large populations of zebra mussels first colonized the nearshore zone as early as 1990 (Fleischer et al., 2001; Karatayev et al., 2014; Nalepa et al., 2014). The results of model test scenarios demonstrate, however, that even with offshore boundary conditions set to values measured *in situ*, thereby accounting for the influence of offshore mussels on the nearshore zone, *Cladophora* growth, nearshore total phosphorus, and primary production decreased substantially. The results of test simulation comparisons provides considerable support for the critical role nearshore dreissenid mussels are playing in Lake Michigan nutrient dynamics and energy pathways through their support of *Cladophora* growth, despite lower concentrations of phosphorus in the pelagic ecosystem.

In the late summer and fall, much of the *Cladophora* biomass and stored phosphorus in the nearshore is lost due to *Cladophora* detachment and sloughing. Sloughed *Cladophora* is either advected offshore, pooled into nearshore settling pits, or accumulated along shoreline beaches (Auer et al., 2010; Higgins et al., 2008b; Tyner, 2013). The fate of sloughed *Cladophora* likely plays an important role in the net influence of dreissenid mussels on Lake Michigan carbon and phosphorus dynamics. If *Cladophora* accumulates on beaches it may produce conditions suitable for *E coli*

(Verhougstraete et al., 2010; Whitman et al., 2003). However, little is known about the fate of excreted and respired phosphorus and carbon associated with sloughed *Cladophora* on the shoreline. If sloughed *Cladophora* accumulates in depositional areas, recent observations suggest that anoxia forms within these pits producing conditions that may promote the production of the botulism toxin (Chun et al., 2013; Tyner, 2013). If *Cladophora* is advected offshore, it may play a role in the pelagic and profundal food web, expanding the reach of nearshore mussels across the lake, and providing a mechanism by which losses of nutrients and energy from the pelagic zone are partially compensated for (Turschak et al., 2014). After detachment from nearshore benthos the fate of *Cladophora* is likely a combination of these three end points, dependent on local hydrodynamic conditions.

Cladophora growth in the near bottom layer is dependent on mussel phosphorus excretion as well as mussel water column clearing which are both controlled by turbulent vertical mixing. Intuitively it would be expected that low vertical mixing between the near bottom layer and overlying water column would allow mussel excreted dissolved phosphorus to accumulate in the near bottom layer increasing its availability for *Cladophora* uptake (Bootsma and Liao, 2013; Dayton et al., 2014). It was found that low vertical mixing rates near the lake bottom would only increase nutrient concentrations until mussels no longer have access to food, which is delivered to the near bottom layer by vertical mixing. Mussel phosphorus excretion decreases over time with decreasing food quality and quantity (Bootsma and Liao, 2013; Johengen et al., 2013). In addition, because vertical mixing delivers particulate material to the near bottom layer where mussels have access to it, vertical mixing controls the ability of mussels to clear the water

column and modify the nearshore light climate, which directly impacts *Cladophora* growth and phosphorus uptake. It is hypothesized that there is likely an optimal combination of food supply and dissolved phosphorus retention in the near bottom layer, controlled by vertical mixing, which produces the maximum amount of *Cladophora* growth. This hypothesis will be extremely difficult to confirm by collecting empirical data alone. Combining techniques for measuring mussel clearance rate and vertical mixing, such as *in-situ* particle imaging velocimetry in the nearshore bottom layer (Liao et al., 2009), with benthic chambers and portable CO₂ monitoring systems to measure *Cladophora* and mussel production rates in the bottom layer (Malkin et al., 2010) will provide useful data on these individual processes, but will not be able to fully capture all of the critical processes acting in concert. Simulating the nearshore zone and the bottom layer mussel-*Cladophora* complex with a model provides a useful and necessary method for calculating the net result of vertical mixing and mussel grazing and phosphorus excretion on *Cladophora* growth. Although identified and quantified at a general level here, future studies should focus on refining model simulations of this process using models with higher vertical resolution which will be able to put this process in the context of the entire water column. These models should be validated against detailed observations of vertical mixing, nutrient concentrations, *Cladophora* biomass, and mussel grazing and phosphorus recycling in the nearshore zone.

It was shown that the nearshore mussel-*Cladophora* complex controls cross-shore phosphorus and carbon fluxes and produces a net sink for atmospheric CO₂ in the nearshore during the summer. Nearshore Lake Michigan biogeochemistry and the role of the nearshore zone in lake nutrient dynamics and energy pathways is therefore sensitive

to nearshore vertical mixing through these interactions. In this context, the spatial distribution and time scales of vertical mixing change must be accurately accounted for when modeling lake biogeochemical dynamics (Dayton et al., 2014). Future research should focus on measurement and parameterizations of nearshore vertical mixing, with attention paid to the *Cladophora* mat itself (Escartín and Aubrey, 1995; Nepf, 2012) and benthic structure such as rocks, boulders, different substrate types, and in situ measurements over mussel beds (Liao et al., 2009; Nowell and Jumars, 1984).

The nearshore zone is a sink for offshore particulate phosphorus and, to a lesser extent, a source of dissolved phosphorus through the summer due to mussel grazing of particulate phosphorus, excretion of dissolved phosphorus, and *Cladophora* phosphorus uptake and storage. Quagga mussel dissolved phosphorus excretion supported *Cladophora* growth through nearly the entire 2013 growth season, agreeing with empirical results suggesting that mussels support *Cladophora* growth at nuisance levels in the Great Lakes (Bootsma et al. 2009; Ozersky et al. 2009). The net result of mussel activity in the nearshore is to produce a sink for lake phosphorus during the summer. These results from Chapter 3 agree with the nearshore shunt hypothesis (Hecky et al., 2004) and other statistical and modeling studies (Bocaniov et al., 2014; Cha et al., 2011). However, confirmation of the critical role of *Cladophora* in the nearshore shunt represents an important, novel finding.

Based on research conducted in Lake Erie and Lake Ontario showing that *Cladophora* photosynthesis was often greater than that of phytoplankton in the nearshore (Davies and Hecky, 2005; Malkin et al., 2010), it was hypothesized that *Cladophora* production likely dominates in the Lake Michigan nearshore. The results of this study

confirm this hypothesis and suggest that the nearshore shunt hypothesis may extend to lake carbon. By shifting carbon pathways from the water column to the benthos in model simulations, dreissenid mussels increased nearshore carbon through supporting high rates of *Cladophora* photosynthesis and carbon storage in *Cladophora* tissue, which drives a consistent flux of particulate carbon and dissolved inorganic carbon from the offshore to the nearshore. Although the majority of mussel grazed particulate carbon was respired as CO₂ into the nearshore zone, the model calculated such high levels of *Cladophora* photosynthesis, sustained by mussel water column clearing and phosphorus recycling as well as the ability of *Cladophora* to grow at a high tissue C:P ratio, that water column CO₂ was consistently below saturation with respect to the atmosphere causing invasion of CO₂ from the atmosphere to the lake.

Quantifying the impact of the nearshore shunt on lake wide nutrient dynamics and energy pathways remains a critical question for future research. In Chapter 3, the summertime accumulation of phosphorus in the nearshore zone attributable to dreissenid mussels was compared to the inter-annual variability in Lake Michigan southern basin total phosphorus and the estimated annual loading of total phosphorus to the Lake Michigan southern basin on an areal basis. These calculations were based on estimates of the portion of the lake nearshore benthos associated with mussels and *Cladophora* (12 – 100%). It was found that the summer time accumulation of phosphorus in the nearshore likely has a modest impact (~10%) on offshore total phosphorus concentrations. These calculations were made with mean and estimated values and their accuracy will likely improve if repeated using model output produced with a lake wide, 3-D biogeochemical model which incorporates nearshore mussels and *Cladophora* (Pauer et al., 2011).

Detailed characterization of nearshore substrate and *Cladophora* coverage lake wide using technology such as satellite imagery and associated modeling (e.g. Shuchman et al., 2013) should be considered a priority so that these future models will be capable of putting nearshore shunt dynamics into the most accurate, whole-lake setting.

The results of this study demonstrate that *Cladophora* production in the Lake Michigan nearshore zone is much greater than that of nearshore phytoplankton and that this production is sustained through the bottom-up influence of dreissenid mussel water column clearing and phosphorus recycling as well as the ability of *Cladophora* to grow at a high tissue C:P ratio. Top-down and bottom-up manipulations of lake food webs have been shown to dramatically change air-water CO₂ fluxes and impact the autotrophic and heterotrophic state of lakes (Carpenter et al., 1987; Cole et al., 2000; Schindler et al., 1997). Through the trophic cascade, increasing or decreasing predator populations or nutrient inputs forces drastic changes in lake primary production (Bunnell et al., 2013; Carpenter et al., 1985; Nicholls, 1999) reinforcing the importance of an ecosystem based approach to lake management. As ecosystem engineers, bivalves transform lake ecosystems through benthic-pelagic coupling, and transformation of benthic habitat (Atkinson and Vaughn, 2015; Newell, 2004; Strayer et al., 1999). Dreissenid mussels sustain an autotrophic nearshore environment and a nearshore carbon and phosphorus shunt through the summer by recycling offshore energy which traditionally was sustained, to a large extent, by pelagic and offshore benthic recycling (Brooks and Edgington, 1994; Conley et al., 1988; Schelske, 1985; Shafer and Armstrong, 1994). As Lake Michigan continues to become more oligotrophic due to phosphorus loading abatement policies (Barbiero et al., 2002; Evans et al., 2011; Mida et al., 2010), and

profundal quagga mussel impacts on production and nutrient dynamics (Bootsma and Liao, 2013; Johengen et al., 2013; Mida et al., 2010; Rowe et al., 2015; Vanderploeg et al., 2010), the role of nearshore dreissenid mussels in lake nutrient dynamics and energy pathways may become increasingly important.

REFERENCES

- Ackerman, J.D., 1999. Effect of velocity on the filter feeding of dreissenid mussels (*Dreissena polymorpha* and *Dreissena bugensis*): implications for trophic dynamics. *Can. J. Fish. Aquat. Sci.* 56, 1551–1561. doi:10.1139/cjfas-56-9-1551
- Ackerman, J.D., Loewen, M.R., Hamblin, P.F., 2001. Lake Erie Benthic-Pelagic coupling over a zebra mussel reef in western. *Limnol. Oceanogr.* 46, 892–904.
- Arhonditsis, G., Brett, M., 2004. Evaluation of the current state of mechanistic aquatic biogeochemical modeling. *Mar. Ecol. Prog. Ser.* 271, 13–26. doi:10.3354/meps271013
- Atilla, N., McKinley, G.A., Bennington, V., Baehr, M., Urban, N., DeGrandpre, M., Desai, A.R., Wu, C., 2011. Observed variability of Lake Superior pCO₂. *Limnol. Oceanogr.* 56, 775–786. doi:10.4319/lo.2011.56.3.0775
- Atkinson, C.L., Vaughn, C.C., 2015. Biogeochemical hotspots: temporal and spatial scaling of the impact of freshwater mussels on ecosystem function. *Freshw. Biol.* 60, 563–574. doi:10.1111/fwb.12498
- Atkinson, C.L., Vaughn, C.C., Forshay, K.J., Cooper, J.T., 2013. Aggregated filter-feeding consumers alter nutrient limitation: Consequences for ecosystem and community dynamics. *Ecology* 94, 1359–1369. doi:10.1890/12-1531.1
- Auer, M.T., Canale, R.P., 1982. Ecological Studies and Mathematical Modeling of *Cladophora* in Lake Huron: 2. Phosphorus Uptake Kinetics. *J. Great Lakes Res.* 8, 84–92. doi:10.1016/S0380-1330(82)71946-X
- Auer, M.T., Canale, R.P., Grundler, H.C., Matsuoka, Y., 1982. Ecological Studies and Mathematical Modeling of *Cladophora* in Lake Huron: 1. Program Description and Field Monitoring of Growth Dynamics. *J. Great Lakes Res.* 8, 73–83. doi:10.1016/S0380-1330(82)71945-8
- Auer, M.T., Tomlinson, L.M., Higgins, S.N., Malkin, S.Y., Howell, E.T., Bootsma, H. a., 2010. Great Lakes *Cladophora* in the 21st century: same algae—different ecosystem. *J. Great Lakes Res.* 36, 248–255. doi:10.1016/j.jglr.2010.03.001
- Baldwin, B.S., Mayer, M.S., Dayton, J., Pau, N., Mendilla, J., Sullivan, M., Moore, A., Ma, A., Mills, E.L., 2002. Comparative growth and feeding in zebra and quagga mussels (*Dreissena polymorpha* and *Dreissena bugensis*): implications for North American lakes. *Can. J. Fish. Aquat. Sci.* 59, 680–694. doi:10.1139/F02-043

- Barbiero, R.P., Tuchman, M.L., Millard, E.S., 2006. Post-dreissenid increases in transparency during summer stratification in the offshore waters of Lake Ontario: Is a reduction in whiting events the cause? *J. Great Lakes Res.* 32, 131–141.
- Barbiero, R.P., Tuchman, M.L., Warren, G.J., Rockwell, D.C., 2002. Evidence of recovery from phosphorus enrichment in Lake Michigan. *Can. J. Fish. Aquat. Sci.* 59, 1639–1647. doi:10.1139/F02-132
- Beletsky, D., Schwab, D., McCormick, M., 2006. Modeling the 1998-2003 summer circulation and thermal structure in Lake Michigan. *J. Geophys. Res.* 111. doi:10.1029/2005jc003222
- Bennett, N.D., Croke, B.F.W., Guariso, G., Guillaume, J.H. a., Hamilton, S.H., Jakeman, A.J., Marsili-Libelli, S., Newham, L.T.H., Norton, J.P., Perrin, C., Pierce, S. a., Robson, B., Seppelt, R., Voinov, A. a., Fath, B.D., Andreassian, V., 2013. Characterising performance of environmental models. *Environ. Model. Softw.* 40, 1–20. doi:10.1016/j.envsoft.2012.09.011
- Berg, D.J., Fisher, S.W., Landrum, P.F., 1996. Clearance and Processing of Algal Particles by Zebra Mussels (*Dreissena polymorpha*). *J. Great Lakes Res.* 22, 779–788. doi:10.1016/S0380-1330(96)70996-6
- Biddanda, B. a., Cotner, J.B., 2002. Love Handles in Aquatic Ecosystems: The Role of Dissolved Organic Carbon Drawdown, Resuspended Sediments, and Terrigenous Inputs in the Carbon Balance of Lake Michigan. *Ecosystems* 5, 431–445. doi:10.1007/s10021-002-0163-z
- Biddanda, B., Ogdahl, M., Cotner, J., 2001. Dominance of bacterial in oligotrophic metabolism relative to eutrophic waters. *Limnol. Oceanogr.* 46, 730–739.
- Bierman, V.J., Dolan, D.M., 1981. Modeling of Phytoplankton-Nutrient Dynamics in Saginaw Bay, Lake Huron. *J. Great Lakes Res.* 7, 409–439.
- Bierman, V.J., Kaur, J., Depinto, J. V, Feist, T.J., Dilks, D.W., Drive, A., Agency, U.S.E.P., 2005. Modeling the Role of Zebra Mussels in the Proliferation of Blue-green Algae in Saginaw Bay, Lake Huron. *J. Great Lakes Res.* 31, 32–55.
- Bocaniov, S. a., Smith, R.E.H., Spillman, C.M., Hipsey, M.R., Leon, L.F., 2014. The nearshore shunt and the decline of the phytoplankton spring bloom in the Laurentian Great Lakes: insights from a three-dimensional lake model. *Hydrobiologia* 731, 151–172. doi:10.1007/s10750-013-1642-2
- Boegman, L., Loewen, M.R., Culver, D.A., Hamblin, P.F., Charlton, M.N., 2008. Spatial-Dynamic Modeling of Algal Biomass in Lake Erie: Relative Impacts of Dreissenid Mussels and Nutrient Loads. *J. Environ. Eng.* 134, 456–468. doi:10.1061/(ASCE)0733-9372(2008)134:6(456)

- Boegman, L., Loewen, M.R., Hamblin, P.F., Culver, D.A., 2008. Vertical mixing and weak stratification over zebra mussel colonies in western Lake Erie. *Limnol. Oceanogr.* 53, 1093–1110.
- Bootsma, H., Liao, Q., 2013. Nutrient Cycling by Dreissenid Mussels, in: *Quagga and Zebra Mussels*. CRC Press, pp. 555–574. doi:doi:10.1201/b15437-43
- Bootsma, H.A., 2009. Causes , Consequences and Management of Nuisance Cladophora; Final Report Submitted to the Environmental Protection Agency Great Lakes National Program Office. Chicago, IL.
- Bootsma, H.A., Waples, J.T., Liao, Q., 2012. Identifying Major Phosphorus Pathways in the Lake Michigan Nearshore Zone; Final Report Submitted to the Milwaukee Metropolitan Sewerage District. Milwaukee, WI.
- Boyce, F.M., 1974. Some Aspects of Great Lakes Physics of Importance to Biological and Chemical Processes. *J. Fish. Res. Board Canada* 31, 689–730. doi:10.1139/f74-098
- Brooks, A.S., Edgington, D.N., 1994. Biogeochemical control of phosphorus cycling and primary production in Lake Michigan. *Limnol. Oceanogr.* 39, 961 – 968.
- Buesseler, K.O., Antia, A.N., Chen, M., Fowler, S.W., Gardner, W.D., Gustafsson, O., Harada, K., Michaels, A.F., van der Loeff'o, M.R., Sarin, M., Steinberg, D.K., Trull, T., 2007. An assessment of the use of sediment traps for estimating upper ocean particle fluxes. *J. Mar. Res.* 65, 345–416.
- Bunnell, D.B., Barbiero, R.P., Ludsin, S. a., Madenjian, C.P., Warren, G.J., Dolan, D.M., Brenden, T.O., Briland, R., Gorman, O.T., He, J.X., Johengen, T.H., Lantry, B.F., Lesht, B.M., Nalepa, T.F., Riley, S.C., Riseng, C.M., Treska, T.J., Tsehaye, I., Walsh, M.G., Warner, D.M., Weidel, B.C., 2013. Changing Ecosystem Dynamics in the Laurentian Great Lakes: Bottom-Up and Top-Down Regulation. *Bioscience* 64, 26–39. doi:10.1093/biosci/bit001
- Bunnell, D.B., Madenjian, C.P., Claramunt, R.M., 2006. Long-term changes of the Lake Michigan fish community following the reduction of exotic alewife (*Alosa pseudoharengus*). *Can. J. Fish. Aquat. Sci.* 63, 2434–2446. doi:10.1139/F06-132
- Bunnell, D.B., Madenjian, C.P., Holuszko, J.D., Adams, J. V., French, J.R.P., 2009a. Expansion of *Dreissena* into offshore waters of Lake Michigan and potential impacts on fish populations. *J. Great Lakes Res.* 35, 74–80. doi:10.1016/j.jglr.2008.10.002
- Bunnell, D.B., Madenjian, C.P., Holuszko, J.D., Adams, J. V., French, J.R.P., 2009b. Expansion of *Dreissena* into offshore waters of Lake Michigan and potential impacts on fish populations. *J. Great Lakes Res.* 35, 74–80. doi:10.1016/j.jglr.2008.10.002

- Buzzelli, C., Parker, M., Geiger, S., Wan, Y., Doering, P., Haunert, D., 2013. Predicting System-Scale Impacts of Oyster Clearance on Phytoplankton Productivity in a Small Subtropical Estuary. *Environ. Model. Assess.* 18, 185–198. doi:10.1007/s10666-012-9338-y
- Canale, R.P., Auer, M.T., 1982a. Ecological Studies and Mathematical Modeling of Cladophora in Lake Huron: 5. Model Development and Calibration. *J. Great Lakes Res.* 8, 112–125. doi:10.1016/S0380-1330(82)71949-5
- Canale, R.P., Auer, M.T., 1982b. Ecological Studies and Mathematical Modeling of Cladophora in Lake Huron: 7. Model Verification and System Response. *J. Great Lakes Res.* 8, 134–143. doi:10.1016/S0380-1330(82)71951-3
- Cariboni, J., Gatelli, D., Liska, R., Saltelli, a., 2007. The role of sensitivity analysis in ecological modelling. *Ecol. Modell.* 203, 167–182. doi:10.1016/j.ecolmodel.2005.10.045
- Carpenter, S.R., Kitchell, J.F., Hodgson, J.R., 1985. Cascading Trophic Interactions and Lake Productivity. *Bioscience* 35, 634–639.
- Carpenter, S.R., Kitchell, J.F., Hodgson, J.R., Cochran, P.A., Elser, J.J., Elser, M.M., Lodge, D.M., Kretchmer, D., He, X., von Ende, C.N., 1987. Regulation of Lake Primary Productivity by Food Web Structure. *Ecology* 68, 1863 – 1876.
- Carrick, H.J., Lowe, R.L., 2007. Nutrient Limitation of Benthic Algae in Lake Michigan: the Role of Silica. *J. Phycol.* 43, 228–234. doi:10.1111/j.1529-8817.2007.00326.x
- Cecala, R.K., Mayer, C.M., Schulz, K.L., Mills, E.L., 2008. Increased benthic algal primary production in response to the invasive zebra mussel (*Dreissena polymorpha*) in a productive ecosystem, Oneida Lake, New York. *J. Integr. Plant Biol.* 50, 1452–66. doi:10.1111/j.1744-7909.2008.00755.x
- Cha, Y., Stow, C. a, Nalepa, T.F., Reckhow, K.H., 2011. Do invasive mussels restrict offshore phosphorus transport in Lake Huron? *Environ. Sci. Technol.* 45, 7226–31. doi:10.1021/es2014715
- Chapra, S.C., 1997. *Surface Water-Quality Modeling*. Waveland Press, Inc., Long Grove, IL.
- Chapra, S.C., Dolan, D.M., 2012. Great Lakes total phosphorus revisited: 2. Mass balance modeling. *J. Great Lakes Res.* 38, 741–754.
- Chen, C., Ji, R., Schwab, D.J., Beletsky, D., Fahnenstiel, G.L., Jiang, M., Johengen, T.H., Vanderploeg, H., Eadie, B., Budd, J.W., Bundy, M.H., Gardner, W., Cotner, J., Lavrentyev, P.J., 2002. A model study of the coupled biological and physical

- dynamics in Lake Michigan. *Ecol. Modell.* 152, 145–168. doi:10.1016/S0304-3800(02)00026-1
- Chen, C.S., Ji, R.B., Schwab, D.J., Beletsky, D., Fahnenstiel, G.L., Jiang, M.S., Johengen, T.H., Vanderploeg, H., Eadie, B., Budd, J.W., Bundy, M.H., Gardner, W., Cotner, J., Lavrentyev, P.J., 2002. A model study of the coupled biological and physical dynamics in Lake Michigan. *Ecol. Modell.* 152, 145–168. doi:10.1016/S0304-3800(02)00026-1
- Chun, C.L., Ochsner, U., Byappanahalli, M.N., Whitman, R.L., Tepp, W.H., Lin, G., Johnson, E. a, Peller, J., Sadowsky, M.J., 2013. Association of toxin-producing *Clostridium botulinum* with the macroalga *Cladophora* in the Great Lakes. *Environ. Sci. Technol.* 47, 2587–94. doi:10.1021/es304743m
- Colbert, S.L., Hammond, D.E., 2007. Temporal and spatial variability of radium in the coastal ocean and its impact on computation of nearshore cross-shelf mixing rates. *Cont. Shelf Res.* 27, 1477–1500. doi:10.1016/j.csr.2007.01.003
- Cole, J.J., Pace, M.L., Carpenter, S.R., Kitchell, J.F., 2000. Persistence of net heterotrophy in lakes during nutrient addition and food web manipulations. *Limnol. Oceanogr.* 45, 1718–1730. doi:10.4319/lo.2000.45.8.1718
- Combes, V., Chenillat, F., Di Lorenzo, E., Rivière, P., Ohman, M.D., Bograd, S.J., 2013. Cross-shore transport variability in the California Current: Ekman upwelling vs. eddy dynamics. *Prog. Oceanogr.* 109, 78–89. doi:10.1016/j.pocean.2012.10.001
- Conley, D.J., Quigley, M.A., Schelske, C.L., 1988. Silica and Phosphorus Flux from Sediments: Importance of Internal Recycling in Lake Michigan. *Can. J. Fish. Aquat. Sci.* 45, 1030–1035. doi:10.1139/f88-126
- Connelly, N.A., O'Neill, C.R., Knuth, B.A., Brown, T.L., 2007. Economic impacts of zebra mussels on drinking water treatment and electric power generation facilities. *Environ. Manage.* 40, 105–112. doi:10.1007/s00267-006-0296-5
- Conway, H.L., Parker, J.I., Yaguchi, E.M., Mellinger, D.L., 1977. Biological Utilization and Regeneration of Silicon in Lake Michigan. *J. Fish. Res. Board Canada* 34, 537–544. doi:10.1139/f77-085
- Cuhel, R.L., Aguilar, C., 2013. Ecosystem Transformations of the Laurentian Great Lake Michigan by Nonindigenous Biological Invaders. *Ann. Rev. Mar. Sci.* 5, 289–320. doi:10.1146/annurev-marine-120710-100952
- Dame, R.E., Prins., T.C., 1998. Bivalve carrying capacity in coastal ecosystems. *Aquat. Ecol.* 31, 409–421.

- Davies, J.-M., Hecky, R.E., 2005. Initial Measurements of Benthic Photosynthesis and Respiration in Lake Erie. *J. Great Lakes Res.* 31, 195–207. doi:10.1016/S0380-1330(05)70314-2
- Dayton, A.I., Auer, M.T., Atkinson, J.F., 2014. Cladophora, mass transport, and the nearshore phosphorus shunt. *J. Great Lakes Res.* 40, 790–799. doi:10.1016/j.jglr.2014.05.010
- Depew, D.C., Houben, A.J., Guildford, S.J., Hecky, R.E., 2011. Distribution of nuisance Cladophora in the lower Great Lakes: Patterns with land use, near shore water quality and dreissenid abundance. *J. Great Lakes Res.* 37, 656–671. doi:10.1016/j.jglr.2011.08.011
- Diggins, T.P., 2001. A Seasonal Comparison of Suspended Sediment Filtration by Quagga (*Dreissena bugensis*) and Zebra (*D. polymorpha*) Mussels. *J. Great Lakes Res.* 27, 457–466. doi:10.1016/S0380-1330(01)70660-0
- Dodds, W.K., Biggs, B.J.F., Iggs, B.A.J.F.B., 2014. Water velocity attenuation by stream periphyton and macrophytes in relation to growth form and architecture Water velocity attenuation by stream periphyton and macrophytes in 21, 2–15.
- Dolan, D.M., Chapra, S.C., 2012. Great Lakes total phosphorus revisited: 1. Loading analysis and update (1994-2008). *J. Great Lakes Res.* 38, 730–740.
- Edwards, W.J., Rehmann, C.R., McDonald, E., Culver, D.A., 2005. The impact of a benthic filter feeder : limitations imposed by physical transport of algae to the benthos 214, 205–214. doi:10.1139/F04-188
- Escartín, J., Aubrey, D.G., 1995. Flow Structure and Dispersion within Algal Mats. *Estuar. Coast. Shelf Sci.* 40, 451–472.
- Evans, M.A., Fahnenstiel, G., Scavia, D., 2011. Incidental Oligotrophication of North American Great Lakes. *Environ. Sci. Technol.* 45, 3297–3303.
- Fahnenstiel, G., Nalepa, T., Pothoven, S., Carrick, H., Scavia, D., 2010a. Lake Michigan lower food web: Long-term observations and Dreissena impact. *J. Great Lakes Res.* 36, 1–4. doi:10.1016/j.jglr.2010.05.009
- Fahnenstiel, G., Pothoven, S., Vanderploeg, H., Klarer, D., Nalepa, T., Scavia, D., 2010b. Recent changes in primary production and phytoplankton in the offshore region of southeastern Lake Michigan. *J. Great Lakes Res.* 36, 20–29. doi:10.1016/j.jglr.2010.03.009
- Fennel, K., Wilkin, J., Levin, J., Moisan, J., O'Reilly, J., Haidvogel, D., 2006. Nitrogen cycling in the Middle Atlantic Bight: Results from a three-dimensional model and

- implications for the North Atlantic nitrogen budget. *Global Biogeochem. Cycles* 20, n/a–n/a. doi:10.1029/2005GB002456
- Fenton, J.D., McKee, W.D., 1990. On calculating the lengths of water waves. *Coast. Eng.* 14, 499–513. doi:10.1016/0378-3839(90)90032-R
- Fitzgerald, S. a., Gardner, W.S., 1993. An algal carbon budget for pelagic-benthic coupling in Lake Michigan. *Limnol. Oceanogr.* 38, 547–560. doi:10.4319/lo.1993.38.3.0547
- Fleischer, G.W., DeSorcie, T.J., Holuszko, J.D., 2001. Lake-wide Distribution of *Dreissena* in Lake Michigan, 1999. *J. Great Lakes Res.* 27, 252–257. doi:10.1016/S0380-1330(01)70638-7
- Flindt, M.R., Pedersen, C.B., Amos, C.L., Levy, a., Bergamasco, a., Friend, P.L., 2007. Transport, sloughing and settling rates of estuarine macrophytes: Mechanisms and ecological implications. *Cont. Shelf Res.* 27, 1096–1103. doi:10.1016/j.csr.2006.08.011
- Foreman, R.J., Emeis, S., 2010. Revisiting the Definition of the Drag Coefficient in the Marine Atmospheric Boundary Layer. *J. Phys. Oceanogr.* 40, 2325–2332. doi:10.1175/2010JPO4420.1
- Gerritsen, J., Holland, A.F., Irvine, D.E., 1994. Suspension-Feeding Bivalves and the Fate of Primary Production: An Estuarine Model Applied to Chesapeake Bay. *Estuaries* 17, 403–416.
- González, M.J., Downing, A., 1999. Mechanisms underlying amphipod responses to zebra mussel (*Dreissena polymorpha*) invasion and implications for fish-amphipod interactions. *Can. J. Fish. Aquat. Sci.* 56, 679–685. doi:10.1139/f98-211
- Graba, M., Kettab, A., Sauvage, S., Sanchez-Pérez, J.M., 2012. On modeling chronic detachment of periphyton in artificial rough, open channel flow. *Desalin. Water Treat.* 41, 79–87. doi:10.1080/19443994.2012.664681
- Hawley, N., Lesht, B.M., Schwab, D.J., 2004. A comparison of observed and modeled surface waves in southern Lake Michigan and the implications for models of sediment resuspension. *J. Geophys. Res.* 109, C10S03. doi:10.1029/2002JC001592
- Hecky, R.E., Smith, R.E.H., Barton, D.R., Guildford, S.J., Taylor, W.D., Charlton, M.N., Howell, T., 2004. The nearshore phosphorus shunt: a consequence of ecosystem engineering by dreissenids in the Laurentian Great Lakes. *Can. J. Fish. Aquat. Sci.* 61, 1285–1293.
- Henry, P.-Y., Myrhaug, D., 2013. Wave-induced drag force on vegetation under shoaling random waves. *Coast. Eng.* 78, 13–20. doi:10.1016/j.coastaleng.2013.03.004

- Higgins, S.N., Althouse, B., Devlin, S.P., Vadeboncoeur, Y., Vander Zanden, M.J., 2014. Potential for large-bodied zooplankton and dreissenids to alter the productivity and autotrophic structure of lakes. *Ecology* 95, 2257–2267.
- Higgins, S.N., Hecky, R.E., Guildford, S.J., 2005a. Modeling the Growth, Biomass, and Tissue Phosphorus Concentration of *Cladophora glomerata* in Eastern Lake Erie: Model Description and Field Testing. *J. Great Lakes Res.* 31, 439–455. doi:10.1016/S0380-1330(05)70275-6
- Higgins, S.N., Hecky, R.E., Guildford, S.J., 2006. Environmental controls of *Cladophora* growth dynamics in eastern Lake Erie: Application of the *Cladophora* growth model (CGM). *J. Great Lakes Res.* 32, 629–644.
- Higgins, S.N., Hecky, R.E., Guildford, S.J., 2008a. The collapse of benthic macroalgal blooms in response to self-shading. *Freshw. Biol.* 53, 2557–2572. doi:10.1111/j.1365-2427.2008.02084.x
- Higgins, S.N., Malkin, S.Y., Todd Howell, E., Guildford, S.J., Campbell, L., Hiriart-Baer, V., Hecky, R.E., 2008b. An Ecological Review of *Cladophora Glomerata* (Chlorophyta) in the Laurentian Great Lakes. *J. Phycol.* 44, 839–854. doi:10.1111/j.1529-8817.2008.00538.x
- Higgins, S.N., Pennuto, C.M., Howell, E.T., Lewis, T.W., Makarewicz, J.C., 2012. Urban influences on *Cladophora* blooms in Lake Ontario. *J. Great Lakes Res.* 38, 116–123. doi:10.1016/j.jglr.2011.11.017
- Higgins, S.N., Todd Howell, E., Hecky, R.E., Guildford, S.J., Smith, R.E., 2005b. The Wall of Green: The Status of *Cladophora glomerata* on the Northern Shores of Lake Erie's Eastern Basin, 1995–2002. *J. Great Lakes Res.* 31, 547–563. doi:10.1016/S0380-1330(05)70283-5
- Higgins, S.N., Vander Zanden, M.J., 2010. What a difference a species makes: a meta-analysis of dreissenid mussel impacts on freshwater ecosystems. *Ecol. Monogr.* 80, 179–196.
- Ho, D.T., Wanninkhof, R., Schlosser, P., Ullman, D.S., Hebert, D., Sullivan, K.F., 2011. Toward a universal relationship between wind speed and gas exchange: Gas transfer velocities measured with ³He/SF₆ during the Southern Ocean Gas Exchange Experiment. *J. Geophys. Res.* 116, C00F04. doi:10.1029/2010JC006854
- Johengen, T.H., Vanderploeg, H.A., Liebig, J.R., 2013. Effects of algal composition, seston stoichiometry, and feeding rate on zebra mussel (*Dreissena polymorpha*) nutrient excretion in two Laurentian Great Lakes, in: *Quagga and Zebra Mussels: Biology, Impacts, and Control*. CRC Press Boca Raton, FL, pp. 445–459.

- Jones, H.F.E., Pilditch, C. a., Bruesewitz, D. a., Lohrer, A.M., 2011. Sedimentary environment influences the effect of an infaunal suspension feeding bivalve on estuarine ecosystem function. *PLoS One* 6. doi:10.1371/journal.pone.0027065
- Jones, L.A., Ricciardi, A., 2005. Influence of physicochemical factors on the distribution and biomass of invasive mussels (*Dreissena polymorpha* and *Dreissena bugensis*) in the St . Lawrence River. *Can. J. Fish. Aquat. Sci.* 62, 1953–1962. doi:10.1139/F05-096
- Jonsson, P.R., Petersen, J.K., Karlsson, Ö., Loo, L., Nilsson, S., 2014. Particle depletion above experimental bivalve beds : In situ measurements and numerical modeling of bivalve filtration in the boundary layer. *Limnol. Oceanogr.* 50, 1989–1998.
- Karatayev, A.Y., Burlakova, L.E., Padilla, D.K., 2014. Zebra versus quagga mussels: a review of their spread, population dynamics, and ecosystem impacts. *Hydrobiologia* 97–112. doi:10.1007/s10750-014-1901-x
- Kerfoot, W.C., Yousef, F., Green, S.A., Budd, J.W., Schwab, D.J., Vanderploeg, H.A., 2010. Approaching storm: Disappearing winter bloom in Lake Michigan. *J. Great Lakes Res.* 36, 30–41. doi:10.1016/j.jglr.2010.04.010
- Klump, J.V., Fitzgerald, S. a., Waples, J.T., 2009. Benthic biogeochemical cycling, nutrient stoichiometry, and carbon and nitrogen mass balances in a eutrophic freshwater bay. *Limnol. Oceanogr.* 54, 692–712. doi:10.4319/lo.2009.54.3.0692
- Lejart, M., Clavier, J., Chauvaud, L., Hily, C., 2012. Respiration and Calcification of *Crassostrea gigas*: Contribution of an Intertidal Invasive Species to Coastal Ecosystem CO₂ Fluxes. *Estuaries and Coasts* 35, 622–632.
- Lemmin, U., 1989. Dynamics of horizontal turbulent mixing in a nearshore zone of Lake Geneva. *Limnol. Oceanogr.* 34, 420–434. doi:10.4319/lo.1989.34.2.0420
- Leon, L.F., Smith, R.E.H., Malkin, S.Y., Depew, D., Hipse, M.R., Antenucci, J.P., Higgins, S.N., Hecky, R.E., Rao, R.Y., 2012. Nested 3D modeling of the spatial dynamics of nutrients and phytoplankton in a Lake Ontario nearshore zone. *J. Great Lakes Res.* 38, 171–183. doi:10.1016/j.jglr.2012.02.006
- Liao, Q., Bootsma, H.A., Xiao, J., Klump, J.V., Hume, A., Long, M.H., Berg, P., 2009. Development of an in situ underwater particle image velocimetry (UWPIV) system. *Limnol. Oceanogr. Methods* 7, 169–184.
- Limburg, K.E., Luzadis, V. a., Ramsey, M., Schulz, K.L., Mayer, C.M., 2010. The good, the bad, and the algae: Perceiving ecosystem services and disservices generated by zebra and quagga mussels. *J. Great Lakes Res.* 36, 86–92. doi:10.1016/j.jglr.2009.11.007

- Lonsdale, D.J., Cerrato, R.M., Holland, R., Mass, A., Holt, L., Schaffner, R. a., Pan, J., Caron, D. a., 2009. Influence of suspension-feeding bivalves on the pelagic food webs of shallow, coastal embayments. *Aquat. Biol.* 6, 263–279. doi:10.3354/ab00130
- Lowe, R.L., Pillsbury, R.W., 1995. Shifts in Benthic Algal Community Structure and Function Following the Appearance of Zebra Mussels (*Dreissena polymorpha*) in Saginaw Bay, Lake Huron. *J. Great Lakes Res.* 21, 558–566.
- Madenjian, C.P., 1995. Removal of algae by the zebra mussel (*Dreissena polymorpha*) population in western Lake Erie: a bioenergetics approach. *Can. J. Fish. Aquat. Sci.* 52, 381–390. doi:10.1139/f95-040
- Madenjian, C.P., Fahnenstiel, G.L., Johengen, T.H., Nalepa, T.F., Vanderploeg, H.A., Fleischer, G.W., Schneeberger, P.J., Benjamin, D.M., Smith, E.B., Bence, J.R., Rutherford, E.S., Lavis, D.S., Robertson, D.M., Jude, D.J., Ebener, M.P., 2002. Dynamics of the Lake Michigan food web , 1970 – 2000 753, 736–753. doi:10.1139/F02-044
- Madon, S.P., Schneider, D.W., Stoeckel, J. a, Sparks, R.E., 1998. Effects of inorganic sediment and food concentrations on energetic processes of the zebra mussel, *Dreissena polymorpha* : implications for growth in turbid rivers. *Can. J. Fish. Aquat. Sci.* 55, 401–413. doi:10.1139/f97-214
- Mahrt, L., Vickers, D., Frederickson, P., Davidson, K., Smedman, A.S., 2003. Sea-surface aerodynamic roughness. *J. Geophys. Res.* 108, 9. doi:3171 10.1029/2002jc001383
- Malkin, S.Y., 2007. The Ecology of the Nuisance Macroalga , *Cladophora glomerata* , and its Resurgence in Lake Ontario.
- Malkin, S.Y., Bocaniov, S. a., Smith, R.E., Guildford, S.J., Hecky, R.E., 2010. In situ measurements confirm the seasonal dominance of benthic algae over phytoplankton in nearshore primary production of a large lake. *Freshw. Biol.* 55, 2468–2483. doi:10.1111/j.1365-2427.2010.02477.x
- Malkin, S.Y., Guildford, S.J., Hecky, R.E., 2008. Modeling the growth response of *Cladophora* in a Laurentian Great Lake to the exotic invader *Dreissena* and to lake warming. *Limnol. Oceanogr.* 53, 1111–1124. doi:10.4319/lo.2008.53.3.1111
- Malkin, S.Y., Silsbe, G.M., Smith, R.E.H., Howell, E.T., 2012. A deep chlorophyll maximum nourishes benthic filter feeders in the coastal zone of a large clear lake. *Limnol. Oceanogr.* 57, 735–748.

- Malkin, S. Y., Sorichetti, R.J., Wiklund, J. a., Hecky, R.E., 2009. Seasonal abundance, community composition, and silica content of diatoms epiphytic on *Cladophora glomerata*. *J. Great Lakes Res.* 35, 199–205. doi:10.1016/j.jglr.2008.12.008
- Mida, J.L., Scavia, D., Fahnenstiel, G.L., Pothoven, S. a., Vanderploeg, H. a., Dolan, D.M., 2010. Long-term and recent changes in southern Lake Michigan water quality with implications for present trophic status. *J. Great Lakes Res.* 36, 42–49. doi:10.1016/j.jglr.2010.03.010
- Murthy, C.R., 1976. Horizontal Diffusion Characteristics in Lake Ontario. *J. Phys. Oceanogr.* 6, 76 – 84.
- Murthy, C.R., Dunbar, D.S., 1981. Structure of the Flow within the Coastal Boundary Layer of the Great Lakes. *J. Phys. Oceanogr.* 11, 1567–1577.
- Nalepa, T.F., Fanslow, D.L., Foley III, A.J., Lang, G. a, Eadie, B.J., Quigley, M. a, 2006. Continued disappearance of the benthic amphipod *Diporeia* spp. in Lake Michigan: is there evidence for food limitation? *Can. J. Fish. Aquat. Sci.* 63, 872–890. doi:10.1139/f05-262
- Nalepa, T.F., Fanslow, D.L., Lang, G. a, Lamarand, D.B., Cummins, L.G., Carter, G.S., 2014. Lake-Wide Benthic Surveys in Lake Michigan in 1994-95, 2000, 2005, and 2010: Abundances of the Amphipod *Diporeia* spp. and Abundances and biomass of the Mussels *Dreissena Polymorpha* and *Dreissena Rostiformis Bugensis*, NOAA Technical Memorandum GLERL-164. Ann Arbor, Michigan.
- Nalepa, T.F., Fanslow, D.L., Lang, G. a., 2009. Transformation of the offshore benthic community in Lake Michigan: recent shift from the native amphipod *Diporeia* spp. to the invasive mussel *Dreissena rostriformis bugensis*. *Freshw. Biol.* 54, 466–479. doi:10.1111/j.1365-2427.2008.02123.x
- Nalepa, T.F., Fanslow, D.L., Pothoven, S. a., 2010. Recent changes in density, biomass, recruitment, size structure, and nutritional state of *Dreissena* populations in southern Lake Michigan. *J. Great Lakes Res.* 36, 5–19. doi:10.1016/j.jglr.2010.03.013
- Nalepa, T.F., Schloesser, D.W., Pothoven, S. a., Hondorp, D.W., Fanslow, D.L., Tuchman, M.L., Fleischer, G.W., 2001. First Finding of the Amphipod *Echinogammarus ischnus* and the Mussel *Dreissena bugensis* in Lake Michigan. *J. Great Lakes Res.* 27, 384–391. doi:10.1016/S0380-1330(01)70653-3
- Nepf, H.M., 2012. Flow and Transport in Regions with Aquatic Vegetation. *Annu. Rev. Fluid Mech.* 44, 123–142. doi:10.1146/annurev-fluid-120710-101048
- Newell, R.I.E., 2004. Ecosystem influences of natural and cultivated populations of suspension-feeding bivalve molluscs: a review. *J. Shellfish Res.*

- Nicholls, K.H., 1999. Evidence for a Trophic Cascade Effect on North-shore Western Lake Erie Phytoplankton Prior to the Zebra Mussel Invasion. *J. Great Lakes Res.* 25, 942–949. doi:10.1016/S0380-1330(99)70791-4
- Nogaro, G., Steinman, A.D., 2014. Influence of ecosystem engineers on ecosystem processes is mediated by lake sediment properties. *Oikos* 123, 500–512. doi:10.1111/j.1600-0706.2013.00978.x
- North, R.L., Smith, R.E.H., Hecky, R.E., Depew, D.C., León, L.F., Charlton, M.N., Guildford, S.J., 2012. Distribution of seston and nutrient concentrations in the eastern basin of Lake Erie pre- and post-dreissenid mussel invasion. *J. Great Lakes Res.* 38, 463–476. doi:10.1016/j.jglr.2012.06.012
- Nowell, A.R.M., Jumars, P.A., 1984. Flow Environments of Aquatic Benthos. *Annu. Rev. Ecol. Syst.* 15, 303 – 328.
- Okubo, A., 1971. Oceanic diffusion diagrams. *Deep. Res.* 18, 789 – 802.
- Ozersky, T., Barton, D.R., Hecky, R.E., Guildford, S.J., 2013. Dreissenid mussels enhance nutrient efflux, periphyton quantity and production in the shallow littoral zone of a large lake. *Biol. Invasions* 15, 2799–2810. doi:10.1007/s10530-013-0494-z
- Ozersky, T., Evans, D.O., Barton, D.R., 2012. Invasive Mussels Alter the Littoral Food Web of a Large Lake: Stable Isotopes Reveal Drastic Shifts in Sources and Flow of Energy. *PLoS One* 7. doi:10.1371/journal.pone.0051249
- Ozersky, T., Malkin, S.Y., Barton, D.R., Hecky, R.E., 2009. Dreissenid phosphorus excretion can sustain *C. glomerata* growth along a portion of Lake Ontario shoreline. *J. Great Lakes Res.* 35, 321–328. doi:10.1016/j.jglr.2009.05.001
- Padilla, D.K., Adolph, S.C., Cottingham, K.L., Schneider, D.W., 1996. Predicting the consequences of dreissenid mussels on a pelagic food web. *Ecol. Model.* 85, 129–144. doi:10.1016/0304-3800(94)00185-5
- Pauer, J.J., Anstead, A.M., Melendez, W., Taunt, K.W., Kreis, R.G., 2011. Revisiting the Great Lakes Water Quality Agreement phosphorus targets and predicting the trophic status of Lake Michigan. *J. Great Lakes Res.* 37, 26–32. doi:10.1016/j.jglr.2010.11.020
- Pennuto, C.M., Howell, E.T., Makarewicz, J.C., 2012. Relationships among round gobies, Dreissena mussels, and benthic algae in the south nearshore of Lake Ontario. *J. Great Lakes Res.* 38, 154–160. doi:10.1016/j.jglr.2012.02.002

- Petersen, J., Maar, M., Ysebaert, T., Herman, P., 2013. Near-bed gradients in particles and nutrients above a mussel bed in the Limfjorden: influence of physical mixing and mussel filtration. *Mar. Ecol. Prog. Ser.* 490, 137–146. doi:10.3354/meps10444
- Pomeroy, L.R., D’Elia, C.F., Schaffner, L.C., 2006. Limits to top-down control of phytoplankton by oysters in Chesapeake Bay. *Mar. Ecol. Prog. Ser.* 325, 301–309. doi:10.3354/meps325301
- Pothoven, S. a., Madenjian, C.P., 2008. Changes in Consumption by Alewives and Lake Whitefish after Dreissenid Mussel Invasions in Lakes Michigan and Huron. *North Am. J. Fish. Manag.* 28, 308–320. doi:10.1577/M07-022.1
- Pothoven, S.A., Fahnenstiel, G.L., 2013. Recent change in summer chlorophyll a dynamics of southeastern Lake Michigan. *J. Great Lakes Res.* 39, 287–294.
- Prins, T.C., Smaal, A.C., Dame, R.F., 1998. A review of the feedbacks between bivalve grazing and ecosystem processes. *Aquat. Ecol.* 31, 349–359. doi:10.1023/a:1009924624259
- Rao, Y.R., Murthy, C.R., 2001. Coastal boundary layer characteristics during summer stratification in Lake Ontario. *J. Phys. Oceanogr.* 31, 1088–1104. doi:10.1175/1520-0485(2001)031<1088:CBLCD>2.0.CO;2
- Rao, Y.R., Schwab, D.J., 2007. Transport and Mixing Between the Coastal and Offshore Waters in the Great Lakes : a Review. *J. Great Lakes Res.* 33, 202–218. doi:10.3394/0380-1330(2007)33
- Reavie, E.D., Barbiero, R.P., Allinger, L.E., Warren, G.J., 2014. Phytoplankton trends in the Great Lakes, 2001–2011. *J. Great Lakes Res.* 40, 618–639. doi:10.1016/j.jglr.2014.04.013
- Robson, B.J., 2014. State of the art in modelling of phosphorus in aquatic systems: Review, criticisms and commentary. *Environ. Model. Softw.* doi:10.1016/j.envsoft.2014.01.012
- Rowe, M.D., Anderson, E.J., Wang, J., Vanderploeg, H. a., 2015. Modeling the effect of invasive quagga mussels on the spring phytoplankton bloom in Lake Michigan. *J. Great Lakes Res.* doi:10.1016/j.jglr.2014.12.018
- Saurel, C., Petersen, J., Wiles, P., Kaiser, M., 2013. Turbulent mixing limits mussel feeding: direct estimates of feeding rate and vertical diffusivity. *Mar. Ecol. Prog. Ser.* 485, 105–121. doi:10.3354/meps10309
- Schelske, C.L., 1985. Biogeochemical silica mass balances in Lake Michigan and Lake Superior. *Biogeochemistry* 1, 197 – 218.

- Schilder, J., Bastviken, D., van Hardenbroek, M., Kankaala, P., Rinta, P., Stötter, T., Heiri, O., 2013. Spatial heterogeneity and lake morphology affect diffusive greenhouse gas emission estimates of lakes. *Geophys. Res. Lett.* 40, 5752–5756. doi:10.1002/2013GL057669
- Schindler, D.E., Carpenter, S.R., Cole, J.J., Kitchell, J.F., Pace, M.L., 1997. Influence of Food Web Structure on Carbon Exchange between Lake and the Atmosphere. *Science* (80-.). 277, 248 – 251.
- Schwalb, A.N., Bouffard, D., Boegman, L., Leon, L., Winter, J.G., Molot, L. a., Smith, R.E.H., 2015. 3D modelling of dreissenid mussel impacts on phytoplankton in a large lake supports the nearshore shunt hypothesis and the importance of wind-driven hydrodynamics. *Aquat. Sci.* 77, 95–114. doi:10.1007/s00027-014-0369-0
- Schwalb, A.N., Bouffard, D., Ozersky, T., Boegman, L., Smith, R.E.H., 2013. Impacts of hydrodynamics and benthic communities on phytoplankton distributions in a large, dreissenid-colonized lake (Lake Simcoe, Ontario, Canada). *Inl. Waters* 3, 269–284.
- Seelbach, P.W., Fogarty, L.R., Bunnell, D.B., Haack, S.K., Rogers, M.W., 2013. A Conceptual Framework for Lake Michigan Coastal/Nearshore Ecosystems , With Application to Lake Michigan Lakewide Management Plan (LaMP) Objectives. Reston, VA.
- Shafer, M.M., Armstrong, D.E., 1994. Mass Fluxes and Recycling of Phosphorus in Lake Michigan, in: Baker, L. (Ed.), *Environmental Chemistry of Lakes and Reservoirs, Advances in Chemistry*. American Chemical Society, Washington, DC, pp. 285–322. doi:doi:10.1021/ba-1994-0237.ch009
- Shuchman, R. a., Sayers, M.J., Brooks, C.N., 2013. Mapping and monitoring the extent of submerged aquatic vegetation in the Laurentian Great Lakes with multi-scale satellite remote sensing. *J. Great Lakes Res.* 39, 78–89. doi:10.1016/j.jglr.2013.05.006
- Stainton, P., Capel, J., Armstrong, F.A.J., Stainton, M.P., Capel, M.J., Armstrong, F.A.J., 1977. The chemical analysis of fresh water. *Canada. Fish. Mar. Serv. Misc. Spec. Publ., Can. Fish. Mar. Serv. Misc* 25, 101 – 111.
- Strayer, D.L., Caraco, N.F., Cole, J.J., Findlay, S., Pace, M.L., 1999. Transformation of freshwater ecosystems by bivalves. A case study of zebra mussels in the Hudson River. *Bioscience* 49, 19–27.
- Stumm, W., Morgan, J.J., 1981. *Aquatic Chemistry: An Introduction Emphasizing Chemical Equilibria in Natural Waters*, 2nd Edition, Second. ed. John Wiley & Sons Inc.

- Tang, H., Vanderploeg, H.A., Johengen, T.H., Liebig, J.R., 2014. Quagga mussel (*Dreissena rostriformis bugensis*) selective feeding of phytoplankton in Saginaw Bay. *J. Great Lakes Res.* 40, 83–94. doi:10.1016/j.jglr.2013.11.011
- Tomlinson, L.M., Auer, M.T., Bootsma, H.A., Owens, E.M., 2010. The Great Lakes Cladophora Model: Development, testing, and application to Lake Michigan. *J. Great Lakes Res.* 36, 287–297. doi:10.1016/j.jglr.2010.03.005
- Turner, C.B., 2010. Influence of zebra (*Dreissena polymorpha*) and quagga (*Dreissena rostriformis*) mussel invasions on benthic nutrient and oxygen dynamics. *Can. J. Fish. Aquat. Sci.* 67, 1899–1908.
- Turschak, B.A., Bunnell, D., Czesny, S., Höök, T.O., Janssen, J., Warner, D., Bootsma, H.A., 2014. Nearshore energy subsidies support Lake Michigan fishes and invertebrates following major changes in food web structure. *Ecology* 95, 1243–1252. doi:10.1890/13-0329.1
- Tyner, E., 2013. Nearshore Benthic Oxygen Dynamics in Lake Michigan. University of Wisconsin - Milwaukee.
- Upstill-Goddard, R.C., 2006. Air–sea gas exchange in the coastal zone. *Estuar. Coast. Shelf Sci.* 70, 388–404. doi:10.1016/j.ecss.2006.05.043
- Urban, N.R., Auer, M.T., Green, S.A., Lu, X., Apul, D.S., Powell, K.D., Bub, L., 2005. Carbon cycling in Lake Superior. *J. Geophys. Res.* 110.
- Vachon, D., Prairie, Y.T., 2013. The ecosystem size and shape dependence of gas transfer velocity versus wind speed relationships in lakes. *Can. J. Fish. Aquat. Sci.* 70, 1757–1764.
- Vanderploeg, H. a., Liebig, J.R., Nalepa, T.F., Fahnenstiel, G.L., Pothoven, S. a., 2010. *Dreissena* and the disappearance of the spring phytoplankton bloom in Lake Michigan. *J. Great Lakes Res.* 36, 50–59. doi:10.1016/j.jglr.2010.04.005
- Vanderploeg, H.A., Nalepa, T.F., Jude, D.J., Mills, E.L., Holeck, K.T., Liebig, J.R., Grigorovich, I.A., Ojaveer, H., 2002. Dispersal and emerging ecological impacts of Ponto-Caspian species in the Laurentian Great Lakes 1. *Can. J. Fish. Aquat. Sci.* 59, 1209–1228. doi:10.1139/F02-087
- Vanderploeg, H.A., Pothoven, S.A., Fahnenstiel, G.L., Cavaletto, J.F., Liebig, J.R., Stow, C. a., Nalepa, T.F., Madenjian, C.P., Bunnell, D.B., 2012. Seasonal zooplankton dynamics in Lake Michigan: Disentangling impacts of resource limitation, ecosystem engineering, and predation during a critical ecosystem transition. *J. Great Lakes Res.* 38, 336–352. doi:10.1016/j.jglr.2012.02.005

- Vaughn, C.C., Nichols, S.J., Spooner, D.E., 2008. Community and foodweb ecology of freshwater mussels. *J. North Am. Benthol. Soc.* 27, 409–423. doi:10.1899/07-058.1
- Verhougstraete, M.P., Byappanahalli, M.N., Rose, J.B., Whitman, R.L., 2010. Cladophora in the Great Lakes: impacts on beach water quality and human health. *Water Sci. Technol.* 62, 68–76. doi:10.2166/wst.2010.230
- Vickers, D., Mahrt, L., 2006. Evaluation of the air-sea bulk formula and sea-surface temperature variability from observations. *J. Geophys. Res.* 111.
- Wallace, J.B., Webster, J.R., 1996. The role of macroinvertebrates in stream ecosystem function. *Annu. Rev. Entomol.* 41, 115–139. doi:10.1146/annurev.ento.41.1.115
- Wanninkhof, R., 1992. Relationship Between Wind Speed and Gas Exchange Over the Ocean. *J. Geophys. Res.* 97, 7373–7382.
- Wanninkhof, R., Asher, W.E., Ho, D.T., Sweeney, C., McGillis, W.R., 2009. Advances in Quantifying Air-Sea Gas Exchange and Environmental Forcing. *Ann. Rev. Mar. Sci.* 1, 213–244. doi:10.1146/annurev.marine.010908.163742
- Waples, J.T., Klump, J.V., 2013. Vertical and horizontal particle transport in the coastal waters of a large lake: An assessment by sediment trap and thorium-234 measurements. *J. Geophys. Res. Ocean.* 118, 5376–5397. doi:10.1002/jgrc.20394
- Waples, J.T., Paddock, R., Janssen, J., Lovalvo, D., Schulze, B., Kaster, J., Val Klump, J., 2005. High Resolution Bathymetry and Lakebed Characterization in the Nearshore of Western Lake Michigan. *J. Great Lakes Res.* 31, 64–74. doi:10.1016/S0380-1330(05)70290-2
- Wetzel, R., 2001. *Limnology, Third Edition: Lake and River Ecosystems*. Academic Press, San Diego.
- White, B., Austin, J., Matsumoto, K., 2012. A three-dimensional model of Lake Superior with ice and biogeochemistry. *J. Great Lakes Res.* 38, 61–71. doi:10.1016/j.jglr.2011.12.006
- White, B., Matsumoto, K., 2012. Causal mechanisms of the deep chlorophyll maximum in Lake Superior: A numerical modeling investigation. *J. Great Lakes Res.* 38, 504–513. doi:10.1016/j.jglr.2012.05.001
- Whitman, R.L., Shively, D.A., Pawlik, H., Nevers, M.B., Byappanahalli, M.N., 2003. Occurrence of *Escherichia coli* and Enterococci in Cladophora (Chlorophyta) in Nearshore Water and Beach Sand of Lake Michigan Occurrence of *Escherichia coli* and Enterococci in Cladophora (Chlorophyta) in Nearshore Water and Beach Sand of Lake Michigan. doi:10.1128/AEM.69.8.4714

- Wilson, K.A., Howell, E.T., Jackson, D.A., 2006. Replacement of Zebra Mussels by Quagga Mussels in the Canadian Nearshore of Lake Ontario : the Importance of Substrate , Round Goby Abundance , and Upwelling Frequency. *J. Great Lakes Res.* 32, 11–28. doi:10.3394/0380-1330(2006)32
- Wyatt, K.H., Rober, A.R., Schmidt, N., Davison, I.R., 2014. Effects of desiccation and rewetting on the release and decomposition of dissolved organic carbon from benthic macroalgae. *Freshw. Biol.* 59, 407–416. doi:10.1111/fwb.12273
- Wyatt, K.H., Tellez, E., Woodke, R.L., Bidner, R.J., Ian, R., Davison, I.R., 2014. Effects of nutrient limitation on the release and use of dissolved organic carbon from benthic algae in Lake Michigan. *Freshw. Sci.* 33, 557–567. doi:10.1086/675453.
- Zhang, H., Culver, D. a., Boegman, L., 2008. A two-dimensional ecological model of Lake Erie: Application to estimate dreissenid impacts on large lake plankton populations. *Ecol. Modell.* 214, 219–241. doi:10.1016/j.ecolmodel.2008.02.005
- Zhang, H., Culver, D., Boegman, L., 2011. Dreissenids in Lake Erie: an algal filter or a fertilizer? *Aquat. Invasions* 6, 175–194. doi:10.3391/ai.2011.6.2.07
- Zhao, D., Xie, L., 2010. A Practical Bi-parameter Formula of Gas Transfer Velocity Depending on Wave States. *J. Oceanogr.* 66, 663–671.
- Zhu, B., Fitzgerald, D.G., Mayer, C.M., Rudstam, L.G., Mills, E.L., 2006. Alteration of Ecosystem Function by Zebra Mussels in Oneida Lake: Impacts on Submerged Macrophytes. *Ecosystems* 9, 1017–1028. doi:10.1007/s10021-005-0049-y

APPENDIX A

SAMPLING METHODS, MEASUREMENT METHODS, AND DATA

A.1: Phosphorus Sampling, Measurement Method, and Raw Data

Phosphorus was measured using water samples collected in the Lake Michigan nearshore zone at the 9m and 20m stations aboard the RV Osprey owned and operated by the University of Wisconsin-Milwaukee, School of Freshwater Sciences. A Niskin bottle was deployed to 2m and 8m depths at the 9m station and 2m, 10m, and 18m depths at the 20m station on the dates listed in Table A.1.1 and A.1.2. The bottle was lowered to the designated depths using a winch attached to the aft rail of the RV Osprey with calibrated marks on the winch cable indicating when the bottle reached the designated depth below the water surface. Water samples were transferred to 4 L Nalgene bottles which were previously washed with 5% HCl solution and rinsed with deionized water. Samples were rinsed with sampled lake water prior to sample transfer. Sample bottles were immediately stored on ice in a cooler until they were returned to the laboratory within several hours. Sample bottles were stored in a refrigerator in the laboratory and were filtered within 24 hours.

Water samples were filtered using Whatman, 0.2 μm glass fiber filters. Filters were ashed in a muffle furnace at 550°C for two hours prior to their use. The volume of sample water filtered varied depending on sample turbidity; typical volumes ranged from 500 ml to 1 L. Filtered volumes were recorded and used to calculate phosphorus concentrations. Filters were stored in desiccators for several days until analysis. Filtrate was used to determine soluble reactive phosphorus (SRP) concentrations (Table A.1.1), and particulate material collected on the filter ($> 0.2 \mu\text{m}$) was used to determine

particulate phosphorus concentrations (Table A.1.2), both using the acid molybdate method (Stainton et al., 1977). Laboratory phosphorus measurements were conducted by graduate students and laboratory technicians in the Bootsma Lab at the School of Freshwater Sciences.

Particulate phosphorus was measured by placing the filters into pre acid washed and DI rinsed Pyrex tubes. The dry filters and tubes were baked at 550°C for 1 hour. After cooling, 2 ml of 1 normal HCl and 10 ml of distilled, deionized water were added to the tubes containing filters. Caps were screwed onto the tube tops loosely and were placed in an oven at 105°C for 2 hours. After cooling, 2.5 ml of mixed molybdate reagent was added to the tubes and 30 minutes was allowed for the development of blue color. Blanks and standards were prepared in the same fashion with standards prepared using SRP stock solution. A mass spectrometer was used to measure sample absorbance at 885 nm with a 1 cm path length. Sample phosphorus concentration was calculated based on a calculated unit extinction factor, the measured standards, and the volume of sample water filtered. SRP was measured following the method for PP without the initial steps of sample drying and acid digestion. SRP was measured with a 10 cm path length at 885 nm.

Table A.1.1: Soluble reactive phosphorus concentration measured at the 9m and 20m monitoring stations during 2013 at the indicated depths. Units of all values are $\mu\text{g P L}^{-1}$. Zeros values indicate measurements below the method detection limit and dashed lines indicate times when samples were not collected or were excluded due to contamination.

Sample Date	Day of 2013	9m Station		20m Station		
		2m	8m	2m	10m	18m
5/29/2013	149	0.556636	0.313108	--	--	--
7/3/2013	184	0.14077	0.316732	0.193558	0.211154	0.175962
7/8/2013	189	0.248961	0.569053	--	--	--
7/17/2013	198	0	0	0	0	0
7/31/2013	212	--	--	0	0	0
8/7/2013	219	0	0	0	0.213175	0
8/20/2013	232	0	0	0	0	0
9/11/2013	254	1.994963	2.455339	2.30188	2.250727	2.625848
9/20/2013	263	0.072972	0.820939	--	--	--
9/25/2013	268	0.633345	1.095516	0.753167	0.496406	0.992811
10/2/2013	275	1.599265	1.880455	1.634414	1.757435	1.915604
10/16/2013	289	0	0.070904	0	0	0.035452
10/22/2013	295	0.178764	0.178764	0	0	0
10/25/2013	298	0	0	0	0	0
11/7/2013	311	0.42229	0.439885	0	0	0
11/13/2013	317	0	0	0	0	0
11/26/2013	330	0.669438	0.57646	--	--	--

Table A.1.2: Particulate phosphorus concentration measured at the 9m and 20m monitoring stations during 2013 at the indicated depths. Units of all values are $\mu\text{g P L}^{-1}$. Dashed lines indicate times when samples were not collected or were excluded due to contamination.

Sample Date	Day of 2013	9m Station		20m Station		
		2 m	8 m	2 m	8 m	18 m
5/29/2013	149	8.304097	4.789781	--	--	--
7/3/2013	184	1.101592	0.99483	0.982698	1.241515	1.438517
7/8/2013	189	2.014907	2.398506	--	--	--
7/17/2013	198	2.087589	3.033263	5.006983	2.753841	1.562663
7/31/2013	212	--	--	1.868704	2.04533	1.356488
8/7/2013	219	3.230201	1.869958	2.836103	2.909996	1.785508
8/20/2013	232	3.265389	2.952724	2.527459	2.484229	1.828661
9/11/2013	254	1.777646	3.032456	1.433586	3.271949	2.465768
9/20/2013	263	2.821297	1.983408	--	--	--
9/25/2013	268	3.051397	2.208927	2.416014	3.31339	1.490086
10/2/2013	275	1.497542	1.294526	2.732358	1.695781	1.144055
10/16/2013	289	1.437832	1.215708	2.535142	2.882032	1.570389
10/22/2013	295	1.428278	1.024634	2.814929	4.589756	2.722804
10/25/2013	298	0.984031	1.277807	2.201331	2.690958	2.81038
11/7/2013	311	6.420912	8.583	2.12805	2.667794	1.862555
11/13/2013	317	2.838762	2.863269	2.070867	2.908199	2.201572
11/26/2013	330	2.761249	3.034447	--	--	--

A.2: *Cladophora* Sampling, Measurement Method, and Raw Data

Cladophora biomass was measured by collecting triplicate samples from the lake bottom at the 9m station by SCUBA diver. A 20cm by 20cm square area of a flat rock surface was scraped clean with a hand scraper and all attached material was carefully collected into a plastic whirl pack bag. Samples were brought to the surface and immediately placed on ice, in the dark, in a cooler. Upon returning to the laboratory within several hours of collection, the contents of benthic scrapes were separated by hand wearing clean latex gloves. *Cladophora* was placed on trays and freeze dried. Dried *Cladophora* tissue samples were then weighed and normalized to the scraped area to provide measurements of dry weight and biomass (Table A.2). *Cladophora* tissue phosphorus content (Table A.2) was measured by homogenizing tissue samples with a mortar and pestle and placing 4 to 7 mg samples into Pyrex tubes. Measurement of *Cladophora* tissue PP then followed the same procedure as for filtered particulate P samples.

Table A.2: Mean and standard deviation of triplicate *Cladophora* biomass and tissue phosphorus content measurements at the 9m station during 2013.

Sample Date	Day of 2013	Mean Biomass (g DW m ⁻²)	Standard Deviation	Mean Tissue P Content (mg P gDW ⁻¹)	Standard Deviation
5/29/2013	149	10.917	3.760	1.281	0.104
7/8/2013	189	129.030	30.030	0.684	0.098
8/7/2013	219	67.288	7.519	0.517	0.062
9/20/2013	263	21.806	7.092	0.969	0.060
11/7/2013	311	50.970	18.992	1.241	0.292

A.3: Dreissenid mussel measurements of density, biomass, and length distribution

Dreissenid mussels were collected from the lake bottom at the 9m station by SCUBA diver following the same benthic scrape procedure as previously presented for *Cladophora*. In the laboratory, mussels were separated from *Cladophora* and other benthic biota by hand. Mussels in each triplicate benthic scrape were counted to determine areal density (Table A.3.1) and sorted into length classes. Biomass was measured by removing mussel tissue from the shells, freeze drying it, and weighing the shell-free, dry tissue. Size distributions were calculated at 1mm intervals between 5mm and 30 mm (Table A.3.2).

Table A.3.1: Mean and standard deviation of measured mussel density and biomass at the 9m station during 2013.

Sample Date	Day of 2013	Mean Density (ind. m ⁻²)	Standard Deviation	Mean Biomass (g DW m ⁻²)	Standard Deviation
5/29/2013	149	3991.667	274.2414	81.37268	5.590586
7/8/2013	189	5050	1316.957	64.49187	16.81842
8/7/2013	219	5525	261.0077	109.059	6.11155
9/20/2013	263	5133.333	518.6119	95.14233	9.612067
11/7/2013	311	4666.667	518.6119	108.6721	12.07686

Table A.3.2: The fraction of mussels within each length class for one representative sample from each day mussels were collected at the 9m station in 2013.

Length Class (mm)	Sample Date				
	5/29/2013	7/8/2013	8/7/2013	9/20/2013	11/7/2013
5	0.000	0.000	0.000	0.000	0.000
6	0.000	0.000	0.000	0.000	0.000
7	0.000	0.000	0.000	0.000	0.012
8	0.000	0.000	0.000	0.000	0.000
9	0.000	0.000	0.000	0.004	0.000
10	0.000	0.000	0.000	0.000	0.000
11	0.000	0.000	0.000	0.004	0.000
12	0.012	0.008	0.000	0.000	0.000
13	0.012	0.020	0.005	0.009	0.012
14	0.012	0.004	0.014	0.009	0.000
15	0.024	0.032	0.024	0.040	0.012
16	0.012	0.071	0.077	0.085	0.018
17	0.054	0.107	0.096	0.080	0.048
18	0.072	0.107	0.100	0.143	0.060
19	0.145	0.087	0.134	0.152	0.119
20	0.181	0.171	0.115	0.156	0.155
21	0.120	0.091	0.110	0.138	0.167
22	0.175	0.115	0.148	0.107	0.173
23	0.096	0.067	0.086	0.027	0.113
24	0.054	0.060	0.048	0.022	0.048
25	0.018	0.036	0.033	0.009	0.030
26	0.006	0.016	0.005	0.004	0.012
27	0.006	0.000	0.005	0.009	0.012
28	0.000	0.008	0.000	0.000	0.012
29	0.000	0.000	0.000	0.000	0.000
30	0.000	0.000	0.000	0.000	0.000

A.4: Sediment Trap Measurements and Data

Two sets of triplicate sediment traps were deployed at the 9m station during the summer and fall of 2013. The traps were suspended using spherical plastic floats at 4m and 8m depths attached to a line anchored to the lake bottom using 125 pounds of weight. Each trap tube was 1 m in length and had a diameter of 0.09 m, and was covered with black plastic to prevent light from penetrating the trap and allowing algal growth inside or on the inner trap walls. The bottom of each trap tube was equipped with a removable cup which was removed and replaced when sediment samples were collected by SCUBA diver approximately once per month from July to November 2013. For each deployment period, 5 mL of liquid chloroform was added to each trap for sample preservation. Sample cups were sealed and stored on ice until reaching the laboratory. In the laboratory, particulates were allowed to settle while the samples were stored in a refrigerator, after which the surface water was siphoned off with a thin tube. All particulate material was carefully extracted from trap cups and transferred to pre weighed aluminum weigh boats. The sediment samples were then freeze dried and weighed (Table A.4). PP measurements (Table A.4) were made by homogenizing individual samples with a mortar and pestle, followed by digestions and phosphorus analysis following the method for *Cladophora* and particulate phosphorus.

Table A.4: Sediment trap dry mass and particulate phosphorus concentrations measured during 2013 at the 9m station. Collection depth indicates whether the sediment trap was located in the upper apparatus (Top) or lower apparatus (Btm). Contaminated sediment trap samples which were not usable are indicated by a dashed line.

Deployment Date	Collection Date	Collection Depth	Collection Replicate	Dry Weight (g)	Particulate Phosphorus Content ($\mu\text{gP mgDW}^{-1}$)
7/11/2013	8/7/2013	Top	A	1.2136	1.18
7/11/2013	8/7/2013	Top	B	1.0001	1.50
7/11/2013	8/7/2013	Top	C	1.1491	1.31
7/11/2013	8/7/2013	Btm	A	18.4913	0.63
7/11/2013	8/7/2013	Btm	B	18.383	0.61
7/11/2013	8/7/2013	Btm	C	18.3751	0.66
8/7/2013	9/20/2013	Top	A	18.5524	0.73
8/7/2013	9/20/2013	Top	B	18.3992	0.82
8/7/2013	9/20/2013	Top	C	18.6861	0.68
8/7/2013	9/20/2013	Btm	A	80.5913	0.78
8/7/2013	9/20/2013	Btm	B	80.5906	0.65
8/7/2013	9/20/2013	Btm	C	80.3208	0.73
9/20/2013	11/7/2013	Top	A	15.5329	0.82
9/20/2013	11/7/2013	Top	B	15.0173	0.82
9/20/2013	11/7/2013	Top	C	--	--
9/20/2013	11/7/2013	Btm	A	19.1401	1.35
9/20/2013	11/7/2013	Btm	B	57.9604	3.57
9/20/2013	11/7/2013	Btm	C	60.4996	0.78
11/7/2013	11/26/2013	Top	A	21.2978	0.81
11/7/2013	11/26/2013	Top	B	21.5024	0.97
11/7/2013	11/26/2013	Top	C	--	--
11/7/2013	11/26/2013	Btm	A	70.5635	0.90
11/7/2013	11/26/2013	Btm	B	70.5784	0.85
11/7/2013	11/26/2013	Btm	C	--	--

A.5: Chlorophyll *a* Sampling, Measurement, and Data

Chlorophyll *a* samples were collected from the same 4 L sample bottles described for SRP and PP sampling. Water was filtered through pre-ashed Whatman GF/F filters (nominal pore size = 0.7 μm) as for SRP and PP. Filtered sample volumes were typically 1 L. When filtering was complete, filters were immediately placed in clean petri dishes which were wrapped in aluminum foil, labeled, and placed in the freezer. Chlorophyll *a* was extracted from filtered phytoplankton using an extraction solvent containing 680 ml of methanol, 27 ml of acetone, and 5 ml of distilled, deionized water. Sample filters were placed in a 15 ml centrifuge tubes and 10 ml of extraction solvent was added with care that the filter was completely submersed in the solvent. Tubes were then capped and placed in the freezer for approximately 24 hours to allow for complete chlorophyll *a* extraction. Tubes were then spun in a centrifuge at 3,000 to 4,000 rpm for a minimum of 5 minutes. Using a pipette, 5 ml of supernatant was removed from the centrifuge tube and placed in a quartz fluorometer tube. Chlorophyll *a* was then measured fluorometrically using a bench top fluorometer. Concentrations of chlorophyll *a* were calculated using the initial filter sample volume (Table A.5).

Table A.5: Chlorophyll *a* concentration measured at the 9m and 20m stations during 2013. Units of all values are in $\mu\text{g L}^{-1}$. Dashed lines indicate times when samples were not collected or were excluded due to contamination.

Sample Date	Day of 2013	9m Station		20m Station		
		2 m	8 m	2 m	8 m	18 m
5/29/2013	149	0.787	0.754	--	--	--
7/3/2013	184	0.361	0.311	0.344	0.420	0.562
7/8/2013	189	0.607	1.166	--	--	--
7/17/2013	198	0.344	0.374	1.642	0.829	0.607
7/31/2013	212	--	--	--	--	--
8/7/2013	219	1.197	0.475	0.998	1.565	0.408
8/20/2013	232	1.151	1.092	0.934	0.783	0.605
9/11/2013	254	0.752	0.752	0.656	1.934	0.672
9/20/2013	263	0.216	0.492	0.656	1.066	0.418
9/25/2013	268	0.868	0.850	1.621	0.423	0.216
10/2/2013	275	0.372	0.254	1.342	1.581	0.817
10/16/2013	289	--	0.626	1.960	2.072	1.184
10/22/2013	295	0.459	0.512	1.565	1.627	1.765
10/25/2013	298	0.623	0.689	0.629	0.776	0.631
11/7/2013	311	0.947	1.678	0.645	0.614	0.599
11/13/2013	317	0.541	0.553	0.998	1.565	0.408
11/26/2013	330	0.610	0.472	--	--	--

A.6: Particulate Carbon Sampling, Measurement, and Raw Data

Particulate carbon concentrations at the 9m and 20m stations were measured by filtering water samples collected as described for phosphorus sampling and measurements. Approximately 1 L of water was filtered onto ash free Whatman GF/F filters. Filters were placed in clean petri dishes and allowed to dry in desiccators. Filters were then folded into 30mm tin disks and shipped to Washington State University Stable Isotope Core Laboratory in Pullman, WA. There, material on filters packed in the folded, tin disks was converted to N₂ and CO₂ gas using an ECS 4010 Elemental Combustion System. Sample gases were separated using a 3m gas chromatograph column, followed analysis in a continuous flow isotope ratio mass spectrometer. Sample carbon content was converted to particulate carbon concentration using the volume of water filtered (Table A.6).

Table A.6: Particulate carbon concentration measured at the 9m and 20m stations during 2013. Units of all values are in $\mu\text{g L}^{-1}$. Dashed lines indicate times when samples were not collected or were excluded due to contamination.

Sample Date	Day of 2013	9m Station		20m Station		
		2 m	8 m	2 m	8 m	18 m
5/29/2013	149	177.620	115.655	--	--	--
7/3/2013	184	78.799	78.310	64.011	76.302	94.291
7/8/2013	189	104.734	155.114	--	--	--
7/17/2013	198	117.939	211.373	274.146	192.806	145.180
7/31/2013	212	--	--	--	--	--
8/7/2013	219	156.259	99.053	161.850	--	89.237
8/20/2013	232	158.874	147.142	132.917	--	128.718
9/11/2013	254	121.935	139.639	112.658	--	120.391
9/20/2013	263	150.772	102.213	113.704	--	75.418
9/25/2013	268	134.216	140.449	149.898	--	112.012
10/2/2013	275	72.232	63.582	139.716	--	60.703
10/16/2013	289	109.819	70.493	131.371	--	112.938
10/22/2013	295	46.138	56.655	129.119	--	138.044
10/25/2013	298	71.507	69.861	81.422	--	80.975
11/7/2013	311	186.371	387.676	79.149	--	92.280
11/13/2013	317	103.434	100.279	161.850	--	89.237
11/26/2013	330	98.654	170.482	--	--	--

A.7: Surface Water and Air CO₂ Partial Pressure

During the spring, summer, and fall of 2013 air and surface water $p\text{CO}_2$ were measured using an autonomous CO₂ monitoring system mounted on a buoy moored at the 9m station (Figure A.7 and Table A.7). Air and water from approximately 1m above and 0.5m below the water surface were sampled for 10 minutes every hour. The mean of each 10 minute measurement period provided an hourly $p\text{CO}_2$ time series for both air and water. Lake water was sampled using 0.25 inch plastic tubing that was insulated with foam pipe insulation to prevent temperature change during sampling. Water was pumped through the CO₂ system and returned to the lake using a peristaltic pump.

Within the CO₂ system water passed through a gas equilibrator with a semi permeable, gas membrane (Mini Modules Membrane Contractors, item: G543, batch: P0106404 – 1L.7475). Air in the equilibrator head space was pumped in the opposite direction of the water flow with an electric air pump and followed a closed loop through the system to allow for 95% equilibration in 90 seconds. CO₂ partial pressure, normalized to 1 atmosphere, was measured using a LICOR (LI-820) CO₂ infrared gas analyzer. Water temperature was measured using an in-line thermistor. The flow speed of water through the CO₂ system was monitored during operation. For periods during which flow speeds dropped below normal levels, either due to system malfunction or water intake clogging, the data was not included in analyses. Air was desiccated before entering the LICOR to prevent IR light absorption due to water vapor. Measurements were remotely downloaded from a CR10X data logger using radio communication with the buoy.

The CO₂ system was calibrated regularly using standard gasses supplied by Air Gas USA, LLC with known CO₂ mole fraction. Standard gasses used for calibration were

always close to ambient air CO₂ partial pressure. The CO₂ system calibration drift was tested prior to calibration by comparing system output to zero and standard gas partial pressures. A zero CO₂ environment was produced by cycling air in a closed loop through the LICOR and a vial of ascarite. There was generally little or no stray from initial calibration during the deployment period, with monthly drift typically < 1 μatm.

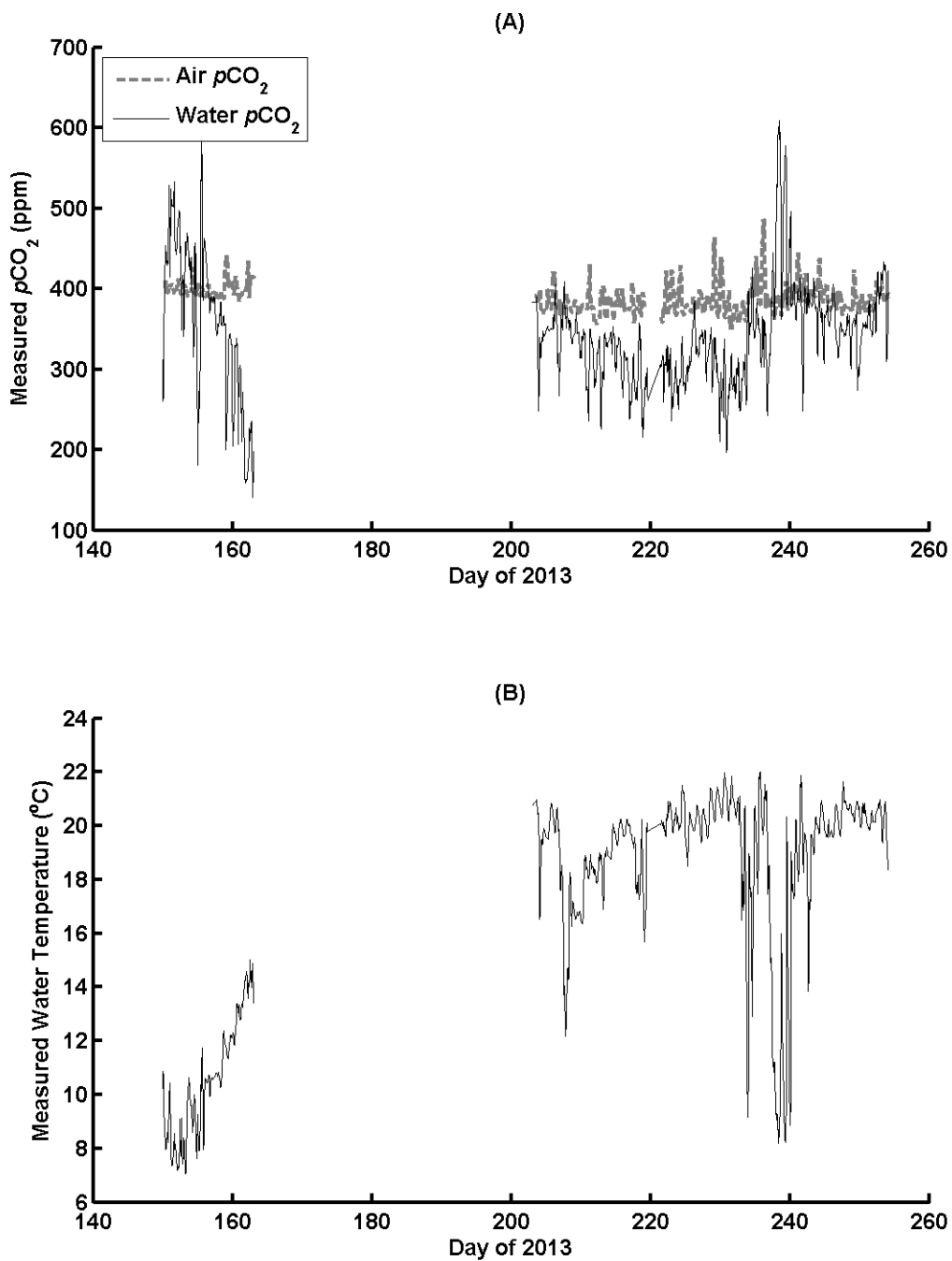


Figure A.7: CO_2 system measured A) air and water $p\text{CO}_2$ (ppm) and B) water temperature ($^{\circ}\text{C}$) during the 2013 monitoring season at the 9m station.

Table A.7: Data collected using the buoy mounted CO₂ monitoring system at the 9m station during 2013. Values listed as NaN represent missing values due to equipment failure. Gaps in the time series were caused by equipment failure and periods of general maintenance.

Day of Year 2013	Water pCO₂ (ppm)	Air pCO₂ (ppm)	System Measured Water Temperature (°C)	Internal Pressure During Water Sampling (kPa)	Internal Pressure During Air Sampling (kPa)
150	312.10	396.33	10.25	103.05	99.30
150.0417	260.60	398.17	10.85	103.47	99.27
150.0833	267.03	397.40	10.74	103.38	99.20
150.125	293.45	398.10	10.30	103.17	99.20
150.1667	352.45	398.47	9.43	102.70	99.20
150.2083	387.15	398.77	8.88	102.40	99.20
150.25	402.48	398.72	8.68	102.37	99.20
150.2917	423.60	397.95	8.54	102.33	99.20
150.3333	437.08	399.50	8.32	102.37	99.20
150.375	454.07	405.33	8.09	102.30	99.20
150.4167	451.55	409.60	7.96	102.35	99.20
150.4583	440.90	407.08	8.01	102.52	99.20
150.5	432.28	404.25	8.16	102.60	99.17
150.5417	435.57	401.27	8.33	102.63	99.10
150.5833	434.50	397.35	8.43	102.72	99.07
150.625	433.70	394.88	8.59	102.77	98.97
150.6667	429.23	395.12	8.52	102.68	98.90
150.7083	434.50	395.53	8.47	102.58	98.90
150.75	430.78	397.85	8.23	102.50	98.90
150.7917	440.92	400.15	8.49	102.47	98.90
150.8333	458.68	395.08	8.94	102.40	98.93
150.875	491.95	396.55	9.25	102.35	99.03
150.9167	528.85	400.02	9.38	102.18	99.10
150.9583	527.35	402.98	9.88	102.20	99.10
151	450.87	405.27	10.45	102.53	99.07
151.0417	415.05	402.58	10.44	102.60	99.00
151.0833	416.28	403.05	10.00	102.40	98.97
151.125	515.40	404.30	8.55	101.77	98.90
151.1667	523.87	405.02	8.01	101.68	98.90
151.2083	517.07	403.05	7.69	101.63	98.93
151.25	505.40	404.70	7.47	101.70	98.97
151.2917	502.28	406.20	7.35	101.70	98.93
151.3333	506.02	404.77	7.37	101.70	99.00
151.375	506.10	402.72	7.40	101.73	99.00

151.4167	502.53	400.20	7.46	101.82	99.00
151.4583	504.35	397.98	7.59	101.95	99.00
151.5	501.85	399.75	7.74	102.10	98.97
151.5417	501.92	395.23	7.84	102.10	98.90
151.5833	509.20	394.63	8.02	102.10	98.90
151.625	532.90	394.40	8.55	102.15	98.87
151.6667	501.20	394.27	8.44	102.25	98.78
151.7083	464.20	393.95	7.96	102.13	98.68
151.75	453.78	393.90	7.98	102.20	98.63
151.7917	456.45	393.70	8.15	102.17	98.70
151.8333	449.15	395.07	8.04	102.08	98.70
151.875	444.35	395.68	7.89	102.00	98.73
151.9167	441.93	396.05	7.79	101.97	98.77
151.9583	448.07	397.33	7.53	101.85	98.70
152	452.78	399.10	7.37	101.67	98.67
152.0417	457.98	397.50	7.39	101.58	98.58
152.0833	467.60	400.20	7.20	101.48	98.50
152.125	474.53	405.38	7.20	101.40	98.50
152.1667	479.47	410.77	7.32	101.37	98.47
152.2083	483.60	412.65	7.22	101.30	98.43
152.25	485.68	410.47	7.26	101.33	98.53
152.2917	490.12	405.48	7.29	101.45	98.60
152.3333	494.15	404.30	7.43	101.62	98.60
152.375	497.52	398.57	7.61	101.75	98.60
152.4167	495.35	397.40	8.07	102.05	98.57
152.4583	479.35	398.47	9.11	102.62	98.50
152.5	444.53	394.37	8.87	102.80	98.50
152.5417	452.87	391.48	7.75	102.23	98.50
152.5833	440.78	392.17	7.78	102.30	98.50
152.625	425.90	392.57	7.71	102.27	98.50
152.6667	392.97	392.58	8.04	102.60	98.47
152.7083	348.40	393.62	9.14	103.45	98.40
152.75	404.98	393.68	7.85	102.30	98.40
152.7917	409.10	395.35	7.54	102.00	98.37
152.8333	406.90	399.83	7.42	101.97	98.35
152.875	417.28	405.40	7.42	101.90	98.50
152.9167	406.40	403.32	7.78	102.05	98.50
152.9583	359.28	398.98	8.26	102.55	98.50
153	340.78	400.68	8.38	102.65	98.50
153.0417	357.77	404.50	8.21	102.45	98.53
153.0833	378.30	403.20	8.09	102.25	98.60
153.125	406.05	404.60	7.75	102.02	98.63
153.1667	437.10	403.10	7.37	101.78	98.75
153.2083	450.42	400.05	7.14	101.70	98.95
153.25	458.30	401.55	7.07	101.70	99.13

153.2917	458.27	400.95	7.09	101.70	99.22
153.3333	452.25	399.77	7.09	101.75	99.32
153.375	441.65	397.00	7.17	101.93	99.43
153.4167	447.08	394.68	7.65	102.02	99.50
153.4583	469.32	392.80	9.12	102.10	99.53
153.5	463.60	391.65	9.61	102.15	99.60
153.5417	462.98	390.68	9.73	102.30	99.63
153.5833	464.37	390.43	9.85	102.33	99.70
153.625	453.92	391.70	10.06	102.45	99.70
153.6667	449.23	391.62	10.23	102.62	99.73
153.7083	445.37	391.27	10.44	102.72	99.80
153.75	436.12	391.03	10.63	102.80	99.80
153.7917	427.98	391.30	10.57	102.77	99.80
153.8333	431.63	391.00	10.38	102.68	99.80
153.875	438.35	391.10	10.17	102.57	99.80
153.9167	432.05	391.93	9.96	102.53	99.80
153.9583	413.15	394.50	9.70	102.60	99.80
154	417.55	397.73	9.64	102.57	99.83
154.0417	429.95	399.43	9.60	102.50	99.90
154.0833	439.65	400.90	9.61	102.47	99.90
154.125	433.52	398.23	9.49	102.40	99.90
154.1667	408.33	405.67	9.24	102.43	99.90
154.2083	387.68	409.07	9.00	102.47	99.90
154.25	394.13	413.00	8.69	102.43	99.93
154.2917	385.65	424.57	8.59	102.58	100.00
154.3333	329.00	426.80	9.07	102.87	100.00
154.375	315.40	420.57	9.31	103.18	100.00
154.4167	322.68	416.70	9.59	103.45	100.00
154.4583	333.65	406.20	9.75	103.70	100.00
154.5	360.98	395.55	9.99	103.92	99.97
154.5417	452.62	396.33	9.89	103.60	99.90
154.5833	440.42	396.77	9.69	103.33	99.90
154.625	400.43	394.87	9.72	103.45	99.87
154.6667	431.05	393.75	9.82	103.42	99.80
154.7083	456.65	392.75	9.17	102.98	99.80
154.75	431.95	390.92	8.79	103.20	99.83
154.7917	400.65	390.20	8.46	103.20	99.90
154.8333	366.03	390.30	7.96	103.25	99.90
154.875	339.90	393.38	7.84	103.37	99.90
154.9167	341.05	397.35	7.63	103.20	99.93
154.9583	321.20	402.53	7.86	103.43	100.00
155	180.88	406.82	9.25	104.92	100.03
155.0417	202.92	401.58	8.91	104.57	100.07
155.0833	225.75	402.10	8.59	104.15	100.00
155.125	241.08	403.00	8.38	103.92	100.03

155.1667	260.97	402.87	8.11	103.65	100.12
155.2083	272.62	400.60	7.94	103.50	100.20
155.25	272.37	393.45	7.92	103.55	100.23
155.2917	251.58	389.45	8.21	103.67	100.30
155.3333	255.85	390.90	8.40	103.60	100.30
155.375	340.00	392.63	8.90	103.47	100.30
155.4167	531.90	394.77	10.32	103.10	100.33
155.4583	535.42	397.27	10.36	103.18	100.37
155.5	534.50	399.78	10.12	103.40	100.30
155.5417	588.00	401.15	10.27	103.53	100.30
155.5833	601.27	403.42	11.07	104.05	100.30
155.625	534.00	402.50	11.73	104.63	100.27
155.6667	455.95	402.48	11.70	105.12	100.23
155.7083	394.15	401.97	11.07	105.32	100.30
155.75	385.50	397.55	9.39	104.50	100.25
155.7917	421.32	395.35	8.50	103.40	100.15
155.8333	448.75	392.83	7.97	102.75	100.27
155.875	452.85	392.70	8.28	102.70	100.23
155.9167	462.50	391.95	9.75	103.02	100.30
155.9583	456.40	391.45	10.17	103.10	100.30
156	458.65	391.20	10.21	103.07	100.30
156.0417	459.60	390.62	10.34	102.98	100.27
156.0833	453.93	389.85	10.54	102.90	100.18
156.125	448.02	389.77	10.59	102.90	100.10
156.1667	444.47	389.25	10.57	102.87	100.10
156.2083	438.18	389.95	10.53	102.80	100.13
156.25	434.55	391.18	10.50	102.80	100.17
156.2917	428.92	392.95	10.46	102.77	100.08
156.3333	420.98	394.37	10.45	102.73	100.00
156.375	415.22	396.23	10.46	102.80	100.03
156.4167	409.53	399.73	10.45	102.80	100.10
156.4583	404.30	403.97	10.46	102.83	100.10
156.5	399.77	404.93	10.53	102.95	100.07
156.5417	398.65	405.63	10.66	103.12	99.98
156.5833	397.27	404.50	10.73	103.20	99.88
156.625	391.95	398.38	10.71	103.20	99.80
156.6667	384.85	398.05	10.70	103.35	99.80
156.7083	382.05	394.28	10.41	103.72	99.80
156.75	369.98	389.95	9.93	103.45	99.77
156.7917	376.88	387.68	9.97	103.25	99.73
156.8333	386.60	386.63	10.42	103.08	99.80
156.875	388.58	386.63	10.50	102.95	99.77
156.9167	390.12	387.35	10.58	102.80	99.70
156.9583	389.42	387.32	10.58	102.80	99.70
157	386.40	388.48	10.59	102.80	99.70

157.0417	387.10	392.10	10.62	102.75	99.67
157.0833	386.67	386.70	10.64	102.60	99.58
157.125	384.73	383.23	10.62	102.60	99.50
157.1667	386.38	383.98	10.58	102.60	99.50
157.2083	388.52	387.83	10.57	102.57	99.50
157.25	385.80	396.23	10.62	102.47	99.50
157.2917	384.68	396.85	10.63	102.38	99.53
157.3333	384.85	396.88	10.65	102.33	99.60
157.375	386.63	396.97	10.64	102.43	99.63
157.4167	391.60	395.45	10.62	102.50	99.70
157.4583	387.27	394.65	10.64	102.50	99.70
157.5	379.75	394.55	10.67	102.50	99.67
157.5417	372.40	394.67	10.69	102.53	99.60
157.5833	365.38	394.63	10.74	102.60	99.60
157.625	361.50	394.70	10.76	102.63	99.60
157.6667	353.47	394.17	10.79	102.72	99.60
157.7083	344.28	391.62	10.81	102.77	99.57
157.75	342.57	387.87	10.81	102.70	99.53
157.7917	341.93	386.63	10.81	102.67	99.60
157.8333	346.13	389.47	10.76	102.58	99.57
157.875	353.90	387.30	10.67	102.47	99.53
157.9167	356.02	388.15	10.73	102.43	99.57
157.9583	355.00	387.95	10.80	102.50	99.50
158	353.62	388.20	10.82	102.50	99.50
158.0417	353.63	388.92	10.78	102.47	99.53
158.0833	361.27	387.63	10.68	102.38	99.57
158.125	365.43	389.25	10.60	102.27	99.50
158.1667	369.00	392.00	10.53	102.18	99.50
158.2083	366.40	389.28	10.50	102.10	99.53
158.25	383.15	390.55	10.37	102.10	99.63
158.2917	383.03	393.38	10.27	102.10	99.70
158.3333	382.77	395.35	10.29	102.18	99.70
158.375	363.55	388.05	10.30	102.45	99.70
158.4167	356.35	388.33	10.46	102.62	99.70
158.4583	354.18	388.90	10.78	102.72	99.67
158.5	357.28	389.75	11.00	102.85	99.60
158.5417	357.85	390.10	11.19	103.02	99.60
158.5833	358.28	388.85	11.46	103.15	99.60
158.625	360.03	388.62	11.73	103.35	99.57
158.6667	363.47	388.45	11.99	103.52	99.50
158.7083	365.90	388.32	12.22	103.62	99.50
158.75	366.30	387.35	12.38	103.70	99.47
158.7917	361.42	386.78	12.30	103.65	99.40
158.8333	354.73	386.12	12.10	103.48	99.43
158.875	356.72	389.28	12.06	103.40	99.50

158.9167	356.38	404.37	11.97	103.37	99.50
158.9583	356.97	417.77	11.89	103.28	99.50
159	356.97	429.07	11.83	103.20	99.50
159.0417	315.22	428.35	11.83	103.38	99.47
159.0833	199.45	432.25	11.84	103.82	99.43
159.125	222.58	438.82	11.72	103.55	99.50
159.1667	224.62	433.88	11.59	103.38	99.50
159.2083	231.23	441.25	11.51	103.30	99.50
159.25	259.55	425.52	11.39	103.25	99.53
159.2917	278.42	412.58	11.38	103.13	99.60
159.3333	284.68	415.60	11.37	103.20	99.63
159.375	300.23	411.57	11.34	103.23	99.70
159.4167	316.83	407.62	11.41	103.27	99.70
159.4583	336.87	402.55	11.53	103.25	99.70
159.5	338.68	403.02	11.70	103.48	99.70
159.5417	342.60	402.33	11.88	103.67	99.70
159.5833	342.47	402.42	11.90	103.63	99.70
159.625	341.80	402.63	12.01	103.75	99.70
159.6667	343.60	406.02	12.19	103.90	99.73
159.7083	341.77	406.85	12.18	103.87	99.77
159.75	335.55	406.27	12.13	103.77	99.73
159.7917	332.75	406.00	12.20	103.70	99.80
159.8333	331.00	406.80	12.17	103.67	99.80
159.875	331.15	408.53	12.11	103.63	99.80
159.9167	313.80	408.65	12.11	103.85	99.80
159.9583	249.33	406.35	12.20	104.35	99.80
160	220.15	402.65	12.24	104.58	99.83
160.0417	205.95	399.40	12.29	104.82	99.87
160.0833	204.35	404.60	12.31	104.77	99.80
160.125	220.53	401.45	12.30	104.37	99.80
160.1667	226.72	399.30	12.21	104.30	99.80
160.2083	224.43	397.62	12.02	104.25	99.80
160.25	233.08	392.48	11.88	104.07	99.80
160.2917	254.38	398.90	11.83	103.92	99.77
160.3333	299.95	410.45	11.90	103.70	99.70
160.375	329.80	409.63	12.13	103.75	99.70
160.4167	327.63	414.40	12.28	104.00	99.70
160.4583	329.32	415.50	12.49	104.30	99.67
160.5	328.90	413.97	12.51	104.30	99.57
160.5417	329.40	412.12	12.68	104.38	99.50
160.5833	338.62	408.25	13.28	104.65	99.47
160.625	337.40	403.17	13.37	104.77	99.37
160.6667	328.58	399.58	13.23	104.73	99.30
160.7083	323.55	400.37	13.38	104.80	99.30
160.75	304.95	398.40	13.36	104.77	99.27

160.7917	261.57	394.78	13.28	104.88	99.20
160.8333	206.85	391.45	13.09	105.25	99.20
160.875	246.13	386.05	13.03	104.72	99.20
160.9167	286.02	383.15	13.33	104.40	99.20
160.9583	301.25	384.17	13.15	104.05	99.20
161	299.93	385.90	12.95	103.85	99.17
161.0417	303.22	388.82	12.84	103.68	99.08
161.0833	304.62	389.50	12.79	103.58	99.00
161.125	302.67	389.73	12.79	103.50	99.00
161.1667	299.03	390.70	12.81	103.47	99.00
161.2083	292.15	391.67	12.91	103.48	99.00
161.25	259.42	391.72	13.19	103.75	99.00
161.2917	231.15	391.25	13.34	103.98	99.00
161.3333	210.53	391.40	13.38	104.05	99.03
161.375	232.73	391.80	13.30	103.63	99.10
161.4167	247.30	393.42	13.28	103.75	99.10
161.4583	257.43	395.02	13.25	103.92	99.10
161.5	271.17	396.18	13.28	104.05	99.07
161.5417	255.83	396.45	13.45	104.25	99.03
161.5833	244.37	395.30	13.59	104.50	99.10
161.625	217.68	394.10	13.76	104.80	99.10
161.6667	221.90	394.13	13.81	104.88	99.07
161.7083	207.50	394.28	14.03	105.10	99.03
161.75	187.25	394.65	14.06	105.18	99.10
161.7917	167.13	395.27	14.24	105.47	99.10
161.8333	159.15	395.65	14.25	105.70	99.10
161.875	159.70	395.30	14.25	105.62	99.13
161.9167	162.85	397.43	14.34	105.40	99.20
161.9583	160.63	402.20	14.51	105.37	99.20
162	161.43	399.22	14.57	105.22	99.23
162.0417	163.30	396.63	14.50	104.93	99.30
162.0833	163.20	400.05	14.40	104.57	99.27
162.125	166.78	409.17	14.31	104.15	99.23
162.1667	171.27	412.48	13.98	104.18	99.30
162.2083	174.05	432.00	13.59	104.62	99.30
162.25	174.18	434.77	13.79	104.40	99.30
162.2917	180.90	426.02	14.15	104.53	99.33
162.3333	199.17	405.00	14.14	104.95	99.37
162.375	213.50	389.55	14.25	105.20	99.27
162.4167	227.12	388.40	14.01	105.60	99.20
162.4583	222.95	392.12	14.55	106.08	99.23
162.5	211.30	396.73	15.03	106.60	99.27
162.5417	218.67	408.85	14.86	106.45	99.18
162.5833	223.12	413.87	14.37	105.95	99.13
162.625	224.85	409.70	14.46	105.77	99.17

162.6667	228.38	410.60	14.59	105.68	99.10
162.7083	233.37	413.40	14.38	105.50	99.10
162.75	236.15	415.30	13.99	105.17	99.10
162.7917	226.82	412.45	13.98	105.18	99.13
162.8333	193.25	414.25	14.37	105.63	99.20
162.875	151.65	415.78	14.87	106.48	99.20
162.9167	141.10	415.92	14.71	106.82	99.20
162.9583	153.52	414.38	14.34	106.13	99.20
163	164.98	412.92	14.09	105.55	99.23
163.0417	176.45	412.45	13.82	105.33	99.27
163.0833	197.32	415.25	13.42	104.97	99.23
203	382.64	390.47	20.74	101.89	98.74
203.0417	382.70	390.49	20.76	101.89	98.74
203.0833	382.75	390.52	20.77	101.88	98.74
203.125	382.81	390.55	20.78	101.88	98.73
203.1667	382.86	390.58	20.80	101.87	98.73
203.2083	382.92	390.60	20.81	101.86	98.73
203.25	382.97	390.63	20.82	101.86	98.73
203.2917	383.02	390.66	20.84	101.85	98.72
203.3333	383.08	390.69	20.85	101.85	98.72
203.375	383.13	390.71	20.86	101.84	98.72
203.4167	383.19	390.74	20.87	101.83	98.72
203.4583	383.24	390.77	20.89	101.83	98.71
203.5	383.30	390.80	20.90	101.82	98.71
203.5417	383.35	390.82	20.91	101.82	98.71
203.5833	383.40	390.85	20.93	101.81	98.70
203.625	383.46	390.88	20.94	101.80	98.70
203.6667	387.23	390.45	20.96	101.77	98.70
203.7083	389.75	387.30	20.89	101.70	98.67
203.75	354.32	381.42	20.58	101.78	98.60
203.7917	324.10	380.45	20.53	101.97	98.60
203.8333	313.65	383.78	20.43	101.93	98.60
203.875	286.10	389.98	20.45	102.08	98.57
203.9167	248.53	391.12	20.46	102.32	98.53
203.9583	252.30	389.65	20.10	102.37	98.60
204	281.00	384.38	19.21	102.25	98.57
204.0417	327.60	391.37	18.42	102.15	98.50
204.0833	339.70	394.88	17.14	102.38	98.53
204.125	334.05	398.40	16.53	102.55	98.57
204.1667	330.40	399.35	16.70	102.35	98.53
204.2083	322.15	396.22	17.47	102.07	98.62
204.25	314.00	377.37	18.33	101.70	98.73
204.2917	315.93	374.75	18.66	101.67	98.82
204.3333	333.80	374.87	19.28	101.63	98.92
204.375	332.85	373.12	19.46	101.70	99.00

204.4167	336.08	371.28	19.50	101.75	99.00
204.4583	339.42	372.02	19.37	101.92	99.03
204.5	334.25	370.90	19.30	101.97	99.10
204.5417	335.13	373.40	19.38	101.90	99.13
204.5833	347.00	372.45	19.63	101.90	99.20
204.625	346.12	370.85	19.75	101.87	99.23
204.6667	344.32	368.75	19.88	101.78	99.30
204.7083	341.33	369.15	19.90	101.68	99.30
204.75	341.02	374.20	19.88	101.60	99.30
204.7917	340.88	373.68	19.88	101.60	99.33
204.8333	341.38	373.87	19.82	101.57	99.42
204.875	342.53	374.05	19.75	101.50	99.50
204.9167	343.75	375.00	19.69	101.47	99.53
204.9583	345.10	375.77	19.63	101.40	99.60
205	347.25	376.25	19.58	101.37	99.60
205.0417	348.55	376.00	19.57	101.30	99.60
205.0833	349.57	375.75	19.58	101.27	99.60
205.125	350.83	375.93	19.57	101.20	99.63
205.1667	352.05	376.05	19.55	101.17	99.70
205.2083	352.35	381.78	19.54	101.10	99.70
205.25	353.52	399.25	19.52	101.10	99.73
205.2917	352.95	399.17	19.51	101.10	99.80
205.3333	352.30	390.35	19.51	101.13	99.83
205.375	350.30	383.25	19.65	101.20	99.90
205.4167	348.98	378.45	19.77	101.23	99.90
205.4583	349.02	377.93	19.82	101.32	99.90
205.5	347.73	377.75	19.89	101.43	99.90
205.5417	348.33	377.70	20.09	101.50	99.90
205.5833	349.25	376.70	20.28	101.50	99.87
205.625	349.95	375.53	20.48	101.50	99.80
205.6667	350.10	375.47	20.62	101.50	99.80
205.7083	350.97	374.93	20.77	101.50	99.80
205.75	350.70	374.32	20.83	101.50	99.80
205.7917	349.75	374.08	20.84	101.47	99.80
205.8333	348.70	374.10	20.80	101.40	99.77
205.875	348.93	376.23	20.74	101.37	99.73
205.9167	349.60	384.55	20.68	101.30	99.80
205.9583	349.70	396.75	20.60	101.30	99.80
206	352.60	411.65	20.47	101.27	99.80
206.0417	362.62	421.60	20.36	101.18	99.80
206.0833	368.00	413.68	20.27	101.10	99.80
206.125	359.80	410.33	20.19	101.10	99.80
206.1667	351.13	420.77	20.08	101.07	99.83
206.2083	367.12	419.77	19.98	100.98	99.90
206.25	380.25	410.42	19.81	100.87	99.90

206.2917	391.62	402.58	19.72	100.80	99.90
206.3333	398.92	396.68	19.76	100.83	99.90
206.375	405.13	391.47	20.00	100.90	99.90
206.4167	397.77	384.48	20.17	100.98	99.90
206.4583	360.73	383.20	20.31	101.22	99.90
206.5	359.30	383.77	20.46	101.30	99.87
206.5417	357.77	379.40	20.58	101.27	99.80
206.5833	355.08	377.63	20.66	101.20	99.80
206.625	347.07	377.75	20.68	101.30	99.77
206.6667	324.65	375.88	20.54	101.65	99.70
206.7083	307.30	377.00	20.36	101.77	99.70
206.75	311.75	374.15	20.18	101.67	99.70
206.7917	320.05	374.75	19.95	101.63	99.67
206.8333	309.70	380.00	19.83	101.70	99.60
206.875	295.82	386.80	19.73	101.73	99.60
206.9167	266.53	383.10	19.88	101.75	99.60
206.9583	290.52	367.65	19.48	101.58	99.57
207	303.48	368.07	18.94	101.58	99.50
207.0417	313.45	368.80	18.16	101.87	99.50
207.0833	316.20	372.88	17.67	102.10	99.50
207.125	326.80	377.95	17.60	102.05	99.50
207.1667	345.85	379.05	17.79	101.80	99.50
207.2083	366.05	381.57	18.14	101.50	99.50
207.25	357.20	381.55	18.52	101.50	99.50
207.2917	361.52	383.67	18.33	101.58	99.50
207.3333	353.73	379.92	18.18	101.80	99.50
207.375	348.65	374.57	18.12	101.77	99.47
207.4167	356.98	371.67	17.87	101.70	99.40
207.4583	377.32	368.20	17.18	101.83	99.40
207.5	385.28	367.98	15.60	102.25	99.37
207.5417	402.57	371.55	14.44	102.42	99.30
207.5833	397.95	373.90	13.72	102.50	99.27
207.625	408.80	374.90	14.01	102.50	99.20
207.6667	382.80	374.83	14.04	102.50	99.20
207.7083	375.73	375.95	13.63	102.58	99.20
207.75	375.80	375.30	12.61	102.75	99.20
207.7917	376.42	377.35	12.22	102.68	99.17
207.8333	369.45	378.55	12.18	102.90	99.13
207.875	356.17	383.63	12.67	102.90	99.20
207.9167	350.90	387.55	12.72	102.85	99.20
207.9583	363.00	390.90	13.27	102.57	99.20
208	368.53	393.38	14.24	102.17	99.20
208.0417	372.18	391.35	14.36	102.02	99.23
208.0833	376.42	383.83	14.62	101.78	99.30
208.125	370.97	381.90	14.68	101.70	99.30

208.1667	357.55	383.65	14.73	101.73	99.30
208.2083	361.62	385.20	14.34	101.82	99.33
208.25	361.52	385.03	14.29	101.87	99.40
208.2917	360.67	385.22	14.32	101.78	99.40
208.3333	356.35	383.70	15.18	101.57	99.40
208.375	348.30	380.37	17.51	101.07	99.37
208.4167	355.07	379.15	18.10	100.70	99.30
208.4583	358.47	377.97	18.26	100.67	99.33
208.5	360.62	376.00	18.26	100.60	99.40
208.5417	355.77	373.73	17.99	100.63	99.40
208.5833	350.68	372.60	17.57	100.75	99.37
208.625	345.40	371.00	17.01	101.00	99.30
208.6667	332.15	371.62	16.26	101.27	99.30
208.7083	333.70	371.65	16.51	101.18	99.30
208.75	332.52	371.37	16.65	101.07	99.27
208.7917	332.18	371.33	16.81	100.95	99.20
208.8333	339.05	372.52	17.17	100.80	99.20
208.875	339.40	373.78	17.18	100.77	99.20
208.9167	340.15	376.07	17.14	100.68	99.20
208.9583	340.83	378.12	17.07	100.63	99.20
209	341.73	379.65	16.95	100.67	99.20
209.0417	342.72	381.52	16.85	100.60	99.20
209.0833	343.85	382.45	16.75	100.60	99.17
209.125	344.48	383.55	16.68	100.60	99.10
209.1667	345.63	384.87	16.61	100.60	99.10
209.2083	348.45	385.87	16.54	100.60	99.13
209.25	356.40	386.00	16.52	100.52	99.20
209.2917	370.10	384.25	16.59	100.33	99.20
209.3333	364.93	381.47	16.59	100.42	99.20
209.375	364.03	377.97	16.62	100.53	99.23
209.4167	363.05	377.53	16.66	100.62	99.30
209.4583	355.12	376.72	16.74	100.72	99.30
209.5	345.55	375.08	16.80	100.83	99.30
209.5417	343.90	374.67	16.73	100.90	99.33
209.5833	345.00	372.25	16.72	100.93	99.40
209.625	345.47	370.27	16.70	101.00	99.40
209.6667	345.30	369.30	16.67	101.03	99.40
209.7083	346.90	369.40	16.70	101.10	99.40
209.75	346.25	369.07	16.80	101.10	99.40
209.7917	334.33	367.45	16.78	101.10	99.40
209.8333	329.20	368.20	16.80	101.10	99.43
209.875	320.55	368.73	16.82	101.13	99.50
209.9167	313.73	370.20	16.80	101.20	99.53
209.9583	314.33	370.63	16.71	101.17	99.60
210	323.45	373.25	16.57	101.10	99.60

210.0417	323.05	375.00	16.48	101.13	99.60
210.0833	314.50	376.17	16.43	101.17	99.63
210.125	329.78	376.50	16.39	101.07	99.70
210.1667	340.45	377.97	16.39	101.00	99.73
210.2083	340.23	379.53	16.37	101.03	99.80
210.25	338.80	381.45	16.37	101.10	99.83
210.2917	335.65	380.50	16.42	101.10	99.92
210.3333	340.05	380.03	16.67	101.02	100.02
210.375	349.28	380.22	17.41	100.75	100.10
210.4167	348.92	379.63	17.86	100.63	100.13
210.4583	345.80	379.15	18.18	100.72	100.17
210.5	342.95	378.37	18.50	100.83	100.10
210.5417	346.25	378.12	18.71	100.92	100.13
210.5833	342.87	377.58	18.88	101.02	100.20
210.625	333.52	377.37	18.87	101.18	100.20
210.6667	312.48	376.93	18.70	101.42	100.20
210.7083	303.45	376.73	18.73	101.50	100.20
210.75	301.90	376.65	18.84	101.53	100.20
210.7917	288.97	376.18	18.67	101.65	100.20
210.8333	273.65	375.90	18.37	101.77	100.20
210.875	273.75	375.25	18.36	101.70	100.23
210.9167	274.90	375.00	18.40	101.65	100.30
210.9583	277.67	374.70	18.45	101.50	100.30
211	272.60	375.13	18.34	101.53	100.30
211.0417	265.93	380.70	18.22	101.60	100.27
211.0833	254.85	395.22	18.06	101.65	100.20
211.125	235.75	397.37	18.05	101.80	100.20
211.1667	244.03	390.65	18.03	101.75	100.20
211.2083	280.22	398.48	18.02	101.47	100.23
211.25	317.95	417.38	18.31	101.07	100.30
211.2917	337.05	430.25	18.53	100.98	100.30
211.3333	350.15	392.35	18.64	100.93	100.30
211.375	349.37	387.92	18.80	101.05	100.27
211.4167	343.00	376.33	18.92	101.17	100.20
211.4583	340.43	375.08	18.75	101.18	100.20
211.5	338.72	376.60	18.61	101.43	100.17
211.5417	332.25	376.67	18.48	101.50	100.10
211.5833	332.30	375.88	18.40	101.50	100.10
211.625	333.57	375.65	18.49	101.50	100.07
211.6667	329.70	377.03	18.50	101.47	100.00
211.7083	328.13	379.07	18.48	101.43	100.00
211.75	325.62	376.20	18.42	101.50	100.00
211.7917	316.78	370.72	18.45	101.50	100.00
211.8333	306.50	360.18	18.31	101.55	100.00
211.875	295.30	359.75	18.20	101.67	100.00

211.9167	293.87	361.02	18.18	101.65	100.00
211.9583	277.35	357.45	18.41	101.77	100.00
212	280.30	358.25	18.37	101.67	99.97
212.0417	287.05	358.75	18.26	101.60	99.90
212.0833	288.50	360.10	18.24	101.57	99.90
212.125	283.48	360.92	18.24	101.50	99.87
212.1667	283.83	360.40	18.10	101.53	99.80
212.2083	285.53	358.82	17.94	101.60	99.80
212.25	292.65	356.52	17.88	101.57	99.83
212.2917	304.80	355.65	17.86	101.48	99.87
212.3333	314.80	355.98	17.92	101.38	99.80
212.375	320.30	357.40	17.93	101.30	99.80
212.4167	319.98	357.40	17.94	101.30	99.80
212.4583	321.55	357.80	18.08	101.30	99.77
212.5	324.58	358.90	18.22	101.33	99.70
212.5417	327.15	358.80	18.40	101.42	99.67
212.5833	328.85	359.60	18.49	101.47	99.60
212.625	334.25	360.45	18.69	101.43	99.57
212.6667	340.95	361.10	19.01	101.45	99.48
212.7083	336.98	361.80	18.89	101.28	99.43
212.75	324.82	365.23	18.69	101.30	99.50
212.7917	285.45	371.00	18.79	101.72	99.47
212.8333	243.08	385.65	18.87	102.12	99.43
212.875	231.70	391.53	18.92	102.23	99.50
212.9167	226.05	398.67	18.89	102.30	99.50
212.9583	235.70	397.30	18.85	102.15	99.50
213	272.73	392.67	18.64	101.62	99.47
213.0417	283.62	387.35	18.47	101.38	99.40
213.0833	289.92	386.80	18.16	101.30	99.40
213.125	295.75	390.90	17.69	101.33	99.40
213.1667	297.32	397.25	17.09	101.40	99.40
213.2083	295.02	401.57	16.89	101.40	99.40
213.25	287.77	403.20	17.00	101.40	99.43
213.2917	287.23	399.10	17.41	101.30	99.50
213.3333	323.22	385.70	17.94	100.95	99.50
213.375	336.68	377.70	18.37	100.77	99.50
213.4167	341.42	370.83	18.69	100.73	99.50
213.4583	345.42	367.58	18.98	100.80	99.50
213.5	342.57	365.80	18.93	100.80	99.50
213.5417	339.05	365.60	18.84	100.83	99.50
213.5833	338.70	364.10	18.88	100.90	99.50
213.625	336.05	363.92	18.98	100.95	99.47
213.6667	328.55	363.33	19.04	101.10	99.40
213.7083	332.62	362.87	19.14	101.07	99.37
213.75	332.27	362.20	19.19	101.00	99.30

213.7917	330.05	362.83	19.12	101.00	99.30
213.8333	327.63	368.33	19.04	101.00	99.30
213.875	329.78	381.80	18.93	100.97	99.33
213.9167	333.02	389.70	18.88	100.88	99.40
213.9583	334.92	389.97	18.91	100.80	99.37
214	335.18	389.17	18.88	100.77	99.30
214.0417	335.85	386.93	18.86	100.70	99.27
214.0833	336.63	386.00	18.82	100.67	99.20
214.125	337.55	384.28	18.83	100.60	99.17
214.1667	338.33	386.08	18.81	100.60	99.13
214.2083	341.42	388.40	18.79	100.57	99.20
214.25	343.05	386.35	18.78	100.47	99.20
214.2917	344.82	378.95	18.79	100.43	99.20
214.3333	345.15	383.55	18.76	100.50	99.17
214.375	346.05	384.12	18.77	100.55	99.10
214.4167	337.30	381.40	18.89	100.80	99.10
214.4583	324.60	375.03	19.23	101.15	99.10
214.5	318.72	375.70	19.40	101.40	99.10
214.5417	323.38	375.67	19.80	101.57	99.10
214.5833	352.82	372.85	19.99	101.20	99.10
214.625	345.92	363.35	20.06	101.20	99.07
214.6667	345.47	359.58	20.05	101.17	99.03
214.7083	344.90	359.53	19.97	101.15	99.15
214.75	344.62	360.28	19.92	101.25	99.25
214.7917	343.35	363.45	19.81	101.10	99.13
214.8333	344.55	367.72	19.74	101.13	99.22
214.875	338.42	370.90	19.74	101.20	99.30
214.9167	315.98	373.65	19.80	101.17	99.30
214.9583	302.25	377.15	19.78	101.08	99.33
215	308.45	382.53	19.68	101.03	99.43
215.0417	302.13	384.15	19.60	101.12	99.50
215.0833	296.95	382.73	19.53	101.17	99.53
215.125	306.23	384.53	19.45	101.02	99.60
215.1667	328.07	389.78	19.40	100.80	99.63
215.2083	330.15	396.62	19.34	100.80	99.70
215.25	328.82	399.75	19.28	100.80	99.70
215.2917	327.88	397.40	19.28	100.80	99.73
215.3333	330.05	393.80	19.36	100.85	99.80
215.375	331.00	387.12	19.51	101.00	99.80
215.4167	336.37	380.03	19.70	101.03	99.80
215.4583	339.55	377.48	19.87	101.10	99.80
215.5	338.70	377.60	19.98	101.15	99.83
215.5417	338.87	385.45	20.09	101.27	99.90
215.5833	337.28	384.60	20.06	101.20	99.90
215.625	334.10	380.87	20.12	101.25	99.90

215.6667	326.73	378.98	20.19	101.40	99.87
215.7083	322.47	379.52	20.24	101.40	99.80
215.75	311.92	378.37	20.23	101.45	99.83
215.7917	296.10	377.63	20.22	101.60	99.90
215.8333	290.10	379.23	20.14	101.57	99.90
215.875	283.50	384.43	20.04	101.55	99.90
215.9167	278.90	393.47	20.02	101.65	99.93
215.9583	281.07	399.00	19.95	101.53	100.00
216	269.75	399.90	19.84	101.65	100.03
216.0417	264.75	395.77	19.78	101.75	100.10
216.0833	274.87	382.13	19.73	101.58	100.13
216.125	281.50	385.42	19.64	101.50	100.20
216.1667	289.90	380.37	19.60	101.40	100.20
216.2083	316.57	373.85	19.62	101.08	100.20
216.25	322.92	373.07	19.61	101.03	100.23
216.2917	320.70	371.98	19.60	101.12	100.30
216.3333	319.95	371.58	19.63	101.22	100.33
216.375	316.00	371.47	19.66	101.35	100.40
216.4167	313.23	372.03	19.72	101.50	100.40
216.4583	311.78	373.67	19.81	101.53	100.40
216.5	310.83	373.28	19.95	101.63	100.37
216.5417	311.60	374.12	20.11	101.67	100.30
216.5833	313.95	374.25	20.19	101.60	100.30
216.625	315.10	374.00	20.22	101.60	100.27
216.6667	314.50	372.85	20.24	101.60	100.20
216.7083	307.60	373.18	20.17	101.60	100.20
216.75	301.50	373.88	20.11	101.60	100.17
216.7917	295.40	374.47	20.08	101.60	100.10
216.8333	290.63	374.77	20.02	101.60	100.10
216.875	287.12	374.85	20.00	101.60	100.10
216.9167	280.87	374.25	20.01	101.63	100.10
216.9583	262.35	373.78	20.07	101.78	100.10
217	237.55	373.57	20.08	102.03	100.10
217.0417	238.80	373.10	19.98	102.00	100.07
217.0833	259.90	373.80	19.83	101.68	99.98
217.125	260.70	378.30	19.78	101.57	99.90
217.1667	256.40	382.90	19.68	101.48	99.90
217.2083	256.08	383.40	19.65	101.38	99.87
217.25	258.70	383.85	19.69	101.30	99.80
217.2917	259.78	384.35	19.67	101.30	99.83
217.3333	263.52	389.30	19.61	101.30	99.90
217.375	266.58	399.43	19.58	101.27	99.85
217.4167	274.58	407.22	19.52	101.15	99.65
217.4583	291.30	398.78	19.40	101.00	99.50
217.5	308.97	401.20	19.35	101.05	99.50

217.5417	311.80	384.60	19.34	101.17	99.50
217.5833	319.65	377.67	19.30	101.15	99.47
217.625	305.77	361.52	19.17	101.30	99.40
217.6667	292.75	357.65	19.31	101.33	99.37
217.7083	283.70	361.45	19.47	101.37	99.30
217.75	284.32	362.00	19.57	101.30	99.30
217.7917	275.40	361.03	19.57	101.33	99.27
217.8333	268.88	364.68	19.14	101.48	99.23
217.875	264.87	371.45	18.45	101.78	99.30
217.9167	262.58	373.92	17.83	102.02	99.27
217.9583	265.95	375.42	17.50	102.02	99.20
218	276.97	373.15	17.70	101.77	99.20
218.0417	266.48	375.77	17.77	101.70	99.20
218.0833	261.43	377.65	17.88	101.70	99.17
218.125	266.23	377.48	17.54	101.73	99.10
218.1667	281.17	379.55	17.53	101.65	99.10
218.2083	289.13	384.45	18.17	101.25	99.10
218.25	305.13	389.08	17.75	101.35	99.10
218.2917	330.37	391.70	17.63	101.28	99.10
218.3333	342.22	390.65	17.25	101.55	99.10
218.375	348.13	392.20	17.29	101.75	99.13
218.4167	357.02	379.18	17.24	101.98	99.20
218.4583	352.77	370.43	17.55	102.30	99.17
218.5	327.97	369.10	17.80	102.65	99.07
218.5417	326.10	369.63	18.09	102.80	99.00
218.5833	321.90	375.47	18.32	102.75	99.00
218.625	326.00	372.52	18.20	102.63	98.97
218.6667	337.97	365.68	18.29	102.75	98.90
218.7083	318.07	365.52	18.83	102.98	98.95
218.75	233.92	366.35	20.19	103.30	99.13
218.7917	229.15	372.08	20.24	103.32	99.20
218.8333	241.70	379.52	19.65	102.60	99.20
218.875	239.27	380.93	18.63	102.87	99.12
218.9167	232.10	390.07	17.97	102.93	98.93
218.9583	215.98	395.20	17.82	103.27	98.97
219	235.38	387.80	17.18	103.17	98.90
219.0417	247.45	384.47	16.51	103.15	98.90
219.0833	250.45	379.70	16.19	103.27	98.90
219.125	256.20	380.95	16.05	103.15	98.90
219.1667	263.50	378.68	15.70	102.93	98.90
219.2083	277.17	379.57	16.09	102.63	98.90
219.25	274.48	379.50	16.30	102.37	98.90
219.2917	279.53	378.45	16.36	102.28	98.93
219.3333	291.02	378.15	16.50	102.23	99.00
219.375	286.80	378.37	17.29	102.02	99.00

219.4167	278.58	377.63	19.62	101.23	99.00
219.4583	289.33	377.43	19.80	101.38	99.00
219.5	301.47	377.78	20.11	101.70	99.00
219.5417	289.02	378.47	19.92	102.15	99.03
219.5833	269.85	NaN	19.78	102.83	NaN
219.625	261.85	NaN	19.79	103.49	NaN
219.6667	262.86	NaN	19.79	103.46	NaN
219.7083	263.86	NaN	19.80	103.42	NaN
219.75	264.86	NaN	19.81	103.39	NaN
219.7917	265.87	NaN	19.81	103.36	NaN
219.8333	266.87	NaN	19.82	103.32	NaN
219.875	267.88	NaN	19.83	103.29	NaN
219.9167	268.88	NaN	19.83	103.26	NaN
219.9583	269.89	NaN	19.84	103.22	NaN
220	270.89	NaN	19.85	103.19	NaN
220.0417	271.90	NaN	19.85	103.16	NaN
220.0833	272.90	NaN	19.86	103.12	NaN
220.125	273.90	NaN	19.87	103.09	NaN
220.1667	274.91	NaN	19.87	103.06	NaN
220.2083	275.91	NaN	19.88	103.02	NaN
220.25	276.92	NaN	19.89	102.99	NaN
220.2917	277.92	NaN	19.89	102.96	NaN
220.3333	278.93	NaN	19.90	102.92	NaN
220.375	279.93	NaN	19.91	102.89	NaN
220.4167	280.94	NaN	19.91	102.86	NaN
220.4583	281.94	NaN	19.92	102.82	NaN
220.5	282.94	NaN	19.93	102.79	NaN
220.5417	283.95	NaN	19.93	102.76	NaN
220.5833	284.95	NaN	19.94	102.72	NaN
220.625	285.96	NaN	19.94	102.69	NaN
220.6667	286.96	NaN	19.95	102.66	NaN
220.7083	287.97	NaN	19.96	102.62	NaN
220.75	288.97	NaN	19.96	102.59	NaN
220.7917	289.98	NaN	19.97	102.56	NaN
220.8333	290.98	NaN	19.98	102.52	NaN
220.875	291.98	NaN	19.98	102.49	NaN
220.9167	292.99	NaN	19.99	102.46	NaN
220.9583	293.99	NaN	20.00	102.42	NaN
221	295.00	NaN	20.00	102.39	NaN
221.0417	296.00	NaN	20.01	102.36	NaN
221.0833	297.01	NaN	20.02	102.32	NaN
221.125	298.01	NaN	20.02	102.29	NaN
221.1667	299.02	NaN	20.03	102.26	NaN
221.2083	300.02	NaN	20.04	102.22	NaN
221.25	301.02	NaN	20.04	102.19	NaN

221.2917	302.03	NaN	20.05	102.16	NaN
221.3333	303.03	NaN	20.06	102.12	NaN
221.375	304.04	NaN	20.06	102.09	NaN
221.4167	305.04	NaN	20.07	102.06	NaN
221.4583	306.05	NaN	20.08	102.02	NaN
221.5	305.90	365.70	20.06	102.03	99.47
221.5417	303.10	363.00	20.05	102.15	99.48
221.5833	303.03	362.60	20.15	102.32	99.67
221.625	304.43	360.42	20.21	102.37	99.60
221.6667	308.50	357.58	20.14	102.28	99.63
221.7083	314.35	357.80	20.10	102.18	99.67
221.75	315.58	358.40	20.05	102.07	99.63
221.7917	317.50	360.67	20.07	101.98	99.70
221.8333	316.08	362.07	19.92	101.90	99.73
221.875	299.15	365.23	19.90	102.05	99.77
221.9167	258.83	374.20	20.15	102.37	99.70
221.9583	284.22	371.78	19.91	102.00	99.73
222	289.83	371.20	19.79	101.90	99.80
222.0417	306.30	373.53	19.84	101.58	99.80
222.0833	308.62	381.03	19.85	101.50	99.83
222.125	307.70	393.95	19.77	101.50	99.90
222.1667	305.53	398.28	19.68	101.50	99.90
222.2083	304.95	410.60	19.60	101.53	99.93
222.25	307.78	421.95	19.71	101.42	100.00
222.2917	321.80	416.03	20.23	100.90	100.00
222.3333	329.65	409.05	20.38	100.90	100.00
222.375	323.00	397.35	20.43	101.10	100.00
222.4167	295.55	385.05	20.19	101.80	100.03
222.4583	300.05	368.88	20.37	101.92	100.10
222.5	327.05	371.70	20.84	101.40	100.10
222.5417	319.90	376.22	20.92	101.43	100.10
222.5833	305.35	376.52	20.65	101.58	100.10
222.625	287.42	374.50	20.58	101.88	100.07
222.6667	279.95	374.40	20.49	102.07	100.00
222.7083	277.85	374.20	20.63	101.98	100.00
222.75	282.25	374.63	20.79	101.82	100.00
222.7917	294.50	375.33	20.90	101.53	100.00
222.8333	314.85	376.98	20.92	101.25	100.00
222.875	324.23	381.13	20.82	101.07	100.00
222.9167	326.35	387.92	20.80	101.00	100.00
222.9583	316.75	394.80	20.72	101.10	100.00
223	285.18	413.20	20.50	101.40	100.00
223.0417	275.00	419.22	20.34	101.55	100.00
223.0833	235.55	423.27	20.24	101.92	100.00
223.125	266.20	421.22	20.19	101.73	100.00

223.1667	263.20	409.78	19.94	101.82	100.00
223.2083	263.17	403.05	19.76	101.87	100.00
223.25	254.72	399.15	19.74	101.83	100.00
223.2917	253.93	396.70	19.74	101.87	100.00
223.3333	260.70	396.12	19.86	101.72	100.00
223.375	281.80	385.35	20.13	101.50	100.00
223.4167	282.57	374.98	20.22	101.53	100.00
223.4583	277.95	369.18	20.23	101.57	100.00
223.5	287.40	371.15	20.19	101.45	100.00
223.5417	296.27	370.92	20.21	101.30	99.97
223.5833	297.48	367.15	20.46	101.25	99.90
223.625	310.40	365.13	20.55	101.10	99.90
223.6667	308.87	366.60	20.68	101.15	99.87
223.7083	298.02	366.30	20.60	101.38	99.80
223.75	280.90	366.43	20.28	101.60	99.77
223.7917	275.40	367.90	20.07	101.63	99.70
223.8333	270.38	371.25	20.07	101.62	99.70
223.875	278.93	372.20	20.33	101.37	99.70
223.9167	277.50	378.50	20.35	101.35	99.70
223.9583	259.85	392.97	20.24	101.58	99.70
224	249.90	400.47	20.02	101.80	99.70
224.0417	252.98	400.40	19.89	101.77	99.67
224.0833	267.20	402.05	19.86	101.65	99.60
224.125	277.90	386.00	19.84	101.45	99.60
224.1667	282.05	389.75	19.92	101.25	99.57
224.2083	285.45	397.70	19.98	101.08	99.53
224.25	287.42	407.38	20.02	101.03	99.60
224.2917	285.08	420.87	19.98	101.12	99.57
224.3333	283.85	428.70	19.98	101.20	99.50
224.375	286.25	419.80	20.01	101.20	99.50
224.4167	293.13	410.42	20.20	101.12	99.50
224.4583	312.82	394.25	20.79	100.90	99.50
224.5	326.25	375.17	21.17	100.87	99.47
224.5417	339.32	371.85	21.45	100.80	99.40
224.5833	340.52	370.00	21.50	100.83	99.37
224.625	329.25	369.27	21.41	101.00	99.30
224.6667	305.35	368.80	21.21	101.32	99.27
224.7083	289.13	368.35	21.26	101.42	99.20
224.75	279.70	368.00	21.31	101.53	99.25
224.7917	282.65	368.25	21.20	101.55	99.37
224.8333	282.83	368.03	21.08	101.38	99.30
224.875	284.23	367.50	21.02	101.30	99.33
224.9167	282.82	367.08	20.85	101.27	99.42
224.9583	272.80	370.48	20.21	101.25	99.52
225	269.00	376.75	19.68	101.35	99.60

225.0417	276.57	378.05	19.45	101.18	99.60
225.0833	282.20	379.30	19.25	101.08	99.63
225.125	291.60	381.03	19.25	100.95	99.70
225.1667	296.05	381.35	19.16	100.80	99.70
225.2083	298.25	380.30	19.01	100.80	99.73
225.25	301.68	380.38	18.87	100.80	99.83
225.2917	305.27	380.42	18.79	100.83	99.92
225.3333	296.10	379.42	18.65	100.95	100.00
225.375	285.15	377.25	18.51	101.13	100.00
225.4167	291.80	375.03	18.77	101.15	100.03
225.4583	302.67	374.87	19.26	101.00	100.10
225.5	304.13	374.02	19.60	101.00	100.10
225.5417	304.37	373.48	19.93	101.03	100.10
225.5833	302.08	373.50	20.12	101.10	100.07
225.625	306.38	373.75	20.31	101.07	100.00
225.6667	316.40	373.07	20.51	101.00	100.00
225.7083	304.70	371.53	20.41	101.00	100.00
225.75	305.88	371.47	20.37	101.00	100.00
225.7917	307.23	371.20	20.31	100.97	100.00
225.8333	310.85	371.12	20.20	100.88	100.03
225.875	318.38	370.10	20.12	100.80	100.10
225.9167	324.55	370.42	20.11	100.80	100.13
225.9583	332.80	370.73	20.06	100.77	100.20
226	341.25	371.50	20.02	100.70	100.20
226.0417	348.80	375.38	20.01	100.67	100.20
226.0833	352.25	387.02	19.94	100.60	100.20
226.125	353.53	389.10	19.87	100.57	100.20
226.1667	358.03	387.78	19.83	100.50	100.23
226.2083	364.87	389.52	19.81	100.50	100.32
226.25	369.80	388.30	19.80	100.50	100.40
226.2917	379.85	387.65	19.80	100.47	100.40
226.3333	385.67	379.90	19.86	100.40	100.40
226.375	377.87	375.42	19.91	100.45	100.40
226.4167	359.15	373.65	20.02	100.65	100.43
226.4583	344.88	373.58	20.09	100.82	100.47
226.5	331.75	373.93	20.14	100.93	100.37
226.5417	320.65	373.97	20.25	101.00	100.30
226.5833	318.15	373.03	20.41	101.00	100.30
226.625	326.28	373.02	20.64	100.97	100.30
226.6667	328.30	372.95	20.74	100.90	100.27
226.7083	326.87	373.35	20.78	100.90	100.20
226.75	324.92	373.30	20.78	100.87	100.17
226.7917	323.35	373.80	20.73	100.80	100.10
226.8333	321.68	377.65	20.64	100.80	100.10
226.875	320.67	385.47	20.57	100.80	100.13

226.9167	319.22	379.68	20.54	100.80	100.20
226.9583	315.55	381.15	20.44	100.77	100.20
227	320.40	385.10	20.33	100.67	100.17
227.0417	332.72	387.18	20.22	100.58	100.10
227.0833	339.42	398.45	20.14	100.48	100.10
227.125	341.40	394.27	20.00	100.40	100.07
227.1667	337.35	392.90	19.84	100.40	100.03
227.2083	341.27	393.70	19.71	100.40	100.10
227.25	343.22	397.43	19.52	100.43	100.10
227.2917	341.80	397.77	19.39	100.55	100.10
227.3333	340.93	393.10	19.38	100.72	100.10
227.375	341.33	385.02	19.50	100.85	100.10
227.4167	344.08	377.18	19.80	101.08	100.10
227.4583	348.52	374.95	20.30	101.25	100.07
227.5	342.57	373.87	20.53	101.07	100.00
227.5417	332.53	370.95	20.61	100.98	100.00
227.5833	331.90	370.73	20.51	100.90	99.97
227.625	332.00	370.97	20.57	100.90	99.90
227.6667	335.60	369.58	20.62	100.90	99.90
227.7083	335.35	369.30	20.50	100.87	99.90
227.75	341.00	369.52	20.36	100.77	99.90
227.7917	348.15	369.88	20.27	100.75	99.93
227.8333	339.95	372.78	20.24	100.87	100.00
227.875	347.65	378.10	20.23	100.83	100.00
227.9167	330.95	383.35	20.17	100.95	100.00
227.9583	303.58	384.28	20.11	101.12	100.00
228	285.43	386.90	20.03	101.17	100.00
228.0417	292.75	382.83	19.92	101.05	100.00
228.0833	303.17	384.70	19.81	100.90	100.00
228.125	307.85	387.43	19.69	100.87	100.00
228.1667	310.12	390.82	19.56	100.80	100.00
228.2083	310.58	390.90	19.55	100.80	100.03
228.25	314.95	386.48	19.58	100.80	100.10
228.2917	317.58	388.90	19.59	100.83	100.13
228.3333	321.35	387.20	19.63	100.90	100.20
228.375	324.48	386.30	19.81	100.98	100.20
228.4167	326.17	384.30	20.22	101.22	100.20
228.4583	327.65	380.98	20.51	101.27	100.20
228.5	332.02	381.50	20.81	101.23	100.20
228.5417	331.80	382.90	21.08	101.32	100.20
228.5833	333.67	381.23	21.31	101.42	100.20
228.625	337.73	379.27	21.40	101.50	100.20
228.6667	349.95	377.15	21.34	101.50	100.20
228.7083	352.12	375.03	21.36	101.53	100.20
228.75	349.50	373.55	21.37	101.60	100.20

228.7917	323.80	373.70	21.28	101.83	100.25
228.8333	271.40	375.10	21.04	102.37	100.35
228.875	281.28	377.68	20.90	102.00	100.23
228.9167	281.92	380.52	20.85	102.00	100.30
228.9583	278.75	383.48	20.80	101.97	100.30
229	285.15	394.62	20.68	101.80	100.30
229.0417	312.65	401.03	20.52	101.43	100.30
229.0833	338.67	435.92	20.43	101.18	100.33
229.125	331.67	456.83	20.28	101.13	100.40
229.1667	319.35	463.22	20.18	101.15	100.40
229.2083	339.22	447.45	20.16	101.00	100.40
229.25	339.00	417.50	20.14	101.03	100.43
229.2917	338.60	411.78	20.22	101.12	100.50
229.3333	337.28	405.95	20.38	101.22	100.50
229.375	338.10	401.52	20.62	101.35	100.50
229.4167	328.35	388.85	20.92	101.73	100.55
229.4583	295.90	379.00	21.09	102.35	100.70
229.5	317.45	373.13	21.24	102.15	100.62
229.5417	312.08	374.75	21.24	102.03	100.40
229.5833	304.93	371.07	21.36	102.12	100.37
229.625	296.07	365.00	21.43	102.20	100.30
229.6667	290.08	364.92	21.40	102.20	100.30
229.7083	288.22	364.80	21.35	102.23	100.30
229.75	283.38	364.97	21.27	102.27	100.27
229.7917	287.32	365.35	21.24	102.18	100.20
229.8333	281.90	367.97	21.11	102.13	100.20
229.875	256.50	370.43	20.98	102.30	100.20
229.9167	223.00	375.10	20.92	102.62	100.20
229.9583	216.15	378.53	20.85	102.70	100.20
230	209.53	386.08	20.79	102.65	100.20
230.0417	234.35	411.00	20.69	102.27	100.23
230.0833	296.05	439.60	20.62	101.60	100.30
230.125	293.68	405.43	20.56	101.60	100.30
230.1667	281.87	432.05	20.48	101.68	100.30
230.2083	248.18	436.02	20.36	101.87	100.30
230.25	259.15	417.70	20.29	101.80	100.33
230.2917	265.98	412.15	20.36	101.80	100.40
230.3333	280.05	410.65	20.50	101.80	100.40
230.375	288.17	401.00	20.72	101.88	100.37
230.4167	280.38	388.45	20.93	102.17	100.35
230.4583	272.20	385.70	21.19	102.63	100.50
230.5	240.15	387.45	21.40	103.02	100.50
230.5417	315.37	381.75	21.70	102.08	100.42
230.5833	336.00	367.65	21.81	101.70	100.18
230.625	336.97	366.17	21.96	101.67	100.10

230.6667	332.42	362.85	21.91	101.60	100.07
230.7083	319.25	362.70	21.88	101.65	100.00
230.75	295.25	364.20	21.73	101.83	100.00
230.7917	282.35	363.35	21.68	101.92	100.00
230.8333	259.12	364.25	21.48	102.15	100.00
230.875	215.50	368.28	21.43	102.68	100.00
230.9167	199.35	374.67	21.43	102.90	100.00
230.9583	196.65	379.35	21.42	102.85	100.00
231	202.55	384.03	21.24	102.62	100.00
231.0417	218.02	384.25	20.93	102.30	99.97
231.0833	235.22	382.35	20.69	101.93	99.90
231.125	250.33	383.70	20.45	101.65	99.90
231.1667	264.32	385.63	20.33	101.45	99.90
231.2083	267.37	388.75	20.25	101.30	99.93
231.25	264.20	391.48	20.17	101.30	100.00
231.2917	268.18	397.50	20.28	101.30	100.00
231.3333	281.30	386.35	20.64	101.35	100.00
231.375	274.25	364.45	20.90	101.55	99.97
231.4167	276.50	352.15	20.97	101.78	99.95
231.4583	285.03	349.88	20.94	102.02	100.10
231.5	296.33	352.22	20.84	102.10	100.07
231.5417	303.92	351.40	20.81	102.10	100.00
231.5833	315.13	354.23	21.28	102.13	99.97
231.625	320.00	360.12	21.78	102.23	99.90
231.6667	282.93	351.93	21.83	102.25	99.90
231.7083	282.15	350.18	21.65	102.08	99.87
231.75	280.55	351.03	21.40	102.00	99.80
231.7917	276.65	357.10	21.16	101.97	99.83
231.8333	275.13	359.22	21.06	101.85	99.90
231.875	283.50	361.30	21.00	101.67	99.90
231.9167	286.55	366.15	20.96	101.52	99.85
231.9583	289.60	371.42	20.94	101.28	99.70
232	290.87	373.53	20.82	101.23	99.70
232.0417	286.75	375.50	20.76	101.25	99.70
232.0833	291.42	378.72	20.74	101.13	99.70
232.125	280.15	376.98	20.70	101.35	99.73
232.1667	263.78	377.45	20.64	101.67	99.80
232.2083	281.90	378.15	20.57	101.35	99.80
232.25	271.72	383.63	20.44	101.53	99.83
232.2917	270.83	382.85	20.35	101.57	99.90
232.3333	294.25	375.70	20.30	101.53	99.90
232.375	300.75	365.92	20.44	101.68	99.90
232.4167	301.97	361.65	20.63	101.95	99.95
232.4583	301.05	360.45	20.75	102.15	100.07
232.5	295.50	359.10	20.90	102.33	100.00

232.5417	292.05	361.62	20.97	102.40	100.00
232.5833	297.20	363.15	21.05	102.32	99.97
232.625	313.63	368.47	20.93	102.10	99.90
232.6667	304.00	364.83	20.72	102.23	99.90
232.7083	252.05	360.48	20.05	102.45	99.85
232.75	254.15	358.05	20.63	101.87	99.70
232.7917	273.00	358.07	21.09	101.55	99.70
232.8333	251.25	358.60	20.68	101.75	99.70
232.875	248.18	361.98	20.21	101.90	99.70
232.9167	250.32	365.13	20.14	101.85	99.70
232.9583	250.48	368.52	20.03	101.75	99.70
233	258.70	369.20	19.62	101.98	99.70
233.0417	260.72	371.22	18.84	102.33	99.70
233.0833	266.68	371.80	17.57	102.80	99.70
233.125	287.82	372.28	16.50	103.05	99.70
233.1667	287.22	375.50	17.50	102.75	99.70
233.2083	286.00	378.82	17.89	102.23	99.70
233.25	287.40	381.83	18.19	102.05	99.70
233.2917	293.92	385.40	17.71	102.30	99.70
233.3333	300.15	384.82	17.19	102.67	99.70
233.375	307.10	380.62	17.09	103.00	99.70
233.4167	309.30	376.77	16.84	103.35	99.75
233.4583	305.95	370.30	17.29	103.42	99.90
233.5	302.67	367.07	18.47	103.00	99.87
233.5417	299.55	365.70	20.55	102.35	99.78
233.5833	318.42	363.25	20.74	102.30	99.75
233.625	313.87	361.20	20.06	102.80	99.90
233.6667	292.25	358.90	18.78	103.50	99.87
233.7083	266.70	360.40	17.87	103.90	99.78
233.75	255.75	358.45	15.82	103.82	99.73
233.7917	265.42	358.28	14.31	102.70	99.77
233.8333	261.30	359.90	14.09	103.08	99.70
233.875	284.20	362.38	12.74	104.00	99.70
233.9167	337.37	367.38	10.82	103.28	99.75
233.9583	381.70	382.22	9.25	102.75	99.85
234	387.10	382.95	9.32	102.27	99.73
234.0417	396.35	380.63	9.17	102.10	99.77
234.0833	396.32	384.83	11.07	101.80	99.70
234.125	318.28	393.27	18.13	101.62	99.70
234.1667	337.17	389.30	18.95	101.13	99.70
234.2083	348.37	394.57	18.81	101.25	99.67
234.25	355.08	389.70	18.06	101.45	99.60
234.2917	357.07	392.75	17.81	101.65	99.60
234.3333	356.95	394.25	17.52	101.82	99.63
234.375	357.67	397.30	17.35	101.85	99.73

234.4167	352.95	401.57	17.68	101.65	99.82
234.4583	361.93	396.47	17.42	101.60	99.95
234.5	386.48	388.45	16.01	101.93	100.07
234.5417	400.45	389.08	14.74	101.95	99.98
234.5833	406.80	395.70	13.73	101.85	99.90
234.625	420.48	408.08	12.90	102.03	99.87
234.6667	425.20	414.02	13.07	102.12	99.80
234.7083	411.47	410.37	14.72	102.10	99.83
234.75	387.80	404.02	16.15	101.80	99.90
234.7917	375.22	399.47	16.27	101.83	99.93
234.8333	349.53	390.88	16.90	101.77	100.00
234.875	346.35	391.65	18.71	101.35	100.03
234.9167	341.05	395.50	19.82	101.13	100.10
234.9583	338.33	399.10	20.59	100.88	100.10
235	339.53	405.75	20.75	100.80	100.10
235.0417	343.45	405.13	20.48	100.80	100.10
235.0833	348.87	406.75	20.27	100.80	100.10
235.125	353.30	404.43	20.13	100.77	100.10
235.1667	359.60	423.28	19.96	100.73	100.10
235.2083	370.90	440.67	19.57	100.80	100.13
235.25	381.33	390.70	19.24	100.83	100.20
235.2917	382.20	426.52	19.15	100.90	100.23
235.3333	374.37	417.90	18.68	100.98	100.30
235.375	365.07	412.32	17.45	101.38	100.30
235.4167	362.65	402.85	17.69	101.90	100.30
235.4583	355.43	395.45	18.18	101.93	100.30
235.5	354.20	381.05	18.45	102.03	100.30
235.5417	363.57	381.62	19.46	101.87	100.27
235.5833	349.20	382.75	21.72	101.20	100.20
235.625	348.78	385.15	21.99	101.23	100.20
235.6667	349.52	384.47	21.87	101.32	100.20
235.7083	348.80	381.25	21.74	101.45	100.25
235.75	340.95	381.65	22.00	101.60	100.40
235.7917	326.48	381.15	21.81	101.57	100.32
235.8333	312.40	379.57	21.55	101.55	100.13
235.875	302.30	382.55	21.17	101.73	100.20
235.9167	306.60	398.75	20.72	101.75	100.20
235.9583	314.20	409.50	20.40	101.58	100.23
236	316.23	427.13	20.16	101.55	100.30
236.0417	344.65	454.40	20.02	101.67	100.30
236.0833	364.92	458.97	19.84	101.58	100.30
236.125	362.10	451.37	19.83	101.50	100.33
236.1667	361.50	450.18	19.79	101.47	100.42
236.2083	361.75	460.25	19.66	101.45	100.50
236.25	346.60	486.38	19.67	101.55	100.50

236.2917	302.98	485.12	20.32	101.40	100.50
236.3333	326.78	457.55	20.87	101.32	100.50
236.375	361.00	436.42	20.97	101.15	100.50
236.4167	358.60	417.70	21.25	101.48	100.55
236.4583	352.37	385.33	21.53	102.00	100.70
236.5	342.18	376.25	21.08	101.95	100.62
236.5417	343.65	378.05	20.95	101.80	100.40
236.5833	341.40	386.70	21.23	101.83	100.40
236.625	324.97	393.10	21.27	101.95	100.37
236.6667	299.68	393.02	21.31	102.18	100.30
236.7083	276.30	385.45	21.08	102.47	100.27
236.75	252.12	381.32	20.28	102.75	100.20
236.7917	242.43	378.68	19.34	102.90	100.23
236.8333	268.07	379.50	18.17	102.82	100.30
236.875	281.90	378.15	17.48	102.60	100.30
236.9167	282.65	377.83	17.82	102.55	100.30
236.9583	287.73	387.00	18.12	102.33	100.30
237	301.28	382.60	18.49	102.10	100.30
237.0417	305.85	388.00	18.53	102.10	100.30
237.0833	303.75	389.35	18.14	102.13	100.27
237.125	319.52	387.32	16.93	102.30	100.23
237.1667	316.80	385.85	15.83	102.57	100.30
237.2083	322.38	387.47	15.36	102.48	100.30
237.25	341.58	387.50	14.91	102.40	100.30
237.2917	347.80	387.37	14.92	102.43	100.30
237.3333	356.10	385.48	14.88	102.52	100.30
237.375	372.50	382.90	15.08	102.65	100.27
237.4167	383.95	380.75	14.86	102.90	100.20
237.4583	381.70	379.55	14.34	103.32	100.25
237.5	409.28	376.00	12.96	103.73	100.37
237.5417	418.82	374.38	11.52	103.80	100.30
237.5833	428.37	373.03	11.18	103.80	100.27
237.625	441.30	372.10	11.31	103.77	100.17
237.6667	444.40	369.78	11.06	103.75	100.08
237.7083	397.75	369.15	10.97	103.85	100.03
237.75	386.00	368.22	10.84	103.78	100.10
237.7917	362.15	364.13	11.19	103.97	100.10
237.8333	367.27	362.00	11.19	103.88	100.13
237.875	367.53	364.20	11.13	103.77	100.20
237.9167	383.98	367.48	10.47	103.42	100.20
237.9583	417.70	371.70	9.76	102.50	100.12
238	439.53	374.90	9.66	102.17	99.90
238.0417	462.28	378.47	9.48	102.08	99.90
238.0833	504.10	379.00	9.07	102.00	99.87
238.125	517.30	379.00	9.29	101.97	99.80

238.1667	529.97	382.65	9.06	101.88	99.83
238.2083	526.68	386.22	9.28	101.83	99.90
238.25	555.93	389.08	8.90	101.90	99.90
238.2917	583.62	391.37	8.68	101.87	99.90
238.3333	600.95	391.30	8.68	101.83	99.90
238.375	600.70	388.63	8.60	101.82	99.93
238.4167	595.88	388.40	8.20	101.68	100.00
238.4583	608.70	386.92	8.67	101.87	100.00
238.5	595.65	386.48	8.59	101.83	99.92
238.5417	585.15	388.90	9.06	101.92	99.70
238.5833	583.85	382.98	9.31	102.05	99.67
238.625	592.43	377.00	9.74	102.25	99.60
238.6667	594.90	373.85	10.23	102.50	99.57
238.7083	562.20	370.25	10.82	103.05	99.55
238.75	493.72	366.85	12.55	103.65	99.67
238.7917	393.35	368.57	15.76	102.95	99.60
238.8333	361.98	368.58	16.00	102.48	99.63
238.875	367.30	372.53	14.53	103.33	99.70
238.9167	373.98	378.67	13.12	103.35	99.67
238.9583	403.50	380.32	12.25	102.90	99.60
239	438.63	382.08	11.64	102.00	99.63
239.0417	468.17	383.25	11.22	101.97	99.67
239.0833	499.82	385.95	10.72	102.00	99.52
239.125	511.90	389.20	10.32	102.27	99.30
239.1667	525.27	393.25	10.03	102.15	99.33
239.2083	529.03	393.97	9.37	101.85	99.42
239.25	538.38	386.00	8.57	101.40	99.50
239.2917	555.70	384.40	8.34	101.37	99.50
239.3333	563.12	387.65	8.32	101.28	99.50
239.375	568.85	397.03	8.22	101.17	99.47
239.4167	577.25	408.60	8.47	101.20	99.38
239.4583	575.07	405.65	9.04	101.57	99.28
239.5	553.07	401.57	9.41	101.90	99.20
239.5417	503.32	390.37	12.67	101.95	99.17
239.5833	382.05	378.10	20.33	101.45	99.10
239.625	378.58	376.10	18.50	102.23	99.15
239.6667	385.65	374.35	16.89	102.48	99.27
239.7083	387.83	373.33	15.44	102.97	99.23
239.75	392.47	372.88	14.04	103.10	99.30
239.7917	392.13	374.80	13.40	103.27	99.33
239.8333	413.90	377.75	12.91	102.08	99.40
239.875	426.38	383.18	12.68	102.17	99.35
239.9167	451.30	395.70	11.49	101.88	99.23
239.9583	461.45	399.50	9.81	102.00	99.25
240	451.70	400.15	9.57	101.62	99.13

240.0417	456.25	400.55	9.03	101.35	99.20
240.0833	463.65	401.25	8.88	101.15	99.23
240.125	483.95	400.30	9.01	101.03	99.30
240.1667	496.47	397.43	9.74	101.12	99.33
240.2083	449.97	395.60	12.58	101.02	99.40
240.25	377.83	392.75	19.03	100.60	99.43
240.2917	379.25	390.00	18.42	100.95	99.50
240.3333	379.33	395.77	17.93	101.15	99.50
240.375	380.95	391.67	17.58	101.30	99.53
240.4167	381.20	386.65	17.83	101.33	99.60
240.4583	383.93	386.78	17.76	101.42	99.63
240.5	393.33	388.73	17.62	101.53	99.70
240.5417	400.65	392.53	17.40	101.62	99.70
240.5833	404.57	402.95	17.32	101.70	99.67
240.625	407.88	405.65	17.28	101.70	99.63
240.6667	408.02	403.10	17.46	101.73	99.70
240.7083	401.45	399.38	17.95	101.77	99.70
240.75	382.05	398.95	18.64	101.65	99.70
240.7917	377.50	398.67	19.38	101.43	99.73
240.8333	365.73	398.50	20.06	101.15	99.80
240.875	361.60	398.50	20.23	101.00	99.80
240.9167	361.43	396.05	20.19	101.00	99.80
240.9583	366.58	394.38	19.90	101.05	99.80
241	377.90	394.52	19.29	101.25	99.80
241.0417	388.55	393.40	18.77	101.40	99.77
241.0833	396.12	405.85	18.67	101.32	99.73
241.125	389.88	436.73	18.67	101.20	99.80
241.1667	397.87	442.45	18.03	101.50	99.80
241.2083	399.95	444.25	17.93	101.50	99.80
241.25	388.77	435.70	18.09	101.50	99.83
241.2917	384.30	414.75	18.25	101.50	99.90
241.3333	383.45	408.50	18.46	101.55	99.90
241.375	383.45	407.57	18.86	101.73	99.90
241.4167	386.42	406.25	19.04	101.88	99.90
241.4583	391.58	408.10	19.63	102.28	99.95
241.5	406.23	412.98	20.71	102.88	100.07
241.5417	412.85	417.60	21.28	102.87	100.00
241.5833	381.48	391.93	21.88	102.18	99.97
241.625	383.50	388.73	21.54	102.15	99.90
241.6667	384.62	388.62	21.43	102.35	99.90
241.7083	372.62	387.10	21.62	102.50	99.87
241.75	349.67	384.07	20.87	102.55	99.80
241.7917	317.28	384.23	20.27	102.72	99.80
241.8333	294.65	385.17	19.97	102.77	99.75
241.875	261.20	385.55	19.64	102.73	99.60

241.9167	247.98	384.78	18.82	102.70	99.57
241.9583	292.55	391.23	18.26	102.33	99.53
242	335.18	404.32	19.02	101.97	99.57
242.0417	363.37	401.85	19.24	101.58	99.50
242.0833	376.88	404.30	19.51	101.45	99.47
242.125	396.90	406.58	19.70	101.25	99.37
242.1667	401.77	412.80	19.74	101.10	99.30
242.2083	399.43	417.05	19.68	101.10	99.30
242.25	397.02	419.10	19.54	101.10	99.27
242.2917	394.42	416.22	19.51	101.13	99.20
242.3333	383.98	404.10	19.48	101.28	99.17
242.375	372.57	394.05	19.34	101.60	99.15
242.4167	368.28	386.15	19.29	102.00	99.27
242.4583	369.78	382.33	18.76	102.40	99.20
242.5	379.10	380.82	18.51	102.83	99.23
242.5417	393.55	379.60	17.85	103.22	99.27
242.5833	396.45	379.60	16.91	103.35	99.20
242.625	406.70	381.78	15.08	103.07	99.23
242.6667	418.47	386.15	13.84	101.88	99.25
242.7083	383.03	387.80	13.94	101.90	99.08
242.75	376.53	388.13	14.35	101.40	99.00
242.7917	394.55	388.37	15.90	101.65	99.05
242.8333	391.42	387.78	17.09	101.48	99.20
242.875	382.93	391.90	17.26	101.37	99.23
242.9167	384.60	389.80	17.16	101.28	99.27
242.9583	385.85	389.28	16.88	101.20	99.20
243	385.15	392.10	17.47	101.07	99.20
243.0417	382.35	397.60	19.25	100.65	99.17
243.0833	381.53	398.90	19.65	100.50	99.10
243.125	380.37	397.05	19.65	100.53	99.13
243.1667	377.38	390.28	19.68	100.60	99.20
243.2083	377.60	390.00	19.61	100.57	99.17
243.25	381.28	392.25	19.53	100.47	99.13
243.2917	385.05	393.03	19.41	100.43	99.20
243.3333	390.15	394.00	19.29	100.52	99.20
243.375	398.85	393.52	19.12	100.60	99.20
243.4167	405.23	392.00	19.05	100.60	99.20
243.4583	413.12	391.45	18.92	100.60	99.20
243.5	406.65	390.65	19.04	100.63	99.20
243.5417	400.82	390.65	19.31	100.80	99.20
243.5833	389.17	391.10	19.61	101.05	99.17
243.625	375.42	390.77	20.11	100.90	99.10
243.6667	375.18	389.70	20.21	100.93	99.07
243.7083	375.47	389.70	20.31	101.00	99.00
243.75	374.98	391.60	20.25	101.00	99.00

243.7917	377.62	394.82	20.35	100.95	99.00
243.8333	375.02	396.08	20.12	100.80	99.03
243.875	368.00	397.77	20.03	100.80	99.10
243.9167	347.22	398.98	20.03	100.80	99.10
243.9583	322.23	403.70	20.08	100.83	99.10
244	316.68	405.45	19.99	100.85	99.07
244.0417	320.42	402.58	19.89	100.70	99.00
244.0833	325.80	405.78	19.94	100.62	99.00
244.125	357.50	412.82	19.96	100.35	98.97
244.1667	397.02	411.45	19.92	100.20	98.90
244.2083	383.30	432.52	19.85	100.17	98.90
244.25	387.75	435.25	19.71	100.18	98.90
244.2917	382.27	437.57	19.74	100.37	98.90
244.3333	374.30	424.33	19.94	100.33	98.90
244.375	373.35	414.07	20.30	100.43	98.90
244.4167	371.08	396.25	20.35	100.50	98.90
244.4583	371.25	386.23	20.51	100.60	98.93
244.5	369.05	385.50	20.76	100.98	99.00
244.5417	358.33	392.70	20.95	101.12	98.97
244.5833	375.77	398.00	20.84	100.88	98.90
244.625	372.25	398.25	20.84	100.77	98.87
244.6667	368.87	392.88	20.76	100.70	98.80
244.7083	357.35	392.42	20.59	100.65	98.77
244.75	350.67	382.15	20.59	100.55	98.70
244.7917	331.93	384.30	20.49	100.67	98.73
244.8333	331.55	385.10	20.45	100.60	98.82
244.875	316.25	388.95	20.31	100.68	98.90
244.9167	307.25	391.43	20.12	100.80	98.90
244.9583	347.90	395.20	20.05	100.45	98.90
245	368.00	398.72	19.90	100.30	98.93
245.0417	365.65	397.75	19.78	100.30	99.00
245.0833	364.38	399.28	19.80	100.30	99.00
245.125	365.93	403.23	19.76	100.30	99.03
245.1667	367.82	404.67	19.71	100.30	99.12
245.2083	370.47	402.10	19.63	100.30	99.20
245.25	372.50	401.83	19.60	100.30	99.23
245.2917	371.90	405.02	19.64	100.33	99.30
245.3333	372.17	402.25	19.65	100.40	99.33
245.375	370.80	390.58	19.66	100.40	99.40
245.4167	376.20	390.40	19.64	100.40	99.43
245.4583	385.97	384.48	19.57	100.43	99.50
245.5	377.15	380.72	19.67	100.53	99.50
245.5417	364.43	379.15	19.91	100.57	99.50
245.5833	353.88	377.40	20.24	100.50	99.50
245.625	355.10	376.05	20.13	100.53	99.50

245.6667	355.85	375.30	19.72	100.60	99.50
245.7083	353.20	374.30	19.69	100.60	99.50
245.75	357.98	373.87	19.63	100.57	99.50
245.7917	360.10	373.45	19.60	100.50	99.50
245.8333	362.15	373.68	19.61	100.47	99.53
245.875	366.48	374.62	19.73	100.40	99.60
245.9167	372.75	374.10	19.78	100.37	99.60
245.9583	375.10	375.05	19.80	100.28	99.60
246	374.55	378.60	19.84	100.20	99.63
246.0417	377.82	381.12	19.81	100.20	99.70
246.0833	380.93	383.73	19.73	100.17	99.70
246.125	389.00	387.45	19.68	100.10	99.70
246.1667	399.32	386.65	19.62	100.07	99.73
246.2083	406.02	387.28	19.57	100.00	99.82
246.25	403.10	391.00	19.59	100.03	99.90
246.2917	402.05	394.80	19.62	100.12	99.90
246.3333	400.70	391.35	19.70	100.22	99.93
246.375	396.92	383.10	19.84	100.33	100.00
246.4167	389.65	378.08	20.03	100.42	99.97
246.4583	377.88	376.28	20.25	100.52	99.90
246.5	372.37	375.68	20.41	100.65	99.87
246.5417	351.95	376.00	20.68	100.80	99.80
246.5833	349.07	376.83	20.77	100.77	99.77
246.625	345.37	378.98	20.80	100.70	99.70
246.6667	344.25	380.15	20.80	100.70	99.67
246.7083	339.15	377.85	20.80	100.70	99.60
246.75	333.22	375.05	20.73	100.70	99.60
246.7917	332.80	374.10	20.70	100.67	99.63
246.8333	332.28	383.90	20.59	100.60	99.70
246.875	329.15	397.02	20.50	100.60	99.70
246.9167	317.70	392.65	20.44	100.60	99.70
246.9583	313.98	395.67	20.32	100.57	99.70
247	316.68	392.27	20.15	100.50	99.70
247.0417	322.15	389.53	20.01	100.47	99.70
247.0833	326.80	391.12	19.88	100.40	99.73
247.125	330.15	389.33	19.83	100.37	99.80
247.1667	344.65	394.95	19.77	100.30	99.83
247.2083	351.10	396.42	19.69	100.30	99.90
247.25	355.55	397.18	19.61	100.30	99.90
247.2917	358.27	397.70	19.64	100.33	99.90
247.3333	358.32	393.45	19.78	100.40	99.90
247.375	356.00	383.52	20.03	100.43	99.90
247.4167	351.50	374.28	20.20	100.52	99.90
247.4583	346.05	369.28	20.52	100.62	99.90
247.5	346.55	367.72	20.67	100.73	99.90

247.5417	348.85	366.55	20.89	100.88	99.95
247.5833	349.65	365.95	21.16	101.12	100.07
247.625	348.42	368.00	21.42	101.20	100.00
247.6667	347.83	369.87	21.50	101.20	100.00
247.7083	349.02	371.88	21.65	101.17	100.03
247.75	343.90	379.77	21.29	101.00	100.05
247.7917	340.23	379.28	20.95	100.70	99.93
247.8333	341.40	379.05	20.88	100.70	100.00
247.875	343.18	379.12	20.92	100.70	100.03
247.9167	343.92	378.23	20.93	100.70	100.10
247.9583	343.57	378.70	20.90	100.73	100.10
248	342.85	377.70	20.85	100.80	100.10
248.0417	341.70	375.93	20.80	100.80	100.13
248.0833	343.30	374.33	20.89	100.80	100.20
248.125	348.62	374.67	20.84	100.80	100.23
248.1667	348.85	374.60	20.77	100.77	100.30
248.2083	354.52	374.73	20.70	100.70	100.33
248.25	362.75	375.30	20.64	100.70	100.43
248.2917	369.07	375.80	20.61	100.75	100.50
248.3333	356.43	376.00	20.61	100.90	100.53
248.375	353.85	377.27	20.65	100.90	100.60
248.4167	360.50	376.28	20.58	100.90	100.60
248.4583	361.20	375.48	20.62	100.90	100.60
248.5	357.25	376.15	20.58	100.90	100.60
248.5417	365.92	376.62	20.67	100.93	100.60
248.5833	354.50	376.37	20.67	101.02	100.60
248.625	344.65	375.15	20.79	101.10	100.57
248.6667	338.58	374.35	20.78	101.10	100.50
248.7083	328.65	374.05	20.82	101.13	100.50
248.75	309.85	373.65	20.77	101.23	100.50
248.7917	300.65	373.95	20.73	101.22	100.50
248.8333	320.12	374.52	20.53	100.98	100.50
248.875	339.55	374.95	20.49	100.87	100.50
248.9167	343.70	374.87	20.44	100.80	100.50
248.9583	348.43	374.18	20.41	100.77	100.47
249	354.78	373.82	20.40	100.70	100.40
249.0417	358.87	372.90	20.37	100.70	100.40
249.0833	360.17	372.58	20.46	100.70	100.40
249.125	359.38	385.48	20.40	100.67	100.40
249.1667	361.42	423.15	20.26	100.60	100.40
249.2083	363.40	420.23	20.15	100.60	100.40
249.25	363.50	423.25	20.15	100.60	100.40
249.2917	360.42	415.92	20.19	100.60	100.40
249.3333	353.05	390.23	20.36	100.60	100.37
249.375	353.70	393.35	20.55	100.60	100.27

249.4167	355.77	392.68	20.55	100.60	100.20
249.4583	358.10	393.65	20.64	100.60	100.20
249.5	359.60	387.85	20.65	100.60	100.15
249.5417	364.20	388.90	20.72	100.57	99.98
249.5833	373.25	391.62	20.79	100.53	99.90
249.625	342.50	391.02	20.91	100.65	99.87
249.6667	311.48	388.45	20.90	100.82	99.80
249.7083	288.48	385.55	20.88	100.90	99.77
249.75	273.83	380.47	20.82	100.87	99.70
249.7917	283.65	375.80	20.90	100.75	99.67
249.8333	297.07	374.38	20.71	100.60	99.63
249.875	302.13	376.65	20.63	100.57	99.67
249.9167	302.42	378.68	20.60	100.53	99.60
249.9583	292.73	378.82	20.69	100.57	99.60
250	294.93	369.25	20.65	100.53	99.60
250.0417	300.93	374.87	20.44	100.60	99.57
250.0833	314.17	379.12	20.25	100.60	99.50
250.125	325.70	381.45	20.05	100.57	99.50
250.1667	329.00	385.02	19.97	100.50	99.50
250.2083	331.80	386.80	19.95	100.47	99.47
250.25	332.88	388.30	19.97	100.40	99.40
250.2917	338.20	389.70	20.02	100.37	99.40
250.3333	345.50	393.72	20.09	100.33	99.40
250.375	341.75	390.47	20.32	100.40	99.37
250.4167	347.55	381.23	20.62	100.48	99.35
250.4583	353.32	377.55	20.84	100.67	99.50
250.5	355.63	376.85	20.85	100.57	99.50
250.5417	357.20	378.80	20.50	100.42	99.42
250.5833	354.70	377.40	20.47	100.15	99.23
250.625	352.95	373.30	20.56	100.00	99.30
250.6667	354.15	373.67	20.70	100.03	99.30
250.7083	354.83	374.20	20.72	100.10	99.30
250.75	354.92	374.95	20.83	100.10	99.30
250.7917	352.88	377.45	20.71	100.07	99.30
250.8333	353.83	384.52	20.54	100.03	99.33
250.875	359.15	380.25	20.42	100.10	99.43
250.9167	355.62	379.80	20.48	100.10	99.52
250.9583	350.60	370.85	20.56	100.15	99.60
251	354.85	378.30	20.18	100.30	99.63
251.0417	354.05	384.20	20.15	100.30	99.70
251.0833	352.87	384.65	20.15	100.30	99.70
251.125	350.45	383.82	20.06	100.30	99.70
251.1667	353.83	382.38	20.01	100.30	99.70
251.2083	361.33	381.45	19.99	100.27	99.70
251.25	373.23	381.65	19.98	100.20	99.73

251.2917	379.22	381.85	19.93	100.23	99.80
251.3333	376.00	382.80	19.89	100.30	99.80
251.375	369.55	385.65	19.95	100.33	99.80
251.4167	367.00	388.05	19.93	100.37	99.83
251.4583	384.42	392.10	19.82	100.30	99.90
251.5	378.82	393.15	19.82	100.33	99.90
251.5417	363.43	387.10	19.87	100.40	99.90
251.5833	350.95	383.63	20.04	100.40	99.87
251.625	347.50	382.65	20.14	100.40	99.80
251.6667	347.12	380.63	20.25	100.40	99.77
251.7083	346.23	378.50	20.43	100.37	99.68
251.75	345.90	378.30	20.56	100.27	99.60
251.7917	342.33	378.25	20.52	100.20	99.60
251.8333	341.08	376.85	20.44	100.17	99.60
251.875	343.73	375.27	20.37	100.13	99.60
251.9167	349.80	373.68	20.28	100.20	99.60
251.9583	358.47	373.27	20.12	100.17	99.60
252	362.85	372.05	20.13	100.07	99.57
252.0417	365.58	371.75	20.14	99.98	99.50
252.0833	373.72	373.88	20.16	99.90	99.47
252.125	373.08	378.15	20.18	99.90	99.37
252.1667	376.27	384.37	20.17	99.87	99.30
252.2083	379.25	386.10	20.16	99.80	99.30
252.25	381.03	389.18	20.14	99.80	99.30
252.2917	383.45	393.72	20.14	99.80	99.33
252.3333	374.37	396.62	20.23	99.82	99.38
252.375	345.12	397.37	20.44	99.90	99.30
252.4167	348.43	393.57	20.49	99.90	99.30
252.4583	359.11	398.88	20.55	99.90	99.28
252.5	378.21	409.91	20.51	99.88	99.20
252.5417	414.39	405.43	20.62	99.80	99.18
252.5833	420.50	402.63	20.60	99.82	99.10
252.625	402.75	399.14	20.61	99.90	99.08
252.6667	400.72	395.74	20.73	99.88	98.98
252.7083	421.17	392.05	20.79	99.78	98.90
252.75	405.38	389.33	20.68	99.73	98.90
252.7917	384.46	388.95	20.64	99.77	98.90
252.8333	381.51	393.69	20.65	99.75	98.90
252.875	390.76	394.47	20.87	99.95	98.95
252.9167	395.07	392.03	20.94	100.12	99.10
252.9583	388.16	390.82	20.96	100.22	99.10
253	389.88	392.85	20.85	100.37	99.15
253.0417	393.87	394.36	20.66	100.57	99.32
253.0833	410.76	397.14	20.64	100.45	99.35
253.125	419.81	400.04	20.49	100.30	99.20

253.1667	416.39	401.48	20.19	100.35	99.22
253.2083	411.56	400.81	19.86	100.52	99.30
253.25	413.18	401.94	19.52	100.62	99.32
253.2917	411.47	403.23	19.38	100.72	99.42
253.3333	409.01	400.98	19.54	100.80	99.50
253.375	405.84	396.43	19.65	100.82	99.50
253.4167	412.19	393.19	19.77	100.92	99.55
253.4583	434.07	390.09	19.99	101.05	99.70
253.5	423.98	386.50	20.28	101.22	99.70
253.5417	426.86	383.17	20.37	101.27	99.68
253.5833	429.89	382.36	20.47	101.23	99.60
253.625	423.93	381.73	20.66	101.30	99.60
253.6667	424.12	382.07	20.76	101.30	99.60
253.7083	424.00	382.25	20.86	101.30	99.60
253.75	426.02	383.63	20.91	101.28	99.60
253.7917	429.46	386.59	20.61	101.18	99.62
253.8333	412.44	389.78	20.48	101.27	99.72
253.875	342.61	390.49	20.26	101.89	99.80
253.9167	309.53	391.04	19.63	102.20	99.78
253.9583	316.75	390.06	19.25	102.13	99.70
254	343.39	391.19	19.03	101.88	99.68
254.0417	336.99	394.53	18.90	101.78	99.60
254.0833	350.70	393.96	18.64	101.68	99.62
254.125	362.23	388.54	18.35	101.43	99.67
254.1667	422.46	388.35	18.73	100.78	99.60

APPENDIX B
MODEL AND FUNCTION MATLAB CODES

B.1: MATLAB code for the Nearshore Phosphorus Flux Model

```

% -----The Nearshore Phosphorus Flux Model-----
%
% Code Written by: Joe Fillingham
% Code Date: January 6, 2015
%
%-----
% Load Model Input Variables:
%
% Required Input Variables:
%
% T = Water Temperature (oC)
% PAR = Surface PAR (uE/m2/s)
% PO1 = Upper Layer Boundary Dissolved Phosphorus Concentration (ug/L)
% PO2 = Lower Layer Boundary Dissolved Phosphorus Concentration (ug/L)
% PPO1 = Upper Layer Boundary Particulate Phosphorus Concentration (ug/L)
% PPO2 = Lower Layer Boundary Particulate Phosphorus Concentration (ug/L)
% u1 = Upper Water Column cross shore current velocity (m/s)
% u2 = Lower Water Column cross shore current velocity (m/s)
% Wtao = Wave driven, benthic shear stress threshold (N/m2)
% Dvw = Vertical diffusivity between the upper and lower water column (m2/s)
% Dvb = Vertical diffusivity between the near bottom and lower layers (m2/s)
%
%-----
% Model Time:
%
n = length(inputvariable); % Available time (hours) - insert input variable
dt = 20; % time step (s)
t = 0:dt:n*3600; % time index (s)
days = daysh(1):1/24/(3600/dt):daysh(end); % Julian days every dt
N = length(days);
%
%-----
% Model Space:
dx = 1000; % m
dy = 1000; % m
dz = 0.2; % m
dzw = 4.5; % m
z = 2*dzw+dz; % m
%
%-----
% Ratios and Constants:
vs = 0.5/24/3600; % Particulate settling velocity (m/s)
CCtoP = 145.44; % Cladophora (g/g or 375 molar)
CtoP = 80; % Seston (g/g)
CtoChla = 35; % Seston (g/g)
Cgtom = 12; % g/mol
Pgtom = 31; % g/mol
Topt = 17; % Optimum Cladophora Sloughing Temperature (oC)
Lmax = 0.176/24/3600; % Maximum Cladophora Sloughing Rate (1/s)

```

```

%-----
% Dependent Variables:

I = zeros(1,N);           % PAR at depth (uE/m2/s)
Ke = zeros(1,N);         % Light extinction coefficient (1/m)
Pb = zeros(1,N);         % BBL DP (ugP/L = mgP/m3)
PPb = zeros(1,N);        % BBL PP (ugP/L = mgP/m3)
P1 = zeros(1,N);         % Surface Water DP (ugP/L = mgP/m3)
PP1 = zeros(1,N);        % Surface Water PP (ugP/L = mgP/m3)
P2 = zeros(1,N);         % Bottom Water DP (ugP/L = mgP/m3)
PP2 = zeros(1,N);        % Bottom Water PP (ugP/L = mgP/m3)

Jbpp = zeros(1,N);       % PP Water to BBL Flux (mgP/m2/s)
Jbp = zeros(1,N);        % DP Water to BBL Flux (mgP/m2/s)
Jwpp = zeros(1,N);       % PP Surface to Bottom Flux (mgP/m2/s)
Jwp = zeros(1,N);        % DP Surface to Bottom Flux (mgP/m2/s)
Jsusp = zeros(1,N);      % PP Resuspension Flux from Sediment storage to BBL
(mgP/m2/s)
Jslpp = zeros(1,N);      % Settling Flux (mgP/m2/s)
Js2pp = zeros(1,N);      % Settling Flux (mgP/m2/s)
Jsbpp = zeros(1,N);      % Settling Flux (mgP/m2/s)
Jo1pp = zeros(1,N);      % Nearshore Offshore Flux of PP (mgP/m2/s)
Jo2pp = zeros(1,N);      % Nearshore Offshore Flux of PP (mgP/m2/s)
Jo1p = zeros(1,N);       % Nearshore Offshore Flux of DP (mgP/m2/s)
Jo2p = zeros(1,N);       % Nearshore Offshore Flux of DP (mgP/m2/s)

MX = zeros(1,N);         % Mussel Excretion (mgP/m2/s)
MG = zeros(1,N);         % Mussel Grazing (mgP/m2/s)
ME = zeros(1,N);         % Mussel Egestion (mgP/m2/s)
X = zeros(1,N);          % Cladophora Biomass (gDM/m2)
S = zeros(1,N);          % Cladophora Phosphorus Storage (mgP/m2/10)
Q = zeros(1,N);          % Cladophora Tissue Phosphorus Content (mgP/gDM/10)
SD = zeros(1,N);         % Sediment Phosphorus Storage (mgPP/m2)
Bsedtrap = zeros(1,N);   % Sediment Accumulated in a Sediment Trap (mgPP/m2)
Tsedtrap = zeros(1,N);   % Sediment Accumulated in a Sediment Trap (mgPP/m2)
dPC = zeros(1,N);        % Cladophora Phosphorus Uptake (mgP/m2/s)
Lloss = zeros(1,N);      % Cladophora Sloughed Phosphorus (mgP/m2/s)

%-----
% Mussel Constants:
vp = zeros(1,N);         % L/m2/s
ex = 0.80;               % excretion/egestion ratio

%-----
% Cladophora Sloughing Algorithm:
SL = zeros(1,N);
x1 = find(T>=Topt);
x2 = find(Wtao >= 0.4);
SL(x1) = Lmax;
SL(x2) = Lmax;

%-----
% Resuspension Parameter:
rtao = zeros(1,N);
rtao(find(Wtao >= 0.40)) = 1;

%-----
% Initial conditions based on measured values:
% SRP13 = measured dissolved phosphorus concentration

```

```

% PP13 = measured particulate phosphorus concentration
% EmpData13 = measured Cladophora biomass, tissue P content, and stored P

Pb(1) = SRP13(1,3);      % ug/L
P2(1) = Pb(1);          % ug/L

PPb(1) = PP13(1,3);     % ug/L
PP2(1) = PPb(1);        % ug/L

PP1(1) = PP13(1,2);     % ug/L
P1(1) = SRP13(1,2);     % ug/L

X(1) = EmpData13(1,2);   % gDM/m2
Q(1) = EmpData13(1,4)/10; % mgP/gDM/10
S(1) = Q(1)*X(1);        % mgP/m2/10

%-----
% Time Loop:

b = dt/dz;      % s/m
b1 = dt/dzw;   % s/m
b2 = dt/dzw;   % s/m

for i = 1:N-1;

    % Light Extinction Coefficient (1/m):
    Ke(i) = 0.0383*mean([PP1(i) PP2(i)]) + 0.162;

    % Light at Depth (uE/m2/s):
    I(i) = PAR(i)*exp(-Ke(i).*z);

    % Mussel Model:
    % Mussel Water Pumping:
    vp(i) = MPfunc(T(i),MD(i),PropSC1(:,i)); % L/m2/s
    vp(i) = vp(i)/1000; % m/s
    % Mussel Phosphorus Fluxes:
    MG(i) = (vp(i)*PPb(i))*(1-rtao(i)); % mgP/m2/s
    MX(i) = ex*MG(i); % mgP/m2/s
    ME(i) = (1-ex)*MG(i); % mgP/m2/s

    % Cladophora Model:
    [S(i+1),Q(i+1),X(i+1),dPC(i),Lloss(i)] = Cfunc2(z,dz,I(i),T(i),Pb(i),...
        Q(i),S(i),X(i),dt,sloughing,SL(i));

    % Calculate Fluxes:

    % Settling:
    Js1pp(i) = vs*PP1(i);
    Js2pp(i) = vs*PP2(i);
    Jsbpp(i) = vs*PPb(i);

    % Resuspension Flux (mgP/m2/s):
    Jsusp(i) = rtao(i)*SD(i)/dt;

    % Vertical Turbulent Diffusion Flux (mgP/m2/s):
    Jbpp(i) = Dvb(i)*(PP2(i)-PPb(i))/dz;
    Jwpp(i) = Dvw(i)*(PP1(i)-PP2(i))/dzw;
    Jbp(i) = Dvb(i)*(P2(i)-Pb(i))/dz;

```

```

Jwp(i) = Dvw(i)*(P1(i)-P2(i))/dzw;

% Offshore to Nearshore Dispersion and Advection (mgP/m2/s):
Jo1pp(i) = abs(u1(i))*PPO1(i) - abs(u1(i))*PP1(i);
Jo2pp(i) = abs(u2(i))*PPO2(i) - abs(u2(i))*PP2(i);
Jo1p(i) = abs(u1(i))*PO1(i) - abs(u1(i))*P1(i);
Jo2p(i) = abs(u2(i))*PO2(i) - abs(u2(i))*P2(i);

% Solve Mass Balance Equations:

% PP in the Water Column (ugP/L):
PP1(i+1) = PP1(i) - Jwpp(i)*b1 - Js1pp(i)*b1 + ...
    Jo1pp(i)*dt/dx + JloadPP(i)*dt;

PP2(i+1) = PP2(i) - Jbpp(i)*b2 + Jwpp(i)*b2 - Js2pp(i)*b2 + ...
    Js1pp(i)*b2 + Jo2pp(i)*dt/dx + JloadPP(i)*dt;

% PP in the BBL (ugP/L):
PPb(i+1) = PPb(i) - b*MG(i) + Jbpp(i)*b...
    - Jsbpp(i)*b + Js2pp(i)*b + Jsusp(i)*b + JloadPPb(i)*dt;

% Water Column DP (ugP/L):
P1(i+1) = P1(i) - Jwp(i)*b1 + Jo1p(i)*dt/dx + JloadDP(i)*dt;
P2(i+1) = P2(i) - Jbp(i)*b2 + Jwp(i)*b2 + Jo2p(i)*dt/dx + JloadDP(i)*dt;

% DP in the BBL (ugP/L):
Pb(i+1) = Pb(i) + b*MX(i) - b*dPC(i) + Jbp(i)*b + JloadDPb(i)*dt;

% Sediment Accumulated PP (mgP/m2):
SD(i+1) = SD(i) + ME(i)*dt + Jsbpp(i)*dt - Jsusp(i)*dt;

% Model Simulated Sediment traps:
if Jbpp(i) >=0;
    Bsedtrap(i+1) = Bsedtrap(i) + Js2pp(i)*dt + Jbpp(i)*dt; % mg PP/m2
else Bsedtrap(i+1) = Bsedtrap(i) + Js2pp(i)*dt; % mg PP/m2
end

if Jwpp(i) >=0;
    Tsedtrap(i+1) = Tsedtrap(i) + Js1pp(i)*dt + Jwpp(i)*dt; % mg PP/m2
else Tsedtrap(i+1) = Tsedtrap(i) + Js1pp(i)*dt; % mg PP/m2
end

end

% End of Model Code
%-----

```

B.2: MATLAB code for the Nearshore Carbon and Phosphorus Model

```

% -----The Nearshore Phosphorus Flux Model-----
%
% Code Written by: Joe Fillingham
% Code Date: January 6, 2015
%-----
% Load Model Input Variabls:
%
% Required Input Variables:
%
% Ts = Surface Water Temperature (oC)
% T = Bottom Water Temperature (oC)
% PAR = Surface PAR (uE/m2/s)
% PO = Boundary Dissolved Phosphorus Concentration (ugP/L)
% PSO = Boundary Phytoplankton Concentration (umolC/L)
% DO = Boundary Particulate Detritus Concentration (umolC/L)
% DIC01 = Boundary Dissolved Inorganic Carbon Concentrations (mol/L)
% Hi01 = Boundary Hydrogen concentration (mol/L)
% u = Water Column mean cross shore current velocity (m/s)
% Wtao = Wave driven, benthic shear stress threshold (N/m2)
%-----
% Model Time:
%
n = length(inputvariable); % Available time (hours) - insert input variable
daysh = floor(inputvariable(1)):1/24:floor(inputvariable(end));
dt = 7200; % time step (s)
t = 0:dt:n*3600; % time index (s)
xday = 310;
days = daysh(1):1/24/(3600/dt):xday; % Julian days every dt
N = length(days); % Length of Simulation
%-----
% Model Space:
dx = 1000; % m
dy = 1000; % m
dz = 9.2; % m
z = dz;
%-----
% Ratios and Constants:
CCtoP = 145.44; % Cladophora (g/g or 375 molar)
CtoP = 80; % Seston (g/g)
CtoChla = 27; % Seston (gC/gChla)
Cgtom = 12; % g/mol
Pgtom = 31; % g/mol
O2gtom = 32; % g/mol (O = 15.999 g/mol -> O2 = 32 g/mol)
Tmin = 17; % Minimum Sloughing Temperatures (oC)
Topt = 17; % Optimum Sloughing Temperatures (oC)
Lmax = 0.176/24/3600; % Maximum Sloughing Rate (1/s)
vs = 0.5/24/3600; % Particulate settling velocity (m/s)
%-----
% Mussel Constants:
vp = zeros(1,N); % L/m2/s
ex = 0.80; % excretion/egestion ratio
%-----

```



```

% Cladophora Sloughing Algorithm:
SL = zeros(1,N);
x1 = find(T>=Topt);
x2 = find(Wtao >= 0.4);
SL(x1) = Lmax;
SL(x2) = Lmax;

%-----
% Resuspension Parameter:
rtao = zeros(1,N);
rtao(find(Wtao >= 0.40)) = 1;

%-----
% Schmidt Number (Temp in oC) (as in Wanninkof 1992)
Sc = 1911.1 - 118.11.*Ts + 3.4527.*(Ts.^2) - 0.041320.*(Ts.^3);

% Solubility Constant in units: mol/(m^3 Pa)
sigma = 2.71828.^(-574.70126+21541.52./(Ts+273)-0.000147759.*...
    (Ts+273).^2+89.892.*log(Ts+273))/101325*1000;

% Air-Water Exchange Velocity:
% Wanninkhof 1992 Model:
k = ((0.31*(uw.^2)).*(Sc./600).^(-0.5))/100/3600; % m/s
% Zhao and Xie k Model:
kzx = min([(6.81*(uw.*WH).^0.63))' (0.75*(uw.^1.89))'], [],2)'.*...
    ((Sc./600).^(-0.5))/100/3600; % m/s

% DIC Equilibrium Constants:
K0 = 10.^(-((-8e-5)*Ts.^2 + 0.0165*Ts + 1.1082));
K1 = 10.^(-((8e-7)*Ts.^3 + 0.0002*Ts.^2 - 0.0133*Ts + 6.5791));
K2 = 10.^(-(0.0001*Ts.^2 - 0.0146*Ts + 10.625));

%-----
% Dependent Variables and Fluxes:

I = zeros(1,N); % PAR at depth (uE/m2/s)
Ke = zeros(1,N); % Light Extinction Coefficient (1/m)

P1 = zeros(1,N); % Surface Water DP (ugP/L = mgP/m3)
PP1 = zeros(1,N); % Surface Water PP (ugP/L = mgP/m3)
dP = zeros(1,N); % Change in Dissolved Phosphorus (ugP/L/s)
PS = zeros(1,N); % Phytoplankton Concentration (umolC/L)
D = zeros(1,N); % Detritus Concentration (umolC/L)
dPS = zeros(1,N); % Change in Phytoplankton (umolC/L/s)
SPmort = zeros(1,N); % Mortality flux of Phytoplankton to Detritus
(umolC/L/s)
DIC = zeros(1,N); % Disolved Inorganic Carbon Concentration (mol/L)
CO2 = zeros(1,N); % Carbon dioxide concentration (mol/L)
HCO3 = zeros(1,N); % Bicarbonate Concentration (mol/L)
CO3 = zeros(1,N); % Carbonate Cocentration (mol/L)
pH = zeros(1,N); % pH
Hi = zeros(1,N); % Hydrogen ion concentration (mol/L)
pCO2w = zeros(1,N); % CO2 partial pressure (uatm)
FCO2 = zeros(1,N); % Air-Water CO2 Flux (mmolC/m2/s)
deltaC = zeros(1,N); % Difference between air and water pCO2 (pa)
dPCC = zeros(1,N); % Cladophora production (molC/m2/s)
MXc = zeros(1,N); % Mussel respiration (molC/m2/s)
dPSc = zeros(1,N); % Phytoplankton Production (molC/m2/s)
Jsusp = zeros(1,N); % PP Resuspension Flux from Sediment storage to BBL
(mgP/m2/s)

```

```

Jslpp = zeros(1,N);      % Settling Flux (mgP/m2/s)
JolPS = zeros(1,N);     % Nearshore Offshore Flux of PS (mmolC/m2/s)
JolD = zeros(1,N);      % Nearshore Offshore Flux of D (mmolC/m2/s)
Jolp = zeros(1,N);      % Nearshore Offshore Flux of DP (mgP/m2/s)
JodIC = zeros(1,N);     % Nearshore Offshore Flux of DIC (mmolC/m2/s)
Johi = zeros(1,N);      % Nearshore Offshore Flux of H+ (mmolC/m2/s) %

MX = zeros(1,N);        % Mussel Phosphorus Excretion (mgP/m2/s)
MGps = zeros(1,N);      % Mussel Phytoplankton Grazing (mmolC/m2/s)
MGd = zeros(1,N);       % Mussel Detritus Grazing (mmolC/m2/s)
MG = zeros(1,N);        % Mussel Grazing (mgP/m2/s)
MGC = zeros(1,N);       % Mussel Grazing (mmolC/m2/s)
ME = zeros(1,N);        % Mussel Egestion (mgP/m2/s)
MEc = zeros(1,N);       % Mussel Egestion (mmolC/m2/s)
X = zeros(1,N);         % Cladophora Biomass (gDM/m2)
S = zeros(1,N);         % Cladophora Phosphorus Storage (mgP/m2/10)
Q = zeros(1,N);         % Cladophora Tissue Phosphorus Content (mgP/gDM/10)
SD = zeros(1,N);        % Sediment Phosphorus Storage (mgPP/m2)
Bsedtrap = zeros(1,N);  % Sediment Accumulated in a Sediment Trap (mgPP/m2)
dPC = zeros(1,N);       % Cladophora Phosphorus Uptake (mgP/m2/s)
Lloss = zeros(1,N);     % Cladophora Sloughed Phosphorus (mgP/m2/s)
dXC = zeros(1,N);       % Change in Cladophora stored Carbon (mgC/m2/s)
LlossC = zeros(1,N);    % Cladophora Sloughed Phosphorus (mgP/m2/s)

%-----
% Initial Conditions:

PS(1) = Chla13(1,2)*CtoChla/Cgtom;      % umol C/L
D(1) = mean(PC13(1,2:3))/Cgtom - (PS(1)); % umol C/L

PP1(1) = (PS(1)+D(1))*Cgtom/CtoP; % ug PP/L
P1(1) = SRP13(1,2); % ug DP/L

X(1) = EmpData13(1,2); % gDM/m2
Q(1) = EmpData13(1,4)/10; % mgP/gDM/10
S(1) = Q(1)*X(1); % mgP/m2/10

% Alkalinity:
Alkm = 2.22*ones(1,N); % meq/L Lake Michigan
Alkm = Alkm/1000; % mol/L

% Initial pCO2 from observations:
pCO2w(1) = pCO2w_obs(1); % uatm
pCO2pa = zeros(1,N) + (pCO2w(1)/1e6)*101325; % pa
CO2(1) = (pCO2w(1)*10^-6)*K0(1); % mol/L

% First Guess:
pH(1) = 8.2;
Hi(1) = 10^(-pH(1)); % mol/L

H1 = 0.1*Hi(1):0.0001e-9:3*Hi(1); % mol/L

% Use the H+ guess range to calculate Alk:
CO21 = CO2(1);
HCO31 = K1(1)*CO21./H1;
CO31 = K2(1)*HCO31./H1;
Alk1 = 2*CO31 + HCO31 - H1;

% Find the difference between the Alk guesses and the constant Lake Alk:

```

```

DAlk = Alk1 - Alkm(1);
[x,i] = min(abs(DAlk));
Hf = H1(i); pHf = -log10(Hf);

% Set initial conditions:
Hi(1) = Hf;
pH(1) = pHf;
HCO3(1) = K1(1)*CO2(1)./Hi(1);           % mol/L
CO3(1) = K2(1)*HCO3(1)./Hi(1);          % mol/L
DIC(1) = CO2(1) + HCO3(1) + CO3(1);      % mol/L
Alk(1) = HCO3(1) + 2*CO3(1) - Hi(1);

%-----
% Time Loop:

a = dt/dz; % s/m

for i = 1:N-1;

    deltaC(i) = (CO2(i)/K0(i))*101325 - pCO2pa(i); % Pa
    FCO2(i) = k(i)*sigma(i)*deltaC(i); % mol/m2/s

    % Light Extinction Coefficient:
    Ke(i) = 0.0383*PP1(i) + 0.162;

    % Light at Depth (uE/m2/s):
    I(i) = PAR(i)*exp(-Ke(i).*9);

    % Mussel Model:
    % Mussel Water Pumping:
    vp(i) = MPfunc(T(i),MD(i),PropSC1(:,i)); % L/m2/s
    vp(i) = vp(i)/1000; % m3/m2/s = m/s
    % Mussel Phosphorus Fluxes:
    MGps(i) = (vp(i)*PS(i))*(1-rtao(i)); % mmolC/m2/s
    MGd(i) = (vp(i)*D(i))*(1-rtao(i)); % mmolC/m2/s
    MG(i) = (MGps(i) + MGd(i))*Cgtom/CtoP; % mgP/m2/s
    MGC(i) = MGps(i) + MGd(i); % mmolC/m2/s
    MX(i) = ex*MG(i); % mgP/m2/s
    ME(i) = (1-ex)*MG(i); % mgP/m2/s
    MXc(i) = ex*MGC(i); % mmolC/m2/s
    MEc(i) = (1-ex)*MGC(i); % mmolC/m2/s

    % Cladophora Model:
    [S(i+1),Q(i+1),X(i+1),dPC(i),Lloss(i),dXC(i),LlossC(i)] = ...
        Cfunc(z,dz,I(i),T(i),P1(i),Q(i),S(i),X(i),dt,sloughing,SL(i));

    % Fluxes:

    % Settling (mgPP/m2/s):
    Jslpp(i) = (vs*PS(i) + vs*D(i))*Cgtom/CtoP;

    % Resuspension (mmolC/m2/s):
    Jsusp(i) = (rtao(i)*SD(i)/dt)*CtoP/Cgtom;

    % Boundary Advection:
    Jo1PS(i) = abs(u(i))*PSo(i) - abs(u(i))*PS(i); % mmol C/m2/s
    Jo1D(i) = abs(u(i))*Do(i) - abs(u(i))*D(i); % mmol C/m2/s
    Jo1p(i) = abs(u(i))*PO(i) - abs(u(i))*P1(i); % mg P/m2/s
    JoDIC(i) = abs(u(i))*(DICO1(i)*1000 - DIC(i)*1000); % mol C/m2/s

```

```

        JoHi(i) = abs(u(i))*(HiO1(i)*1000 - Hi(i)*1000);      % mol Hi/m2/s

% Phytoplankton Model:
[dP(i),dPS(i),SPmort(i)] = phyfunc(Ts(i),z/2,Ke(i),PAR(i),PS(i),P1(i));

% Solve Mass Balance Equations:

% Phytoplankton (umolC/L):
PS(i+1) = PS(i) + dPS(i)*dt - vs*PS(i)*a - MGps(i)*a + ...
        JolPS(i)*dt/dx;

% Detritus (umolC/L):
D(i+1) = D(i) + SPmort(i)*dt - vs*D(i)*a - MGd(i)*a + ...
        Jsusp(i)*a + JolD(i)*dt/dx;

% Water Column PP (ugP/L):
PP1(i+1) = (PS(i+1)+D(i+1))*Cgtom/CtoP; % ugPP/L

% Water Column DP (ugP/L):
P1(i+1) = P1(i) + Jolp(i)*dt/dx + MX(i)*a - dPC(i)*a + dP(i)*dt;

% Sediment Accumulated PP (mgP/m2):
SD(i+1) = SD(i) + ME(i)*dt + Js1pp(i)*dt - (Jsusp(i)*Cgtom/CtoP)*dt;

% Photosynthesis and Respiration:
dPCc(i) = dXC(i)*0.30/Cgtom;      % mol C/m2/s
MXc(i) = MXc(i)/1000;            % mol C/m2/s
dPSc(i) = SPup(i) - SPresp(i);   % mmol C/m3/s
dPSc(i) = dPSc(i)*dz/1000;      % mol C/m2/s

% Solve Mass Balance Equations:

% DIC:
DIC(i+1) = DIC(i) + JoDIC(i)*dt/dx/1000 - FCO2(i)*a/1000 ...
        - dPCc(i)*a/1000 + MXc(i)*a/1000 - dPSc(i)*a/1000 ;

% Hydrogen:
Hi(i+1) = Hi(i) + JoHi(i)*dt/dx/1000;

% Upper Water Column Chemistry:
[Hi(i+1),pH(i+1),CO2(i+1),HCO3(i+1),CO3(i+1),pCO2w(i+1)] = ...

DICfunc1(T(i),dt,dz,DIC(i),DIC(i+1),Hi(i+1),Alkm(i),K0(i),K1(i),K2(i));

end

% End of Model Code
%-----

```

B.3: *Cladophora* model function and *Cladophora* model multipliers function

```

function [si,Qi,Xi,dPC,Lloss,dXC,LlossC] = ...
CfuncC(z,dz,I,T,P,Q,s,X,dt,sloughing,SL);

dt1 = dt;
dt = (1/24/3600);

% Constants:
umax = 1.53;           % Maximum growth coefficient (1/day)
Q0 = 0.05;            % Minimum P Quota (P as %DW)
Xmax = 800;           % Maximum biomass density (gDW/m2)
rhomax = 4.5;         % Maximum phosphorus uptake rate (%P/day =
mgP/gDW/day/10)
Km = 125;              % Half saturation constant for uptake as a function of
% external phosphorus concentration (ugP/L)
Rmax = 0.23;          % Maximum specific light-enhanced respiration rate
% coefficient (1/day)

% Cladophora Model:
if I > 1235;
    I = 1235;
end

% Polynomials:
[Rmult,umult] = multipliers(I,T);
RLT = Rmax*Rmult*dt; % Respiration due to temp and light (1/sec)

if I < 35;
    umult = 0;
end

Mgross = umult;

% Respiration:

% Basal respiration (1/sec)
RB = (0.003*T + 0.0199)*dt;

if I < 35;
    RLT = 0;
end
if I > 35;
    RB = 0;
end

% Gross Respiration Coefficient (1/sec)
R = RLT + RB;

% Sloughing Rate (1/sec):
Lz = 0;

% Sloughing Algorithm:
if sloughing == 1;
    Lz = SL;
end

% Multipliers Based on Phosphorus Tissue Content and Biomass Capacity:

```

```

Mp = 1 - (Q0/Q);
Mx = 1 - (X/Xmax);

% Time Step Growth Rate:
u = umax*Mgross*Mx*Mp*dt;          % 1/s

% Time Step Phosphorus Uptake (i+0.5):
rho = (rhomax*(P/(Km + P))*0.016556*Q^(-1.5963))*dt; % mgP/gDW/sec/10

% Change in Phosphorus Storage :
ds = rho*X - R*s;                  % mgP/m2/sec/10

% Change in Biomass:
dX = (u - R - Lz)*X;               % gDW/m2/sec
dXC = (u - R)*X;                   % gDW/m2/sec
% New (i+1) Stored Phosphorus (including loss due to sloughing):
si = (ds)*dt1 - (Lz*s)*dt1 + s;   % (mgP/m2/10)

% New (i+1) Biomass
Xi = dX*dt1 + X;                   % (gDW/m2)

% New (i+1) Tissue Phosphorus Content:
Qi = (si/Xi);                       % mgP/gDW/10

% Sloughed Phosphorus Loss Flux:
Lloss = Lz*(s*10);                 % mgP/m2/sec
LlossC = Lz*X;                     % gDW/m2/s

% Net Cladophora Phosphorus Flux Due to Uptake and Respiration:
dPC = ds*10;                       % mgP/m2/sec

% End of Model Function

function [Rmult,umult] = multipliers(x1,x2);

r1 = 9.57964430724275e-2;
r2 = 5.90365507708485e-4;
r3 = 2.25715188890411e-2;
r4 = -4.72010300767978e-7;
r5 = 1.90990816538341e-5;
r6 = -1.16739190002568e-3;
r7 = 7.87726632078466e-11;
r8 = -2.51393854052121e-8;
r9 = -1.94496751357286e-8;
r10 = 2.33853164223086e-5;
r11 = 4.20154521630618e-11;
r12 = -1.90416382375698e-9;
r13 = 3.03917511652015e-8;

g1 = -3.10189820044715e-2;
g2 = 1.21097828989578e-3;
g3 = 3.12062696338505e-2;
g4 = -2.99494257852711e-6;
g5 = 2.87556463159981e-4;
g6 = -1.06206957408835e-3;
g7 = 1.6875291852178e-9;
g8 = -2.59743951456656e-7;
g9 = -8.88202634153844e-6;
g10 = 5.41146607284034e-6;

```

```

g11 = 8.94172679669356e-11;
g12 = 2.67412430299216e-9;
g13 = 7.18690371326443e-8;

Rmult = r1 + r2*x1 + r3*x2 + r4*x1^2 + r5*x1*x2 + r6*x2^2 + r7*x1^3 + ...
        r8*x1^2*x2 + r9*x1*x2^2 + r10*x2^3 + r11*x1^3*x2 + r12*x1^2 * x2^2 + ...
        r13*x1*x2^3;

umult = g1 + g2*x1 + g3*x2 + g4*x1^2 + g5*x1*x2 + g6*x2^2 + g7*x1^3 + ...
        g8*x1^2*x2 + g9*x1*x2^2 + g10*x2^3 + g11*x1^3*x2 + g12*x1^2*x2^2 + ...
        g13*x1*x2^3;

```

B.4: Dreissenid Mussel Function:

```

function [MP] = MPfunc(T,MD,PropSC);

sc = [5:30]'; % mussel size classes (mm)
n = length(sc); % number of size classes

% Model Variables:
mp = zeros(n,1); % Mussel Pumping for each size class (L/m2/s)
MP = 0;          % Areal P Excretion (mg P/m2/hr)

MP1 = (0.633*exp(0.074*T))/1000/3600; % mL/mgDW/hr -> L/mgDW/sec

% Equation Components: Excretion (mg P/mgDW/hr) X size correction factor X
% mussel density X size class proportion X length to weight conversion

mp = MP1.*(1207.8*sc.^-2.3689).*...
     MD.*...
     PropSC.*...
     (0.0018.*sc.^3.11); % L/m2/sec

% Add excretion over all size classes:
MP = sum(mp); % L/m2/sec

```

B.4: Phytoplankton Function:

```

function [dP,dPS,SPmort] = phyfunc(T,z,Ke,PAR,PS,P)

% Depth:
Z = z;

% Ratios:
CtoP = 80;      % g/g
Cgtom = 12;     % g/mol
Pgtom = 31;     % g/mol

%Max Growth Rate:
Vpsmax = 1.4/24/3600; % 1/s

% Half Saturation Constants:
kps = 0.1;      % umolP/L
P = P/Pgtom;   % umol P/L

```

```

% Rates:
respPS = 0.05/24/3600;    % respiration rate (1/s)
alphaPS = 0.01/24/3600;  % mortality rate (1/s)

% Temperature Dependence Coefficient
alpha = 0.0693;

% Light Function:
Fips = exp(-Ke*Z);

% Change in Phytoplankton and Phosphorus:
SPup = Vpsmax*(P./(kps + P))*Fips*PS;          % umol C/L/sec
SPmort = alphaPS*PS^2;                          % umol C/L/sec
SPresp = respPS*PS;                             % umolC/L/sec
dPS = SPup - SPmort - SPresp;                  % umol C/L/sec
dP = - (SPup*Cgtom/CtoP) + (SPresp*Cgtom/CtoP); % ug P/L/s

% End of Function

```

B.5: Hydrogen ion iteration function:

```

function [Hf1,pHf1,CO2f1,HCO3f1,CO3f1,pCO2wf] = ...
    DICfunc1(T,dt,dz,DIC,DICf,Hf,Alkm,K0,K1,K2)

% DIC in the water column:
DIC1 = DICf; % mol/L

if DIC1 ~= DIC;

% Iteration to Determine H+ Concentration:
%   Guess at the new H+ concentration with a range (+/-) around the
%   prior H+ concentration:
H1 = 0.1*Hf:0.0001e-9:3*Hf; % mol/L

% Use the H+ guess range to calculate Alk:
a0 = (1+(K1./H1)+((K1*K2)./(H1.^2))).^(-1);
a1 = ((H1/K1) + 1 + (K2./H1)).^(-1);
a2 = (((H1.^2)/(K1*K2)) + (H1/K2) + 1).^(-1);
CO21 = DIC1.*a0;
HCO31 = DIC1.*a1;
CO31 = DIC1.*a2;
Alk1 = 2*CO31 + HCO31 - H1;

% Find the difference between the Alk guesses and the constant Lake Alk:
DAlk = Alk1 - Alkm;
[x,I] = min(abs(DAlk));

% Find the point where the difference between the constant Alk and Alk
% guesses is near zero:
Hf1 = H1(I);
clear H1 CO21 HCO31 CO31 Alk1 x I DAlk

% Double Check:
a0 = (1+(K1./Hf1)+((K1*K2)./(Hf1.^2))).^(-1);
a1 = ((Hf1/K1) + 1 + (K2./Hf1)).^(-1);
a2 = (((Hf1.^2)/(K1*K2)) + (Hf1/K2) + 1).^(-1);

```



```

CO2f1 = DIC1.*a0;
HCO3f1 = DIC1.*a1;
CO3f1 = DIC1.*a2;
pHf1 = -log10(Hf1);

Alk2 = 2*CO3f1 + HCO3f1 - Hf1;
% Make sure DAlk2 is very very small!
DAlk2 = Alk2 - Alkm;

pCO2wf = (CO2f1./K0).*10^6; % uatm
pHfm = pHf1;

end

if DIC1 == DIC;
    Hf1 = Hf;
    a0 = (1+(K1./Hf1)+((K1*K2)./(Hf1.^2))).^(-1);
    a1 = ((Hf1/K1) + 1 + (K2./Hf1)).^(-1);
    a2 = (((Hf1.^2)/(K1*K2)) + (Hf1/K2) + 1).^(-1);
    CO2f1 = DIC1.*a0;
    HCO3f1 = DIC1.*a1;
    CO3f1 = DIC1.*a2;
    pHf1 = -log10(Hf1);
    pCO2wf = (CO2f1./K0).*10^6; %uatm
end

% End of Function

```

CURRICULUM VITAE

Joseph H Fillingham

Place of Birth: Milwaukee, WI

Education:

B.S., University of Wisconsin, May 2007
Major: Atmospheric and Oceanic Sciences

M.S., Mathematical Sciences and Atmospheric Sciences
Thesis Title: Evaluation of the influence of surface atmospheric stability and fetch on wave and air-water gas exchange modeling on Lake Michigan

Dissertation Title: Modeling Lake Michigan Nearshore Carbon and Phosphorus Dynamics

Publications:

Wang, B., Q. Liao, J. H. Fillingham, and H. A. Bootsma (2015), On the coefficients of small eddy and surface divergence models for the air-water gas transfer velocity, *J. Geophys. Res. Oceans*, 120, 2129–2146, doi:10.1002/2014JC010253

Presentations:

Fillingham, J.H., Bootsma, H.A., 2014. Modeling Carbon and Phosphorus Cycles in the Nearshore Zone of Lake Michigan. International Association for Great Lakes Research Annual Conference. McMaster University, Hamilton, ON, Canada. Scheduled for: May 30, 2014.

Fillingham, J.H., Wang, B., Bootsma, H.A., Liao, Q., 2013. Towards a Parameterization for the CO₂ Gas Transfer Velocity Useful for Biogeochemical Modeling of the Great Lakes. International Association for Great Lakes Research Annual Conference. Purdue University, West Lafayette, IN. June 4, 2013.

Fillingham, J.H., Bootsma, H.A., Roebber, P.J., 2009. Modeling waves and their influence on air-water gas exchange in Lake Michigan. International Association for Great Lakes Research Annual Conference. University of Toledo, Toledo, OH. May 19, 2009.

Awards:

HYDROLAB/IAGLR Student Oral Paper award for the 2014 IAGLR Conference, May 2015

PhD Scholarship, International Association for Great Lakes Research, May 2014

Knauss Marine Policy Fellowship, NOAA Sea Grant, February 2011

Research Excellence Award, UW-Milwaukee Graduate School, September 2010

Professional Positions:

Science Lead, WellIntel Inc., Milwaukee, WI
February 2015 to Present

Research Assistant, School of Freshwater Sciences, University of Wisconsin-Milwaukee
February 2012 to January 2015

Program Analyst, Knauss Marine Policy Fellow, Office of Laboratories and Cooperative
Institutes, Oceanic and Atmospheric Research, National Oceanic and Atmospheric
Administration
February 2011 to January 2012

Teaching Assistant, Atmospheric Science 100 Laboratory, Department of Mathematical
Sciences, University of Wisconsin-Milwaukee
August 2009 to May 2010

Research Assistant, Great Lakes WATER Institute, University of Wisconsin-Milwaukee
May 2008 to August 2009 and May 2010 to January 2011

Sailing Instructor, Milwaukee Community Sailing Center, Milwaukee, WI
May 2002 to Present